Design, Synthesis and Characterization of Targeted and Calcium Responsive Nano-size Contrast Agents for Magnetic Resonance Neuroimaging

Design, Synthese und Charakterizierung von zielspezifischen und Kalziumempfindlichen Molekülen als MRT-Kontrastmittel für das Neuroimaging

Dissertation

der Mathematisch-Naturwissenschaftlichen Fakultät

der Eberhard Karls Universität Tübingen

zur Erlangung des Grades eines

Doktors der Naturwissenschaften

(Dr. rer. nat.)

vorgelegt von

Serhat Gündüz

aus Yerköy/Türkei

Tübingen

2014

Tag der mündlichen Prüfung:	17.07.2014
Dekan:	Prof. Dr. Wolfgang Rosenstiel
1. Berichterstatter:	Prof. Dr. Martin E. Maier
2. Berichterstatter:	Priv.–Doz. Dr. Goran Angelovski

This doctoral thesis was carried out at the Dept. of Physiology of Cognitive Processes of the Max Planck Institute for Biological Cybernetics, Tübingen under the supervision of Prof. Nikos K. Logothetis, Priv.–Doz. Dr. Goran Angelovski and in collaboration with the Institute for Organic Chemistry, Eberhard-Karls-University, Tübingen under the guidance of Prof. Dr. Martin E. Maier during the period from October 2010 to May 2014.

Hereby I declare the fact that I am writing this work and no different than the indicated aids have been used.

Tübingen, May, 2014

To my wife and our kids

Acknowledgements

First and foremost, I would like thank Prof. Nikos K. Logothetis, Director of Department Physiology of Cognitive Processes, Max Planck Institute for Biological Cybernetics, for giving me an opportunity to work in his research group providing his support and funding.

I would like to thank Prof. Martin E. Maier who constantly supervised my work, teaching in his Wednesday seminars.

I would like to express my special thanks to my supervisor Priv. –Doz. Dr. Goran Angelovski who helped me during my PhD study for his helpful advices, encouragement, motivation and patience.

I would like to thanks my project collaborators: Dr. Anthony Power for help with biological experiments and his advices, Dr. Aoki Ichio and his group members for performing *in vivo* MR experiments in rat brain. I also would like to thank Dipl. –Ing. Michael Bayerlein for performing *in vitro* MR experiments.

I wish to express my deepest thanks to all my colleagues and group members of chemistry groups in Logothetis department: Dr. Ilgar Mamedov, Dr. Pascal Kadjane, Dr. Sandip M. Vibhute, Dr. Karolina Jankowska, Dr. Matteo Placidi, Dr. Fatima Oukhatar, Dr. Aneta Keliris, and Dr. Nevenka Cakic for their helpful discussions, help and wonderful atmosphere in the laboratory. I also would like to thank Dr. Joern Engelmann, Dr. Rajendra Joshi and Ms. Hildegard Schulz for their help. Thanks to Conchy Moya and Rainer Hirt for all the help on the administrative arrangements. Furthermore I would like to thank Dr. Dorothee Wistuba for her comprehensive help with high resolution mass spectrometry.

I would like to thank members of the exam committee, Prof. Dr. Thomas Ziegler and Prof. Dr. Hermann A. Mayer.

The financial support of the Max-Planck Society, the Turkish Ministry of Education (PhD fellowship) and European COST CM1006 and TD1004 Actions is gratefully acknowledged.

Finally, I thank all my family for their support throughout my life. Especially, I thank my wife, Fatma for her love, understanding, encouragement and support.

Abstract

Magnetic resonance imaging (MRI) is a powerful imaging technique for biomedicine and neuroscience. The contrast agents (CAs) have been developed to help increasing signal intensity for high resolution MR images. Here we report the synthesis of novel multimodal and multivalent CA targeted to the protein (Neutr/strept) avidin and Ca^{2+} responsive multivalent CAs for MR neuroimaging.

In the first project, the avidin-targeted monomeric (**MCA-2**) and dendrimeric (**DCA-2**) CAs containing fluorescence label (FITC) and biotin were synthesized and characterized. The relaxometric analysis, avidin binding assay, MRI experiment and fluorescence measurements were performed. G4 PAMAM dendron with 32 surface amino groups was used as a multivalent scaffold. Avidin binding assay showed the binding efficiency of **MCA-2** to avidin beads is higher than **DCA-2**, while the beads bound **DCA-2** provided higher MR signal intensity than **MCA-2**. A number of diverse applications could consequently be envisaged for **DCA-2** to investigate living systems**.** For instance, the polypeptide avidin could be introdruced as a transgene in living cells with techniques of molecular biology for creating model organisms.

The second project focused on the synthesis and characterization of the monomeric Ca^{2+} responsive CA (**SCA-1**) and dendrimeric Ca^{2+} responsive CAs (**DSCA-1**, **DSCA-2**, and **DSCA-3**) using G0, G1 or G2 PAMAM dendrimers, which contains 4, 8, and 16 surface amino groups, respectively, as multivalent scaffolds. The relaxometric Ca^{2+} titrations and *in vivo* MR experiments in rat brain were performed. In the presence of Ca^{2+}, the longitudinal relaxivity of these SCAs increased. *In vivo* experiments showed that the DSCAs stayed longer period of time in tissue than **SCA-1** providing higher signal intensity. Since the short retention time of the commercial low molecular CAs reduces the quality of MR images, making the diagnosis difficult, the use of DSCAs with a comparably longer retention time may enable development of new imaging protocols with the high quality MR image.

Abstrakt

Die Magnetresonanztomographie (MRT) ist ein leistungsfähiges bildgebendes Verfahren für Biomedizin und Neurowissenschaft. Kontrastmittel (engl. CAs: contrast agents) wurden entwickelt, um die Signalintensität hochauflösender MR-Bilder zu erhoehen. Wir berichten hier über die Synthese von neuartigen multimodalen und multivalenten avidinbindenden CAs sowie ueber kalziumsensitive multivalente CAs für das MR- neuroimaging.

Im ersten Projekt, wurden fluoreszenz (FITC) und biotin markiertes (Monomere (**MCA -2**) und Dendrimere (**DCA-2**)) Kontrastmitteln, die an Avidin bindet, synthetisiert und charakterisiert. Es wurden relaxometrische Analysen, Avidin-Bindungsassays, MRI Experimente und Fluoreszenzmessungen durchgeführt. G4 PAMAM Dendron, das 32 Oberflächenaminogruppen aufweist, wurde als multivalentes Gerüst verwendet. Avidin-Bindungstests zeigten, dass die Bindungseffizienz von **MCA-2** an Avidinbeads höher als **DCA-2** ist, während an Avidinbeads gebundenes **DCA-2** höhere MR-Signalintensität als **MCA-2**.zeigte. Eine Reihe verschiedener Anwendungen könnten für **DCA-2** entwickelt werden, um damit lebende Systeme zu untersuchen. Zum Beispiel könnte das Polypeptid Avidin mittels molekularbiologischer Techniken als Transgen in Zellen eingefuehrt werden und in Modellorganismen untersucht werden.

Das zweite Projekt konzentrierte sich auf die Synthese und Charakterisierung des monomeren kalziumsensitiven CA (**SCA-1**), sowie der kalziumsensitiven CA (**DSCA-1**, **DSCA-2** und **DSCA-3**) die G0, G1 oder G2 PAMAM-Dendrimere, mit 4, 8 und 16 Oberflächen aminogruppen als multivalentes Gerüste enthielten. Es wurden relaxometrische Ca^{2+}-Titrationen und *in vivo* MR-Experimente am Rattenhirn durchgeführt. In Gegenwart von Kalzium erhoehte sich die longitudinale Relaxivität der SCAs. In-vivo-Experimente zeigten, dass die DSCAs längere Zeit als **SCA-1** im Gewebe verblieben, und somit eine höhere Signalintensität zeigten. Da die kurze Retentionszeit kommerzieller, niedermolekularer CAs die Qualität der MR-Bilder beeintraechtigte, koennte der Einsatz von DSCAs mit vergleichsweise längerer Retentionszeit die Entwicklung neuer Bildgebungsverfahren mit hoher MR-Bildqualität ermöglichen.

Abbreviations

AAZTA	6-amino-6-methylperhydro-1,4-diazepinetetraacetic acid
Boc	*tert*-butoxycarbonyl
BOLD	Blood-oxygen-level dependent
CA	Contrast agent
Cbz	Carboxybenzyl
$CDCl_3$	Chloroform deuterated
CT	Computed tomography
Cys	Cystamine
D_2O	Deuterium oxide
DCA	Dendrimeric contrast agent
DCC	N,N'-Dicyclohexylcarbodiimide
DMAP	4-Dimethylaminopyridine
DMSO	Dimethyl sulfoxide
DOTA	1,4,7,10-tetraazacyclododecane-N,N',N",N'"-tetraacetic acid
DOTP	1,4,7,10-tetraazacyclododecane-N,N',N",N'"-tetra(methylene phosphonic acid)
DO3A	1,4,7,10-tetraazacyclododecane-1,4,7-*tris*(acetic acid)
DPDP	Dipyridoxyl diphosphate
DSCA	Dendrimeric smart contrast agent
DTPA	Diethylene triamine pentaacetic acid
DTT	Dithiothreitol
EDC	1-Ethyl-3-(3’-dimethylaminopropyl) carbodiimide
EDTA	Ethylenediaminetetraacetic acid
EGTA	Ethylene glycol bis(2-aminoethylether)-N,N,N’,N’-tetraacetic acid

EGad	(4,7,10-tri(acetic acid)-l-(2-β-galactopyranosylethoxy)-1,4,7,10-tetraazacyc1ododecane) gadolinium
Eq	Equation
Equiv	Equivalent
EMEA	European Medicines Agency
ESI-MS	Electrospray ionization mass spectrometry
ESI-TOF-MS	Electrospray ionization/time of flight mass spectrometry
FDA	U.S. Food and Drug Administration
FITC	Fluorescein isothiocyanate
FT-ICR-MS	Fourier transform ion cyclotron resonance mass spectrometry
ICP-MS	Inductively coupled plasma – mass spectrometry
J	Coupling constant
Ln	Lanthanide
m	Multiplet (NMR)
MALDI-TOF	Matrix-assisted laser desorption/ionization-time of flight
MCA	Monomeric contrast agent
MHz	Megahertz
MR	Magnetic resonance
MRI	Magnetic resonance imaging
MWCO	Molecular weight cutoff
m/z	Mass/charge ratio
NCS	Isothiocyanate
NHS	N-Hydroxysuccinimide
NMR	Nuclear magnetic resonance
PAMAM	Poly(amido amine)

PAS	p-aminosalicylic acid
PBS	Phosphate buffer saline
Pd/C	Palladium/carbon
PET	Positron emission tomography
PPI	Poly(propylenimine)
q	Quartet (NMR)
R	Relaxation rate
ROI	Region of interest
RF	Radio frequency
rt	Room temperature
s	Singlet
SCA	Smart contrast agent
SMCC	Succinimidyl-4-(*N*-maleimidomethyl)cyclohexane-1-carboxylate
SPIO	Superparamagnetic iron oxide
T	Tesla (MRI)
T_1	Spin lattice relaxation time
T_2	Spin spin relaxation time
t-Bu	*tert*-butyl
TCEP	*Tris*(2-carboxyethyl)phosphine
tert	Tertiary
TLC	Thin layer chromatography
TPEN	*Tetrakis*-(2-Pyridylmethyl)ethylenediamine
USPIO	Ultra small seperparamagnetic iron oxide
δ	Chemical shift

Table of Contents

1. Introduction

1.1. Magnetic resonance Imaging (MRI)

MRI has become one of the essential noninvasive techniques for studying soft tissues and diseases in biomedicine and neurosience. Neuroimaging includes the use of various techniques such as MRI, CT, PET, and SPECT to image the structure and the function of brain. MRI has various advantages versus other imaging techniques. It does not involve any ionizing radiation and it provides higher contrast between different soft tissues. The noninvasive nature of MRI makes it indispensable in visualization and understanding of the limited structure and function of human body in clinical diagnosis.

MR images are generated using powerful magnetic field to align the nuclear magnetization of water hydrogen nuclei. The signal intensity depends on several intrinsic properties of the tissue such as spin density, spin lattice relaxation time (T_1), and spin-spin relaxation time (T_2). Because of the differences between relaxation times and the random distribution of water in the body, an intrinsic contrast is produced in different tissues. This allows obtaining 3D model of the investigated tissue, e.g. human anatomy. Although water proton in the body provides a contrast in the magnetic field, this contrast is sometimes not sufficient to get good resolution MR images for the region of interest. Consequently the contrast agents (CAs) have been developed to help increasing signal intensity for high resolution MR images. Generally CAs are classified into two groups, T_1-weighted CAs and T_2-weighted CAs. The most commonly used CAs agents contain gadolinium metal ion (Gd^{3+}). Gadolinium is a lanthanide element which has seven unpaired electron pair, symmetric S-state, large magnetic moment, and slow relaxation of electron spin. Since Gd^{3+} ion is toxic like the other paramagnetic ions such as Mn^{3+}, Fe^{3+}, it is complexed with a proper ligand to reduce the toxicity. Gd^{3+} is complexed with the polydentate ligands in order to minimize its toxicity.[1-4]

1.2. Basic Principle of MRI

MRI works based on the principle of NMR. Due to the abundance of hydrogen in the body and its quite large magnetic moment, the hydrogen proton is used in clinical imaging applications. A proton has a positive charge and spin angular momentum. Although the proton does not have very large electrical charge, it rotates very fast providing a magnetic field.

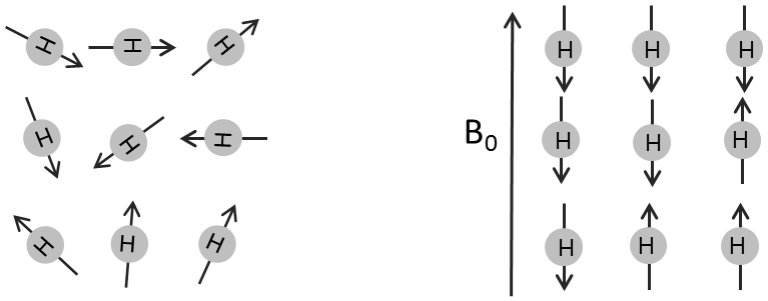

Figure 1-1. Alignment of randomly distributed protons (left) with an external magnetic field, B_0 (right).

The direction of this magnetic field is randomly distributed. The magnetic moment of atomic nuclei and its nuclear spin, ***I*** are proportional each other. The hydrogen atom has a spin of ½ and there are two possible orientations, +½ and -½. When a large external magnetic field is applied, the protons are aligned either with or against the applied magnetic field (Figure 1-1). When the proper resonant energy (ΔE) is applied, the spin transitions occur between these two states. ΔE is expressed by Eq. 1:

$$\Delta E = h\nu = \frac{\gamma h B_0}{2\pi} \tag{1}$$

Here γ is the magnetogyric ratio, ν is the applied frequency, B_0 is external magnetic field, and h is Planck's constant. The needed frequency relies on the external magnetic field and the magnetogyric ratio. In case of the difference in the population of spins between the +½ and -½ states, an absorption energy will occur when frequency, ν is applied. The Boltzmann equation gives the ratio of the population ($N_{-1/2}$ / $N_{+1/2}$) between these two states (Eq. 2).

$$\begin{aligned} \frac{N_{-1/2}}{N_{+1/2}} &= \exp(-h\nu / kT) \\ &= 1 - h\nu / kT; \quad \text{since } h\nu << kT \end{aligned} \tag{2}$$

The excess population of spins is nearly 1 in 100.000, because NMR deals with frequency in the megahertz range. For this basic reason, NMR has the low sensitivity. The detectable hydrogen is only 0.001%. According to these two equations (Eq. 1, 2), the studies should be done with a high γ and at high magnetic fields to increase the sensitivity. Frequency and sensitivity are directly proportional each other. Therefore hydrogen which has the second highest γ among all nuclei is often used and MR images are generated in higher field. Because

water contains largest amount of proton among all the other molecules containing proton, it is used for imaging.

1.2.1 Relaxation rates

After nuclei are placed in a magnetic field, the vectors of water protons need a certain time to align with or against the magnetic field. When the aligned spins turn to their initial equilibrium distribution, the rate defined as relaxation is formed. The time constant for this rate of the alignment is called relaxation time. Where the nuclear spin magnetization is parallel with the external magnetic field, the time constant is called the longitudinal (spin-lattice) relaxation time, T_1 and where the nuclear spin magnetization is perpendicular to the external magnetic fields, the time constant is called the transverse (spin-spin) relaxation time, T_2. There are two reasons to generate transverse relaxation. Those are the magnetic interactions between neighboring molecules and distortions in the homogenous external magnetic field. The sum of these two effects is called T_2^*. Even if only the water protons are detected by imaging experiments, the relaxation times are different for water in different tissues. Therefore the contrast can be generated by making the image acquisition sensitive to differences in T_1, T_2, T_2*.

The measurement of difference between signal intensity of water in the different tissues can give the contrast between these tissues. A radio frequency (RF) can provide an additional energy for nuclei spins to change their orientation and transit to a higher energy level. This frequency is called Larmor frequency which is proportional to the magnetogyric ratio and the strength of the external magnetic field (Eq. 1). The applied RF causes the alignment of the spins through the z-axis and perpendicular to x- and y-axis. When the RF is stopped, the nuclear spins return to their ground state level by interacting with their surroundings. This process is called spin-lattice relaxation characterized by the time constant T_1 (Figure 1-2a). T_1 is the required time for returning to initial value of the longitudinal magnetization M_z. T_1 and M_z are defined by the Eq. 3 and Eq. 4, respectively. When the spins are realigned to their equilibrium state due to the external magnetic field, the transverse component of the magnetization vector rotates in the xy- plane (Figure 1-2b). Then dephasing is occurred due to the fact that all spins are interacting with the surrounding spins. This process is called spin-spin relaxation characterized by the time constant T_2. T_2 is the required time for returning to initial value of the transverse magnetization, M_{xy}. T_2 and M_{xy} are defined by Eq. 3 and Eq. 5, respectively:

$$\frac{1}{T_{i,obs}} = \frac{1}{T_{i,d}} + ri\,[Gd] \qquad i = 1,2 \tag{3}$$

$$M_z = M_0(1 - e^{-t/T_1}) \tag{4}$$

$$M_{xy} = M_0(1 - e^{-TR/T_1})e^{-t/T_2} \tag{5}$$

Here $1/T_{i,obs}$ is the observed solvent relaxation rate, $1/T_{i,d}$ is diamagnetic term, $1/T_{i,p}$ is paramagnetic term, r_i is relaxivity, M_0 is the equilibrium at applied external magnetic field, B_0 and t is time after the spin is realigned with B_0, TR is the time between two successive RF pulses and e^{-t/T_2} is the spin-spin decay factor characterized by the time constant T_2.[1, 5]

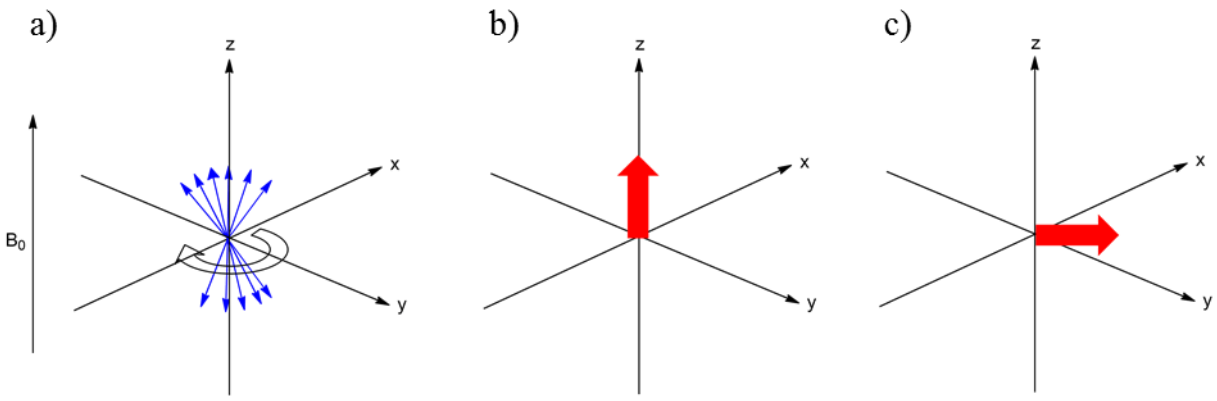

Figure 1-2. a) The magnetic field applied; b) The form of relaxation involves the return to equilibrium of spin up and spin down states, this is known as T_1 relaxation or longitudinal (spin-lattice) relaxation. This has the effect of restoring the overall magnetisation vector in the Z direction; c)The most rapid form of relaxation is the dephasing of the spins, this is known as T_2 relaxation or transverse (spin-spin) relaxation. This has the effect of reducing the overall magnetisation vector in the XY plane.

1.2.2 Hydration number (*q*)

Hydration number (*q*) is the number of water molecules which directly bind to the metal ion. The inner sphere proton relaxivity is linearly proportional to the hydration number *q*, hence a higher *q* results in an increase in relaxivity. However, thethermodynamic and kinetic stability of complex can reduce due to increasing hydration number. The approved CAs by the drug agencies have one innersphere water molecule.[3]

1.2.3 Water and proton exchange

The residence lifetime of protons, τ_m, plays a dual role in determining proton relaxivity. It modulates the efficiency of chemical exchange from the inner sphere of the metal to the bulk.

It also contributes to the overall correlation time that governs the dipole-dipole interaction between the electron spin and nuclear spin. Therefore the water exchange rate always shows a lower limit for the proton exchange rate. The proton exchange rate for the currently used Gd^{3+} based CAs is usually equal to the water exchange rate at physiological pH. Through acid or base catalyzed pathways, the proton exchange on the Gd^{3+} can be significantly faster than the water exchange.[6, 7]

1.2.4 T_1 and T_2 contrast agents and relaxivity

All CAs shorten T_1, T_2 and T_2*. However, T_1 CAs alter the longitudinal relaxation rate ($1/T_1$) more than the transverse relaxation rate ($1/T_2$). Similarly, T_2 CAs largely increase the transverse relaxation rate ($1/T_2$). T_1 CAs are positive CAs which cause a reduction in T_1 relaxation time and give rise to increase signal intensity. T_2 CAs give rise to decrease T_2 relaxation time and decrease signal intensity; these are negative CAs.

Relaxivity is defined as the relaxation rate enhancement of water protons by CA at a given concentration. The paramagnetic relaxation of the water protons is determined by the dipole-dipole interactions between the proton nuclear spins and the fluctuating local magnetic field caused by the unpaired electron spins of the paramagnetic particles. The overall proton relaxivity enhancement originates from two main components; inner sphere and outer sphere water molecules. The inner sphere water molecules are coordinated with the metal ion and the water protons in the first coordination sphere of the metal ion chemically exchanges with the bulk water (Figure1-3). The paramagnetic effect is also experienced by the bulk water molecules surrounding the paramagnetic centre. The relaxation mechanism comes from this random translational diffusion around the paramagnetic centre. This effect is defined as outer sphere relaxation. The water molecules can also interact with the hydrophilic part of the contrast agent, therefore this can affect relaxivity enhancement. These water molecules are called second sphere water molecules.

The overall paramagnetic relaxation enhancement is described by the sum of inner sphere, second sphere and outer sphere relaxation rate (Eq. 6) or expressed in terms of the relaxivity (Eq. 7), where IS, SS, and OS are inner sphere, second sphere, and outer sphere, respectively.

$$\left(\frac{1}{T_{1,2}}\right) = \left(\frac{1}{T_{1,2}}\right)^{IS} + \left(\frac{1}{T_{1,2}}\right)^{OS} + \left(\frac{1}{T_{1,2}}\right)^{SS} \quad (6)$$

$$r_{1,2} = r_{1,2}^{IS} + r_{1,2}^{OS} + r_{1,2}^{SS} \quad (7)$$

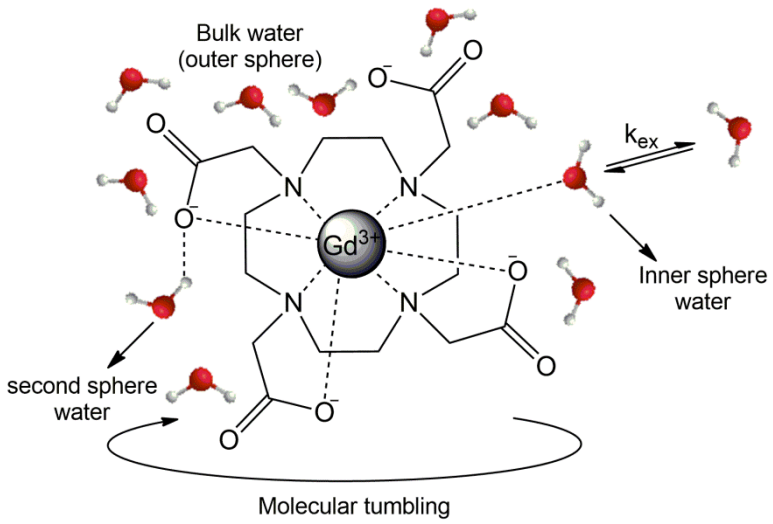

Figure 1-3. Important parameters responsible for the relaxivity of CA.

The inner sphere contribution to proton relaxivity results from the chemical exchange of the coordinated water protons with the bulk. The longitudinal inner sphere relaxataion rate ($1/T_1$) and the transverse inner sphere relaxation rate ($1/T_2$) of the bulk solvent nuclei(the only observable NMR signal) are defined by Eq. 8 and 9, respectively:

$$\left(\frac{1}{T_1}\right)^{IS} = \frac{cq}{55.5}\frac{1}{T_{1m}+\tau_m} = P_m\frac{1}{T_{1m}+\tau_m} \quad (8)$$

$$\left(\frac{1}{T_2}\right)^{IS} = \frac{P_m}{\tau_m}\frac{T_{2m}^{-2}+\tau_m^{-1}T_{2m}^{-1}+\Delta\omega_m^2}{(\tau_m^{-1}+T_{2m}^{-1})^2+\Delta\omega_m^2} \quad (9)$$

Here c is the molal concentration, q is hydration number (the number of bound water nuclei per Gd^{3+}), P_m is the mole fraction of the bound water nuclei, τ_m is the lifetime of a solvent (water) molecule in the inner sphere of the complex (equal to the reciprocal water exchange rate, $1/kex$), $1/T_{1m}$ and $1/T_{2m}$ are the longitudinal and transverse proton relaxation rates in the bound water, and $\Delta\omega_m$ is the chemical shift difference between bound and bulk water.[1, 3]

Considering the magnetic features of CAs, they can be classified as superparamagnetic contrast agents (T_2 agents) and paramagnetic contrast agents (T_1 agents) as described below.

1.2.4.1 Gadolinium and manganese based paramagnetic contrast agents

Ideally, MRI CAs should have many unpaired electrons, because long relaxation time is provided by the high number of their unpaired electrons. Therefore, the paramagnetic metal ions are most useful in MR experiments depending on the number of their unpaired electrons. Mn^{2+} and Gd^{3+} complexes are generally used as paramagnetic contrast agents (T_1 agents), since Mn^{2+} has five unpaired electrons and Gd^{3+} has seven unpaired electrons in their outermost shells.[5, 8]

The most of the contrast agents used in clinical MR applications contain Gd^{3+}. Some properties of Gd^{3+} make it more advantageous over the other lanthanide ions.Gd^{3+} ion has the largest number of unpaired electrons among all the other ions and it can be coordinated with eight ligands and one water molecule. The other advantage of Gd^{3+} is its symmetrical ground state. Although Dy^{3+} and Ho^{3+} have high magnetic moment, their asymmetrical ground states make them less favorable than Gd^{3+} for MRI. However, Gd^{3+} is a toxic metal ion. For instance, gadolinium chloride has an LD_{50} (dose that causes death in 50% of the animals) of 0.5 mmol/kg in rats. To reduce its toxicity, it must be coordinated with a multidentate ligand. For this purpose, the ligands such as DOTA and DTPA have been used (Figure 1-4). The DTPA ligand is also toxic as much as Gd^{3+}. But Gd-DTPA complex has approximately 20 times less toxic (LD_{50}=8 mmol/kg) than both DTPA and Gd^{3+} separately.[9]

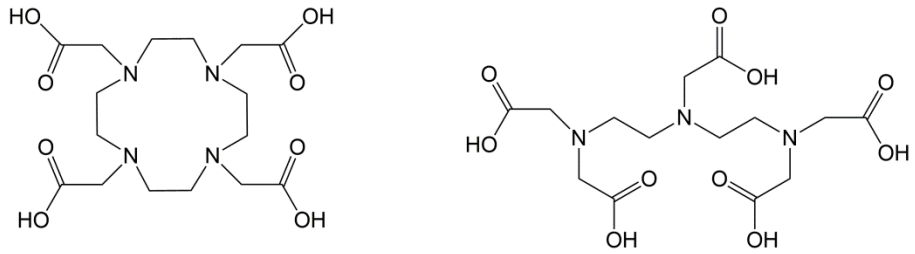

Figure 1-4. Chemical structures of DOTA (left) and DTPA (right) ligands.

Metal-ligand complex stability can be assessed by determining the metal-ligand formation constant (also called the stability constant).[10] Gd^{3+}-complexes used as CAs possess very high stability constants ($K>10^{17}$).[4] Kinetic stablity is also important. Generally, macrocyclic ligands such as DOTA tend to give more kinetically inert complexes than acyclic ligands such as DTPA. In addition, in *in vivo* experiments, the thermodynamically stable macrocyclic

complexes are advantageous regarding their stability toward release of Gd^{3+} from the chelate. Gd-DOTA and Gd-DTPA are thermodynamically stable complexes. The thermodynamic stability constants of Gd-DOTA and Gd-DTPA in water at 20 MHz and 40 °C are LogK= 24.7 and 22.2 respectively.[3]

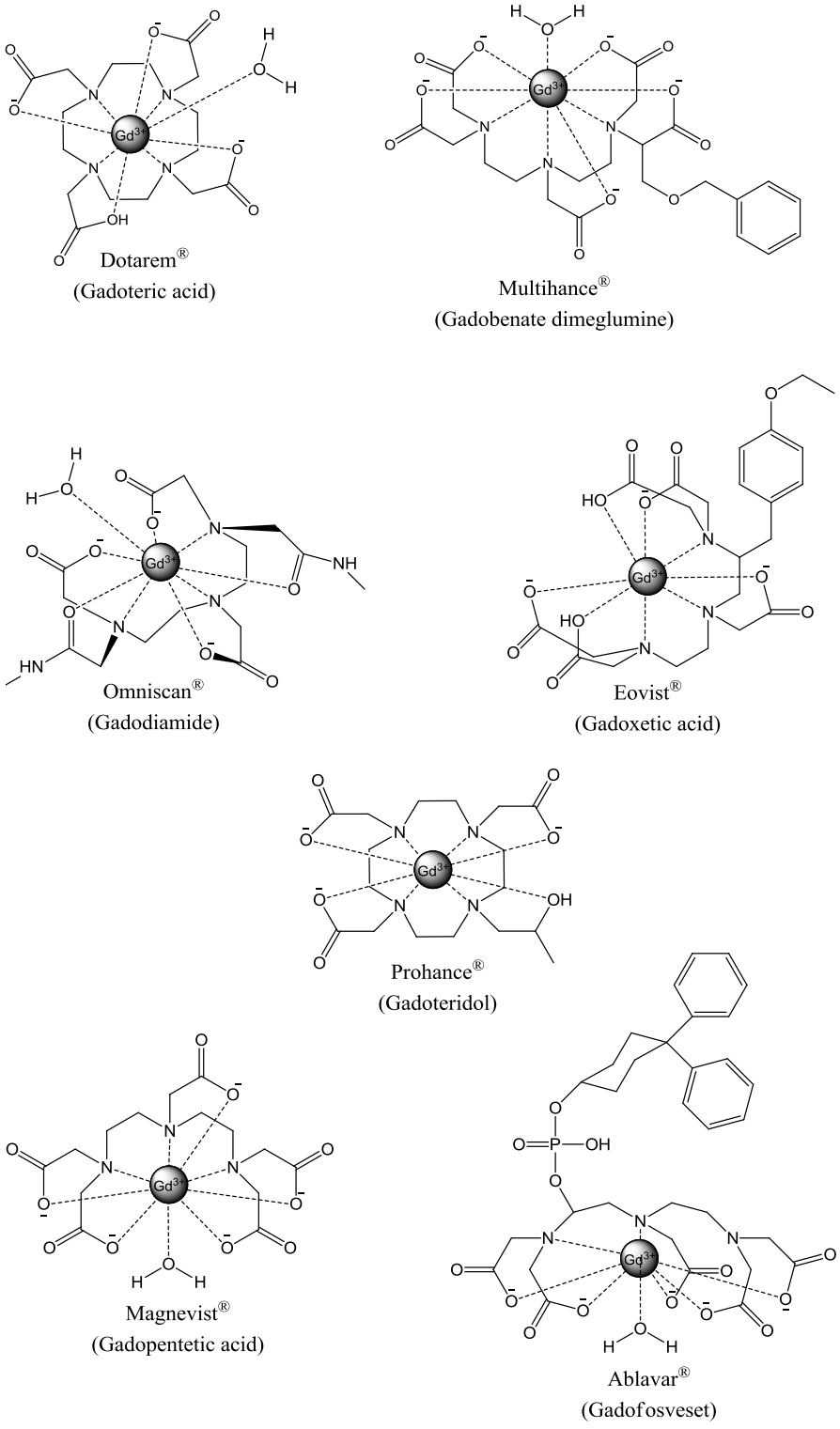

Figure 1-5. Some of the approved low molecular weight MRI contrast agents.

1.2.4.2 Iron oxide based superparamagnetic contrast agents

The paramagnetic contrast agents behave as local magnets when an external magnetic field is applied. The total magnetic susceptibility of a paramagnetic contrast agent is directly proportional to the number of paramagnetic ions in the contrast agent. When the external magnetic field is applied, iron particle exhibits very large magnetic moment. The iron oxide particles such as Fe_3O_4 (Magnetite; mixture of Fe_2O_3 and FeO) have been used as the superparamagnetic contrast agents.[11] Although the superparamagnetic contrast agents shorten T_1 relaxation time, T_2 effect is dominant due to their large magnetic moment.[12] In order to reduce their toxicity and make them biocompatiple CAs, iron oxides are coated.[13] Iron oxide particles can be classified into two categories depending on their particle sizes. The iron oxide particles with diameter more than 50 nm are called superparagmanetic iron oxides (SPIOs), and the iron oxide particles with diameter less than 50 nm are called ultra small superparamagnetic iron oxides (USPIOs). Iron particles do not have inner sphere water molecules, the relaxation of water arises from the water molecules diffusing near particle. The iron oxide crystals have a net magnetization. When the external magnetic field is increased, this magnetization increases. Altough the longitudinal relaxivity of the USPIOs can have fairly high, the iron particle contrast agents cause much greater increase in $1/T_2$. Therefore they work as T_2 agents and lead to T_2-weighted MR images.[5]

Depending on the coating unit, iron oxide particles can be used as targeted CA. For example, dextran coated iron oxide particle, Feridex I.V. has been approved by FDA and it is used for the imaging of liver tumors.[14, 15]

1.3 Dendrimers

Dendrimers are well-defined regular and highly branched monodisperse macromolecules. Those are composed of the branching of same units from a multifunctional core. Dendrimers are also called cascade molecules. The name comes from the Greek words *dendron* meaning tree and *meros* meaning part. Their structures are similar to tree and each repeating unit in dendrimer can be branched with the same repeating units after a certain length.[16, 17] In order to describe the size of dendrimers, the word 'generation' is used. Generation is defined as the layer between each repeating cycle (Figure 1-6) and it is abbreviated with Gn (n=0, 1, 2, 3,….).

Dendrimers have functional surface groups which allow managing the number of generation and their monodispersities. They are synthesized by two main synthetic strategies; divergent and convergent. In the divergent approach, the repeating units are attached to the dendrimer surface groups. Therefore branching of the repeating units starts from the core and continues until reaching the desired generation number. The first synthesis of dendrimer using divergent approach was introduced by Fritz Vögtle *et al*. in 1978.[18] In the convergent approach, the synthesis starts from the surface groups. Firstly, the desired dendrons are prepared and these dendrons are bound to the core molecule. The first convergent approach was introduced by Jean Frechet in 1990.[19] As depicted in Figure 1-7, a dendrimer with desired generation can be synthesized using these two synthetic methods.

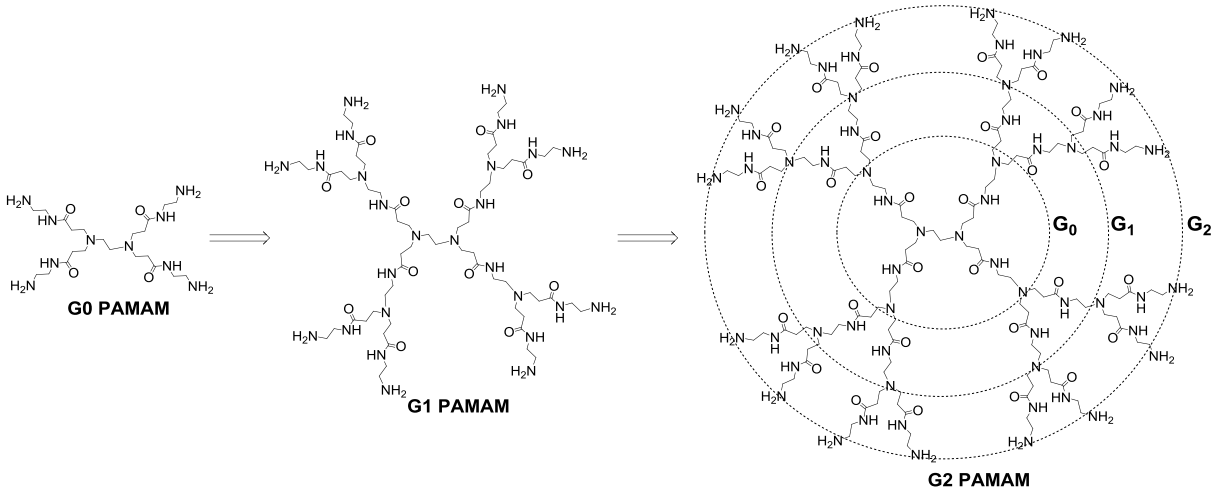

Figure 1-6. Schematic representation of the structure of PAMAM dendrimers with generations.

In contrast to most of linear polymers, which exhibit vast collections of different molecular weights, size and structures, the precise nanoscale sizes and narrow molecular weight distrubutions of dendrimers allow correlation of a specific physical and mechanical property or biological response relative to a discrete chemical structure. The development of such distinct structure-property relationships is extremely useful in the design and evaluation of a macromolecule for a targeted application.[20]

Dendrimers can be used for the therapeutic and diagnostic purposes.[21-23] For example, dendrimers have been developed as drug delivery agents.[24-27] The internal cavities of dendrimers allow encapsulating the guest molecules or their functional surface groups can interact with the drug. Therefore, functional surface groups and macmolecular structure of dendrimers are suitable for use in diagnostic medical imaging.[28, 29]

When their *in vivo* applications are considered, the biocompability of dendrimers is being very important. According to the recent studies, the toxicitiy of the dendrimers with amine surface groups (cationic dendrimers) such as PAMAM and PPI is increasing when the generation is increased.[30] Roberts *et al*. studied generation, 3, 5, and 7 PAMAM dendrimers upon the administrated to the mice.[31] The results showed generation 7 dendrimer has higher toxicity than the generation 3 and 5 dendrimers. The carboxylate surface PAMAM and PPI dendrimers have lower toxicity than the amine surface dendrimers. Since the cell membranes are negatively charged, the dendrimers with cationic nature can interact with the cell membranes, damaging the cell surface. Since the carboxylate groups are negatively charged, they are not harmful for the cells.[32] Therefore, dendrimers containing carboxlyate surface are more biocompatible than the amine surface dendrimers.

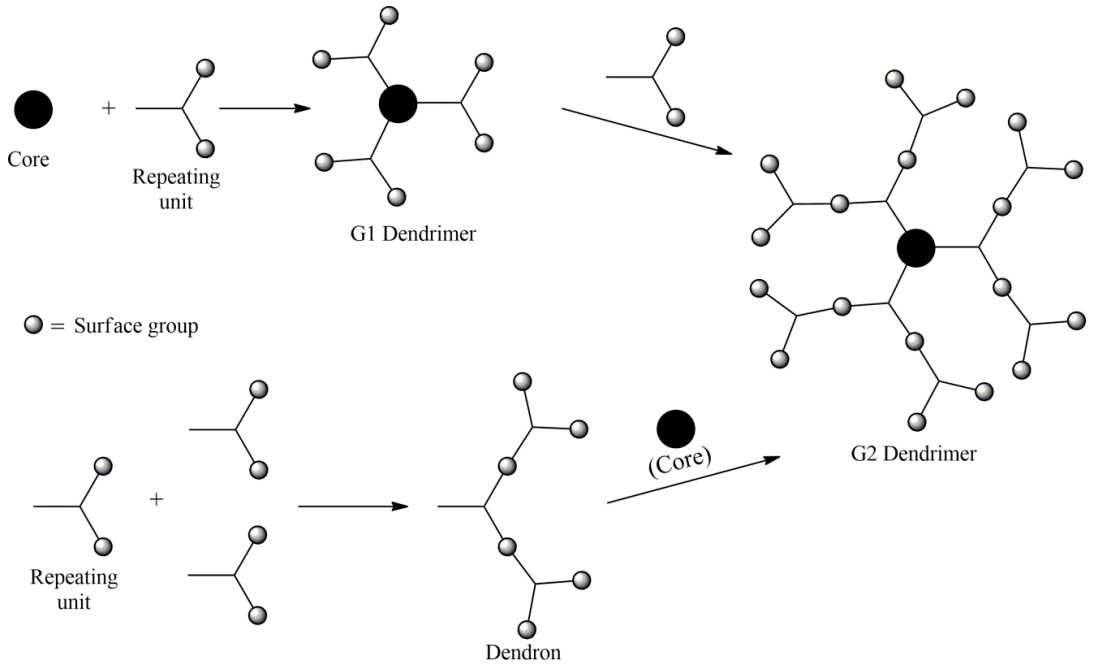

Figure 1-7. Examples for divergent growth (above) and convergent growth (below).

1.3.1 Dendrimeric contrast agents for MRI

The commonly available low molecular weight CAs (Figure 1-5) have disadvantages such as non-specificity, fast renal excretion, low contrast efficiency. Therefore they require higher dosage. To overcome these problems, the classical contrast agents have been modified by the attaching to a targeting unit for increasing tissue specificity such as tumor-specific CA. In addition to target-specific CAs, multivalent and high molecular weight contrast agents have been developed. High molecular weight CAs stay longer in the blood vessel and tissue than

low molecular weight CAs. This gives an opportunity to use lower amount of CAs and produces higher contrast in MRI. Dendrimers are proper scaffolds for the syntheses of high molecular weight and multivalent contrast agents.[33] They are highly-branched molecules that are capable of carrying large number of CAs,[34, 35] and hence the amplification of MRI signal (Figure 1-8).[36, 37]

The longitudinal relaxivity (r_1) value is an important parameter in order to evaluate the efficacy of MRI contrast agent. The studies in the low magnetic field have showed that the dendrimeric contrast agents have higher relaxivity values than their monomeric analogues.[38] For example, the generation six dendrimeric CA, G6 PAMAM funtionalized with Gd-DTPA, displayed an r_1 of 34 $mM^{-1}s^{-1}$ and its monomeric analogue, Gd-DTPA, displayed an r_1 of 5.4 $mM^{-1}s^{-1}$ (0.6 T, 20 ^{o}C).[39] Accordingly, the r_1 relaxivity of the monomeric analogue is nearly six times lower than that of the dendrimeric contrast agent.

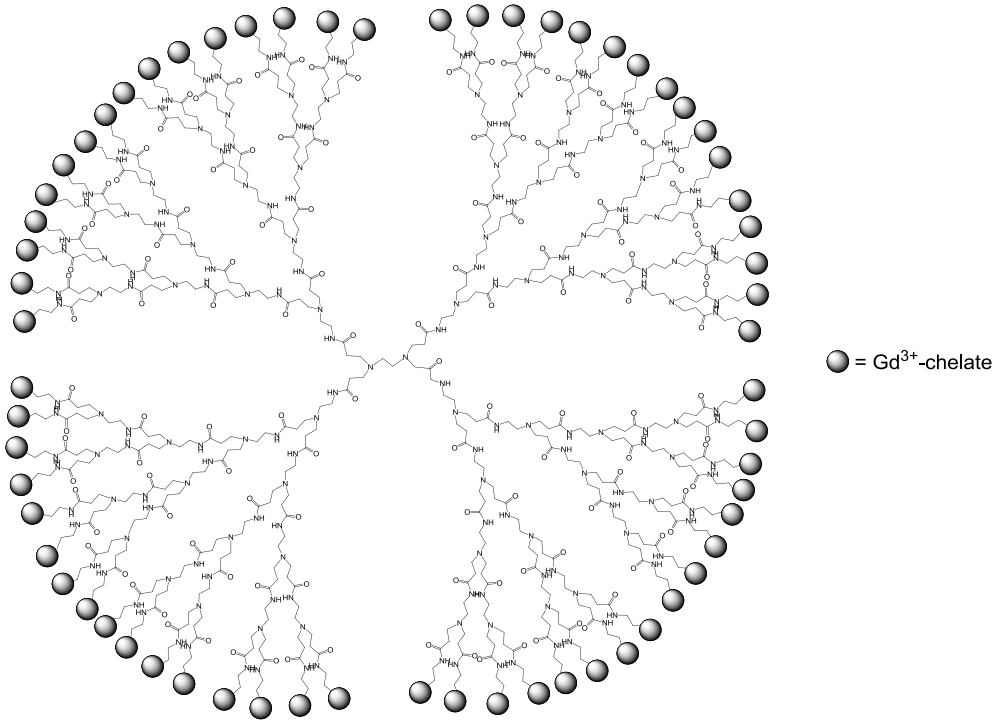

Figure 1-8. Schematic representation of a dendrimeric MRI contrast agent.

In vivo studies have shown that the high molecular weight (i.e. high generation) dendrimeric MRI CAs stay longer time in the bloodstream than low molecular weight (i.e. low generation) dendrimeric MRI CAs and their monomeric analogues such as Gd-DOTA complex. At the same time, high generation dendrimeric MRI CAs possess a large number of Gd^{3+}. This gives rise to increase the signal intensity. For instance, an *in vivo* experiment was performed with mice and Gd-DTPA-functionalized G0, G1, G3 and G5 dendrimers were used.[36] Since

these dendrimeric CAs displayed higher relaxivity and hence the signal enhancement, lower concentrations of CAs could be used.

1.4 Target specific MRI contrast agents

A target specific contrast agent contains a functional moiety that is capable of detecting a particular molecular site or tissue thus resulting in an accumulation of CA at one specific place and signal enhancement on the targeted place.

Misselwitz *et al*. studied with Gadofluorine 8 which is a Gd-DTPA derivative water soluble lipophilic CA.[40] After interstitital injection, Gadofluorine 8 rapidly and highly accumulated in lymph node groups. The attachment of low molecular weight Gd^{3+}-complexes to high molecular weight molecules such as polymer, dextrans, polylysines, and dendrimers or their encapsulations in liposomes can prolong their residence time in the cardiovascular system. Therefore they can be used in magnetic resonance imaging applications. The high molecular weight CAs can also be used in magnetic resonance lympography.[41]

In order to visualize the neuroanatomical connectivity by MRI and optical imaging, a Gd-AAZTA based CA was developed in our institute by Mamedov *et al*.[42] Gd-AAZTA complex was chosen, because it extraordinarily shortens the relaxation times of the surrounding water protons in the tissue. This provides high increase in T_1-weighted MR signal. A dextran as a core molecule was used to link Gd-AAZTA complex and the fluorescence dye (etramethylrhodamine) making this CA suitable for MR and optical imaging. Furthermore, dextran is an excellent marker for neurons, enabling the efficient internalization of this CA into the neurons.

Konda *et al.* introduced G4 PAMAM folate-dendrimer with Gd-complexes. This targeted dendrimeric CA was administered to mouse erythroleukemia cells *in vitro* to test whether the folate-dendrimeric CA was able to bind the cells which express the folate receptor. The results showed over 2700% increase in binding compared with untreated cells. *In vivo* experiment showed that when the folate-dendrimeric CA was administered, ovarian tumor xenografts resulted in a 33% contrast enhancement. It was significantly different compared with results obtained with a non-specific, extracellular fluid space agent, Gd-HP-DO3A. This dendrimeric CA showed the high transverse relaxivitiy (r_2=41.16$\pm$3.14 mM-1s-1) at 4.7 T compared with Gd-HP-DO3A. Therefore it can be used in specifically targeting the hFR on tumor cells and ovarian tumors. [43]

1.5 Smart contrast agents

Smart or responsive agents are the contrast agents that generate a MR signal and display relaxivity changes depending on changes in their environment. The amplitude of the relaxivity change is the one of the most important factor to evaluate the efficiency of SCA. The change in r_1 of Gd^{3+} based SCA can be achieved by modifying the main relaxation parameters, q (inner-sphere hydration number), τ_m (the residence time of the water molecule) and τ_R (the rotational correlation (tumbling) time of the agent). The change in q can provide field independent r_1 change. In this approach, the ligand has a functional group which is weakly coordinated to Gd^{3+}. This coordination restricts the approach of water molecules to the metal center. Therefore this causes reducing q, and thus lower r_1. When a target ion or molecule interacts with the SCA, the weak coordination of Gd^{3+} to the functional group is broken, which leads to an increase in q, and hence higher r_1 (Figure 1-9). In the second approcah, low molecular weight Gd^{3+}-complex can be coupled to a high moleceular weight macromolecules such as proteins, dendrimers etc. This will slow down the rotation of the whole system and result in reduce τ_m and high r_1 at low magnetic field.[44]

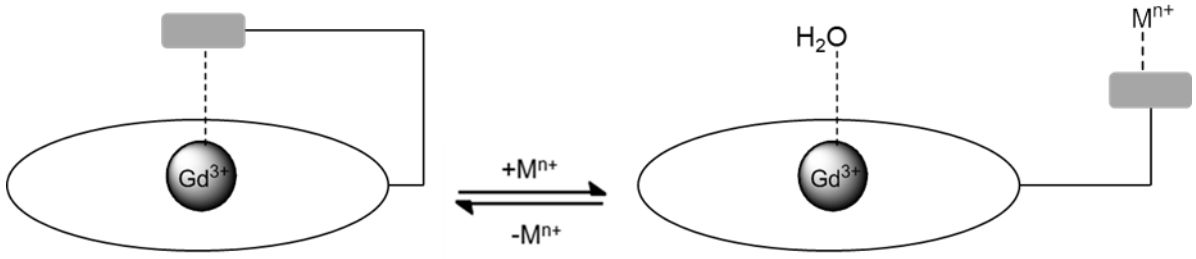

Figure 1-9. Scheme for a mechanism of the cation responsive contrast agent. When the cation interacts with the funtional group, the coordination between the functional gorup and Gd^{3+} ion is broken and water is coordinated with Gd^{3+} ion. This leads to decrease in T_1, thus higher r_1.

1.5.1 Responsive contrast agents to cations

While some cations such as Cd^{2+}, Hg^{2+}, and Pb^{2+} are very toxic and harmful, several metal ions such as Ca^{2+}, Zn^{2+}, Fe^{2+} are beneficial or essential in the body. An ion deficieny or excessiveness in the body leads to some diseases.[45]

Zinc is one of the essential elements in the human body. It is crucial for many biological functions. Over 300 enzymes in the body contain zinc for their activities. Hanaoka *et al*. synthesized a Zn^{2+} sensitive MRI CA (Figure 1-10).[46] This CA contains DTPA based bisamide Gd^{3+} complex and N,N,N',N'-tetrakis(2-pyridylmethyl)ethylenediamine (TPEN)

ligand which is strongly sensitive to Zn^{2+}. TPEN is easily complexed with Zn^{2+}, but it is hardly coordinated with Mg^{2+} and Ca^{2+}. When Zn^{2+} is introduced to the zinc sensitive MRI CA containing solution, Zn^{2+} is coordinated with the TPEN ligand and it restricts to the access of water to Gd^{3+}. Therefore the water proton relaxivity in the solution decreases about 33%.

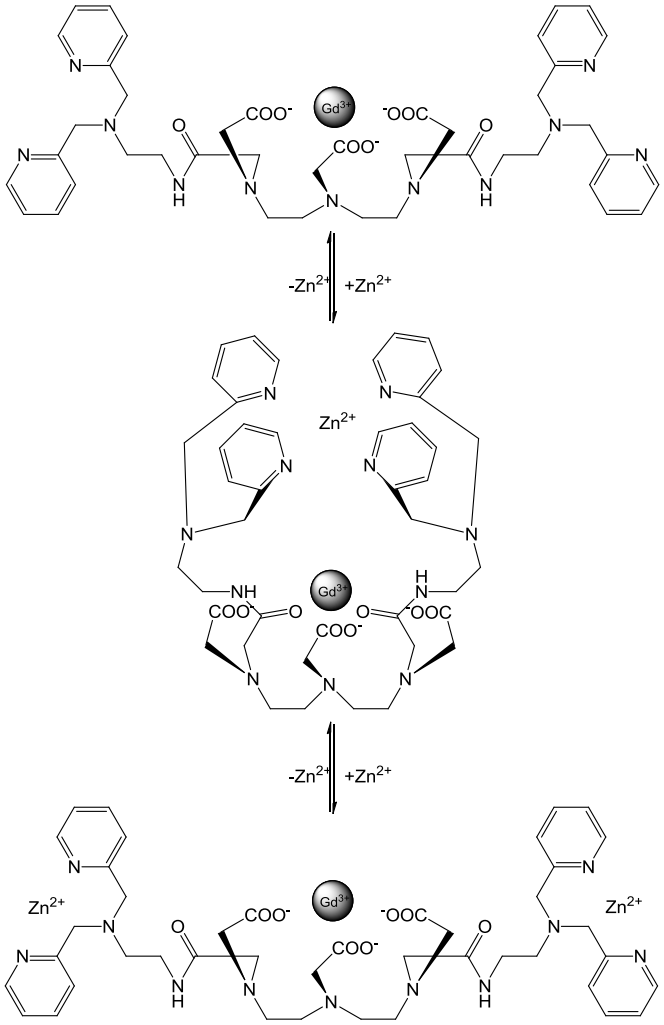

Figure 1-10. Schematic representation of Zn^{2+}-sensitive MRI CA.

Hemoglobin is a metalloprotein that contains Fe^{2+} and carries oxygen from the respiratory organs to the rest of the body. When it releases oxygen, nutrients in the cells are burned and an energy occurs. This energy is needed for the metabolical activities in the organism. The Fe^{2+} deficiency causes anemia. Since all stored Fe^{2+} in the body is consumed and the level of hemoglobin in the blood is not supported. The iron responsive MRI contrast agentwas synthesized by Aime *et al*.[47] The Gd-DTPA based contrast agent (Gd-DTPA-PAS) was prepared and analyzed (Figure 1-11). In the presence of Fe^{3+}, it was coordinated with the functional groups of these CAs. This coordination provided an increase in relaxivity due to the molecular weight increase of the Fe^{2+}-complex.

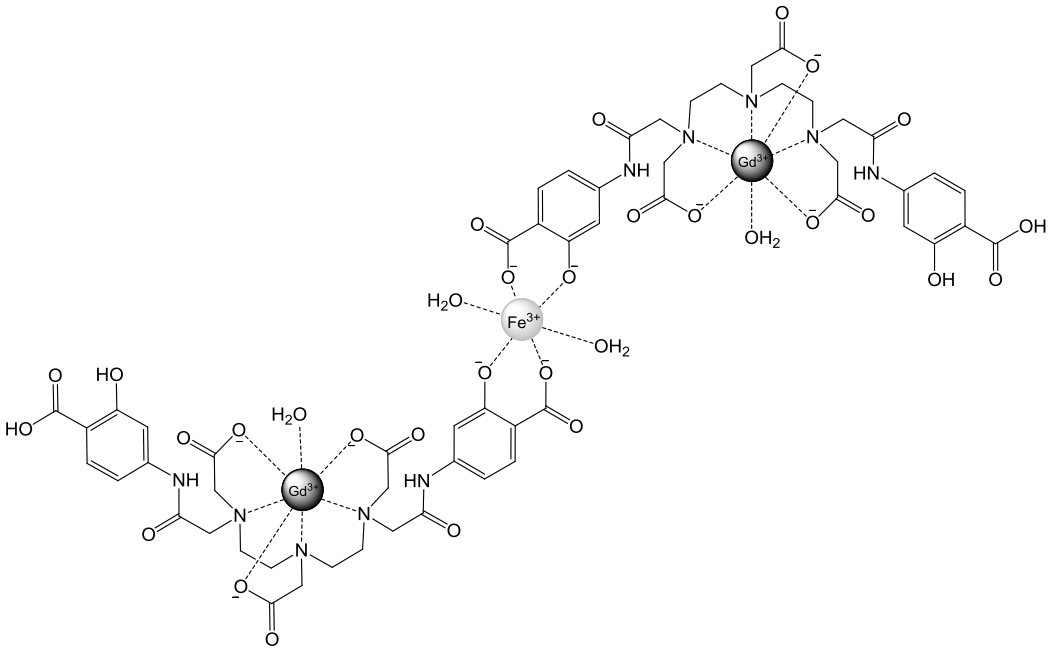

Figure 1-11. Schematic representation of Fe^{3+}-sensitive MRI CA.

Finally, one of the most crucial metal ions for the life is Ca^{2+}. It has many important roles in healthy and damaged tissues. Especially numerous intracellular processes are dependent on Ca^{2+}. The fluorescent probes have been developed to understand the Ca^{2+} role in the body.[48] Because the transparent samples have absorption and scattering problems, these probes cannot be used for the transparent samples. The Ca^{2+} concentration in the extracellular fluid is higher than the intracellular Ca^{2+} concentration (approximately 12,000-fold). Therefore the CAs have been developed for sensing the extracellular Ca^{2+} concentration. The Ca^{2+} responsive CAs will be discussed in detail in Chapter 3.

1.6 Aim of the project

Based on theoretical consideration and previous experimental studies, the standart low molecular weight CAs have the limitations for *in vivo* applications such as fast diffusion, low contrast efficiency, and non-specificity. These limitations could be overcome by either increasing the valency of the CA (number of Gd^{3+} per molecule) or improving the binding affinity between CA and target. The main goal of this thesis was to design and synthesize multivalent targeted MRI CAs and multivalent responsive (smart) CAs carrying multiple copies of Gd-chelates. PAMAM dendrimers were used as multivalent scaffolds.

The chapter 1 focuses on the synthesis of monomeric and dendrimeric MRI CA containing optically-detecable FITC moiety and the high-affinity ligand biotin. The well-established biotin-(strept)avidin targeting system was incorporated into the design as it exhibits the highest known binding affinity of any noncovalent protein/small-molecule coupling. Bead-binding assay was used to determine the ability of the CA to bind the protein target avidin. Its relaxometric, fluorescence and MRI behaviors were also evaluated. For the comparison of contrast enhancement of the dendrimeric CA, its monomeric analogue was synthesized.

The chapter 2 presents the synthesis of monomeric and dendrimeric calcium responsive/sensitive (smart) MRI CAs. EGTA derivative was used as a Ca^{2+} chelator. Since Ca^{2+} plays an important role as second messenger in cellular signaling pathways, this makes it a favorite targeting unit. Relaxometric Ca^{2+} titrations were performed to observe the relaxation time changes of the smart CAs. *In vivo* MRI experiments in the rat brain were performed to observe MRI behaviors of the monomeric and dendrimeric calcium responsive CAs.

2. Chapter 1:

Synthesis of multimodal dendrimeric avidin-targeted MRI contrast agent

2.1 Introduction

Target specific contrast agents (TSCAs) or high affinity contrast agents have been developed for achieving higher local concentration, hence the recorded signal in the region of interest. In order to synthesize TSCAs, the affinity between the targeting unit and the ligand has to be strong and the targeting unit must specifically bind to the ligand.

Avidin-biotin interaction is one of the most commonly used system in molecular and cellular assays. Avidin is a protein that specifically binds biotin and consists of four domains. Biotin is a small hydrophobic molecule that functions as a coenzyme of carboxylases. It is also known as B-vitamin (vitamin B_7, or vitamin H). The dissociation constant (K_d) for avidin-biotin complex is 1.3×10^{-15} M at pH 5. This remarkable affinity of avidin to biotin is the strongest known non-covalent interaction. Because the affinity is too high, the avidin-biotin conjugate is extremely resistant to any type of denaturing agent.[49] Therefore the avidin-biotin system has been used in the MRI applications with regard to the accumulation of MRI CAs in the region of interest.[50]

Dendrimeric contrast agents (DCAs) also provide signal enhancement in MRI. Although DCAs have low renal excretion from the body, they are nonspecifically distributed in the body. In order to increase the efficiency of MRI CAs in the region of interest, DCAs can be targeted by coupling a specific ligand such as biotin or folic acid. Kobayashi *et al*. introduced a tumor targeting agent.[51] For this purpose, a biotinylated DCA was synthesized using G6 PAMAM and Gd-DTPA, which was conjugated with avidin. SHIN3 cells (a human ovarian cancer) were incubated with PBS, Gd-DTPA, G6 DCA or avidin-DCA conjugate containing the same concentration of Gd^{3+}. The T_1 weighted MR images were acquired for each sample. The *in vitro* internalization study showed that avidin-DCA accumulated and was internalized into SHIN3 cells 50- and 3.5-fold greater than Gd-DTPA and DCA.

The studies have shown that multimodal MRI CAs could be synthesized by modifying DCAs. Xu *et al*. introduced lectin-targeted DCA.[52] The cleavable cystamine core G2 PAMAM was used as a multivalent scaffold. After the DCA functionalized with DTPA was cleaved giving thiol group, the dendron was coupled to biotin. The biotinylated DCA-avidin-rhodamine green conjugate was made by the reaction of the bitonylated DCA with the avidin-rhodamine green conjugate. This fluorescently labeled adduct provided the applicability for MR and optical imaging. Boswell *et al*. synthesized Integrin $\alpha_v\beta_3$-targeted DCA by a different approach from the above-mentioned study.[53] In this study the fluorescent dye and the

targeting moiety were coupled to dendrimer surface. These fluorescently labeled targeted-DCAs can also be used in MR and optical imaging.

The above-mentioned studies lead to synthesis of multimodal, multivalent CAs in order to enable detection by means of optical and MR-based techniques.

Here we report the development of a multimodal CA that accomplishes the two-fold goal. First, it targets a protein-based receptor with the highest possible binding affinity. Second, it follows a strategy designed to improve detection of targeted CA by increasing the number of Gd^{3+}-chelates per molecule. Therefore, monomeric CA (MCA) carrying single Gd^{3+}-complex and dendrimeric CA (DCA) containing multiple Gd^{3+}-complexes were prepared. Two different avidin-displaying targets, agarose beads and polystyrene microspheres, were used to assess specific binding of targeted CAs. Relaxometric, fluorescence, MRI and inductive-coupled plasma mass spectrometry (ICP-MS) measurements were carried out to compare the potential of MCA and DCA as targeted imaging agents.

2.2 Result and Discussion

2.2.1 Design of compounds

The desired compounds contain biotin as a ligand which targets the contrast agent to protein avidin and the fluorescent dye fluorescein isothiocyanate (FITC) which enables characterization of the final molecule using fluorescence spectroscopy. Lysine was used as a multifunctional core. The commercially available compound cystamine core G4 PAMAM dendrimer was used as a multivalent scaffold in order to attach a large number of the copies of Gd^{3+}-complex. The structure of the monomeric and dendrimeric CAs were schematically depicted in Figure 2-1. The preferred features of the target molecules are water solubility, efficient binding to desired region/receptor, and sufficient MR signal enhancement to allow high resolution images.

a)

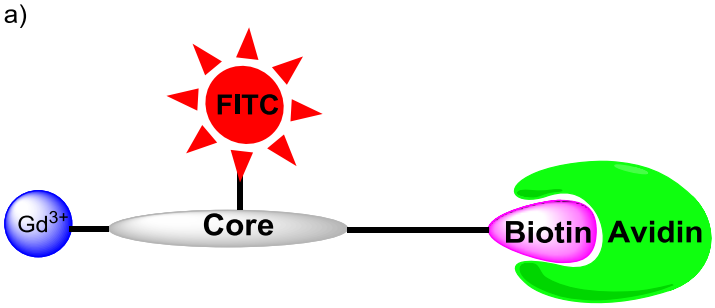

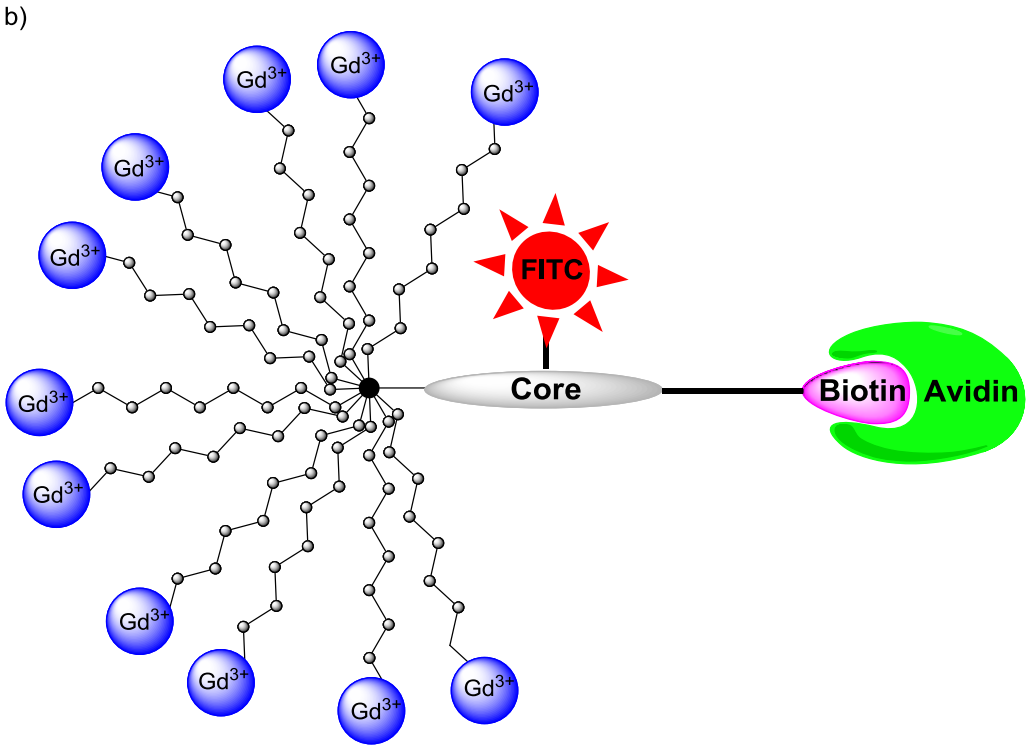

Figure 2-1. Schematic structure of the avidin-targeted monomeric (a) and dendrimeric (b) MRI CA conjugate.

2.2.2 Synthesis of compounds

2.2.2.1 Retrosynthetic analysis of MCA-1

As previously described, **MCA-1** comprises of a Gd^{3+}-complex, biotin, FITC, and lysine including thioamide bonds and amide bonds. The retrosynthetic analysis of the framework of **MCA-1** is shown in Figure 2-2. The thiourea bonds indicated with dashed line can be generated from the macrocyclic compound containing isothiocyanate group, FITC and the biotinylated lysine containing primary amine group. The amide bonds indicated with dashed line can be generated from the starting materials: biotin, protected lysine and ethylenediamine (en). This retrosynthetic analysis suggests the synthesis of a biotinylated and fluorescently labeled building block and a *tetrakis*-alkylated cyclen derivative containing isothiocyanate group.

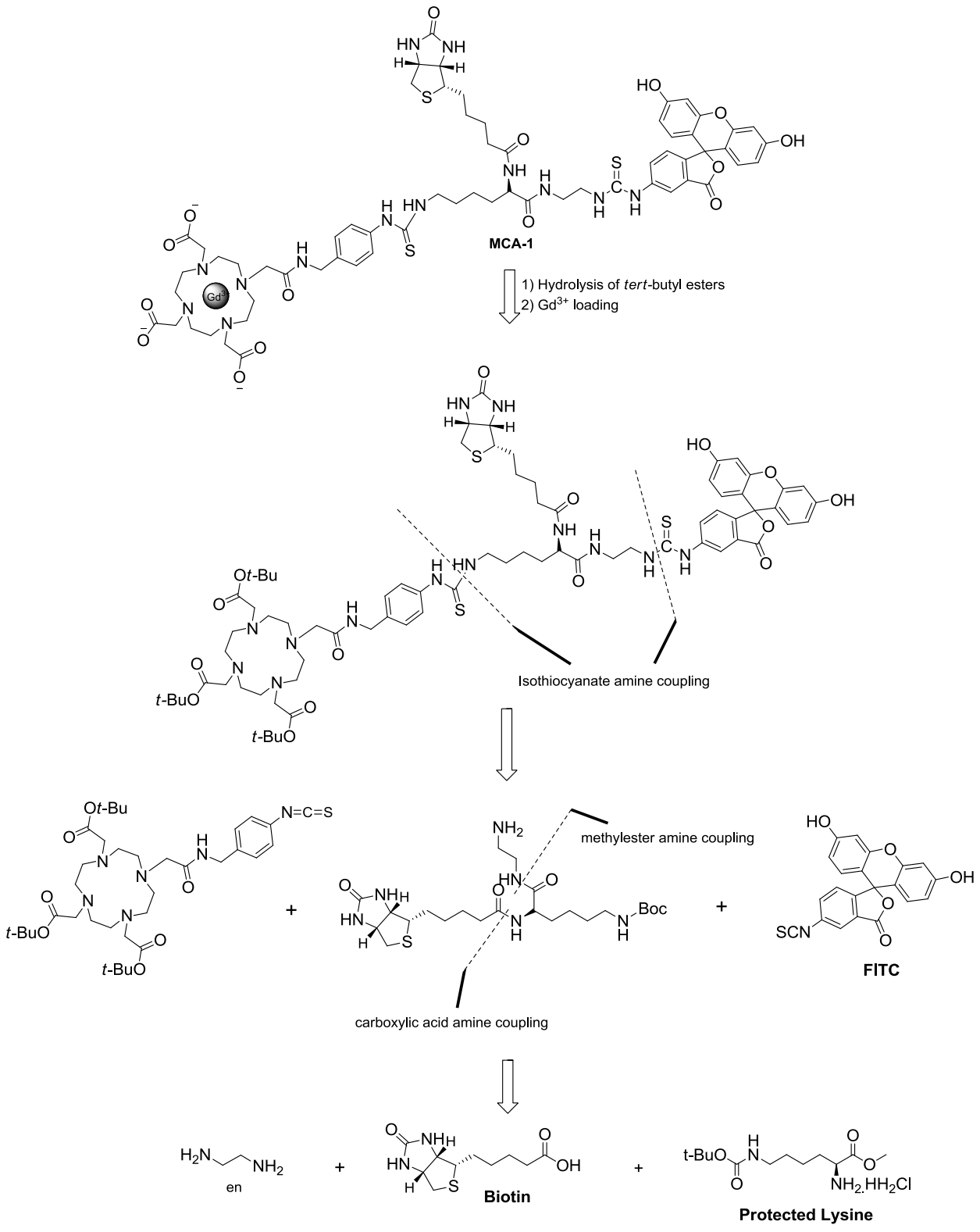

Figure 2-2. Retrosynthetic analysis for **MCA-1**.

2.2.2.2 Synthesis of biotinylated and fluorescently labeled building block (4)

Amine **4** was prepared as a building block for the synthesis of biotinylated and fluorescently labeled MCA and DCA following the retrosynthetic analysis described in section 2.2.2.1 (Figure 2-3).

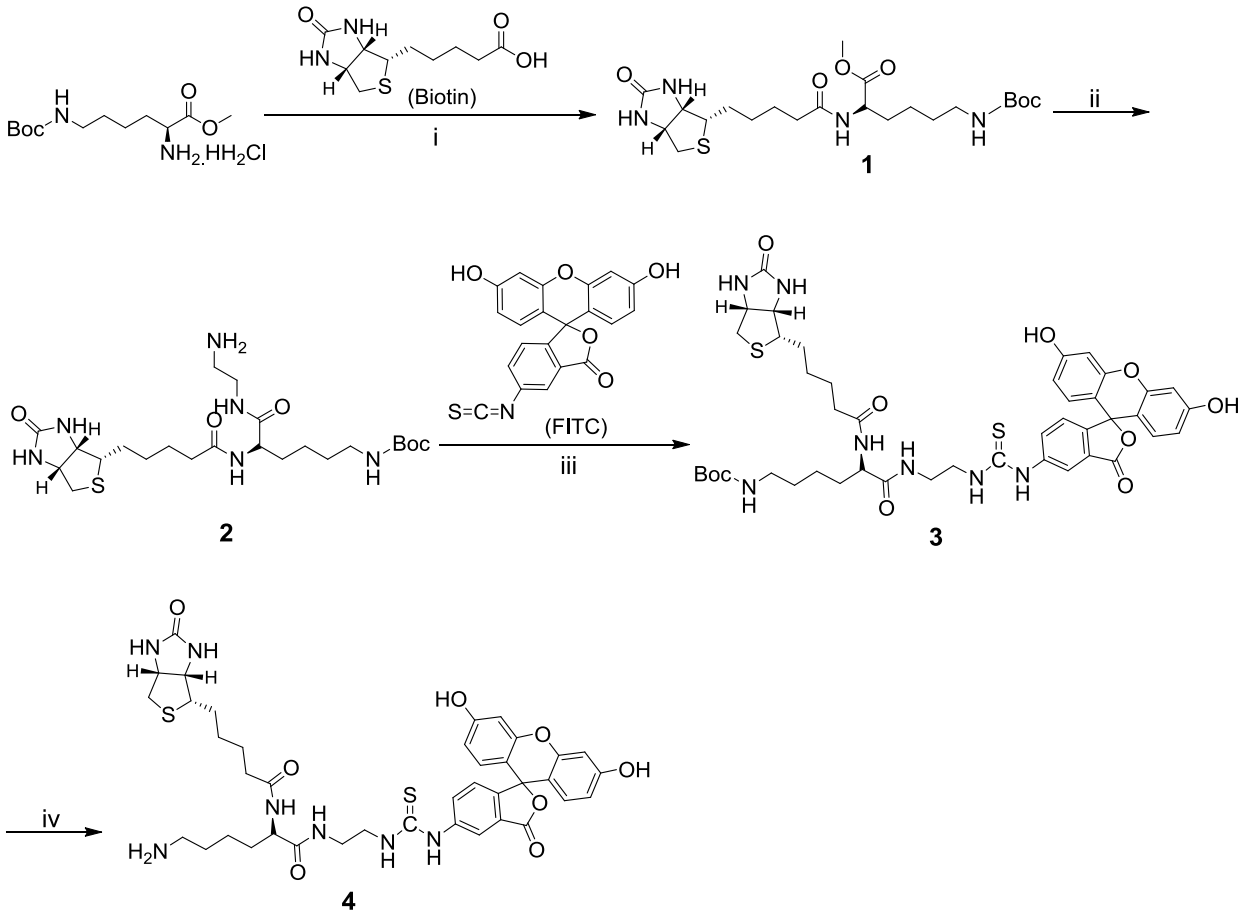

Figure 2-3. Synthetic scheme of the biotinylated and fluorescently labeled building block **4**. Reagents and conditions: (i) EDC·HCl, DMAP, DMF, rt, 48 h, 64%; (ii) ethylenediamine, MeOH, rt, 24 h, 77%; (iii) Et_3N, DMF, rt, 16 h, 88%; (iv) Conc. HCl, MeOH, rt, 1 h, 97%.

The core molecule lysine was biotinylated using EDC coupling reagent to give **1**. The methyl ester group in **1** was transformed to primary amine group using excess amount of ethylenediamine in order to introduce the FITC. FITC was coupled to amine **2** in basic medium to get **3**. The Boc group in **3** was removed using hydrochloric acid in methanol to obtain amine **4**. After deprotection of the Boc group, the amine **4** was coupled to the monomeric and dendrimeric Gd^{3+}-complexes yielding the target specific contrast agents.

2.2.2.3 Synthesis of DO3A-NCS ligand (L-1) and its Gd^{3+}-complex (CA-1)

The synthesis of **L-1** commenced by the alkylation of DO3A-*tris*-*tert*-butylester with chloride **5** in the presence of potassium carbonate in dimethylformamide. Chloride **5** was synthesized by the acylatiom of *p*-nitrophenylbenzylamine with 2-chloroacetyl chloride in dichloromethane with triethylamine as a base.[54]

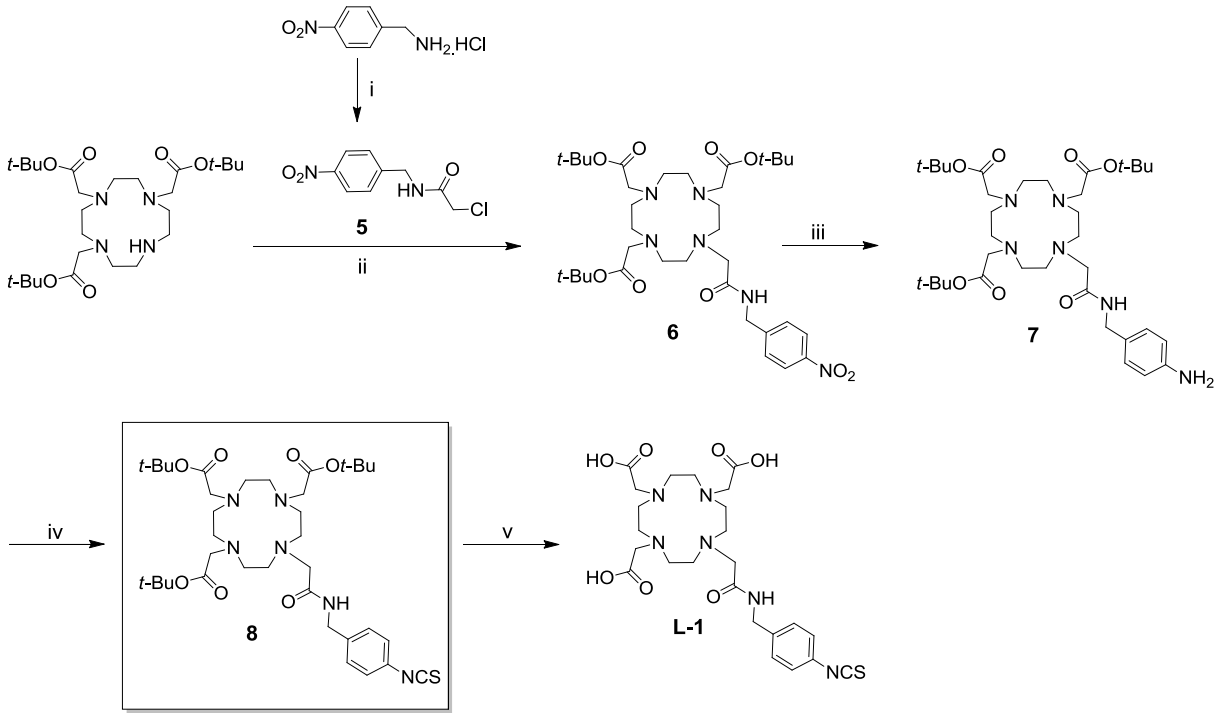

Figure 2-4. Synthetic scheme of **8**, and **L-1**. Reagents and conditions: (i) Chloroacetylchloride, Et_3N, dichloromethane, 0 °C to rt, 2 h, 92%; (ii) K_2CO_3, DMF, 16 h, 84%; (iii) Pd/C, Hydrazine, reflux, 4 h, 96%; (iv) $CSCl_2$, Et_3N, rt, 2 h, 47%; (v) formic acid, 60 °C, 24 h.

Compound **6** containing nitro group was reduced to amine **7** by palladium catalyzed hydrogenation using hydrazine in ethanol at reflux temperature. The primary amine group was converted into isothiocyanate using thiophosgene in dichloromethane to get **8**. For the synthesis of **L-1**, *tert*-butyl esters in **6** were hydrolized using formic acid (Figure 2-4).

2.2.2.4 Synthesis of MCA-1

Compound **8** was directly bound to the amine **4** in a basic medium to get **9**. *Tert*-butyl esters in **9** were hydrolyzed using formic acid to give **L-2**. Gd^{3+} was loaded at neutral pH to obtain **MCA-1** (Figure 2-5). Since compound **9**, **L-2** and **MCA-1** have low solubility, the reliable

NMR data were not obtained. Therefore the synthesis of these compounds was confirmed by means of ESI-MS spectrometry.

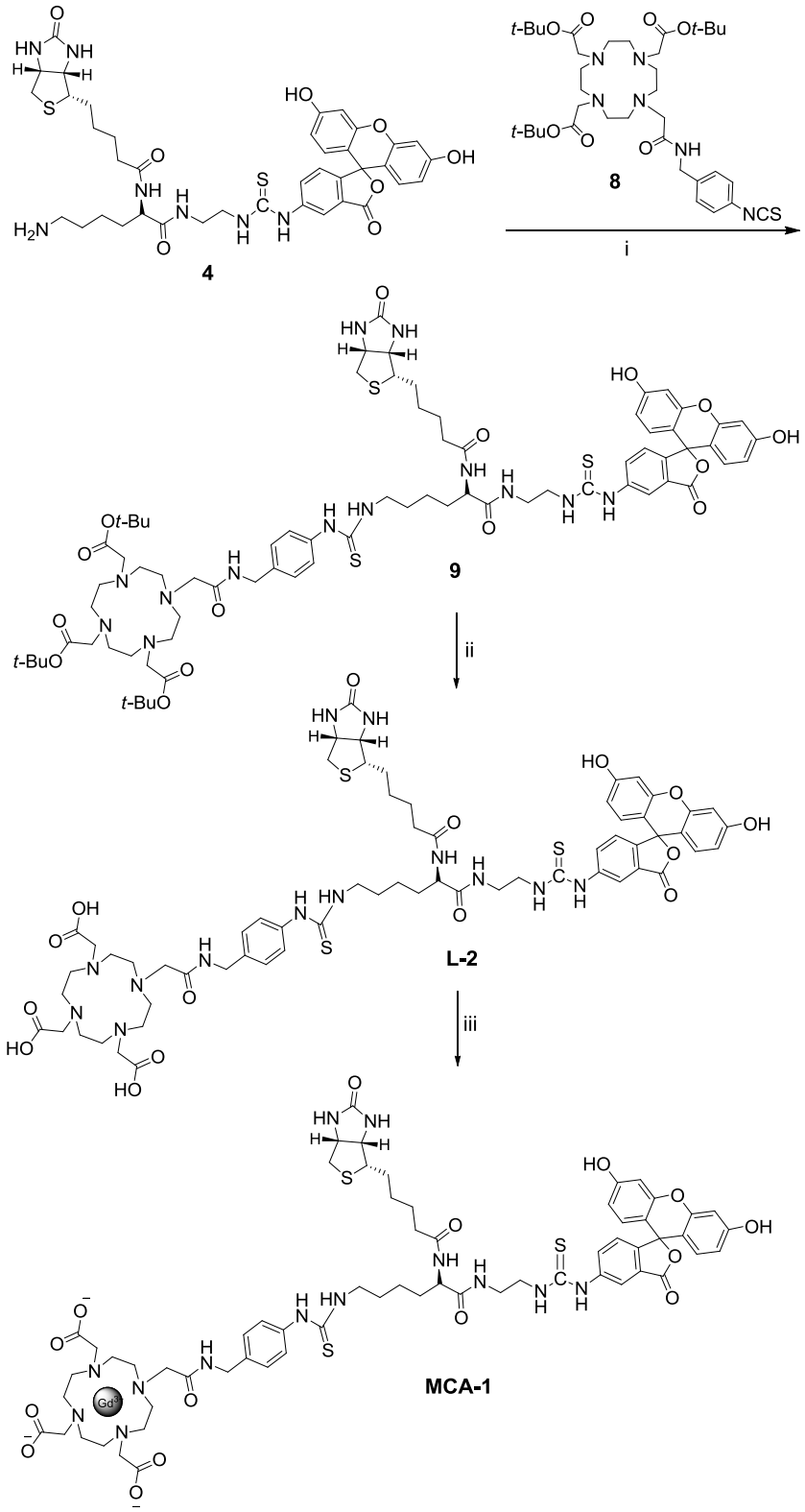

Figure 2-5. Synthetic scheme of **MCA-1**. Reagents and conditions: (i) Et_3N, DMF, 45 ^oC, 16 h; (ii) formic acid, 60 °C, 24 h; (iii) $GdCl_3 \cdot 6H_2O$, pH 7.0, rt, 24 h.

2.2.2.5 Retrosynthetic analysis of DCA-1 (First approach)

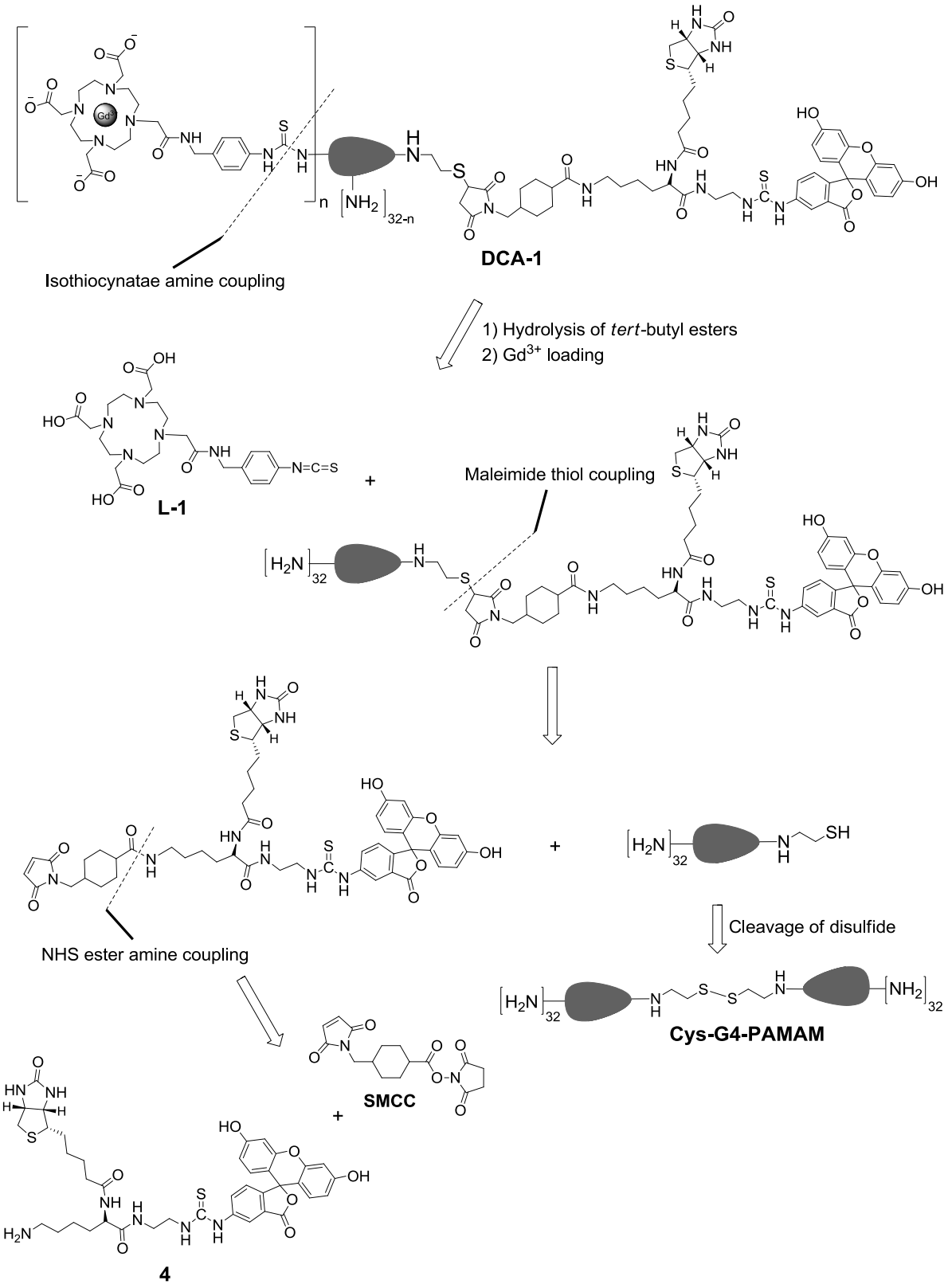

Figure 2-6. Retrosynthetic analysis for the framework of **DCA-1**.

In order to synthesize the targeted multivalent contrast agent, we used a Cys-G4-PAMAM dendrimer, which can be cleaved using a proper reducing agent was used in this study.[52] The retrosynthetic analysis of the framework of **DCA-1** is shown in Figure 2-6. The thioamide bonds indicated with dashed line can be generated from **L-1** and the biotinylated dendrimeric compound containing FITC. The biotinylated and fluorescently labeled compound containing maleimide group and the G4 PAMAM dendron with thiol group can be generated from the thioether linkage indicated with dashed line. Then the amide linkage indicated with dashed line can be generated from amine **4** and SMCC linker. The recoupling of thiol group of the dendron gives cystamine core G4 PAMAM dendrimer (Cys-G4-PAMAM).

2.2.2.6 Synthesis of intermediate compound (10)

In order to bind the biotinylated and fluorescently labeled compound **4** to dendrimer, SMCC linker which contains amine reactive N-hydroxysuccinimide (NHS ester) group and thiol reactive maleimide group was used.[55]

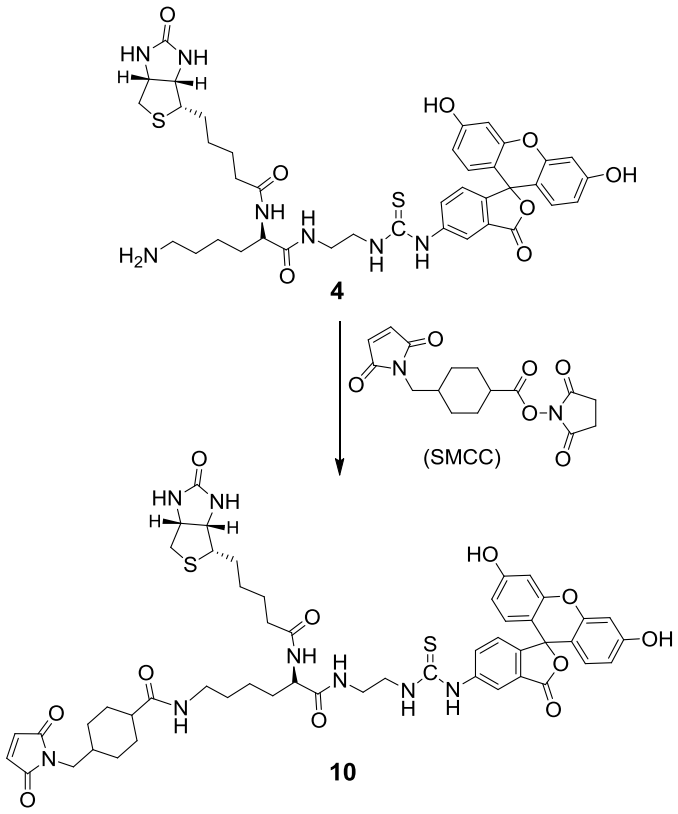

Figure 2-7. Synthetic scheme of intermediate **10**. Reagents and conditions: H_2O/DMF, pH 7.5, rt, 4 h.

The NHS ester group in SMCC linker reacts with the primary amines at pH 7.0–9.0 in order to form stable amide bond. Therefore, pH was maintained at 7.5 until the reaction was completed and intermediate compound **10** was obtained (Figure 2-7). Compound **10** was characterized by ESI-MS and directly coupled to the dendrimeric ligand by changing pH without further purification.

2.2.2.7 First attempt for synthesis of DCA-1

The disulfide bond in Cys-G4-PAMAM was reduced to dendron **11** with thiol group using DTT. Ellman's reagent test was performed for the confirmation of the reduction.[56] The reaction mixture was developed on TLC plate. After treatment with Ellman's reagent, the presence of a yellow band showed that the disulfide bond was reduced to thiol groups. For the synthesis of biotinylated and fluorescently labeled dendrimer, the intermediate compound **10** was used. The maleimide group in **10** was bound to thiol groups at pH 6.5–7.0. After that, the residue was purified by an avidin affinity column to obtain the biotinylated and fluoroscently labeled dendron **12**. Since isothiocyanate group reacts with primary amines in a basic medium, the coupling **L-1** to amino surface groups of dendron **12** was carried out at pH 9.0.[57] After the coupling, the residue was purified by ultrafiltration to get the multivalent ligand **L-3**. Dendron **12** and **L-3** were analyzed by means of ^{1}H-NMR spectroscopy. Then Gd^{3+} was loaded at neutral pH to obtain **DCA-1** (Figure 2-8). After adding Gd^{3+}, the precipitation occured. Two reasons could be an explanation for the precipitation. Firstly, the overall charge of dendrimer changes upon addition of Gd^{3+} which potentially changes the solubility. Secondly, the internal cavities of dendrimer could host metal ions due to the functional architecture which contains tertiary amines and amide linkages. The complexation these functional groups with Gd^{3+} could cause reduced solubility, and thus the precipitation.[58]

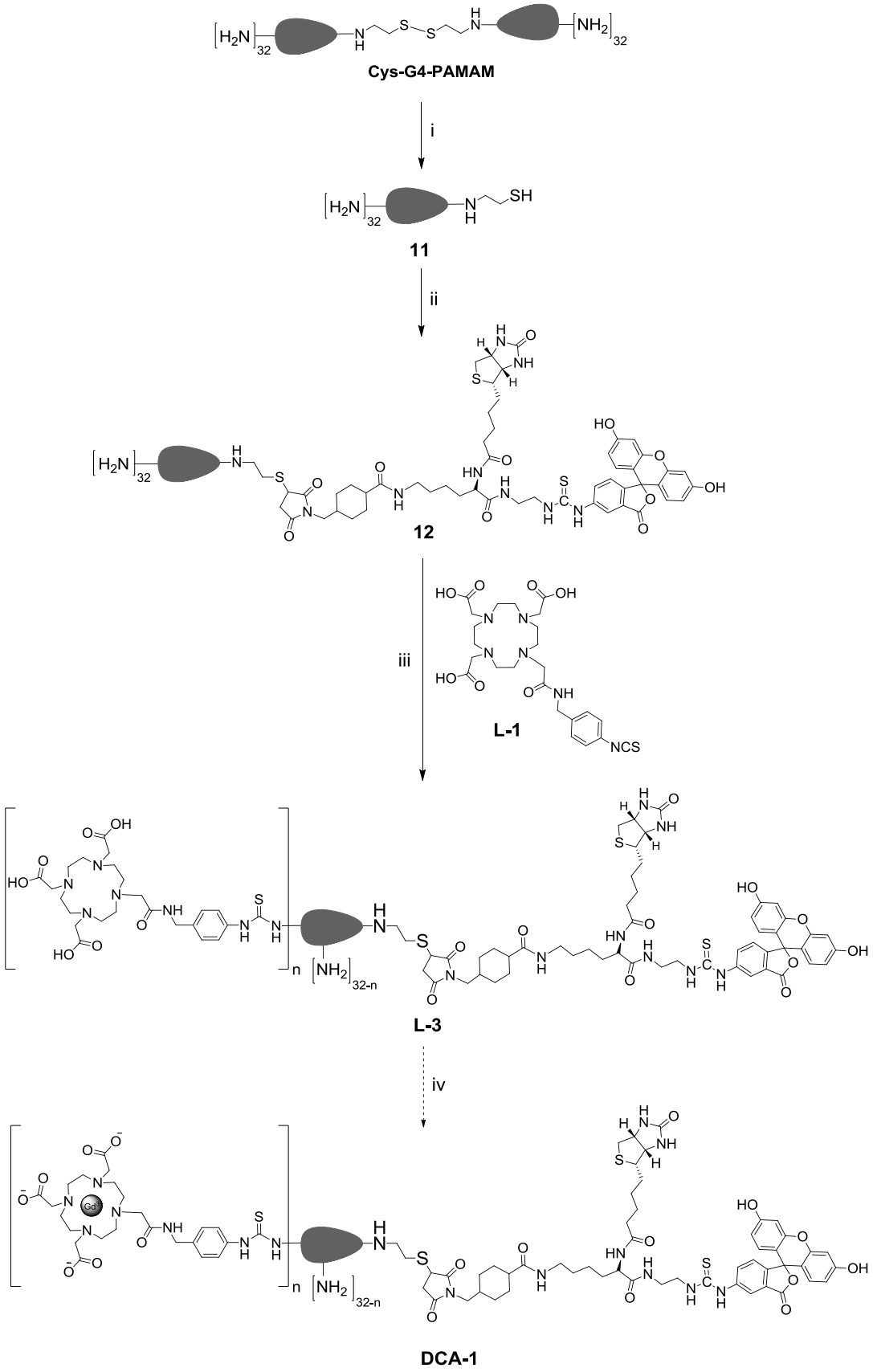

Figure 2-8. Synthetic scheme of **DCA-1**. Reagents and conditions: (i) DTT, CH_3OH/CH_2Cl_2, rt, 48 h; (ii) Intermediate **10**, pH 6.5-7.0, rt, 24 h; (iii) pH 9.0, rt, 24 h; (iv) $GdCl_3 \cdot 6H_2O$, pH 7.0, rt, 24 h.

2.2.2.8 Second attempt for synthesis of DCA-1

In order to eliminate the precipitation of the desired dendrimer product, the Gd-DO3A-NCS complex (**CA-1**) was synthesized using **L-1** (Figure 2-9). **CA-1** was directly attached to the surface of the dendron **12** at pH 9.0 in dimethyl sulfoxide/water mixture (Figure 2-9). Although free Gd^{3+} ions do not exist in the reaction mixture, the precipitation occured again. The reason could be high molecular weight and neutral charge of the final product. To overcome the solubility problem, a new Gd^{3+} chelator was synthesized (Figure 2-10).

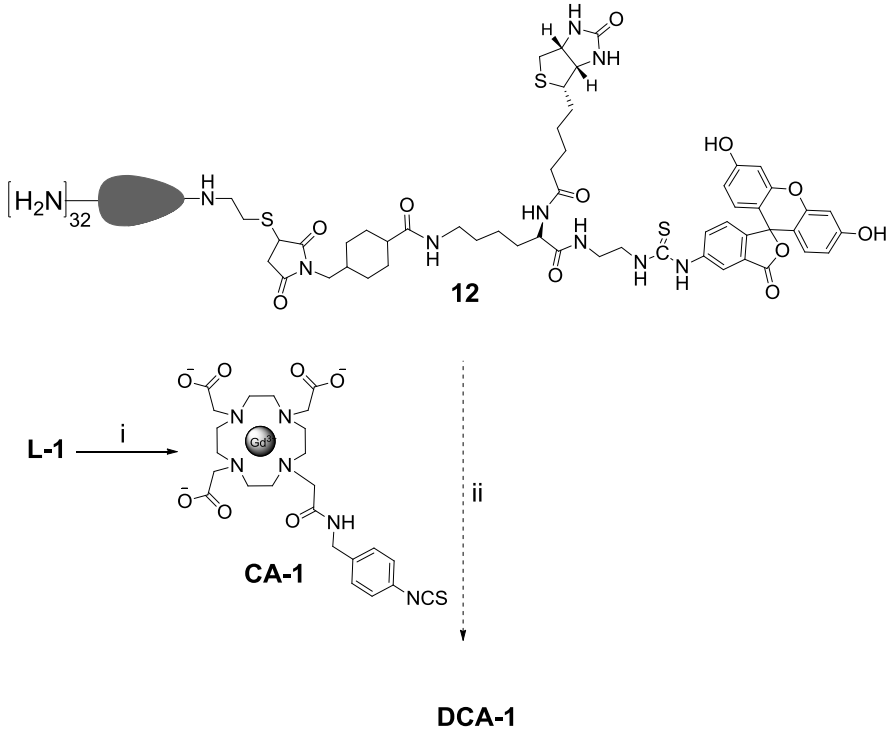

Figure 2-9. Synthetic scheme of **CA-1** and **DCA-1**. Reagents and conditions: (i) DMSO/H_2O, pH 9.0, 45 °C, 48h; (ii) $GdCl_3 \cdot 6H_2O$, pH 7.0, rt, 24 h.

2.2.2.9 Synthesis of DOTA-NCS ligand (16) and CA-2

Compound **16** containing four carboxylic groups was synthesized. Its Gd^{3+}-complex is negatively charged, and this provides an advantage in terms of water solubility (Figure 2-10).

Initially, bromide **13** was prepared by alpha bromination and protection of 4-(4-nitrophenyl)butyric acid according to a published procedure.[59] After the bromination, the carboxylic acid group was protected using *tert*-butyl-2, 2, 2-trichloro acetimidate with the catalyst boron trifluride etherate to give bromide **13**. DO3A-*tris*-*tert*-butyl ester was alkylated

with the bromide **13** in the presence of potassium carbonate in acetonitrile to get **14** in high yield. The nitro group in **14** was reduced to the primary amine **15** by palladium catalyzed hydrogenation and converted into the isothiocyanate by thiophosgene to get **16** in good yield. Compound **16** was used for the synthesis of new monomeric (**MCA-2**) and dendrimeric (**DCA-2**) MRI CAs. *Tert*-butyl esters in **14** were hydolyzed using formic acid. Then Gd^{3+} was loaded at neutral pH to get the Gd-DOTA complex (**CA-2)**

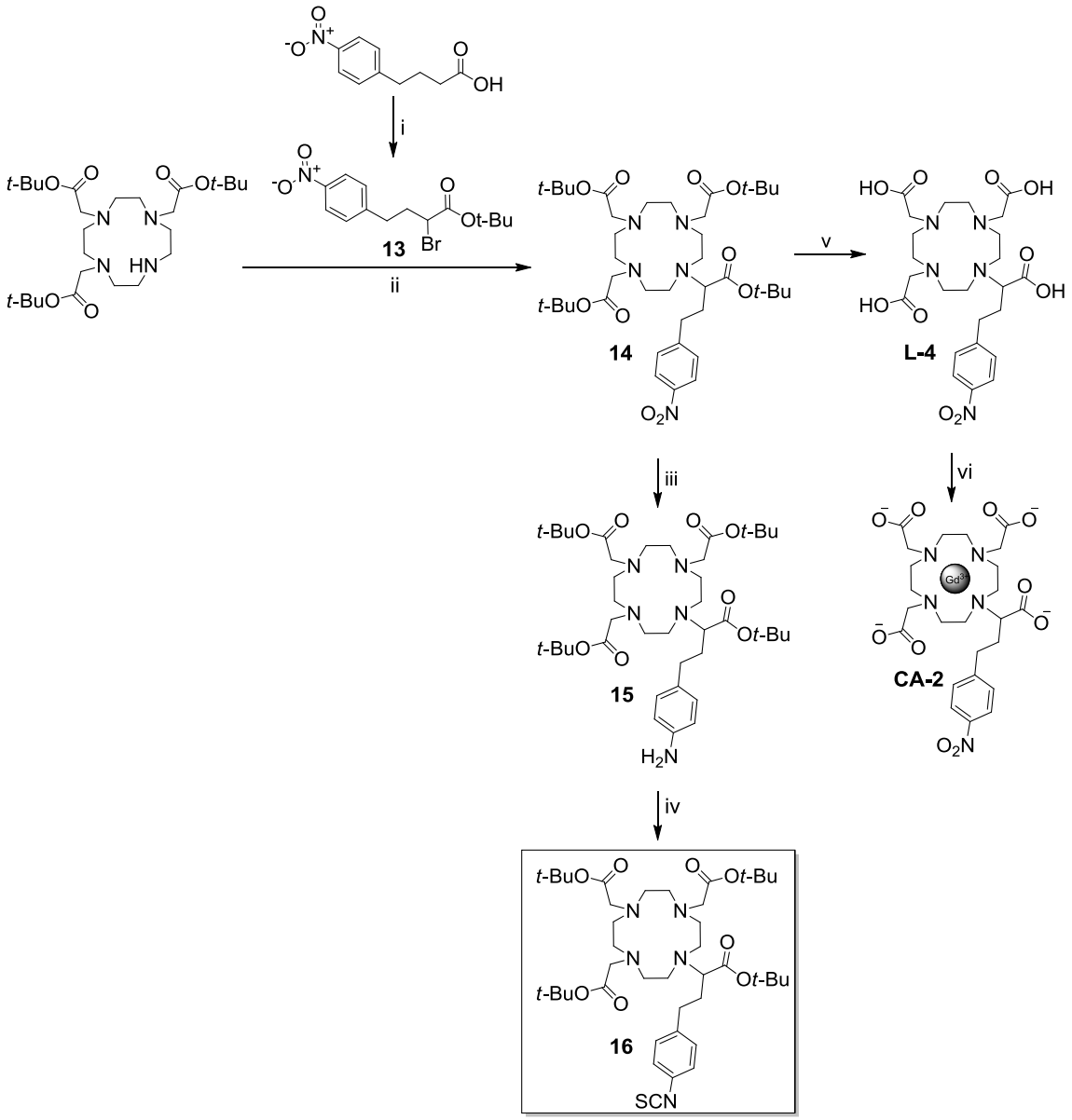

Figure 2-10. Synthetic scheme of **16** and **CA-2**. Reagents and conditions: (i) 1) $SOCl_2$, 75 °C, 24 h, 2) Br_2, 75 °C, 24 h, 3) *tert*-butyl-2, 2, 2-trichloroacetimidate, $CHCl_3$, rt, 16 h, 65%; (ii) K_2CO_3, DMF, 45 °C, 16 h, 96 %; (iii) H_2, Pd/C, EtOH, rt, 16 h, 95%; (iv) $CSCl_2$, Et_3N, rt, 2 h, 71%; (v) formic acid, 60 °C, 24 h, 24%; (vi) $GdCl_3 \cdot 6H_2O$, pH 7.0, rt, 24 h, 47%.

2.2.2.10 Synthesis of MCA-2

Amine **4** was directly coupled to **16** in the presence of triethylamine in dimethylformamide to get **17**. *Tert*-butyl esters were hydrolyzed using formic acid to get **L-5** (Figure 2-11). Finally, **L-5** was complexed with Gd^{3+} to obtain **MCA-2**.

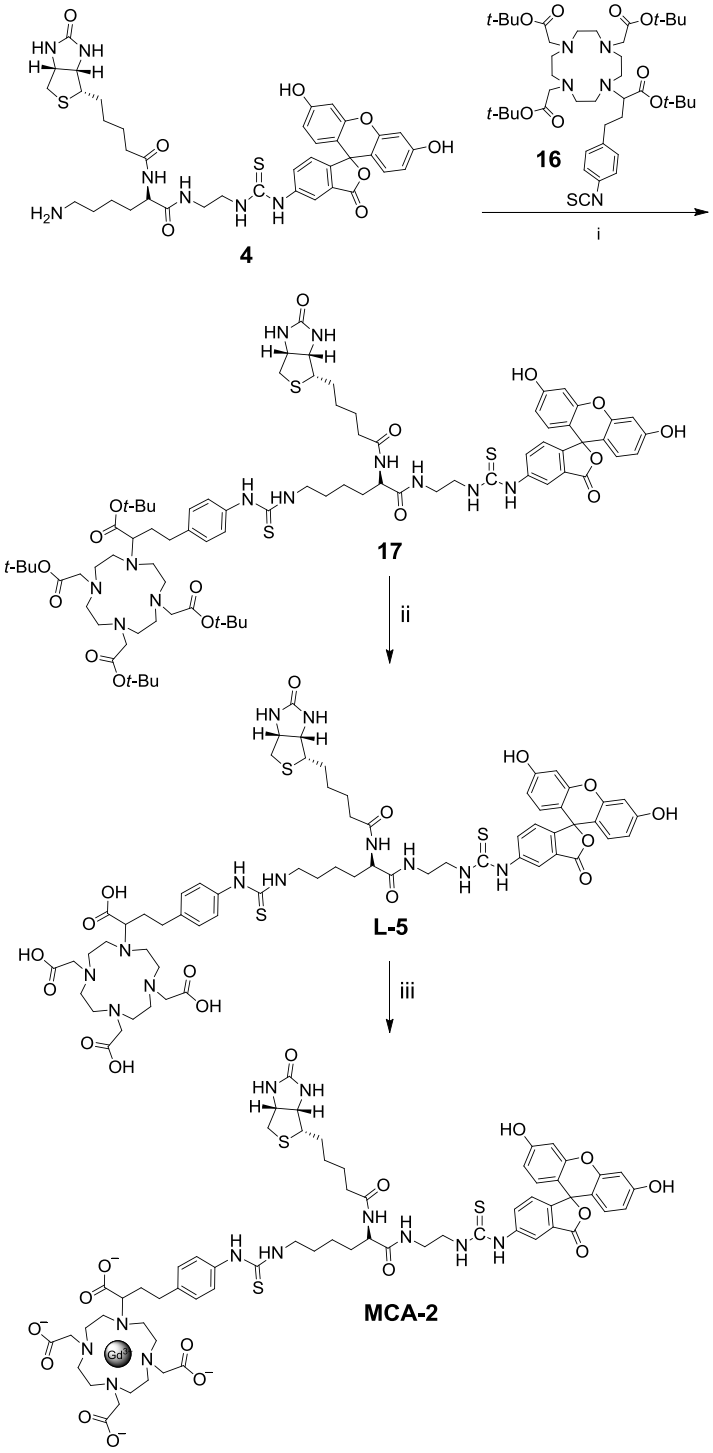

Figure 2-11. Synthetic scheme for preparation of **MCA-2**. Reagents and conditions (i) Et_3N, DMF, 45 °C, 16 h, 68%; (ii) formic acid, 60 °C, 24 h, 95%; (iii) $GdCl_3 \cdot 6H_2O$, pH 7.0, rt, 24 h, 51%.

2.2.2.11 Retrosynthetic analysis of DCA-2

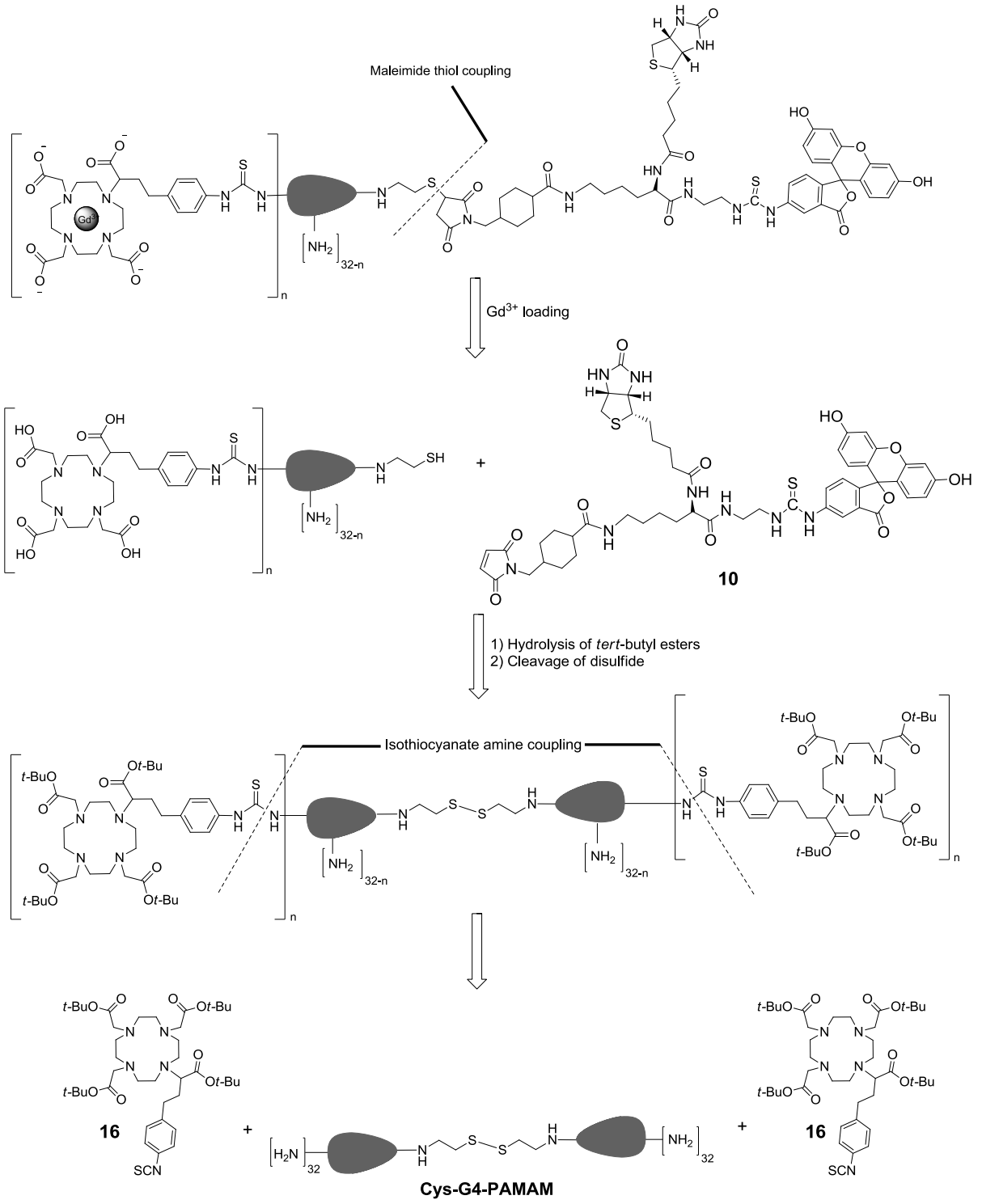

Figure 2-12. Retrosynthetic analysis for the framework of **DCA-2**.

The retrosynthetic analysis of the framework of **DCA-2** is shown in Figure 2-12. The synthetic pathway is different from that of **DCA-1**, simce compound **16** was used instead of **L-1**. In this approach, firstly NCS ligand is bound to the surface groups of dendrimer. Then

the disulfide bond is cleaved using a reducing agent and compound **10** is coupled to the dendron. Finally *tert*-butyl esters are hydrolyzed and Gd^{3+} is loaded.

2.2.2.12 Synthesis of DCA-2

Compound **16** was coupled to the amino surface groups of Cys- G4 PAMAM to get **18**. *Tert*-butyl esters were hydrolyzed using formic acid to get acid **19**. Disulfide bond in **20** was reduced to thiol group using *tris*(2-carboxyethyl)phosphine hydrochloride (TCEP.HCl) to afford the dendron **20**.[52] The presence of thiol group was confirmed by means of Ellman's reagent test.[56] In order to prevent recoupling of thiol compound, the maleimide was immediately added to the reaction mixture without further purification to give **L-6**. In general maleimide groups react with thiol groups in a slightly acidic medium.[55] Therefore, pH was maintained to 6.5-7.0 during the reaction. The unreacted compound **20** was re-oxidized bubbling oxygen gas through to reaction mixture to get acid **19**. Then the excess amount of **10** and acid **19** were removed using G-15 sephadex column and water as eluent to get pure **L-6**. After the purification, **L-6** was complexed with Gd^{3+} at neutral pH to get **DCA-2** (Figure 2-13). To remove the excess amount of Gd^{3+} ions, EDTA was introduced to the reaction mixture. EDTA was complexed with free Gd^{3+} ions and **DCA-2** was purified using centrifugal filter unit with 3 KDa MWCO. The compound **18**, and **19** were analyzed by means of MALDI-TOF/MS and ^{1}H NMR spectroscopy. MALDI-TOF spectra exhibited broad signals with patterns similar to those previously reported for DTPA-functionalized G4 PAMAM dendrimers.[60] The calculated masses indicated the average of 37 DOTA chelates per dendrimer molecule, which corresponds to 55-60% conversion of the amino surface groups into the thiourea product with the DOTA-NCS units. Appearance of aromatic protons in the ^{1}H NMR spectra is a clear evidence of the DOTA-dendrimer conjugate formation (these peaks do not exist in ^{1}H NMR spectra of the commercial PAMAM G4 dendrimer), however integration of spectra was less successful as expected,[60] usually indicating slightly higher amount of DOTA units (when comparing regions of aromatic vs. aliphatic protons) than amounts determined by means of MALDI-TOF. The dendrons **L-6** and **DCA-2** were also analyzed by means of MALDI-TOF showing again broad peaks with an average number of 19 DOTA chelators attached to the G4 PAMAM dendron, which is completely in line with results observed for the initial dendrimers **18** and **19** which have double number of DOTA units. To increase binding efficacy of dendrimeric CA, small size dendrimer can be used or a longer linker than SMCC can be coupled to higher generation dendrimers or a longer core molecule can be used instead of lysine. The structure of **DCA-2** is depicted in figure 2-14.

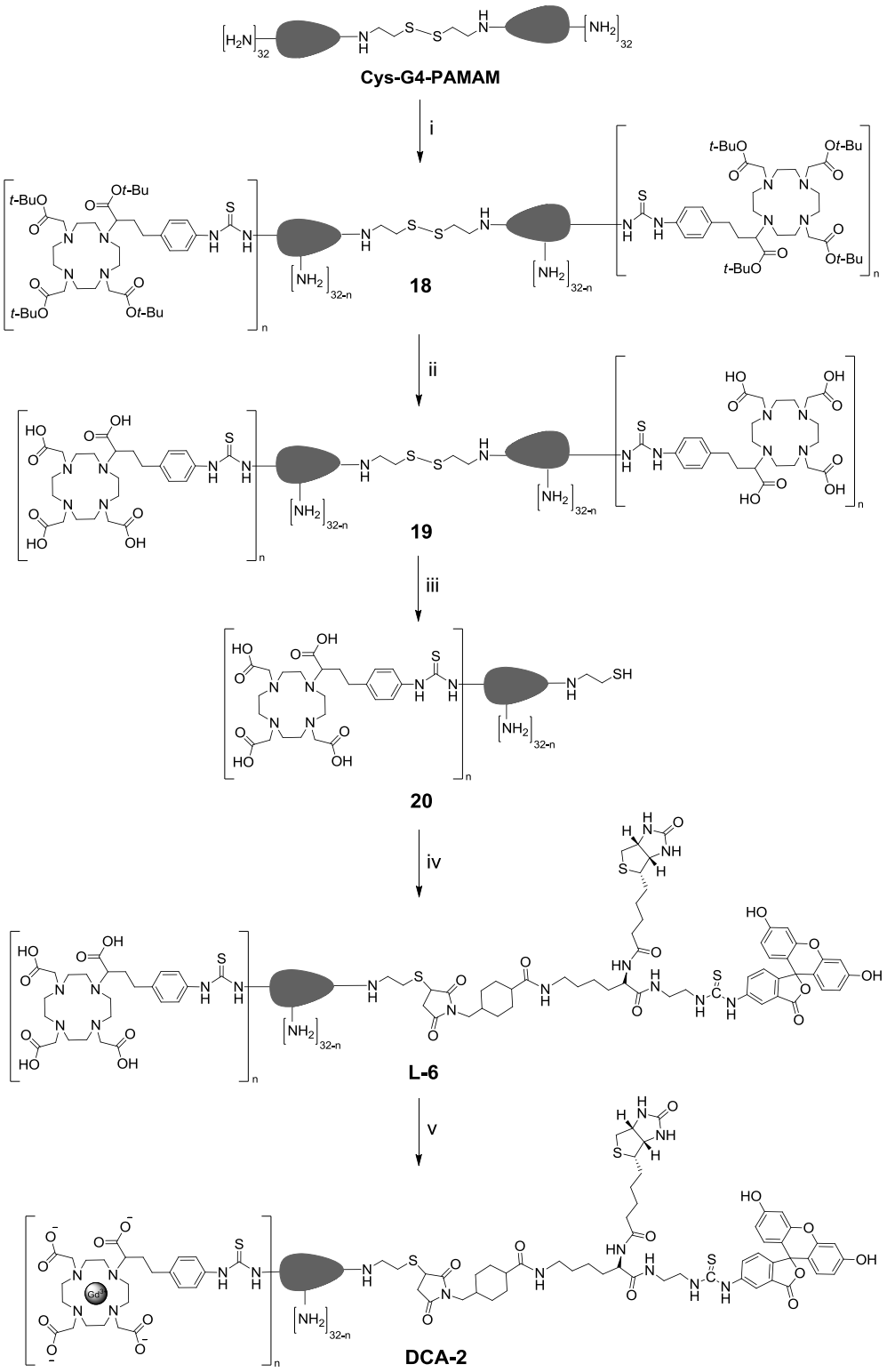

Figure 2-13. Synthetic scheme of **DCA-2**. Reagents and conditions: (i) Compound **16**, Et_3N, DMF, 45 °C, 48 h, 81%; (ii) formic acid, 60 °C, 24 h, 84%; (iii) TCEP.HCl, pH 7.0, rt, 1 h; (iv) **10**, pH 6.5–7.0, rt, 16 h, 87%; (v) $GdCl_3 \cdot 6H_2O$, pH 7.0, rt, 24 h, 79%.

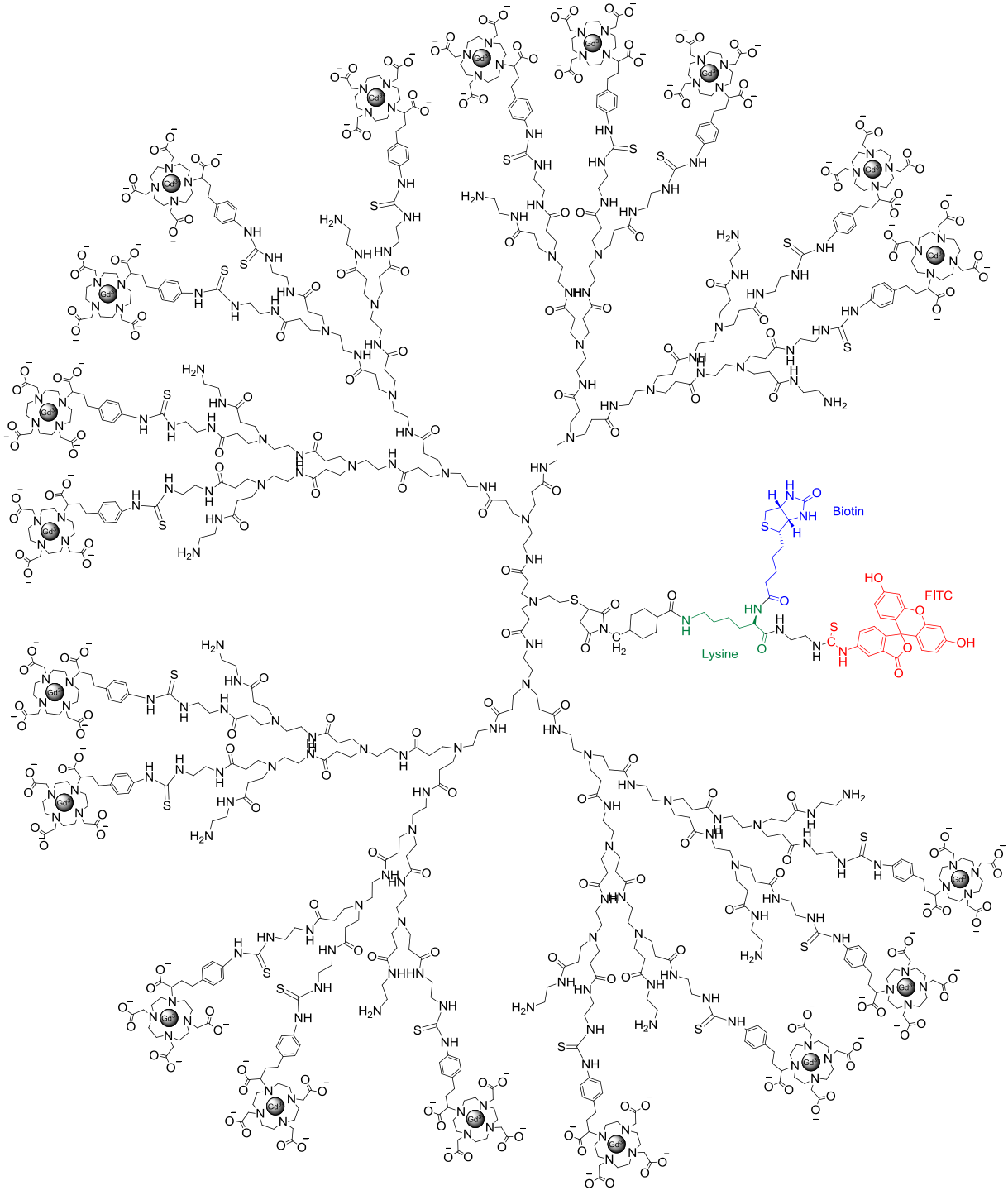

Figure 2-14. Estimated structure of **DCA-2** with 19 Gd-DOTA complex.

When macrocycles are coupled to dendrimer surface, free primary amine groups are remaining. This gives an opportunity to bind more biotin. In case the stoichiometric ratio is not important for desired application, more biotin can be coupled to free amino surface groups in dendrimeric compound to increase the binding efficiency. Similarly, more fluorescent dye can be coupled to free amino groups instead of biotin. When the stoichiometric ratio is

important and it is needed to avoid free amines for desired application, free amines can be inactivated using a proper scavenger such as methyl isothiocyanate.

2.2.3 Longitudinal relaxivity of monomeric and dendrimeric CAs

Longitudinal relaxivity (r_1) relaxivity values of **CA-2**, **MCA-2,** and **DCA-2** were determined at 7 T (300 MHz) and 25 °C. The initial Gd^{3+} concentrations were determined by measuring the bulk magnetic susceptibility shifts.[61] The T_1 relaxation times were recorded at pH 7.0 in PBS at different concentrations of Gd^{3+} prepared by diluting the stock solutions of **CA-2**, **MCA-2,** and **DCA-2** with appropriate amount of PBS. The exact concentration of Gd^{3+} in stock solutions was determined by the bulk magnetic susceptibility shift method.[61] The r_1 relaxivity of each CA was obtained as a slope of the linear regression curve for concentrations of Gd^{3+} plotted against the relaxation rate (R_1) (Figure 2-15). The r_1 values of 4.78±0.24, 6.96±0.32 and 6.09±0.19 $mM^{-1}s^{-1}$ were determined for **CA-2**, **MCA-2**, and **DCA-2** respectively.

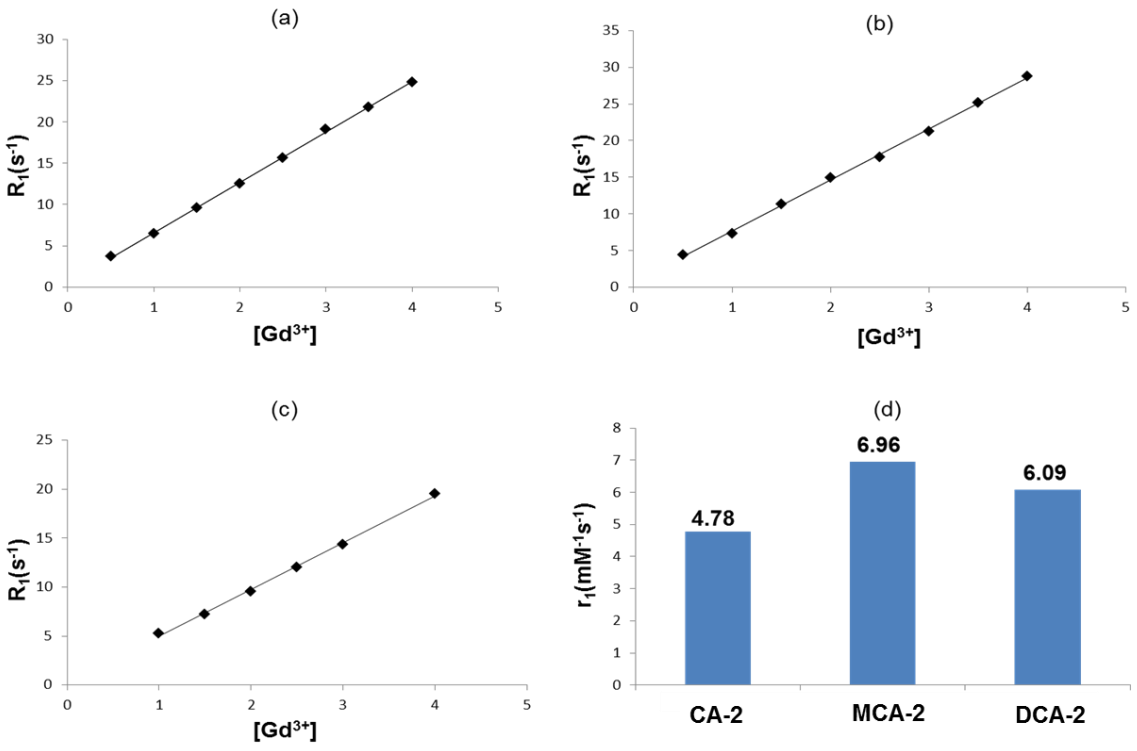

Figure 2-15. The linear regression curves for concentrations of Gd^{3+} for **CA-2 (**a), **MCA-2** (b), **DCA-2** (c), and the comparison of the r_1 relaxivities (d).

As expected, the low molecular weight Gd-DOTA complex **CA-2** has the lowest r_1 relaxivity. Although monomeric **MCA-2** and dendrimeric **DCA-2** agents have higher molecular size than **CA-2**, a dramatic increase in the r_1 was not observed. The studies with high molecular

weight dendrimers have showed that dendrimeric CAs has much higher r_1 value than their low molecular weight analogues in low magnetic field. In our study the relaxivity experiments were performed in high magnetic field (7 T). Probably the high magnetic field has not allowed us to observe a significant increase in the r_1. Namely, it is known that rotational correlation time does not lead to increase in r_1 at frequencies above ~200 MHz. Therefore, a slight increase in r_1 was observed for both **MCA-2** and **DCA-2**, where **DCA-2** displays lower r_1 than **MCA-2**. It is possible that a moderate molecular weight of **MCA-2** leads to a slight increase in r_1, whereas a combination of the dramatic increase in molecular weight, fast local motion of DOTA chelators and possible partial hindrance (and therefore reduction in hydration) of Gd^{3+} by the dendrimer branches leads to a cumulative effects which result is lowering of r_1 for **DCA-2** as compared to **MCA-2**.

2.2.4 Binding of targeted contrast agents to avidin-coated microspheres

An analysis on avidin-coated polystyrene microspheres (avidin beads) by means of fluorescence microscopy was performed to qualitatively evaluate the suitability for targeting avidin and the efficacy of the targeted CAs. In order to allow binding, the avidin coated microspheres were incubated with the solutions of **MCA-2** and **DCA-2** in pH 7.4 PBS. Excess amounts of compounds were removed by washing beads with PBS. The microspheres were also treated with PBS and the solution of FITC in pH 7.4 PBS as negative controls. Finally, the microspheres were imaged by bright-field and epi-fluorescence microscopy to detect the presence of bound CAs.

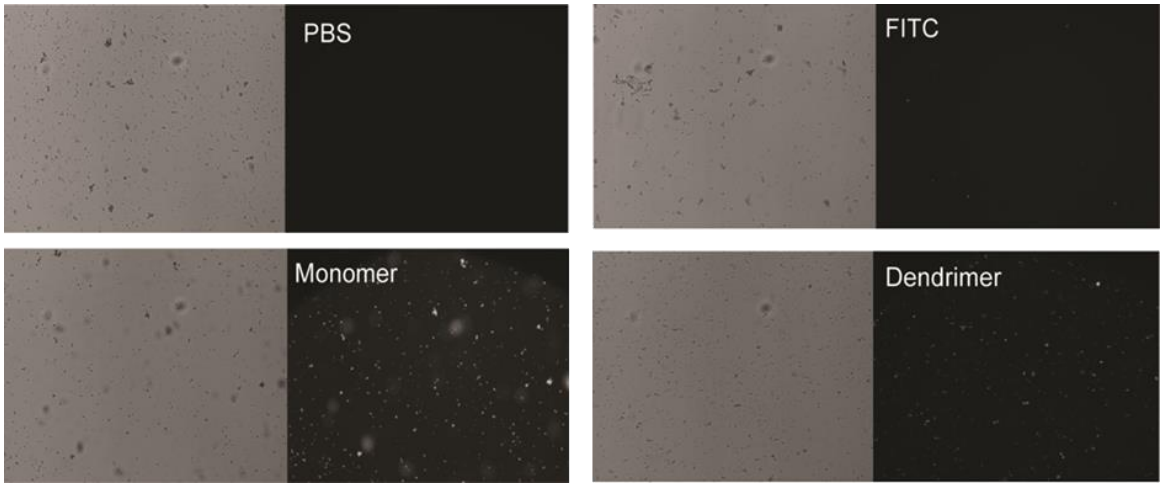

Figure 2-16. Microscopic fluorescence imaging of avidin-coated microspheres treated with PBS, FITC, **MCA-2** (Monomer) and **DCA-2** (Dendrimer).

The beads treated with targeted CAs (**MCA-2** and **DCA-2**) provided bright spots and the beads treated with PBS and FITC did not show detectable fluorescence (Figure 2-16). Since **MCA-2** has less steric hindrance to bind avidin, the microspheres treated with **MCA-2** showed greater fluorescence intensity than that of **DCA-2**.

2.2.5 Binding of targeted contrast agents to NeutrAvidin™-agarose gel beads

Beside qualitative binding ability test, the fluorescence intensities of the targeted CAs were also measured using NeutrAvidin™-agarose gel beads. Solutions containing 1 mM of **MCA-2**, or **DCA-2** in pH 7.4 PBS, as well as a non-targeted Gd-chelate CA Dotarem® were incubated with the beads. The fourth sample was incubated with PBS containing no CA as a control. The beads were then washed to remove excess amount of CAs and then analyzed by fluorescence spectroscopy, MRI and inductively-coupled mass spectrometry (ICP-MS).

2.2.5.1 Fluorescence spectroscopy and microscopy

Contrast agent binding was verified by checking the beads for fluorescence of the FITC moiety (λex=485 nm / λem = 520 nm), which is present on both of **MCA-2** (monomer) and **DCA-2** (dendrimer), but not Dotarem®. Beads treated with **MCA-2** and **DCA-2** were fluorescent when placed on a blue light source and viewed through an amber filter. The beads which had been treated with **MCA-2** appeared brighter than those treated with **DCA-2**. No fluorescence was observed with untreated beads or beads treated with Dotarem® (Figure 2-17).

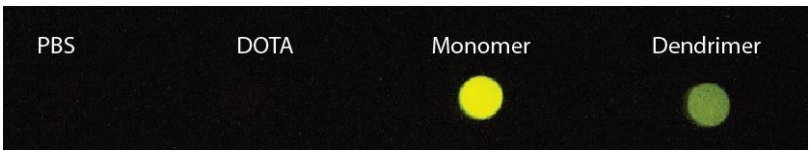

Figure 2-17. The fluorescence images, from left to right: beads treated with PBS, Dotarem® (DOTA), **MCA-2** (Monomer) or **DCA-2** (Dendrimer) were pipetted onto the optical surface of a fluorescent gel imager and digital photographs were acquired.

Quantification of fluorescent signals in a multiplate reader revealed a similar trend. For the PBS and Dotarem®-treated, we recorded fluorescence values below background levels (63-64 arbitrary units) whereas raw values for beads treated with the targeted CAs were more than 3 orders of magnitude greater – ~63 000 and 15 000 a.u. for the monomer and dendrimer respectively (Figure 2-18). **MCA-2** appeared to bind the Neutravidin gel most efficiently, as there was a 3.6-fold increase in fluorescence intensity values compared to **DCA-2** (Table 2-1).

However, these results have to be taken with care since it is not known if the binding of the targeted molecule to the protein affects the emission properties of the fluorescence dye, nor if fluorescence intensity was recorded at the appropriate FITC concentration. Nevertheless, it is expected that **MCA-2** binds more efficiently than **DCA-2** due to the lower size of the former.

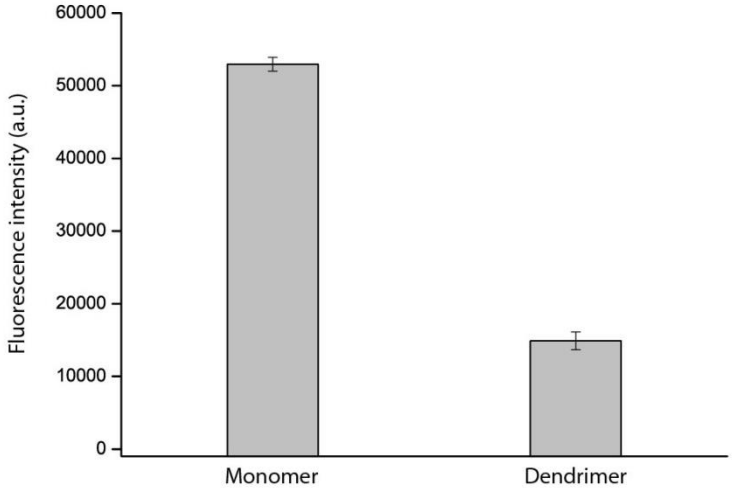

Figure 2-18. Fluorescence measurements of CA-treated agarose beads. CA-treated beads were placed in a 96-well plate and the fluorescence intensity of FITC (λ_{ex}=485 nm /λ_{em}=520 nm) was quantified in a fluorescence plate reader. Bar plots show the mean values of three experiments ± standard deviation.

2.2.5.2 T_1-weighted magnetic resonance imaging

Microtubes containing PBS-, Dotarem®-, **MCA-2-** or **DCA-2-** treated with neutravidin agarose beads were imaged at 7 Tesla. T_1-weighted images were generated with an echo time of 6 ms and a series of 30 repetition times ranging from 21-8000 ms. For each set of parameters, we acquired longitudinal images at an in-plane resolution of 200 µm and slice thickness of 2 mm (Figure 2-19). The signal intensities of the CA-treated samples varied depending on the TR used for image acquisition (Table 2-1). The greatest signal change was found with **DCA-2** at TR=59 ms, therefore further analysis was carried out on this dataset. Binding of **DCA-2** caused a nearly 10-fold increase in bead signal intensity (Figure 2-19, Table 1). Binding of **MCA-2** also led to a noticeable enhancement (~2-fold). Dotarem® treatment caused only a marginal increase (1.08-fold), suggesting a small degree of non-specific bead retention of this non-targeted CA (Figure 2-20, Table 2-1). In summary, binding of both **MCA-2** and **DCA-2** increased target contrast in T_1-weighted images acquired at 7 T. Comparatively, **DCA-2** showed an overall ~5-fold increase in performance over **MCA-2**.

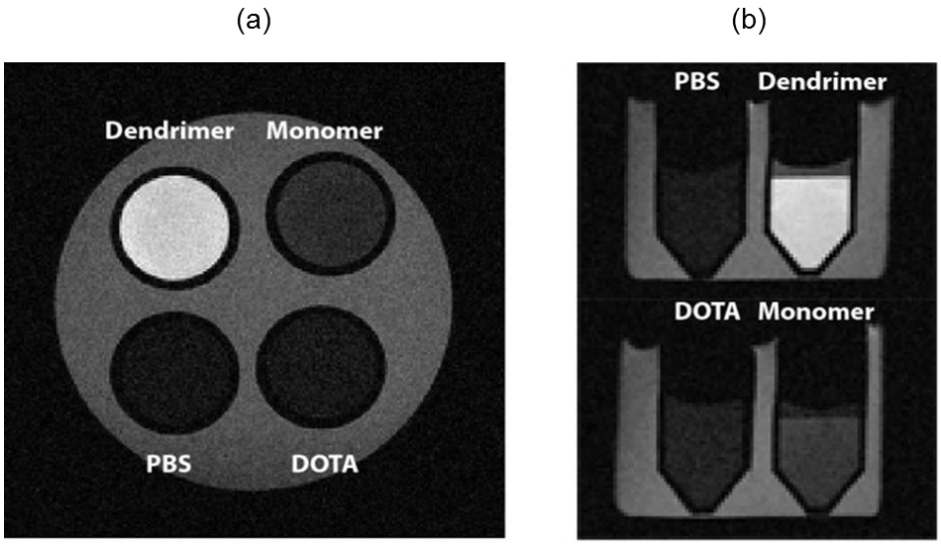

Figure 2-19. Specific MRI contrast enhancement in NeutrAvidin™-agarose gel treated with targeted CAs. NeutrAvidin™-agarose gels were treated with PBS, Dotarem®, **MCA-2** (Monomer) or **DCA-2** (Dendrimer) and imaged at 7 Tesla MRI scanner with TR=58.5ms. a) Coronal and b) sagittal images obtained in a single representative experiment.

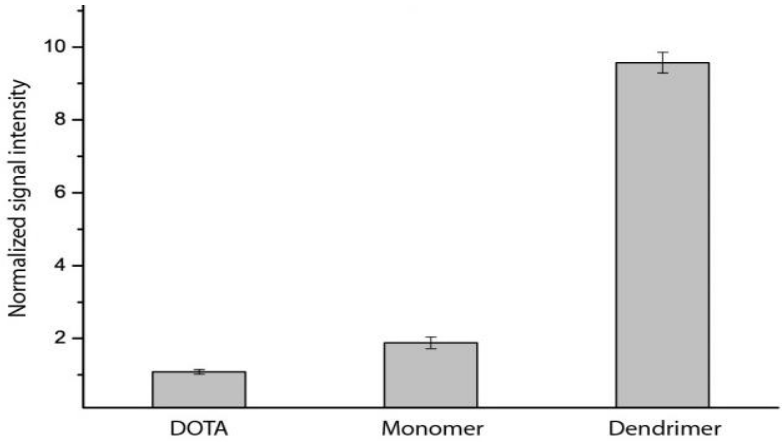

Figure 2-20. Comparison of obtained MRI signal intensities. Signal for each CA sample was normalized to the PBS control. Bars show the average normalized signal from three independent experiments ± standard deviation.

2.2.5.3 Inductively coupled plasma mass spectrometry (ICP-MS) experiments

We attempted to assess the efficacy of the targeted CAs by quantifying the amount of Gd^{3+} that was bound to NeutrAvidin™-agarose gel by means of ICP-MS. The samples containing NeutrAvidin™-agarose gel treated with PBS, Dotarem®, **MCA-2** or **DCA-2** were digested in conc. HNO_3 and the amount of ionic Gd^{3+} was quantified by ICP-MS. The results obtained from these experiments, as well as further quantitative comparisons from the fluorescence

spectroscopy and MRI experiments are summarized in the Table 2-1. The ICP-MS data were consistent with observations derived from the fluorescence and MRI studies. Gadolinium was detectable in the three bead samples treated with Dotarem®, **MCA-2**, or **DCA-2**. The non-specific nature of Dotarem® interaction was indicated by much lower bead-associated Gd^{3+} in comparison to either of **MCA-2** and **DCA-2** (Table 2-1). Consistent with the dendrimer's determination of the ~19:1 content of Gd^{3+}-DOTA:biotin, beads treated with this agent (**DCA-2**) were associated with on the order of ~14 times more Gd^{3+}.

Table 2-1. Analysis of contrast agent binding to NeutrAvidin™-agarose gel

Sample	Fluorescence intensity (a.u.) [(a)]	T1-w MRI intensity (norm.) [(a)]	Relative Gd^{3+} content (norm.) [(a, b)]	Ratio Gd^{3+} **(DCA-2/MCA-2)** [(a,c)]
PBS	-	1.00	-	-
Dotarem®	-	1.08	1.0	-
MCA-2 (Monomer)	52965	1.88	11.2	-
DCA-2 (Dendrimer)	14891	9.6	151.5	13.5

a) Reported results are mean of three independent experiments; b) As determined by ICP-MS;
c) Ratio of Gd^{3+} content of dendrimer/monomer

2.3 Conclusion

We synthesized biontinylated and fluorescently labeled targeted monomeric and dendrimeric CAs which can be detected through both optical fluorescence and T_1 MRI contrast signals. The targeting properties of the synthesized monomeric and dendrimeric CAs were studied using various methods and types of targets. The agents exploit the high affinity biotin-avidin interaction and were found to efficiently label avidin-coated microspheres and NeutrAvidin^{TM}-agarose gel beads. The types of studied targets highlight potential application directions of our dendrimeric targeted CA. Avidin-coated microspheres could be considered as a good model of cells with a higher content of avidin expressed on their surface. Similarly, NeutrAvidin™-agarose gel beads clearly demonstrated the binding efficiency of monomeric CA by both the fluorescence- and MR-based methods. Apart of potential targeted imaging applications mentioned above, these results indicate one additional possibility with these agents. Namely, various nanosize, biocompatible polymer based systems coated with protein-dendrimer conjugates can be envisaged, leading to high load of paramagnetic Gd^{3+} and subsequently strong blood-pool CAs.

3. Chapter 2:

Synthesis of dendrimeric Ca^{2+} responsive ‘smart’ MRI contrast agents

3.1 Introduction

Calcium ion is one of the essential metal ions in the body. Ca^{2+} plays key roles in numerous crucial physiological processes. For instance intracellular calcium is vital for regulating myriad cellular functions, such as differentiation, secretion, proliferation and motility, and it also acts as a cofactor in a number of enzymatic reactions. Especially it has a dual role as a carrier of electrical current and as an intracellular second messenger. Since calcium actions are mediated by a much larger array of proteins including protein kinases, its effects are much more diverse than those of the other second messengers such as cAMP (3',5'-cyclic adenosine monophosphate) and DAG (diacylglycerol). Despite of dependency to some extent on extracellular calcium $[Ca^{2+}]_o$, the levels of free calcium in the cytosol $[Ca^{2+}]_i$ are much lower than $[Ca^{2+}]_o$ (100 nM vs. 1.1–1.3 mM). In contradiction to $Ca^{2+}{}_o$, $Ca^{2+}{}_i$ fluctuates faster and has 10-fold or more wide range in response to hormonal and other stimuli. $Ca^{2+}{}_o$ regulates a variety of physicological functions including blood clotting, neuromuscular excitability and maintenance of skeletal integrity.[62, 63]

Neuronal calcium fluxes are dramatic and directly related to synaptic activity. Beacuse of that, Ca^{2+} is an important target in neuroimaging. Significant changes in Ca^{2+} concentration occur during neuronal activity. Therefore Ca^{2+} concentration changes could contribute to the understanding of basic aspects of neuronal regulation or highlight the abnormalities in the diseased area. Currently, the blood-oxygen-level-dependent (BOLD) functional MRI (fMRI) technique is used for neuroimaging in humans and animals. Neuronal activity is measured indirectly by the BOLD technique detecting changes in blood flow to brain regions with increased energy requirements. The BOLD technique has physiological limitations due to the vascular origin of the signal. The hemodynamic changes take place several seconds after the neurons actually fire. It is too slow to study precise neural activity. Additionally, the relationship between the neural activity and the BOLD signal has not been completely understood yet.[64-66] In order to overcome this problem, bioactivable MRI CAs such as Gd-complexes could be used as functional markers for processes directly linked to neural signaling. Ca^{2+} is the most important biomarker among several possible markers that are responsive to the concentration of certain ions for the tracking the neural activity. In order to develop Ca^{2+} sensitive/responsive MRI CAs two different approaches have been reported: Gd^{3+}-complexes with a T_1 response on interaction with Ca^{2+} ions and a T_2 agent based on Ca^{2+}-related aggregation of superparamagnetic iron nanoparticles conjugated to

calmodulin.[44, 67] In the first approach, Gd^{3+}-based Ca^{2+} responsive CAs involved changes in the coordination sphere of the Gd^{3+} following coordination of Ca^{2+}. These CAs have two coordinating groups that specifically chelate Gd^{3+} and Ca^{2+}. The calcium chelating unit is weakly coordinated to the Gd^{3+} in the absence of Ca^{2+}. When Ca^{2+} interacts with the responsive CA, the Ca^{2+} chelating unit coordinates to Ca^{2+} liberating a coordination site on Gd^{3+}, allowing water molecule to coordinate to this free coordination site. Therefore the relaxivity incerases with the increase of hydration number.[66] According to this approach, Ca^{2+} responsive CAs with two macrocyclic lantanide metal chelators connected by a linker containing calcium selective chelator have been developed. The first Ca^{2+} sensitive MRI contrast agent Gd-DOPTA was synthesized by Li *et al*.[68] This molecule is composed of two Gd-DO3A complexes linked to the Ca^{2+} selective ligand BAPTA. The relaxivity depends on the Ca^{2+} concentration in the medium. When Ca^{2+} is introducued to the solution of this complex, the r_1 relaxivity increases from 3.26 to 5.76 $mM^{-1}s^{-1}$. Before Ca^{2+} is added to the solution, the carboxylate groups in BAPTA are coordinated with Gd^{3+} ions and the access of water molecules to Gd^{3+} is restricted. When Ca^{2+} is added, it is coordinated with the carboxylate groups resulting in increase of hydration number. Then water molecules approach to the Gd^{3+} leading to an increase in the relaxivity (Figure 3-1).

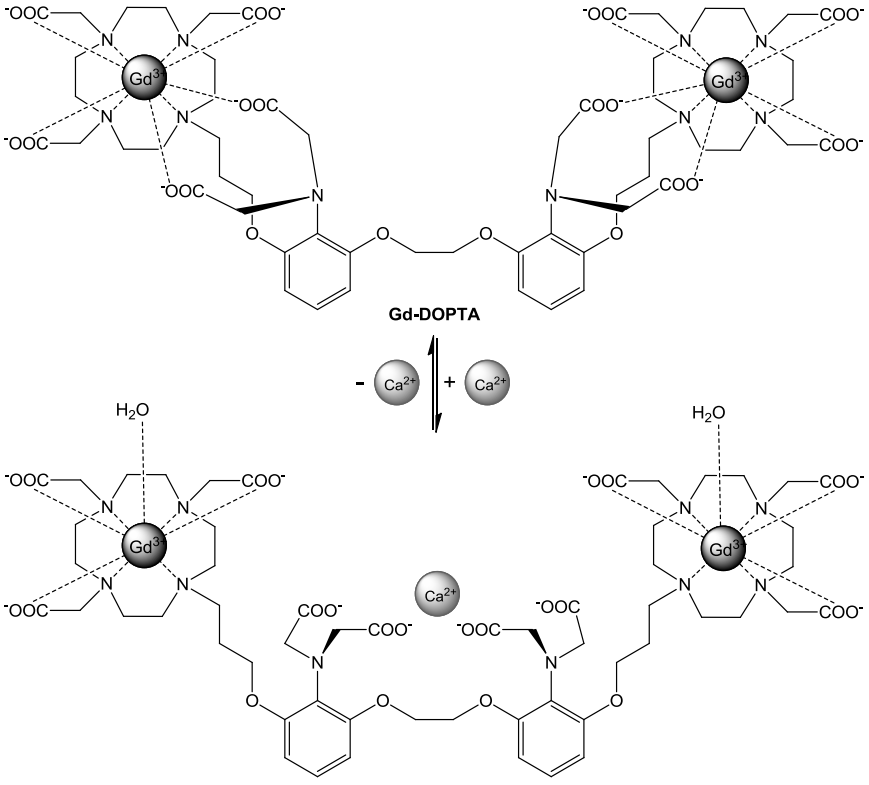

Figure 3-1. Equilibrium reaction of Gd-DOPTA.

Angelovski *et al.* introduced two Ca^{2+} responsive MRI contrast agents (Figure 3-2). They chose a modified EGTA chelator linked to two Gd^{3+} chelates.[69]

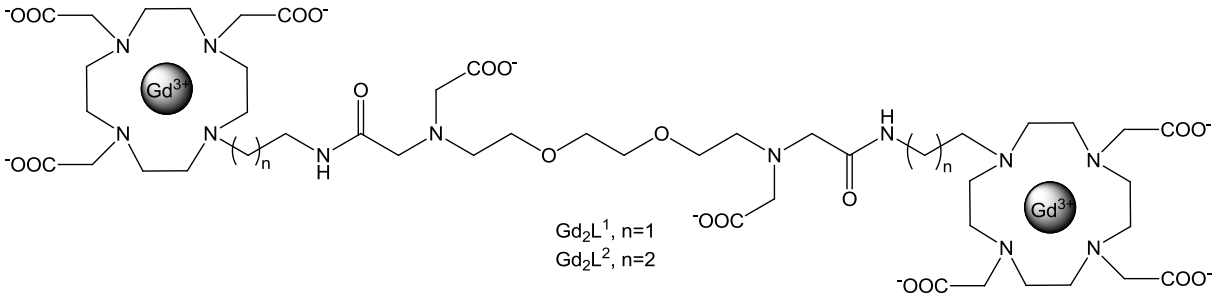

Figure 3-2. Structures of complexes Gd_2L^1 and Gd_2L^2.

They performed a *q* assessment on Eu^{3+} analogues Eu_2L^1 and Eu_2L^2 by means of time-resolved luminescence decay measurements. Estimated values of *q* changed upon addition of one equivalent of Ca^{2+} from 0.3 to 0.7 and 0.5 to 0.9 for Eu_2L^1 and Eu_2L^2, respectively. This means an increase of the inner-sphere hydration number of these complexes induced the observed relaxivity changes. Ca^{2+} titrations were performed in the DMEM/F-12 medium that contained GIBCO^{TM} N-2 supplement (N-2) in order to simulate the biochemical complexity of the brain and investigate the Ca^{2+}-sensing properties of these complexes in a biologically more realistic environment. The DMEM/F-12/N-2 mixture was considered as a very good approximation of the brain extracellular medium (BEM). Upon addition of 1.6–1.8 equiv Ca^{2+}, the relaxivity of Gd_2L^1 increased from 2.61 to 3.94 $mm^{-1}s^{-1}$ whereas for Gd_2L^2 it increased from 2.46 to 3.73 $mm^{-1}s^{-1}$ (51 and 52% change, respectively) (Figure 3-3). A subsequent "reverse" titration with EDTA was performed in order to simulate the transient nature of the Ca^{2+} changes during neural activity. The relaxivities returned to the initial values. This confirmed the reversibility of the Ca^{2+}–contrast agent interaction even in a complex environment.

The behaviors of these CAs in a in a biologically relevant medium, such as the model of the brain extracellular fluid, is extremely promising. These CAs have great potential to function in real *in vivo* condirions, since they are able to alter their magnetic properties in response to Ca^{2+}-concentrations changes. This can be exploited to track *in vivo* changes of extracellular Ca^{2+} flux, and thus, neural activity.[70] These complexes could lead to high-resolution MR imaging of brain function due to their remarkable relaxivity properties.

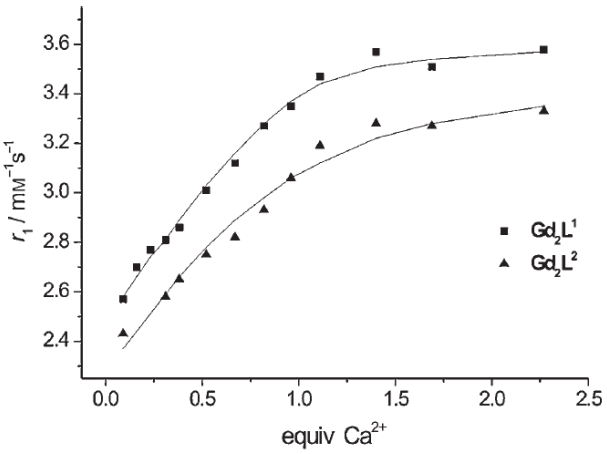

Figure 3-3. Relaxometric titration of Gd_2L^1 (■) and Gd_2L^2 (▲)

However, the diffusion of CAs over time from the region of interest complicates their in vivo applications. When a MR measurement is performed, as fast diffusion leads to a quick decrease signal intensity. This limitation could be overcomed by the synthesis of high molecular weight CAs. In order to reduce the diffusion rate and increase the CA concentration in the region of interest, dendrimers can be used as multivalent scaffolds for the synthesis of high molecular weight Ca^{2+} responsive CAs. A modified EGTA chelator linked to a Gd^{3+} complex can be attach to surface groups of dendrimers. For this purpose, the Ca^{2+} responsive CAs introduced by Angelovski *et al*. can be modified and coupled to amine surface groups of dendrimers to obtain high molecular weight CAs. Due to their high molecular weight, they can stay in the region of interest longer than low molecular weight CAs. Additionally, they can provide MR signal enhancement, since they contain larger amount of Gd^{3+} complexes.

3.2 Results and Discussion

3.2.1 Design of calcium responsive MRI contrast agents

The desired molecules contain G0, G1, or G2 PAMAM dendrimers as a multivalent scaffold, EGTA derivative which is used as a specific Ca^{2+} chelator linked to Gd-DO3A type MRI CA. In the absence of Ca^{2+}, one of the carboxylate group of EGTA part coordinates to Gd^{3+} and this cause reducing hydration number of SCA as previously mentioned. When the SCA was administered to the medium containing Ca^{2+}, EGTA part interacts with Ca^{2+} liberating one coordination site on Gd^{3+}. In order to attach EGTA derivative to amino surface groups of dendrimers, a linker containing nitro group can be prepared. The nitro groups can be converted to isothiocyanate group which easily reacts with primay amine groups. For the comparison of the relaxometric and in vivo behaviors, a monomeric analogue of the dendrimeric CAs can also be synthesized. The schematic structures of the monomeric and dendrimeric Ca^{2+} responsive MRI CAs are depicted in Figure 3-4.

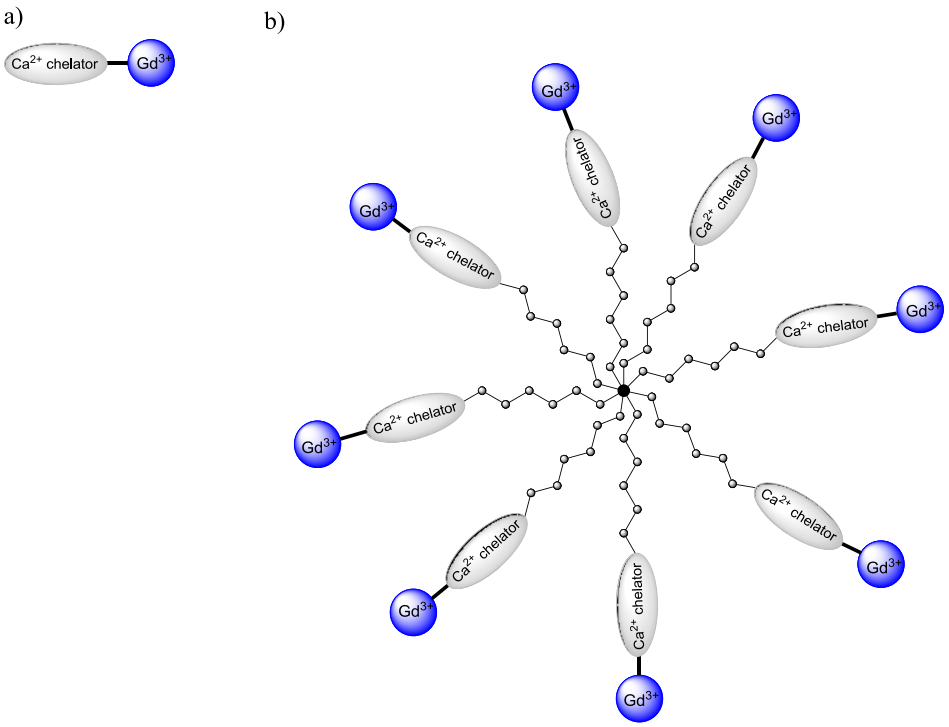

Figure 3-4. Schematic structures of the monomeric (a) and dendrimeric (b) Ca^{2+} responsive MRI CAs.

3.2.2 Synthesis of compounds

3.2.2.1 The retrosynthetic analysis for DSCAs

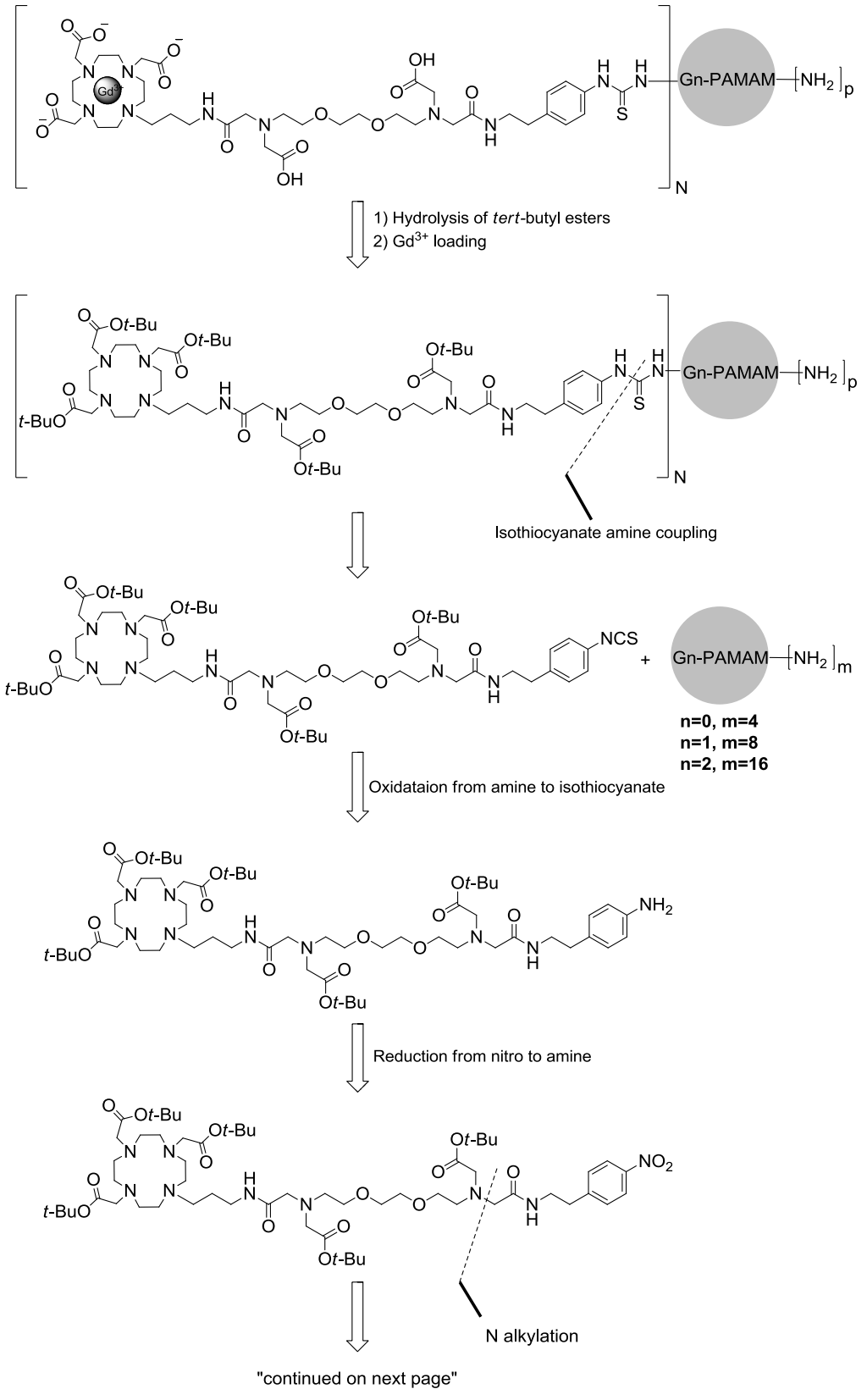

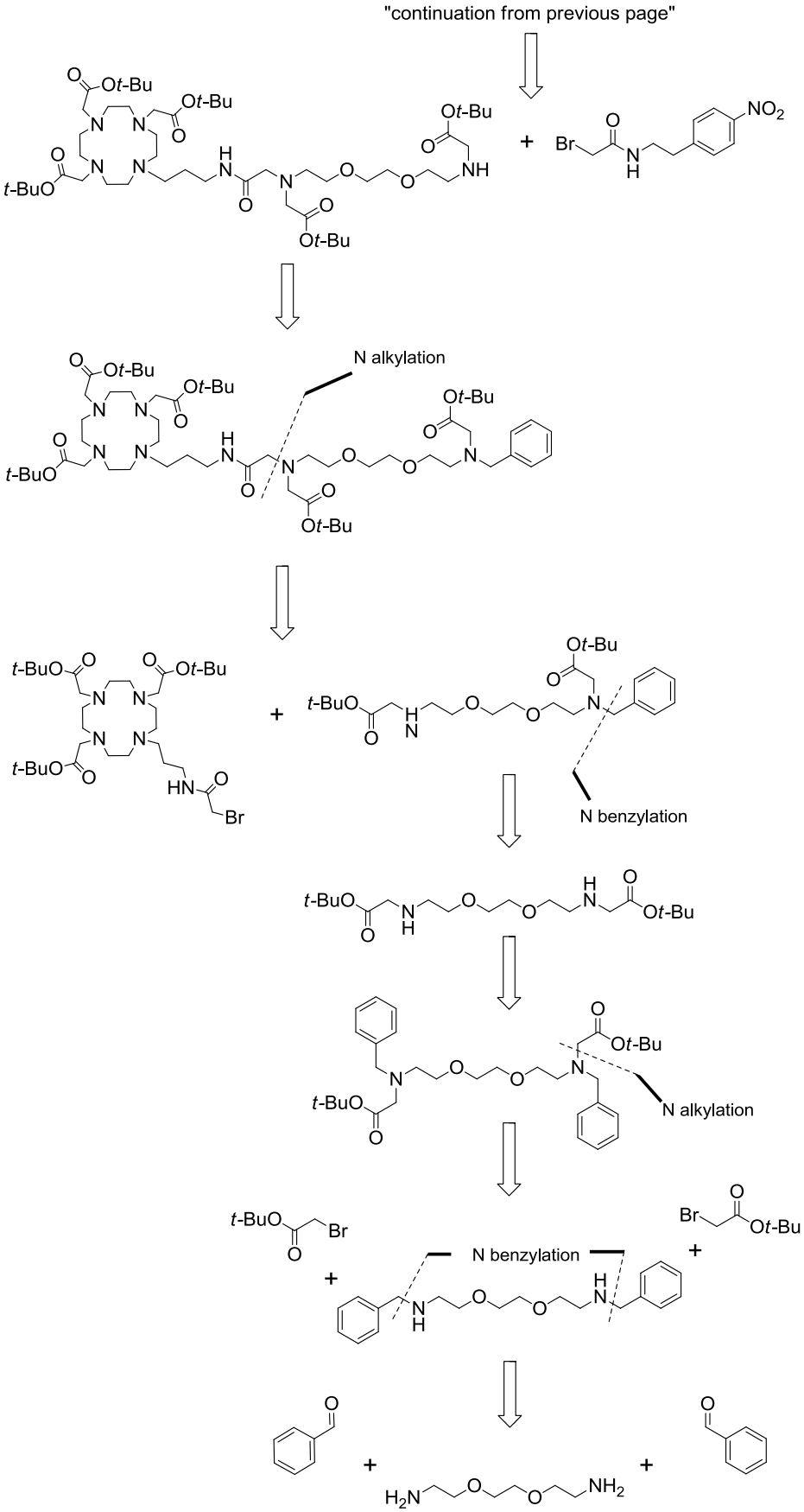

Figure 3-5. Retrosynthetic analysis for the dendrimeric SCAs.

The retrosynthetic analysis of the framework of **DSCAs** shows that DO3A derivative with bromide terminal group, modified EGTA and a bromide compound with aromatic nitro group can be prepared by sequential N-benzylation and N-alkylation reactions. After coupling of these three units, the nitro group can be reduced to amine and converted into isothiocyanate group in order to attached surface groups of dendrimer. Finally *tert*-butyl esters are hydrolyzed and Gd^{3+} ions are loaded (Figure 3-5).

3.2.2.2 Synthesis of DO3A-derived ligand (22)

Bromide **23** was synthesized as a Gd^{3+}-chelator which is attached to Ca^{2+}-chleator according to published procedures.[69, 71] Firstly amino group of 3-bromopropan-1-amine hydrochloride was protected with Cbz in the presence of potassium carbonate in water/dioxane solution to get bromide **21**. Then DO3A-*tris*-*tert*-butyl ester was alkylated with the bromide **21** in acetonitrile with potassium carbonate as a base.

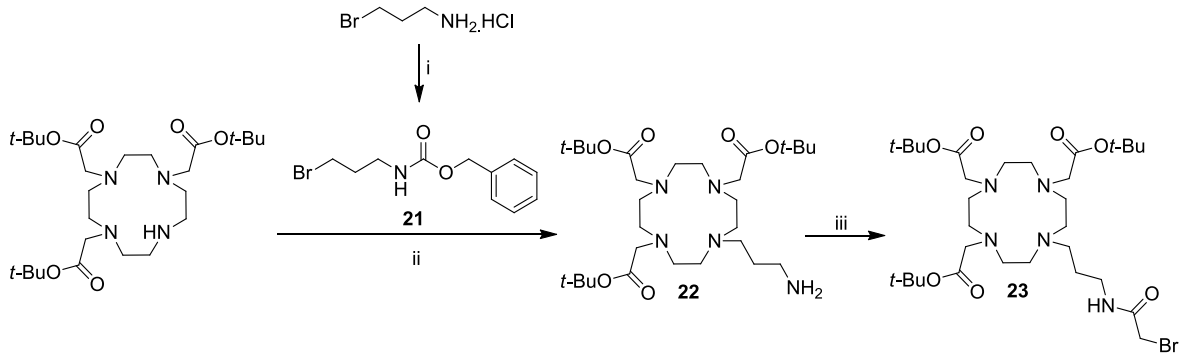

Figure 3-6. Synthetic scheme of DO3A ligand. Reagents and Conditions: (i) Benzylchloroformate, K_2CO_3, H_2O/Dioxane, rt, 1 h, 97%; (ii) 1) K_2CO_3, MeCN, 70 °C, 16 h, 2) Pd/C, EtOH, rt, 16 h, 75%; (iii) bromoacetic acid, DCC, CH_2Cl_2, rt, 1h, 79%.

After the completion of reaction, Cbz was removed by palladium catalyzed hydrogenation in ethanol to get the amine **22**. The amine **22** was acylated with bromoacetic acid to obtain bromide **23** (Figure 3-6).

3.2.2.3 Synthesis of modified EGTA (27)

Amine groups in 1,2-Bis(2-aminoethoxy)ethane were protected by benzylation with benzaldehyde in dichloromethane and reduction using sodium borohydride in ethanol to obtain **24**. After benzylation, **24** was alkylated with *tert*-butyl 2-bromoacetate to give **25**. Benzyl groups were removed by palladium hydroxide-charcoal catalyzed hydrogenation to give **26**. In order to avoid producing bismacrocycle, one of the secondary amines in **26** had to

be protected. The mono protection was performed by benzylation with chloromethyl benzene in the presence of cesium carbonate in dimethylformamide to get the amine **27** (Figure 3-7).

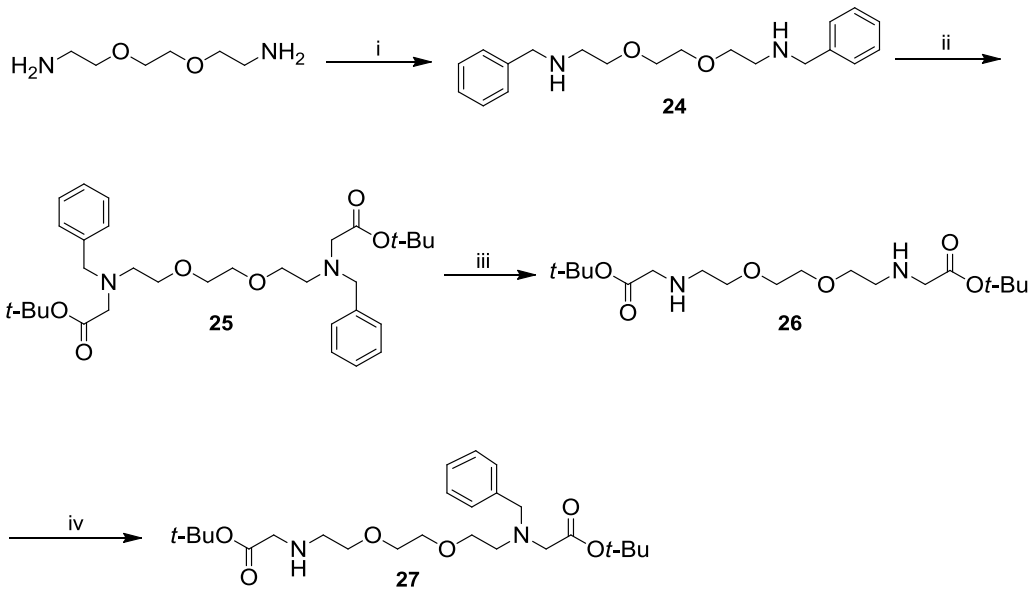

Figure 3-7. Synthetic scheme of modified EGTA (**27**). Reagents and conditions: (i) 1) Benzaldehyde, CH_2Cl_2, rt, 24 h, 2) $NaBH_4$, EtOH, 0 °C → rt, 48 h, 87%; (ii) *tert*-butyl bromoacetate, K_2CO_3, MeCN, 70 °C, 16 h, 75 %; (iii) H_2, $Pd(OH)_2/C$, EtOH, 16 h, 97%; (iv) chloromethyl benzene, Cs_2CO_3, DMF, rt, 24 h, 42%.

3.2.2.4 Synthesis of NCS ligand (33)

The synthesis of NCS ligand started with binding DO3A-ligand **22** to amine **27** in the presence of potassium carbonate in acetonitrile to get benzyl protected amine **28**. After deprotection of benzyl group by palladium hydroxide catalyzed hydrogenation, amine **29** was modified for the preparation of monomeric and dendrimeric MRI contrast agents using a linker containing NCS group. The bromide **30** was prepared by the alkylation of 4-nitrophenylethylamine with bromoacetyl bromide in dichloromethane with triethylamine as a base. Amine **29** was alkylated with bromide **30** in the presence of potassium carbonate in acetonitrile to get **31.** It was reduced to the amine **32** by palladium-charcoal catalyzed hydrogenation in ethanol. Amine **32** was converted into isothiocyanate **33** using thiophosgene with triethylamine as a base in dichloromethane (Figure 3-8). The product was characterized by high resolution mass spectroscopy and carbon and proton NMR spectroscopy.

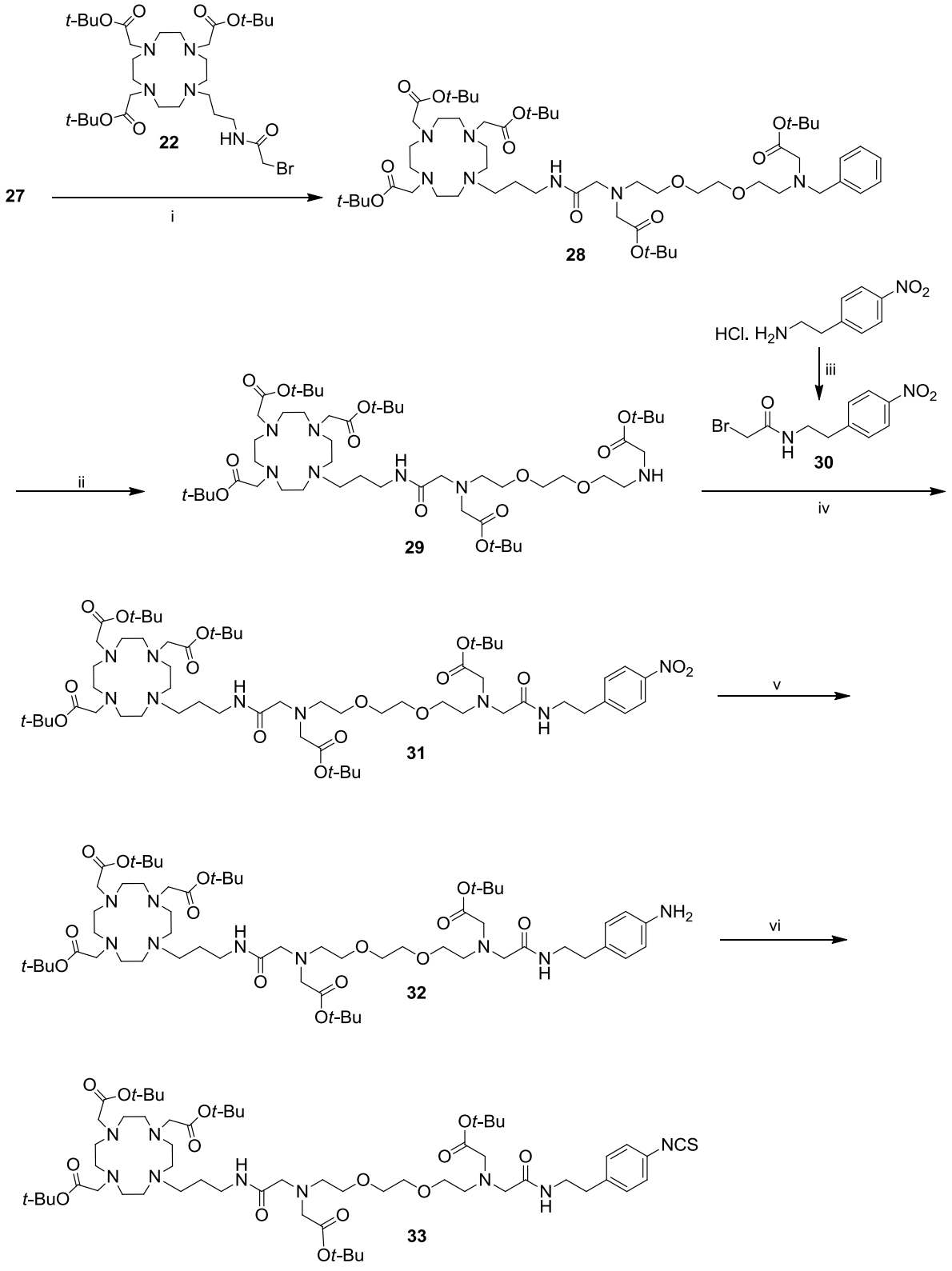

Figure 3-8. Synthetic scheme of compound **33**. Reagents and conditions: (i) K_2CO_3, MeCN, 70 °C, 24 h, 71%; (ii) H_2, $Pd(OH)_2/C$, EtOH, rt, 16 h, 95%; (iii) bromoacetyl bromide, Et_3N, CH_2Cl_2, 0 °C, 20 min, 54%; (iv) K_2CO_3, MeCN, 70 °C, 24 h, 81%; (v)H_2, Pd/C, EtOH, rt, 16 h, 97%; (vi)$CSCl_2$, Et_3N, CH_2Cl_2, rt, 2h, 58%.

3.2.2.5 Synthesis of monomeric calcium responsive/smart contrast agent (SCA-1)

SCA-1 was synthesized starting with the hydrolysis of *tert*-butyl esters of **31** by formic acid to give the acid **L-7**. Then Gd^{3+} ion was added to obtain **SCA-1** (Figure 3-9).

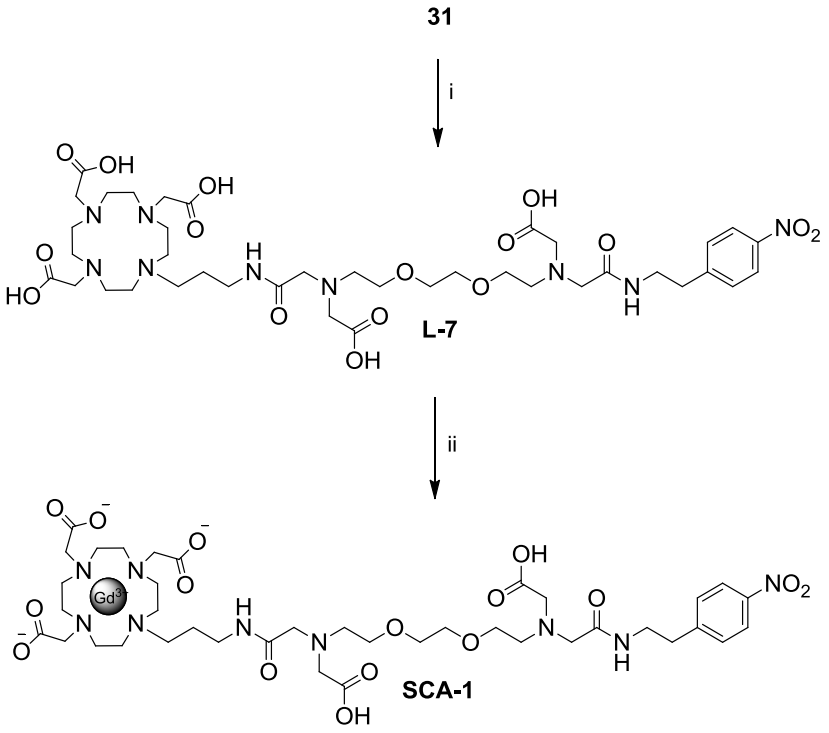

Figure 3-9. Synthetic scheme of monomeric calcium responsive MRI contrast agent. Reagents and Conditions: (i) formic acid, 60 °C, 16 h, 91%; (ii) $GdCl_3 \cdot 6H_2O$, pH 7.0, rt, 24 h, 81%.

3.2.2.6 Synthesis of dendrimeric calcium responsive/smart contrast agents (DSCAs)

All of the dendrimeric SCAs were synthesized in the same manner (Figure 3-10). Compound **33** was attached to dendrimer surface in dimethylformamide with triethylamine as a base to get **34**, **35**, **36**. Excess amount of **33** was removed using liphopilic sephadex column and methanol as eluent. Tert-butyl esters were hydrolyzed using formic acid to give dendrimeric ligand **L-8**, **L-9** or **L-10**. After evaporation of formic acid, dendrimeric ligands were eluted from G-15 sephadex column with water to remove residual formic acid and analyzed by ^1H NMR spectra. Appearance of aromatic protons in the ^1H NMR spectra is a clear evidence of the NCS ligand-dendrimer conjugate formation (these peaks do not exist in ^1H NMR spectra of the commercial PAMAM dendrimers). Then DO3A chelators of the dendrimeric ligands were complexed with Gd^{3+} using $GdCl_3 \cdot 6H_2O$ to obtain **DSCA-1**, **DSCA-2** or **DSCA-3**. EDTA was used for removing free Gd^{3+} ions, since it complexes with excess amount of Gd^{3+}

ions. The final products were purified by centrifugation using centrifugal filter unit with 3 KDa MWCO. Since integration of spectra was not reliable for dendrimeric molecules,[60] the number of EGTA ligand and Gd^{3+} content was determined by MALDI-TOF/MS (Table 3-1). The calculated masses correspond to the average of Gd^{3+} complex per dendrimer molecule, which corresponds to 88%, 50, and 56 conversion of the amino surface groups into the thiourea product with the NCS ligand, respectively.

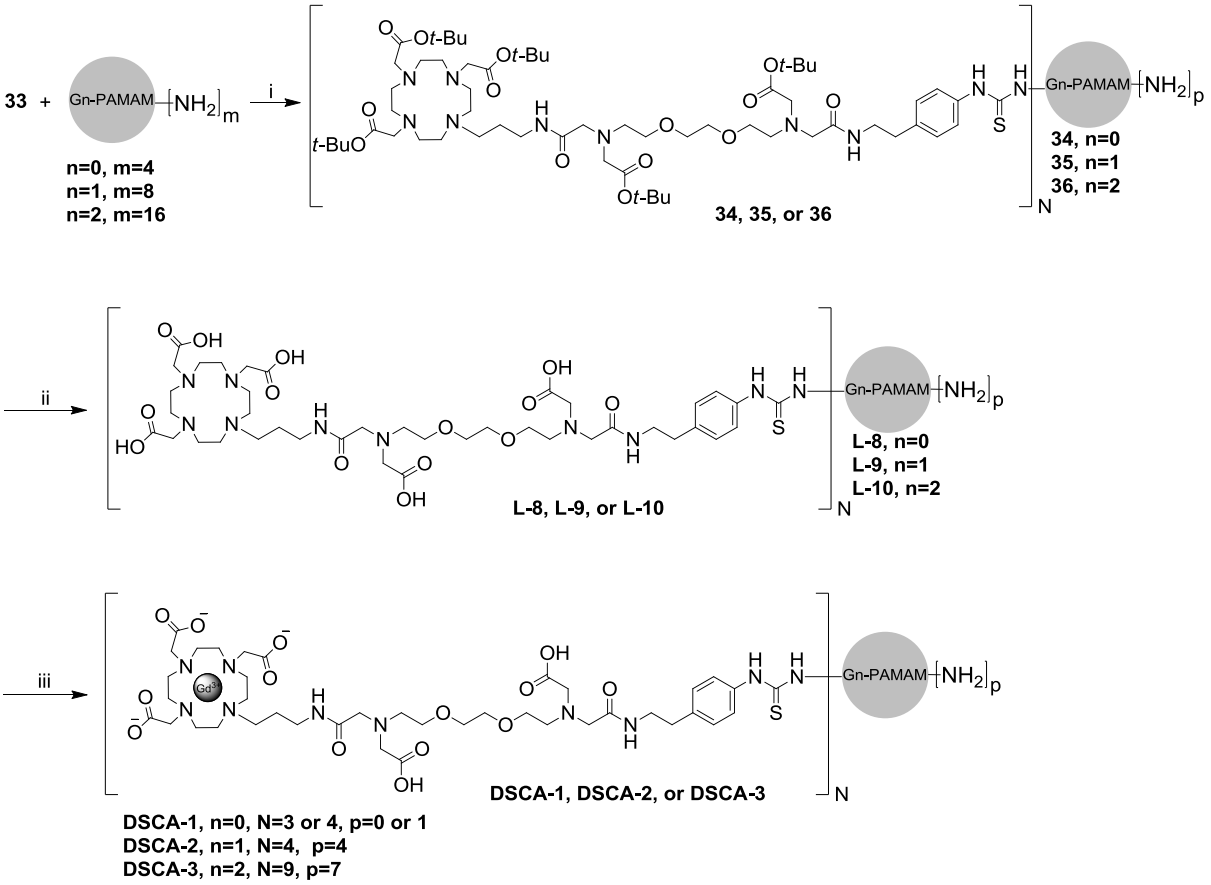

Figure 3-10. Synthetic scheme of **DSCAs**. Reagents and conditions: (i) Et_3N, DMF, 45 °C, 24 h; (ii) formic acid, 60 °C, 16 h; (iii) $GdCl_3 \cdot 6H_2O$, pH 7.0, rt, 24 h.

Table 3-1. Average number of Gd^{3+} ions on DSCAs according to MALDI-TOF/MS.

Sample	Generation of dendrimer	No. of surface groups	Av. no of Gd^{3+} ions	Loading of Gd^{3+} ions (%)
DSCA-1	0	4	3.5	88
DSCA-2	1	8	4	50
DSCA-3	2	16	9	56

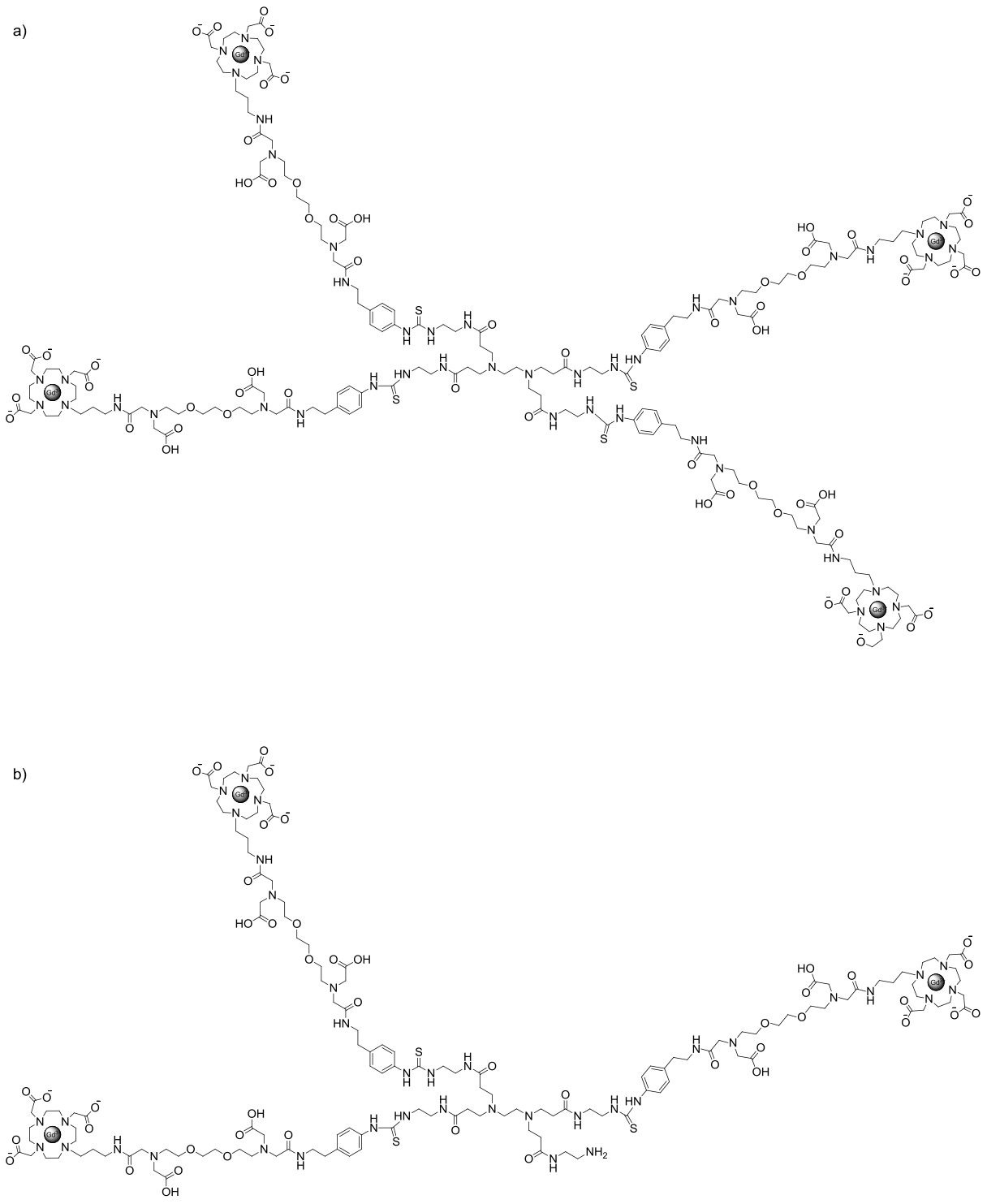

Figure 3-11. Structure of **DSCA-1**; a) with four SCAs; b) with three SCAs.

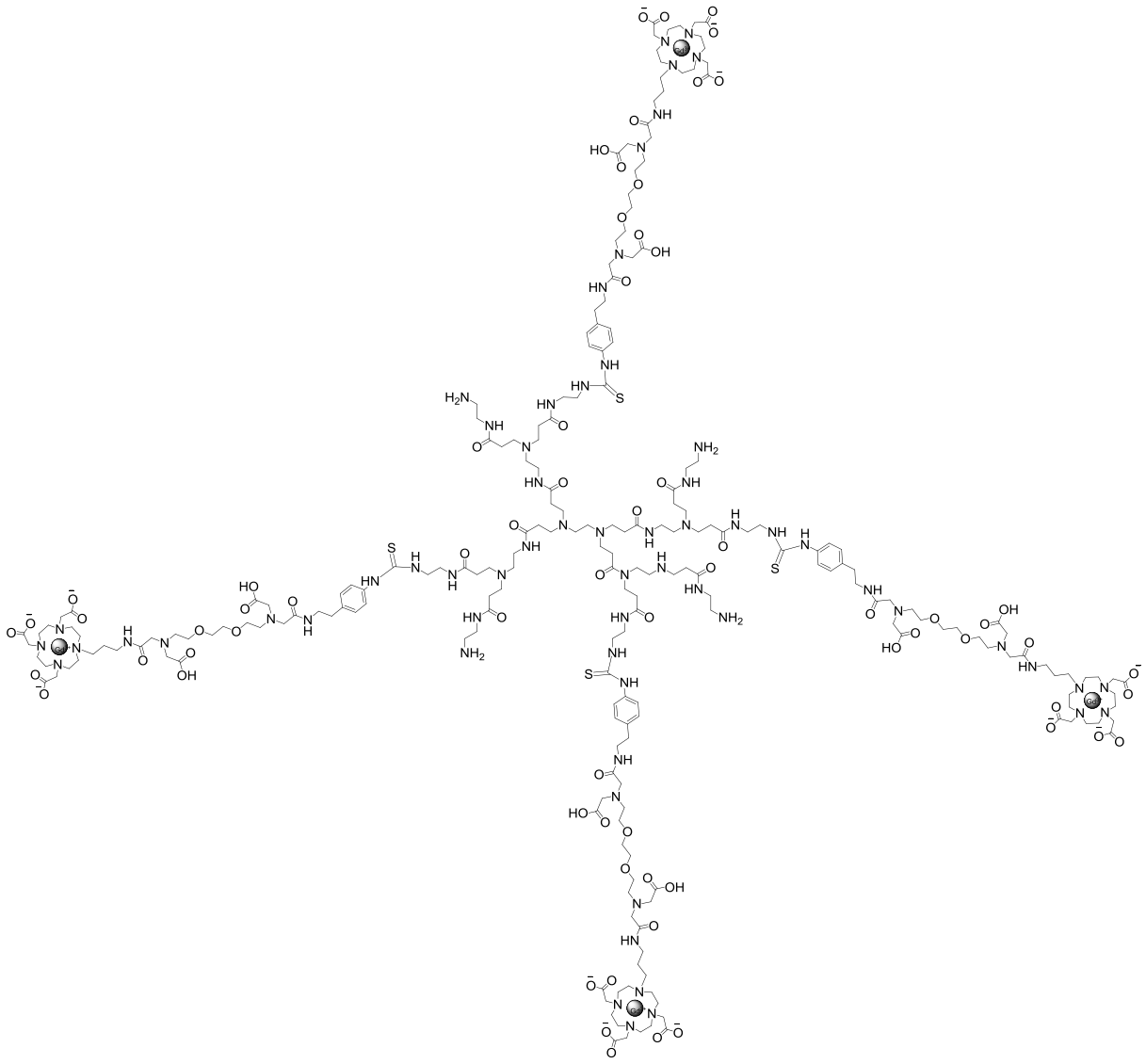

Figure 3-12. Structure of **DSCA-2** with four SCAs.

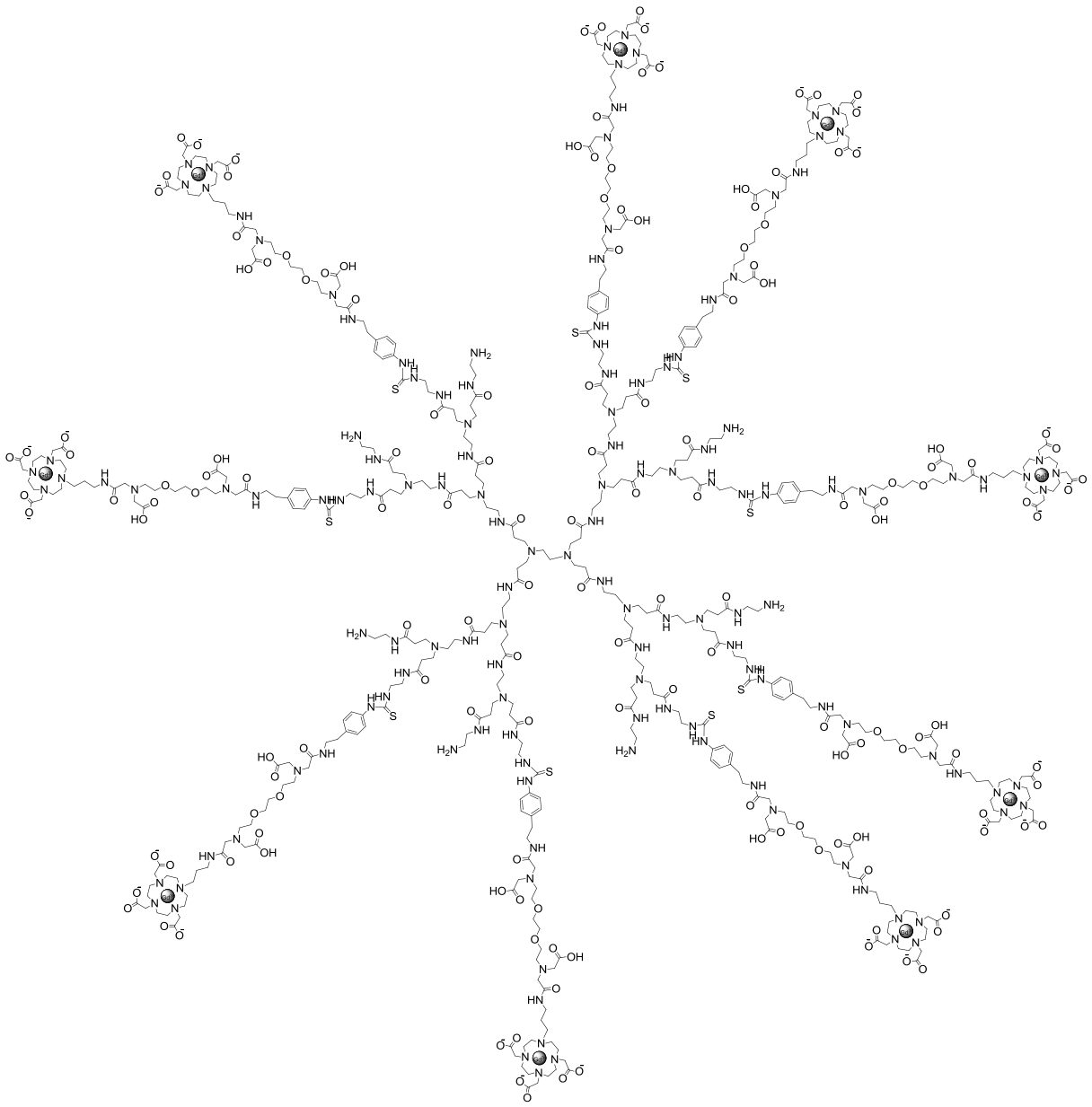

Figure 3-13. Structure of **DSCA-3** with nine SCAs.

3.2.3 Relaxometric Ca^{2+} titrations

The relaxometric titrations of **SCA-1**, **DSCA-1**, **DSCA-2**, or **DSCA-3** were performed at pH 7.4 (HEPES) at 7 T (300 MHz) and 25℃. The initial Gd^{3+} concentrations were determined by measuring the bulk magnetic susceptibility shifts.[61] 3.0 mM Gd^{3+} solutions of the complexes were used in order to determine the longitudinal relaxation times (T_1). 30 mM Ca^{2+} solution (in 0.1 equiv. portions) was added until 1.5 equiv. and 150 mM Ca^{2+} solution (in 0.5 equiv. portions) was added until 4.0 equiv. with respect to number of Gd^{3+} ions in SCA. The results of the relaxivity measurements are summerized in the Figure 3-14 and Table 3-2.

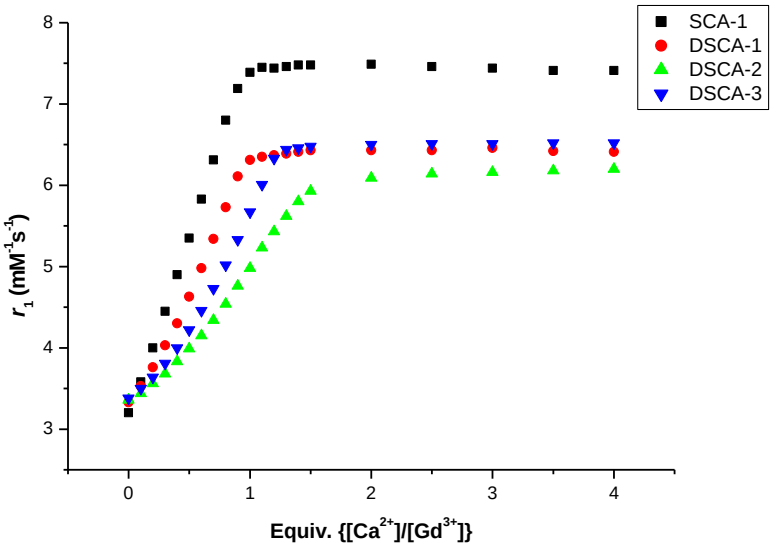

Figure 3-14. Ca^{2+} dependent relaxivity response of SCAs.

Table 3-2. r_1 changes of SCAs upon addition of Ca^{2+}

Sample	Initial r_1 ($mM^{-1}s^{-1}$)	Final r_1 ($mM^{-1}s^{-1}$)	Change (%)
SCA-1	3.20	7.45	132
DSCA-1	3.33	6.35	91
DSCA-2	3.36	6.20	84
DSCA-3	3.38	6.44	91

Before introducing Ca^{2+} to the medium, the initial r_1 relaxivities were measured. The monomeric SCA (**SCA-1**) displayed the slightly lower r_1 than the dendrimeric smart CAs.

Upon saturation with Ca^{2+}, **SCA-1** exhibited the highest r_1 enhancement over the dendrimeric CAs in the high magnetic field (7 T). **SCA-1** has less steric hindrence than the dendrimeric CAs, therefore Ca^{2+} easily coordinates to the EGTA part. The initial and final r_1 relaxivity values of DSCAs at the saturation point are close to each other. However, G1 dendrimeric CA (**DSCA-2**) showed the least relaxivity enhancement among all of the DSCAs. Intramolecular interactions and molecular conformations depending on the chemical structure of **DSCA-2** could prevent reaching Ca^{2+} to all of the calcium chelators in dendrimer. This decreases the hydration number, and thus relaxivity.

3.2.4 *In vivo* MRI experiments

In order to observe activity of SCAs in rat brain, the preliminary *in vivo* MRI experiments were performed. The experiments for each SCA were carried out in the same manner. The SCAs at same concentraion of Gd^{3+} were injected into the brain cortex (example, Figure 3-15). The T_1-weighted images were acquired at 7 T and the relative MR signal intensities were measured as a function of time elapsed from injection.

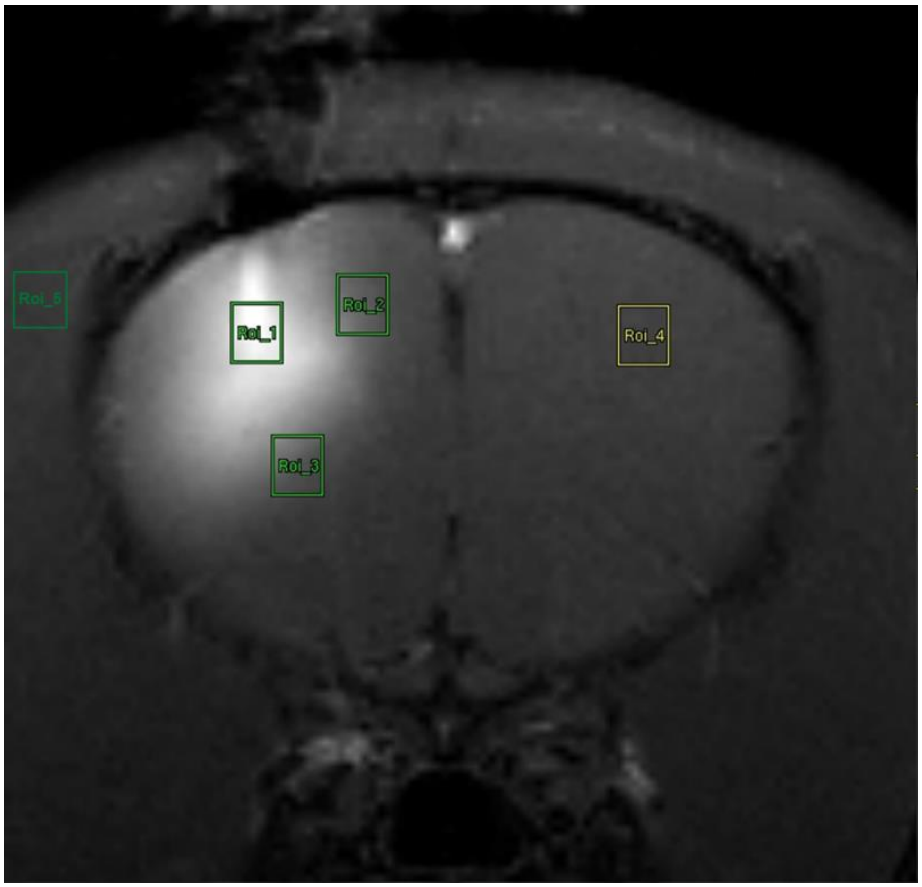

Figure 3-15. Representation for the region of interest with respect to the injection of the contrast agents to rat brain.

ROI1-ROI3 show regions where the SCAwas injected in the brain area, ROI4 shows the site which does not include SCA and ROI5 indicates the tissue outside brain. Total measurements for all MRI acquisitions were completed within approximately 4 hours. The signal intensities measured were normalized and the ROI1/ROI5 ratios for each SCA were plotted versus time in order to compare the signal intensity changes (Figure 3-16).

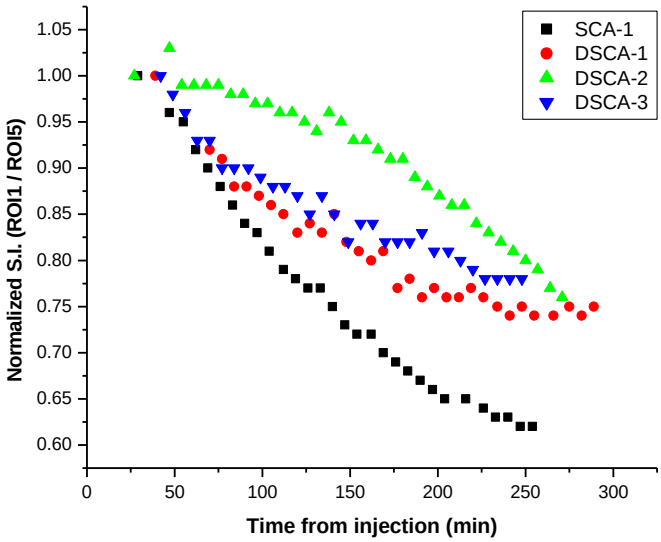

Figure 3-16. Relative MR signal intensity of the SCAs with respect to ROI1/ROI5 ratio.

The signal intensity on T_1-weighted MRI increases with the high concentrations of Gd^{3+}. In our experiment, SCAs at same concentrations of Gd^{3+} were injected. Then the signal intensity changes were measured and summerized in Table 3-3. The results showed the signal intensities of DSCAs were much higher than that of **SCA-1** after 4 hours. Since **SCA-1** has the lowest molecular weight, the signal intensity of **SCA-1** decreased faster than that of DSCAs. In the other words, since the molecular weight of **SCA-1** is lower than that of DSCAs, the diffusion and excretion of **SCA-1** are faster than that of DSCAs, as expected.

Table 3-3. Normalized signal intensity of SCAs versus time from injection

	Normalized signal intensity (%)			
Sample	after 1 h	after 2 h	after 3 h	after 4 h
SCA-1	92	78	68	63
DSCA-1	92	83	78	74
DSCA-2	99	95	91	81
DSCA-3	93	87	82	78

The concentration of extracellular Ca^{2+} changes during neuronal activity. Therefore, the measurement of Ca^{2+} concentration change is one of the important parameters for understanding of basic aspects of neuronal regulations and brain functions. For this purpose, several Ca^{2+} responsive SCAs have been developed. In the presence of high Ca^{2+} concentration, SCAs provide high signal intensity due to high r_1. However, the diffusion mechanism of CAs in the extracellular fluid is quite complicate. Hagberg *et al*. worked on an MRI-based method for determination of diffusion properties of Ca^{2+} responsive CA in rat brain.[72] Their study showed that used CAs have fast diffusion rates. When relatively high molecular weight CAs were used, slower difussion rates were observed. Therefore, in order to ensure detectability, higher amounts of CA must be injected in order to keep the concentration of CA at a stable level. As a result, their study showed that diffusion rates of high molecular weight CAs in brain indicated slower diffusion than for low molecular CAs.

The fast diffusion of low molecular weight SCAs makes difficult to obtain reliable results for quantitative Ca^{2+} determination. In our study the signal insensity values were recorded every 7 min. and the values between two sequential measurements for DSCAs were very close to each other. Therefore, DSCAs possess great application potential for the measurement of Ca^{2+} change, allowing almost constant concentration of SCA during the two consecutive measurements. If the concentration of SCA is known in extracellular fluid, it allows us to observe how Ca^{2+} concentration changes when the brain is stimulated. Additionally, DSCAs remained in a high ratio after 4 h in the region of interest when compared to monomeric **SCA-1**. Thus, DSCAs allows longer time for MRI scans.

In future studies, the effective *in vivo* diffusion of our SCAs can be assigned and thus the local calcium concentration can be quantitatively determined using the diffusion properties of SCAs.

3.3 Conclusion

Three dendrimeric Ca^{2+} responsive MRI CAs with different dendrimer generations and a monomeric analogue were synthesized to sense Ca^{2+} concentration changes in the extracellular matrix of the brain following neural activity. Since dendrimeric SCAs are high molecular weight molecules, they remained in the region of interest longer than low molecular weight SCA. The relaxometric Ca^{2+} titrations showed that all of the SCAs exhibited higher r_1 relaxivity than their initial state after addition of Ca^{2+}. While the monomeric SCA had the highest relaxivity change among all of the SCAs, the G1 DSCA had the highest relaxivity changes among all of the DSCAs. *In vivo* MRI experiments in rat brains showed that after the injection of SCAs, the DSCAs diffused from the region of interest at a slower rate than the monomeric SCA, as expected. In addition, the DSCAs provided higher MR signal intensity than monomeric SCA. The slow diffusion rate of DSCAs allows longer scan times at constant CA concentration, use of lower SCA dose, and also provides higher quality MR images. The efficacy of these Ca^{2+} responsive CAs can be further improved modifying the Ca^{2+} chelator part and Gd^{3+} complex or using higher generation dendrimers.

4. Summary, conclusions and outlook

This thesis describes the development of novel multimodal and multivalent CA targeted to the protein (Neutr/strept) avidin and multivalent Ca^{2+} responsive CAs for MR neuroimaging.

The developed TCA includes biotin which is specifically binds the targeting unit protein avidin, FITC as a fluorescent dye for in *vitro* characterization, lysine as a core molecule and G4 PAMAM dendron as a multivalent scaffold. It has also one biotin per molecule allowing the comparison of the binding ability with the biotinylated agents. Altough high generation dendrimeric CA leads to less binding efficiency, it provided high signal intensity due to carrying multiple copies of Gd^{3+} complexes. In addition to dendrimeric CA (**DCA-2**), its monomeric analogue (**MCA-2**) was synthesized for the comparison of avidin-binding, MRI and relaxometric behaviors.

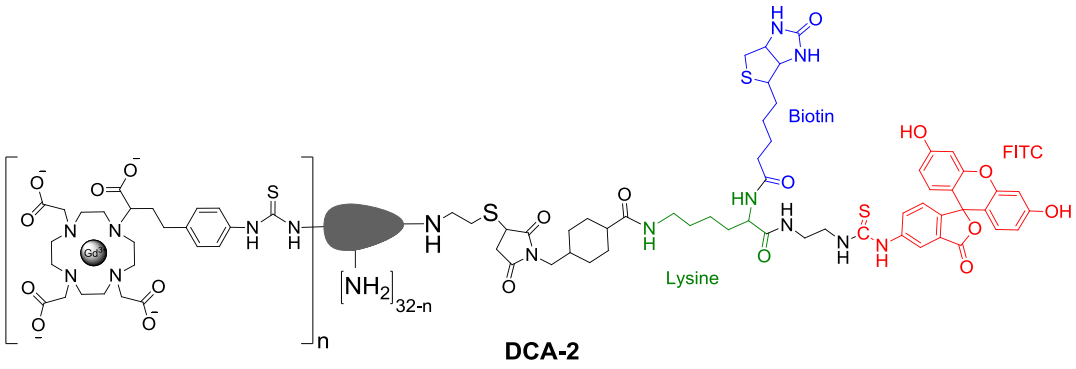

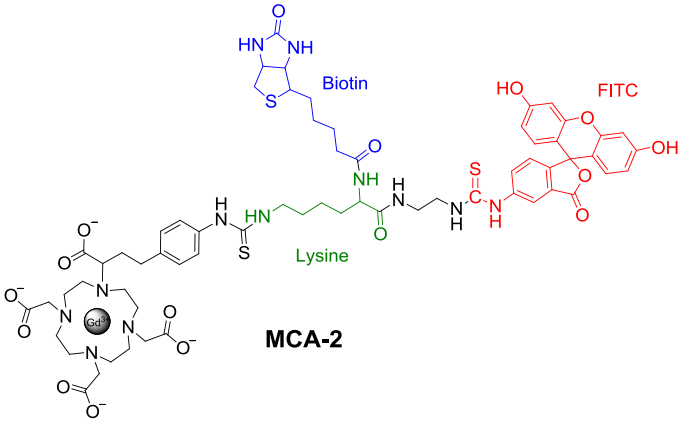

Avidin beads binding assay was performed to observe binding ability of targeted CAs synthesized. *In vitro* fluorescent experiments showed **MCA-2** binds to avidin beads 3.6 times stronger than **DCA-2**. As expected, monomeric analogue **MCA-2** efficiently binds avidin beads when compared to **DCA-2**. Unlike fluorescent intensity, the beads bound **DCA-2** provided brighter MR images than **MCA-2**. The MRI experiments with avidin-coated agarose gel beads showed remarkable signal enhancement of **DCA-2**, providing a promising

application outlook for targeted CA based on this approach. Quantitavively, **DCA-2** has nearly 5.0 times higher MR signal intensity than **MCA-2**.

A number of diverse applications could be envisaged for these targeted probes to investigate living systems. In one possible implementation, the polypeptide target avidin could be encoded as a transgene, manipulated using molecular biology and introduced into living cells of model organisms. For example, a fusion between avidin and a membrane-associated protein can be generated for expression on the outer surface of the cell as a receptor for targeted agents. [73-77]. By deploying genetically-engineered target receptors with the available strategies for spatiotemporal control of transgene expression (e.g. tissue-specific or inducible promoters), the corresponding CA could be used to study the development, physiology or pathology of specific cell types and tissues in multimodal high field MRI-optical experiments.

In the second project, the dendrimeric smart contrast agents **DSCA-1**, **DSCA-2**, and **DSCA-3** were prepared. The monomeric agent **SCA-1** with nitro terminal group was also synthesized for the comparison the relaxometric and *in vivo* MRI behavior. All of CAs contain EGTA derivative which is a Ca^{2+} selective group linked to Gd-DO3A complex. In order to couple **SCA-1** to amino surface groups of dendrimer, the nitro group of the ligand of **SCA-1** was converted into the isothiocyanate group using thiophosgene. In the presence of Ca^{2+}, the r_1 values of all SCAs increased. **SCA-1** showed the highest r_1 change (132%) and **DSCA-2** showed the lowest r_1 change (70%).

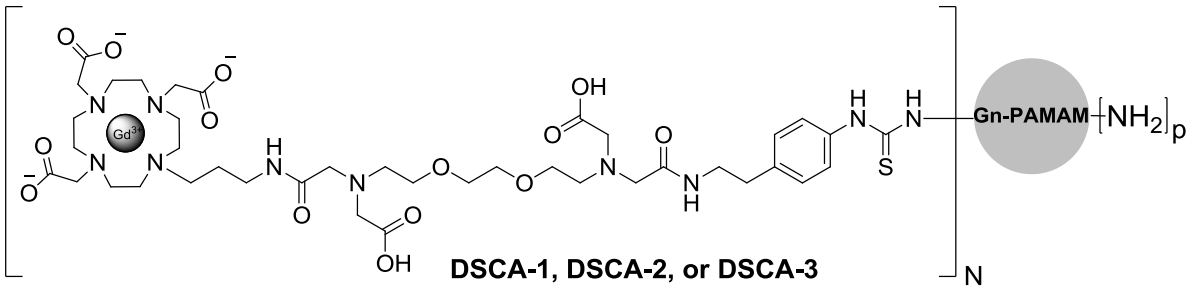

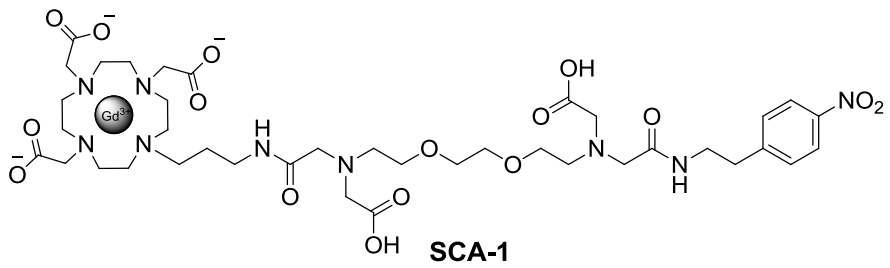

In vivo experiments in rat brain showed that **DSCA-2** provided the highest, and **SCA-1** provided the lowest MR signal intensity among all of the SCAs. Additionally dendrimeric SCAs provides higher MR signal and stay longer in the region of interest than monomeric SCA. In future, dendrimeric SCAs can be used as a new class of Ca^{2+} responsive MRI CAs by optimizing their structural features. These DSCAs can be developed not only for Ca^{2+}-responsive CAs, but also it can be applied for other cation (e.g. Zn^{2+}, Fe^{3+}) responsive CAs. For this purpose the EGTA part can be replaced with a desired cation selective ligand.

In conclusion, we successfully synthesized multimodal and dendrimeric targeted CA and responsive CAs. *In vitro* and *in vivo* experiments in these studies confirmed that dendrimeric CAs are more efficient than their monomeric analogues in MRI. Improvement of efficiency in the synthesis of dendrimeric contrast agent can increase their availability for clinical applications. Additionally, the properties of dendrimers such as water solubility, biocompability, non-toxicity, internal cavities and monodispersity make them ideal candidates as carriers of CAs in MRI applications.

5. Experimental section

5.1 Materials and methods

All commercially available chemicals used without further purification. DO3A-*tris*-*tert*-butyl ester was purchased from Click Chemistry Technology, Beijing, China. Biotin and H-Lys(Boc)-OMe hydrochloride, lipophilic sephadex and G-15 sephadex were purchased from Sigma-Aldrich, Gemany.Fluorescein isothiocyanate (FITC) was purchased from Biomol, Germany. SMCC was purchased from Shangai YFan Chemistry Co., Ltd., Shanghai P.R.China. Cys PAMAM G4 was purchased from Dendritic Nanotechnologies Inc., USA.*Tert*-butyl 2-bromo-4-(4-nitrophenyl)butanoate was prepared according to the literature procedure. Avidin-coated microspheres were purchased from Thermo Fisher Scientific Inc., USA. NeutrAvidin™-agarose gel was purchased from Life Technologies Co., Invitrogen™, USA . Water was purified using a Milipore Milli-Q Synthesis purifier.

5.1.1 Chromotography

Aluminium sheet 0.2-mm-thick silica gel 60 F254 plates (E. Merck, Germany) were used for thin-layer chromatography. The compounds were visualized by UV_{254} light. In order to visualize the invisible compounds under UV light, phosphomolybdic acid, Dragendorff reagent and ninhydrin solutions were used.

5.1.2 Mass spectroscopy

ESI-MS analysis was performed by a Agilent SL 1100 system, Germany. FT-ICR-MS analysis was performed by a Bruker FT-ICR Apex II spectrometer, Germany. ESI-TOF-MS analysis was performed by MAXIS 3G, Bruker Daltonics Inc., Germany. MALDI-TOF-MS analysis was performed by The Scripps Center for Mass Spectrometry, La Jolla, CA. ICP-MS experiments were performed by Currenta GmbH& Co. OHG, Leverkusen, Germany.

5.1.3 NMR spectroscopy

^{1}H, and ^{13}C- NMR spectra were performed on a Bruker Avance III 300 MHz spectrometer, Germany.

5.1.4 Binding of contrast agents to NeutrAvidin™ agarose beads

Packed beads were incubated with 1 mM contrast agent (in 0.01M PBS pH 7.4) for 30 min at 4 °C with rotary shaking. Excess CA was removed and the beads were washed by repeated

centrifugation and re-suspension in PBS. After the final wash step supernatant was removed and packed beads were kept for MRI scanning and subsequent analyses as described in table 6-1.

5.1.5 Fluorescence microscopy

Microscopic images were acquired using the AxioImager. Z1 upright microscope (Zeiss) equipped with an AxioCamHR3 (Zeiss) camera. Images were acquired over identical exposure times across all samples and exported as 16-bit grayscale, 1388 x 1040 pixel TIFF format files.

5.1.6 Fluorescence images of CA-treated NeutrAvidin^{TM} agarose beads

Fluorescent imaging was carried out by placing beads on a SafeImager 2.0 blue (470nm) LED source transilluminator equipped with the supplied amber emission filter. Images were captured with a digital camera and cropped around a region containing the samples using Photoshop CS5 software.

5.1.7 Processing of T_1-weighted MR images for display purposes

The 32-bit grayscale images files (2Dseq format) generated by the Bruker scanner Paravsion software were opened using the ImageJ (ver 1.47d, Fiji package) image processing software. The images were converted to 8-bit files using the "Image-Type-8-bit" command and saved as TIFF format using the "File-Save As" command. The TIFF images were opened with Adobe Photoshop CS5 and rotated 90° clockwise.

5.1.8 Quantitative analysis of T_1-weighted MR images

The original T_1-weighted images generated by the Paravision software (32-bit, 2Dseq format images files) were opened in the ImageJ (ver 1.47d, Fiji package) analysis software. A circular ROI was manually placed around each bead/CA sample outlining the largest possible diameter fitting within the walls of the sample tube, in order to maximize the number of pixels sampled for calculation (1000-1500 pixels). The ImageJ function "Analyze-Measure" was used to calculate the mean pixel intensity and total number of pixels within the ROI. Mean pixel intensities were exported into spreadsheets for further analysis.

5.1.9 ICP-MS determination of Gd^{3+} associated with CA-treated NeutrAvidin™ agarose beads

Equal volumes of the CA-treated NeutrAvidin™ agarose samples were digested with 26% Nitric Acid at 50 °C for 72 h to release chelated Gd^{3+} into solution. The Gd^{3+} concentration was quantified by ICP-MS at Currenta GmbH & Co. (Leverkusen, Germany).

5.1.10 Procedure for MRI scans

For MRI, the 2 ml Eppendorf tubes containing Neutravidin™ agarose bead/CA sample were placed in a 1% Agar solution to avoid susceptibility distortions. Imaging was performed on a 7 T Bruker BioSpec 70/30 scanner, equipped with a BGA-12S gradient insert using a commercial quadrature volume resonator, Bruker 1H 112/086 QSN. For data acquisition a multislice spin-echo sequence (MSME) was used for imaging. T_1-weighted saturation recovery MSME images were performed with a series of varying repetition times and contrast, through the transverse and longitudinal planes of the sample tubes. Acquisition parameters were field of view 4x4cm^2, matrix 200x200, one axial 2mm slice, TE=6ms and TR=21-8000ms (logarithmic steps, 30 images). For longitudinal images the field of view was 4x6cm^2, matrix 200x300 and two slices.

5.1.11 *In vivo* MRI measurement

Normal male Wistar rats (234.4 ± 21.7 g body-weight, 9–11 weeks) were used for MRI experiments. The *in vivo* MRI acquisitions were performed using a 7-T, 40 cm bore MRI magnet (Kobelco and Jastec, Kobe and Tokyo, Japan) interfaced to a Bruker console (BioSpec Avance-I, Bruker Biospin, Ettlingen, Germany). A volume resonator (72 mm inner diameter, transmission, Bruker Biospin) and quadrature surface reception coil (rat brain coil, Rapid Biomedical, Rimpar, Germany) was used.

Prior to the MRI scan, all rats were anesthetized with 2.0% isoflurane (Abbott Japan, Japan). Samples were intracerebrally administrated into the cortex (bregma +1 mm frontal, +3 mm right side, and 1.5 mm depth) using a stereotaxic apparatus (Narisige, Tokyo, Japan) and micro-syringe (Hamilton Company, Nevada, USA). Rectal temperature was continuously monitored and maintained at 37.0 ± 0.5 °C using a heater throughout the experiments. During the MRI scan, the rats were held in place with the help of a handmade ear/bite bar and anesthetized through a facemask with 2% isoflurane.

Prior to MRI acquisitions, scout images were acquired to localize the imaging plain. Imaging registration was carefully adjusted to the injected site based on scout scan. MRI acquisitions were performed following order: one acquisition of T_1-weighted image (T_1WI), one acquisition of diffusion-weighted image (DWI), repeated 29 acquisitions of T_1WI, and one acquisition of DWI. Total measurement time for all MRI acquisitions was approximately 4 hours. The first T_1WI scan began 20 minutes after the intracerebral administration typically.

For the T_1WI, a two-dimensional (2D), single-slice image was obtained using a conventional spin-echo sequence with the following parameters: repetition time (TR) = 400 ms, echo time (TE) = 9.6 ms, matrix size = 256 × 256, field of view (FOV) = 32.0 × 32.0 mm^2, slice thickness (ST) = 1.0 mm, number of acquisitions (NA) = 4, and slice orientation = trans-axial. For this imaging sequence, the nominal voxel resolution was 125× 125 × 1000 µm. The total acquisition time for the T_1WI was 6 min and 42 s. For the DWI, 2D, single-slice diffusion-weighted spin-echo sequence was used with the following parameters: TR = 2500 ms, TE = 27 ms, matrix size = 128 × 128, FOV = 32.0 × 32.0 mm^2, ST = 1.0 mm, NA = 1, b value = 0 and 1000 s/mm^2, gradient strength (G) = 0 or 200 mT/m, gradient duration (δ) = 7 ms, interval between the gradient pulse onsets (Δ) = 14 ms, and slice orientation = trans-axial. The total acquisition time for the DWI was 10 min and 40 s. All calculations and analyses were performed using the ParaVision (Bruker Biospin).

5.2 Synthetic procedures of compounds

methyl 6-((tert-butoxycarbonyl)amino)-2-(5-(2-oxohexahydro-1H-thieno[3,4-d]imidazol-4-yl)pentanamido)hexanoate (1)

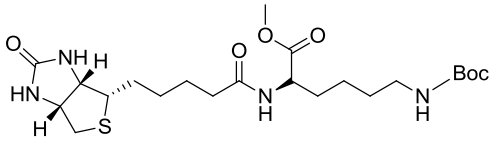

Biotin (3.37 mmol, 0.82 g), EDC·HCl (5.05 mmol, 0.97 g), and DMAP (8.42 mmol, 1.03 g) were dissolved in dimethylformamide (25 mL). H-Lys(Boc)-OMe hydrochloride (3.37 mmol, 1.00 g) was added to the mixture. The reaction mixture was stirred under nitrogen at room temperature for 48 h. The solvent was evaporated and the residue was poured into water (100 mL) and extracted with dichloromethane (3x100 mL). The collected organic phases were dried over sodium sulfate and evaporated under reduced pressure. The crude product was purified by column chromotography (silica gel, 10% methanol/dichloromethane) to give **1** as colorless solid (1.05 g, 64%).

^{1}H NMR (300 MHz, $CDCl_3$): δ 4.86−4.68 (br, 1H; SCH_2CHNH), 4.57−4.40 (br, 1H), 4.37−4.22 (br, 1H), 3.71 (s, 3H; $NHCHCOOCH_3$), 3.19−2.97 (br, 2H; $CH_2NHCOOC(CH_3)_3$), 2.90 (dd, *J*=12.8, 4.8 Hz, 1H; SCH_2CHNH), 2.71 (d, *J*=12.8 Hz, 1H; SCH_2CHNH), 2.24 (br, 2H; CH_2CONH), 1.86−1.56 (br, 6H; $CH_2CH_2CH_2CONHCHCH_2$), 1.54−1.25 (br, 15H; $SCHCH_2$ and $CH_2CH_2CH_2NHCOOC(CH_3)_3$).

^{13}C NMR (75 MHz, $CDCl_3$): δ 173.9, 173.5, 164.4, 156.1(*C*=O), 79.0 ($C(CH_3)_3$), 61.9, 60.2, 55.9 (*C*H ring), 52.2 ($NHCHCOOCH_3$), 52.0 ($NHCHCOOCH_3$), 40.4, 40.1, 35.4, 31.4, 29.5 ($-CH_2-$), 28.4 ($C(CH_3)_3$), 28.2, 27.9, 25.4, 22.7 ($-CH_2-$).

ESI-TOF/MS (m/z): $[M+Na]^+$ calcd. for $C_{22}H_{38}N_4NaO_6S^+$, 509.2404; found 509.2398.

***tert*-butyl (6-((2-aminoethyl)amino)-6-oxo-5-(5-(2-oxohexahydro-1H-thieno[3,4-d]imidazol-4-yl)pentanamido)hexyl)carbamate (2)**

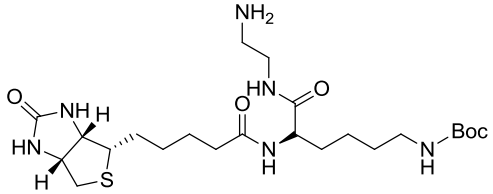

Compound **1** (1.00 g, 2.06 mmol) was dissolved in methanol (10 mL). Ethylenediamine (1 mL, 14.98 mmol) was added into the solution. The reaction mixture was kept at room

temperature for 24 h. The crude product was washed with ethylacetate to remove excess ethylenediamine and yield **2** as colorless solid (0.81 g, 77%)

^{1}H NMR (300 MHz, $CDCl_3$): δ 4.69–4.06 (br, 3H; SCH_2CHCH and $NHCHCONH$), 3.85–2.68 (br, 9H; CH_2SCH, $NH_2CH_2CH_2NH$ and CH_2NHCOO), 2.45-2.00 (br, 2H; CH_2CONH), 1.97−1.13 (br, 21H; $–CH_2–$ and $C(CH_3)_3$).

^{13}C NMR (75 MHz, $CDCl_3$): δ 176.3, 174.9, 174.4, 165.1(*C*=O), 62.1, 60.7 55.1 (*C*H ring), 54.5 (HNC*H*CONH), 40.2, 40.0, 39.9, 37.2, 34.9, 30.7 ($–CH_2–$), 29.1 ($C(CH_3)_3$), 28.3, 27.5, 25.2, 22.6 ($–CH_2–$).

ESI-TOF/MS (m/z): $[M+H]^+$ calcd. for $C_{23}H_{43}N_6O_5S$,515.3010; found 515.3008.

***tert*-butyl (6-((2-(3-(3',6'-dihydroxy-3-oxo-3H-spiro[isobenzofuran-1,9'-xanthen]-5-yl)thioureido)ethyl)amino)-6-oxo-5-(5-(2-oxohexahydro-1H-thieno[3,4-d]imidazol-4-yl)pentanamido)hexyl)carbamate (3)**

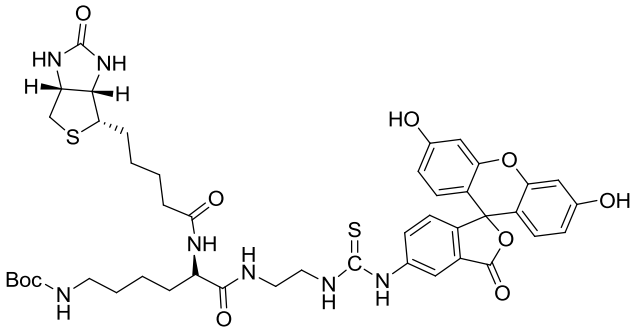

Compound **2** (0.51 mmol, 0.26 g), fluorescein isothiocyanate (0.61 mmol, 0.24 g) and triethylamine (0.72 mmol, 0.10 mL) were dissolved in dimethylformamide (5 mL). The reaction mixture was stirred overnight at room temperature. The solvent was evaporated. The residue was purified by flash column chromotography (silica gel, gradient 10% to 20% methanol/dicholoromethane) to yield **3** as orange solid (0.40 g, 88%).

^{1}H NMR (300 MHz, CD_3OD): δ 7.78 (d, *J*=7.8 Hz, 1H; Ar*H*), 7.54 (s, 1H; Ar*H*), 7.15 (d, *J*=8.2 Hz, 1H; Ar*H*), 6.92 (d, *J*=8.6 Hz, 2H; Ar*H*), 6.66 (d, *J*=2.4 Hz, 2H; Ar*H*), 6.57 (dd, *J*=9.0, 2.5 Hz, 2H; Ar*H*), 4.50−4.40 (br, 1H; SCH_2CHCH), 4.32−4.16 (br, 2H; SCH_2CHCH and $NHCHCONH$), 3.89-3.63 (br, 2H; $NHCH_2CH_2NHCSNH$), 3.56−43.32 (br, 3H; $SCHCH$ and $CH_2NHCOOC(CH_3)_3$), 3.18–3.07 (br, 1H; SC*H*), 2.87 (dd, *J*=12.9, 5.0 Hz, 1H; SCH_2), 2.66 (d, *J*=12.9 Hz, 1H; SCH_2), 2.35−2.12 (br, 2H; $CH_2CONHCHCONH$), 1.85−1.51 (br, 6H; $–CH_2–$ and $C(CH_3)_3$), 1.50−1.27 (br, 16H).

^{13}C NMR (75 MHz, CD_3OD): δ 181.0 (*C*=S), 174.4, 173.3, 169.7, 162.9 (*C*=O), 159.9, 156.5, 152.6, 147.1, 140.3, 130.2, 128.9, 127.4, 124.3, 118.9, 112.5, 109.9, 102.4 (Ar*C*), 78.8

(*C*(CH_3)$_3$), 61.5, 61.4, 59.8, 55.1, 53.32, 43.6, 41.9, 39.8, 39.5, 38.4, 36.2, 34.8, 31.0, 28.9 (–*C*H– and –*C*H_2–), 27.8, 27.6, 27.5 (C(*C*H_3)$_3$), 25.0, 22.5 (–*C*H_2–).

ESI-TOF/MS (m/z): $[M+H]^+$ calcd. for $C_{44}H_{54}N_7O_{10}S_2^+$, 904.33681; found 904.33781.

6-amino-N-(2-(3-(3',6'-dihydroxy-3-oxo-3H-spiro[isobenzofuran-1,9'-xanthen]-5-yl)thioureido)ethyl)-2-(5-(2-oxohexahydro-1H-thieno[3,4-d]imidazol-4-yl)pentanamido)hexanamide (4)

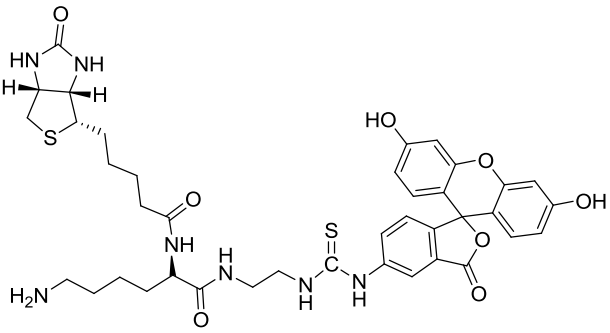

Compound **3** (0.28 mmol, 0,25 g) was dissolved in methanol (5 mL) and conc. HCl (5 mL) was added to the solution. The reaction was kept at room temperature for 1 h. The solvent was evaporated under reduced pressure to get **4** as orange solid (0.22 g, 97%).

^{1}H NMR (300 MHz, CD_3OD): δ 7.78 (d, *J*=7.8 Hz, 1H; Ar*H*), 7.54 (s, 1H; Ar*H*), 7.15 (d, *J*=8.2 Hz, 1H; Ar*H*), 6.92 (d, *J*=8.6 Hz, 2H; Ar*H*), 6.66 (d, *J*=2.4 Hz, 2H; Ar*H*), 6.57 (dd, *J*=9.0, 2.5 Hz, 2H; Ar*H*), 4.50−4.40 (br, 1H; SCH_2CHCH), 4.32−4.16 (br, 2H; SCH_2CHCH and NHC*H*CONH), 3.89-3.63 (br, 2H; $NHCH_2CH_2NHCSNH$), 3.56−43.32 (br, 3H; SC*H*CH and $CH_2NHCOOC(CH_3)_3$), 3.18–3.07 (br, 1H; SC*H*), 2.87 (dd, *J*=12.9, 5.0 Hz, 1H; SCH_2), 2.66 (d, *J*=12.9 Hz, 1H; SCH_2), 2.35−2.12 (br, 2H; $CH_2CONHCHCONH$), 1.85−1.51 (br, 6H; –CH_2– and C(CH_3)$_3$), 1.50−1.27 (br, 16H).

^{13}C NMR (75 MHz, CD_3OD): δ 183.2 (*C*=S), 176.6, 175.1, 172.7, 167.8 (*C*=O), 160.7, 143.7, 134.4, 132.7, 131.6, 127.9, 126.7, 121.2, 118.4, 103.5 (Ar*C*), 63.9, 62.4, 57.1, 55.2, 44.9, 41.1, 40.6, 40.5, 36.5, 34.7, 32.4, 29.8, 29.7, 29.5, 28.2, 26.8, 26.0, 24.2 (–CH– and –CH_2–).

ESI-TOF/MS (m/z): $[M+H]^+$ calcd. for $C_{39}H_{46}N_7O_8S_2^+$, 804.2844; found 804.2839.

2-chloro-N-(4-nitrobenzyl)acetamide (5)

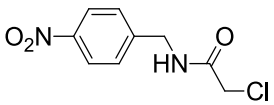

4-nitrobenzylamine hydrochloride (2.00, 10.60 mmol) was dissolved in a mixture of dichloromethane (25 mL) and triethylamine (3.70 mL, 26.15 mmol). 2-chloroacetyl chloride (0.75 mL, 15.91) was dissolved in dichloromethane (10 mL) and added over a period of 30 min to the solution at -8 °C under inert atmosphere. The reaction mixture was kept at 0 °C for 30 min., then it was kept at room temperature for 2 h. The solvent and excess 2-chloroacetylchloride were evaporated under reduced pressure. The residue was dissolved in dichloromethane (100 mL) and extracted with water (2x100 mL). After the extraction, dichloromethane was evaporated under reduced pressure and **5** was obtained as yellow solid (2.24, 92%).

^{1}H NMR (300 MHz, $CDCl_3$): δ 8.16 (d, *J*=9.0 Hz, 2H; Ar*H*), 7.44 (d, *J*=9.0 Hz, 2H; Ar*H*), 4.59 (d, *J*=6.1 2H; ArCH_2NH), 4.06 (s, 2H; COCH_2Cl).

^{13}C NMR (75 MHz, $CDCl_3$): δ 166.3(*C*=O), 128.2, 123.9, 144.9, 147.3 (Ar*C*), 43.0 (Ar*C*H_2NH), 42.5(CO*C*H_2Cl).

ESI-MS (m/z): $[M+Na]^+$ calcd. for $C_9H_9ClN_2NaO_3^+$, 251.0; found 251.0.

***tri-tert*-butyl 2,2',2''-(10-(2-((4-nitrobenzyl)amino)-2-oxoethyl)-1,4,7,10-tetraazacyclododecane-1,4,7-triyl)triacetate (6)**

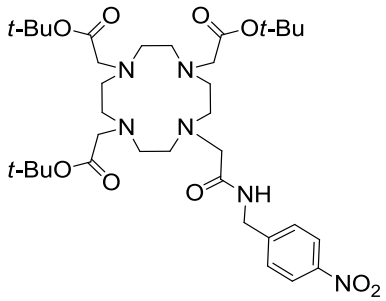

Potassium carbonate (2.42g, 17.5 mmol) was added to a solution of DO3A-tert-butyl ester (2.51 g, 4.88 mmol) in dimethylformamide (25 mL) under nitrogen. A solution of the chloride **5** (1.12 g, 4.88 mmol) in dimethylformamide (5 mL) was added and the mixture was kept at room temperature for 16 h. Then additional 0.5 equiv. of the chloride **5** was added and the reaction mixture was kept for 8 h. The mixture was dissolved in dichloromethane (200 mL) and extracted with water (2x200 mL). Compound **6** was obtained as brown solid by silica gel column chromotography (10% methanol/dichloromethane) (2.60 g, 84%).

^{1}H NMR (300 MHz, $CDCl_3$): δ 8.03 (d, *J*=9.0 Hz, 2H; Ar*H*), 7.55 (d, *J*=8.5 Hz, 2H; Ar*H*), 4.49 (br, 2H; ArCH_2NH), 3.40 (s, 2H; NHCOCH_2) 3.30−1.70 (br, 22H; –CH_2–), 1.40 (s, 9H; C(CH_3)$_3$), 1.33 (s, 18H; C(CH_3)$_3$).

^{13}C NMR (75 MHz, $CDCl_3$): δ 172.3, 172.1 (*C*=O), 147.8, 146.5, 128.6, 123.1 (Ar*C*), 81.8, 81.7 (*C*$(CH_3)_3$, 55. 9, 55.5, 55.4, 50.3, 42.3 (*C*H_2 ring), 27.8 (C(*C*$H_3)_3$).

ESI-MS (m/z): $[M+H]^+$ calcd. for $C_{35}H_{59}N_6O_9$,707.4; found 707.5; $[M+Na]^+$ calcd. for $C_{35}H_{58}N_6NaO_9^+$, 729.4; found 729.5.

***tri-tert*-butyl 2,2',2''-(10-(2-((4-aminobenzyl)amino)-2-oxoethyl)-1,4,7,10-tetraazacyclododecane-1,4,7-triyl)triacetate (7)**

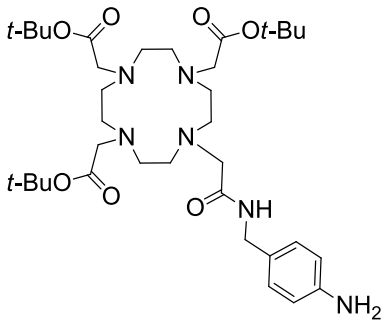

Compound **6** (1.00 g, 1.42 mmol) was dissolved in ethanol (10 mL) and Pd/C catalyst (250 mg) was added to the solution. The reaction mixture was heated to reflux temperature and 22-26% hydrazine (6 mL) was added. The reaction was kept for 4 h. The catalyst was removed by filtration. The solvent and hydrazine were evaporated under reduced pressure to get **7** as brown solid (920 mg, 96%).

^{1}H NMR (300 MHz, $CDCl_3$): δ 6.95 (d, *J*=8.8, 2H; Ar*H*), 6.52 (d, *J*=8.2, 2H; Ar*H*), 4.13 (br, 2H; ArCH_2), 3.88 (NHC(O)CH_2), 3.60−1.70 (br, 24H; CH_2 ring), 1.33 (overlapping m, 27H; C(C$H_3)_3$).

^{13}C NMR (75 MHz, $CDCl_3$): δ 172.3, 172.0 170.8 (C=O), 145.4, 128.7, 128.6, 115.1 (Ar*C*), 81.7, 81.6 (*C*$(CH_3)_3$, 55.9, 55.4, 55.3, 42.4 (*C*H_2 ring), 27.6 (C(*C*$H_3)_3$).

ESI-MS (m/z): $[M+Na]^+$ calcd. for $C_{35}H_{60}N_6NaO_7^+$, 699.4; found 699.5.

***tri-tert*-butyl 2,2',2''-(10-(2-((4-isothiocyanatobenzyl)amino)-2-oxoethyl)-1,4,7,10-tetraazacyclododecane-1,4,7-triyl)triacetate (8)**

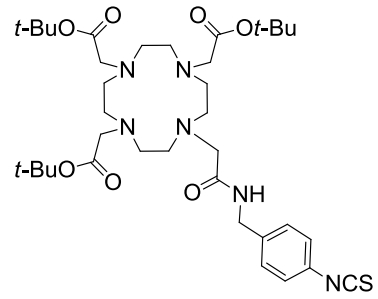

Thiophosgene (618 μL, 4.43 mmol) was added into the mixture of compound **7** (1.00 g, 1.46 mmol) and triethylamine (0.109 mmol, 15 μL) in dichloromethane (5 mL). The reaction mixture was kept at room temperature for 2 h. Compound **9** was obtained by siliga gel column chromotography (10% methanol/dichloromethane) as brown solid (0.50 g, 47.1%).

^{1}H NMR (300 MHz, $CDCl_3$): δ 7.29 (d, *J*=8.0 Hz, 2H; Ar*H*), 7.16 (d, *J*=8.3 Hz, 2H; Ar*H*), 4.46 (d, *J*=6.2 Hz, 2H; ArCH_2), 3.38-2.23 (m, 24H; CH_2 ring), 1.44 (s, 27H; C(CH_3)$_3$).

^{13}C NMR (75 MHz, $CDCl_3$): δ 172.3, 171.9 (*C*=O), 139.8, 134.5, 129.1, 126.6, 125.3 (Ar*C*), 81.8 (*C*(CH$_3$)$_3$, 54.4–56.1, 42.3 *C*H$_2$ ring), 27.9 (C(*C*H$_3$)$_3$).

ESI-MS (m/z): $[M+H]^+$ calcd. for $C_{36}H_{59}N_6NaO_7S^+$,719.4; found 719.3; $[M+Na]^+$ calcd. for $C_{36}H_{58}N_6NaO_7S$ 741.4; found 741.3.

2,2',2''-(10-(2-((4-isothiocyanatobenzyl)amino)-2-oxoethyl)-1,4,7,10-tetraazacyclododecane-1,4,7-triyl)triacetic acid (L-1)

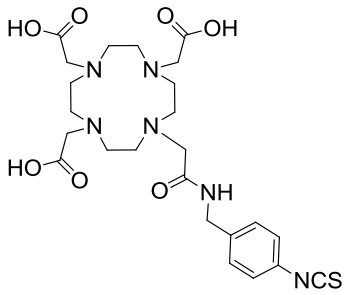

Compound **8** was dissolved in formic acid (3 mL). The reaction was kept at 60 °C for 24 h. Formic acid was evaporated under reduced pressure. The product was dried by lyophilizer to get the ligand **L-1** as off-white solid which was used in the next step without further purification.

^{1}H NMR (300 MHz, D_2O): δ 7.22 (br, 4H; Ar*H*), 4.32 (br, 2H; ArCH_2), 4.22−2.75 (br, 24H; CH_2 ring).

ESI-MS (m/z): $[M-H]^-$ calcd. for $C_{24}H_{33}N_6O_7S^-$ 549.2; found 549.2; $[M-2H+Na]^-$calcd. for $C_{24}H_{32}N_6NaO_7S^-$, 571.2; found 571.2.

Complex CA-1

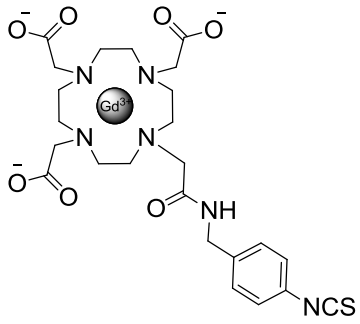

Compound **9** was dissolved in water. pH was adjusted to 7.0 with 0.1 M sodium hydroxide solution. $GdCl_3 \cdot 6H_2O$ was added to the solution and pH was maintained to 7.0. The reaction mixture was kept at room temperature for 24 h and treated with Chelex® 100 sodium form for 24 h to remove free Gd^{3+} ions. The absence of free Gd^{3+} was confirmed by xylenol orange test. After the filtration of chelex, the solvent was evaporated under reduced pressure to obtain **CA-1** and the product was dried by lyophilizer to get as off-white solid.

ESI-MS (m/z): $[M+H]^+$ calcd. for $C_{24}H_{32}GdN_6O_7S^+$, 706.1; found 706.3.

***tri-tert*-butyl 2,2',2''-(10-(2-((4-(3-(6-((2-(3-(3',6'-dihydroxy-3-oxo-3H-spiro[isobenzofuran-1,9'-xanthen]-5-yl)thioureido)ethyl)amino)-6-oxo-5-(5-(2-oxohexahydro-1H-thieno[3,4-d]imidazol-4-yl)pentanamido)hexyl)thioureido)benzyl)amino)-2-oxoethyl)-1,4,7,10-tetraazacyclododecane-1,4,7-triyl)triacetate (9)**

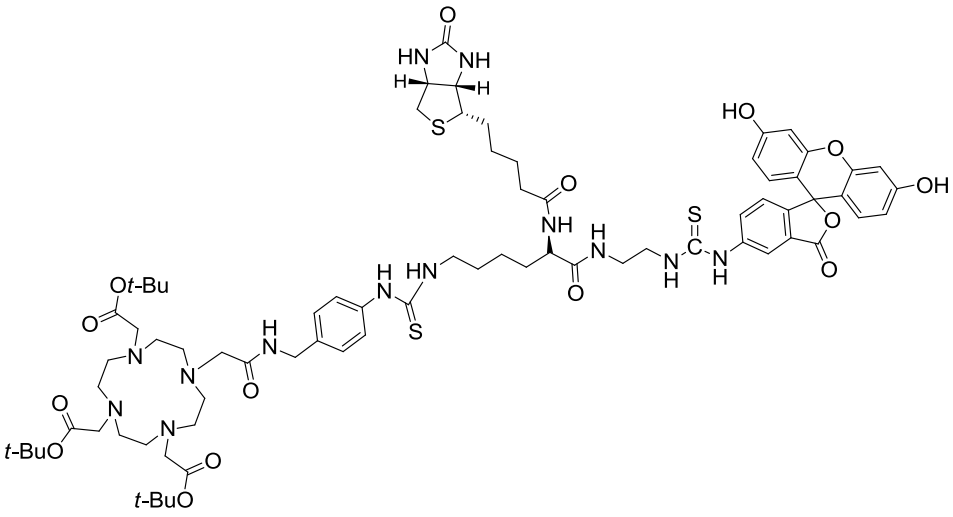

Compound **4** (0.062 mmol, 50 mg), compound **8** (0.062 mmol, 45 mg) and triethylamine (1 mL) were dissolved in dimethylformamide (3 mL). The reaction mixture was stirred at 40 °C

with protection from the light for 16 h. The solvent was evaporated. Protected monomeric chelator **9** was obtained as orange solid by silica gel column chromatography (20% methanol /dichloromethane).

ESI-MS (m/z): $[M+Na]^+$ calcd. for $C_{75}H_{103}N_{13}NaO_{15}S_3^+$, 1544.7; found 1544.7.

2,2',2''-(10-(2-((4-(3-(6-((2-(3-(3',6'-dihydroxy-3-oxo-3H-spiro[isobenzofuran-1,9'-xanthen]-5-yl)thioureido)ethyl)amino)-6-oxo-5-(5-(2-oxohexahydro-1H-thieno[3,4-d]imidazol-4-yl)pentanamido)hexyl)thioureido)benzyl)amino)-2-oxoethyl)-1,4,7,10-tetraazacyclododecane-1,4,7-triyl)triacetic acid (L-2)

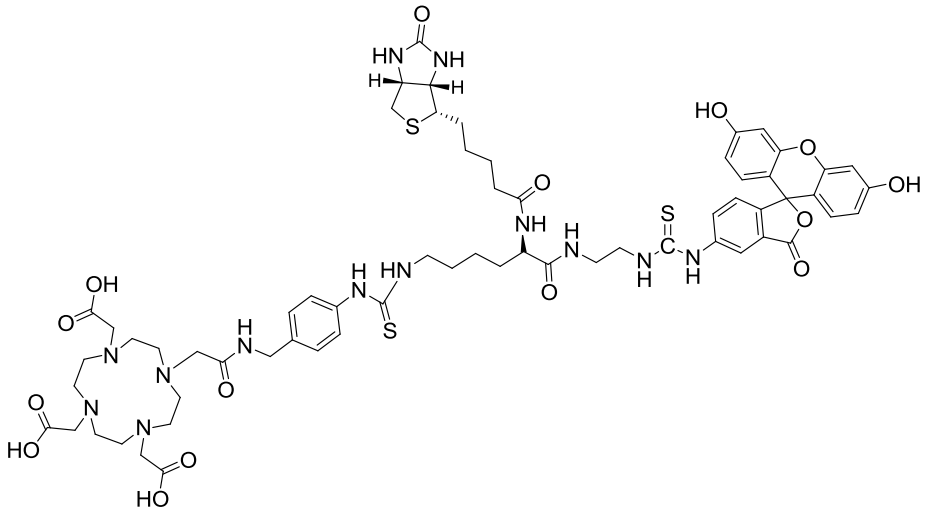

Protected monomeric chelator **9** was dissolved in formic acid. The reaction was kept at rt for 48 h. The solvent was evaporated under reduced pressure and the residue was dissolved in water. The solution was slowly added to diethylether under vigorous stirring. The product was filtered and dried under reduced pressure.

ESI-MS (m/z): $[M+H]^+$ calcd. for $C_{63}H_{80}N_{13}O_{15}S_3^+$, 1354.5; found 1354.5.

Complex CA-2

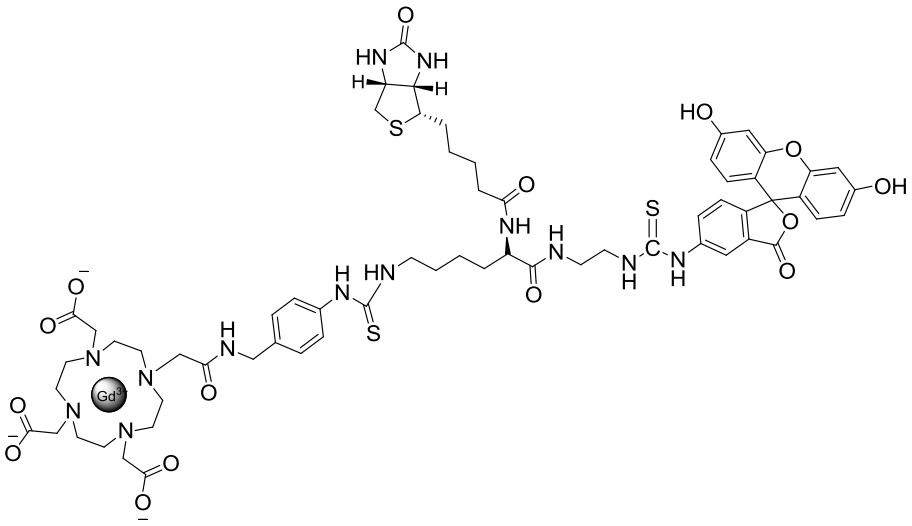

Monomeric chelator **L-2** was dissolved in water. pH was adjusted to 7.0 with NaOH. $GdCl_3 \cdot 6H_2O$ was added to the solution and pH was maintained to 7.0. The mixture was kept at room temperature for 24 h and treated with Chelex® 100 sodium form for 24 h to remove free Gd^{3+} ions. The absence of free Gd^{3+} was confirmed by xylenol orange test. After the filtration of chelex, the solvent was evaporated under reduced pressure to obtain **CA-2** as orange solid. **ESI-MS (m/z):** $[M+H]^+$ calcd. for $C_{64}H_{77}GdN_{13}O_{15}S_3^+$,1509.3; found 1509.4.

N-(6-((2-(3-(3',6'-dihydroxy-3-oxo-3H-spiro[isobenzofuran-1,9'-xanthen]-5-yl)thioureido)ethyl)amino)-6-oxo-5-(5-(2-oxohexahydro-1H-thieno[3,4-d]imidazol-4-yl)pentanamido)hexyl)-4-((2,5-dioxo-2,5-dihydro-1H-pyrrol-1-yl)methyl)cyclohexanecarboxamide (10)

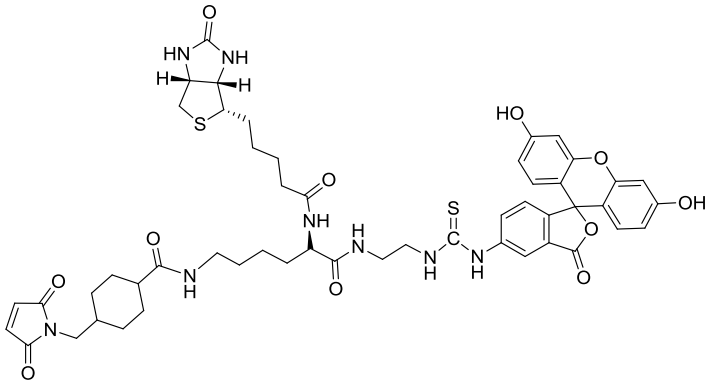

Compound **4** (100 mg, 0.12 mmol) was dissolved in phosphate buffer saline (pH 7.5). SMCC (20mg, 0.60 mmol) was dissolved in ddimethylformamide (0.5 mL) and added to the solution.

The reaction mixture was stirred at room temperature for 4 h to get compound **10**.This reaction mixture was used for the next step without further purification and evaporation.

ESI-MS (m/z): $[M-H]^-$ calcd. for $C_{51}H_{57}N_8O_{11}S_2^-$, 1021.4; found 1021.4.

Dendron 11

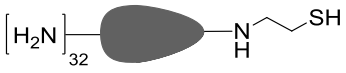

Cys-PAMAM-G4 was dissolved in the methanol-dichloromethane mixture. The solution was purged with nitrogen for 15 min. and DTT (0.26 mg, 1.7 μmol) was added. The reaction mixture was stirred for 48 h at room temperature under inert atmosphere. The reduced product gave a positive test to Ellman's reagent on the TLC plate (chloroform:methanol:ammonium hydroxide, 3:1:0.02).

Dendron 12

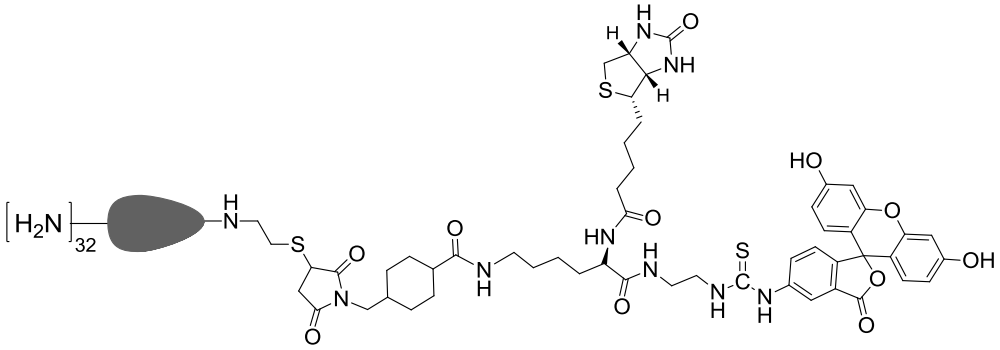

After confirmation of dendron **11**, pH was adjusted to 6.5−7.0 with 0.1 M hydrochloric acid solution. The solution of compound **10** was added to the reaction mixture and the pH was maintained to 6.5−7.0 duting the reaction. The mixture was stirred at room temperature for 16 h. The solvent was evaporated under reduced pressure. The residue was dissolved in water and loaded onto G-15 sephadex column, eluted with Mili-Q water. The water was evaporated under reduced pressure to get dendron **12** as brown solid (110 mg, 87%).

^{1}H NMR (300 MHz, $CDCl_3$): δ 7.29−6.92 (br, Ar*H*), 6.68-6.33 (br, Ar*H*), 4.02-0.64 (br).

Dendronic chelator L-3

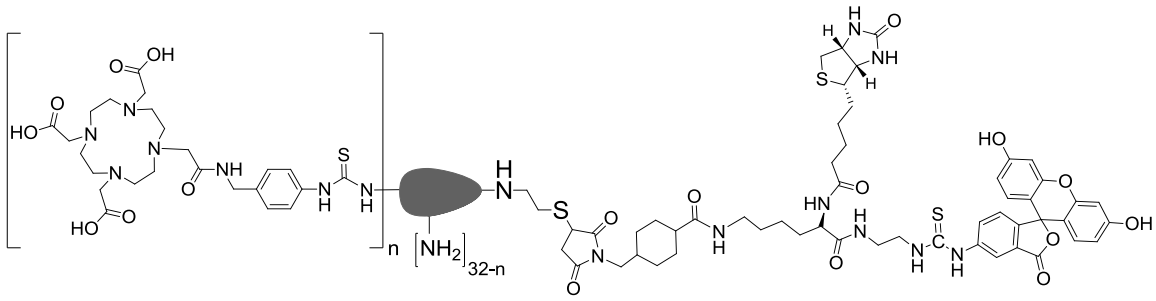

A mixture of **L-1** and dendron **12** was stirred in water at room temperature for 24 h. pH was maintained to 9.0 during the reaction. The solvent was evaporated under reduced pressure to get dendronic chelator **L-3** as brown solid.

^{1}H NMR (300 MHz, D_2O): δ 7.65−6.98 (br, Ar*H*), 4.57−0.80 (br).

Dendrimeric contrast agent DCA-1 (First attempt)

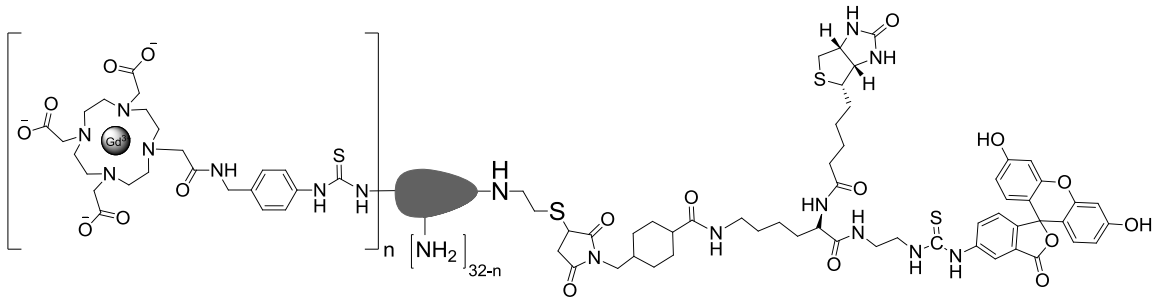

Ligand **L-3** was dissolved in water and pH was adjusted to 7.0 with 0.1 M of sodium hydroxide. $GdCl_3 \cdot 6H_2O$ was added to the solution and a precipitate formed. pH was maintained to 7.0 with the sodium hydroxide solution but the precipitate was not dissolved. EDTA was added to the mixture to remove excess Gd^{3+} and pH was maintained to 7.0 with the sodium hydroxide solution and the precipitate was not dissolved again. The mixture was stirred at room temperature for 24 h. After that, the precipitate was not dissolved. Therefore the product was not recovered.

Dendrimeric contrast agent DCA-1 (Second attempt)

Dendron **12** were dissolved in DMSO/H2O 1:1. pH was adjusted to 9.0 with 0.1 M sodium hydroxide solution. The reaction was kept at 40 °C for 24h. Complex **CA-1** was added to the reaction mixture. pH maintained at 9.0 and stirred at 45 °C for a further 48 h. The

precipitation occured and pH was maintained to 9.0 with the sodium hydroxide solution, but the precipitate was not dissolved. Therefore complex **DCA-1** was not obtained.

***tert*-butyl 2-bromo-4-(4-nitrophenyl)butanoate (13)**

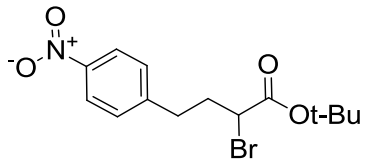

4-(4-nitrophenyl)-butyric acid (2.00 g, 9.56 mmol) was dissolved in thionyl chloride (2.78 mL, 38.2 mmol) and stirred at 75°C for 16 h. Bromine (0.54 mL, 10.48 mmol) was added dropwise at the same temperature and again stirred for 24 h. Cooled reaction mixture was poured on ice and stirred for 2 h. Aqueous layer was extracted with diethyl ether (3 x 200 mL). Combined organic phase was washed by brine (200 mL), dried over sodium sulfate and concentrated to get acid. Acid was redissolved in chloroform (30 mL). Solution of *tert*-butyl-2, 2, 2-trichloro acetimidate (4.18 g, 19.12 mmol) in chloroform (20 mL) was added slowly. Boron triflurideetherate (67 µL, 0.53 mmol) was added and the reaction mixture was stirred at room temperature for 16 h. Solid sodium bicarbonate (1.70 g) was added and stirred for 30 minutes. Solids were removed by filtration; filtrate was concentrated to afford crude. Crude was purified by silica gel column chromatography (2% ethyl acetate/hexane) to afford light yellow oil of bromide **13** (2.14g, 65%).

^{1}H NMR (300 MHz, $CDCl_3$): δ 8.16 (d, *J*=8.5 Hz, 2H; Ar*H*), 7.37 (d, *J*=8.5 Hz, 2H; Ar*H*), 4.07 (dd, *J*=8, 6.5 Hz, 1H; $ArCH_2CH_2CHBr$), 3.01−2.77 (m, 2H; $ArCH_2CH_2CHBr$), 2.44−2.20 (m, 2H; $ArCH_2CH_2CHBr$), 1.48 (s, 9H; $(CH_3)_3C$).

^{13}C NMR (75 MHz, $CDCl_3$): δ 168.2 (*C*=O), 147.8, 146.7, 129.3, 123.8 (Ar*C*), 82.7 ($(CH_3)_3C$), 46.4 ($ArCH_2CH_2CHBr$), 35.6 ($ArCH_2CH_2CHBr$), 33.1 ($ArCH_2CH_2CHBr$), 27.7 ($(CH_3)_3C$).

***tri-tert*-butyl 2,2',2''-(10-(1-(tert-butoxy)-4-(4-nitrophenyl)-1-oxobutan-2-yl)-1,4,7,10-tetraazacyclododecane-1,4,7-triyl)triacetate (14)**

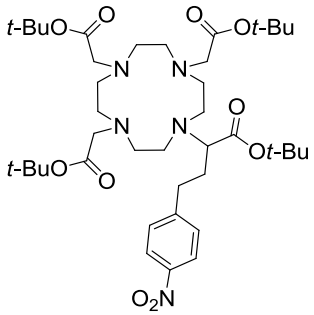

A suspension of tri-tert-butyl 2,2',2''-(1,4,7,10-tetraazacyclododecane-1,4,7-triyl)triacetate (1.54 g, 3.02 mmol), tert-butyl 2-bromo-4-(4-nitrophenyl)butanoate (1.35 g, 3.92 mmol), and potassium carbonate (1.04 g, 7.54 mmol) in dimethylformamide (10 mL) was prepared and stirred at 45 °C for 16 h. Dimethylformamide was removed under reduced pressure. The residue was dissolved in dichloromethane (200 mL) and extracted with water (2×200 mL). Dichloromethane was evaporated under reduced pressure and **14** was obtained by column chromotography (silica gel, 10% methanol/dichloromethane) as light brown solid (2.25 g, 96 %).

^{1}H NMR (300 MHz, $CDCl_3$): δ 8.12 (d, *J*=8.3 Hz, 2H; Ar*H*), 7.34 (d, *J*=8.5 Hz, 2H; Ar*H*), 3.61−1.59 (m, 27H; CH_2 ring, ArCH_2CH_2C*H*COO*t*Bu and CH_2COO*t*Bu), 1.53 (s, 9H; (CH_3)$_3$C), 1.43 (overlapping m, 27H; (CH_3)$_3$C).

^{13}C NMR (75 MHz, $CDCl_3$): δ 174.9 172.8, 170.4 (*C*=O), 149.1, 146.5, 129.6, 123.6 (Ar*C*), 82.4, 81.8, ((CH$_3$)$_3$*C*), 59.3 (*C*HCOO*t*Bu), 55.8, 55.5, 52.6, 52.4, 52.0 (*C*H$_2$ ring), 34.5 (Ar*C*H$_2$CH$_2$), 28.1 (ArCH$_2$*C*H$_2$), 27.9, 27.8, 27.8 ((*C*H$_3$)$_3$C).

FT-ICR/MS (m/z): $[M+H]^+$ calcd. for $C_{40}H_{68}N_5O_{10}^+$, 778.4961; found 778.4957.

***tri-tert*-butyl 2,2',2''-(10-(4-(4-aminophenyl)-1-(tert-butoxy)-1-oxobutan-2-yl)-1,4,7,10-tetraazacyclododecane-1,4,7-triyl)triacetate (15)**

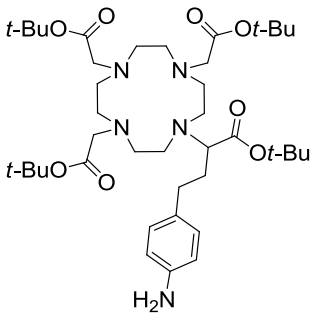

Compund **14** was dissolved in ethanol (10 mL) and Pd/C catalyst (300 mg) was added into the solution. The heterogeneous mixture was shaken for 16 h under a hydrogen atmosphere (30 psi) in a Parr hydrogenator apparatus. The catalyst was removed by filtration through the celite. The solvent was evaporated to obtain **15** as brown solid (2.74, 95%).

^{1}H NMR (300 MHz, $CDCl_3$): δ 6.86 (d, *J*=8.2 Hz, 2H; Ar*H*), 6.59 (d, *J*=8.3 Hz, 2H; Ar*H*), 3.55−1.65 (m, 27H; CH_2 ring, ArCH_2CH_2C*H*COO*t*Bu and CH_2COO*t*Bu), 1.63−1.25 (overlapping m, 36H; C(CH_3)$_3$).

^{13}C NMR (75 MHz, $CDCl_3$): δ 175.6, 172.8, 172.6 (*C*=O), 145.1, 120.0, 129.6, 115.1(Ar*C*), 81.8, 81.7, 81.6 ((CH$_3$)$_3$*C*), 58.2 (*C*HCOO*t*Bu), 55.7, 55.4, 52.5, 52.4, 51.6, 48.5, 48.3, 48.1, 47.0, 44.4 (*C*H$_2$ ring), 33.1 (Ar*C*H$_2$CH$_2$), 28.2 (ArCH$_2$*C*H$_2$), 27.9, 27.8, 26.1 ((*C*H$_3$)$_3$C).

FT-ICR/MS (m/z): $[M+H]^+$ calcd. for$C_{40}H_{70}N_5O_8^+$, 748.5219; found 748.5224.

***tri-tert*-butyl 2,2',2''-(10-(1-(tert-butoxy)-4-(4-isothiocyanatophenyl)-1-oxobutan-2-yl)-1,4,7,10-tetraazacyclododecane-1,4,7-triyl)triacetate (16)**

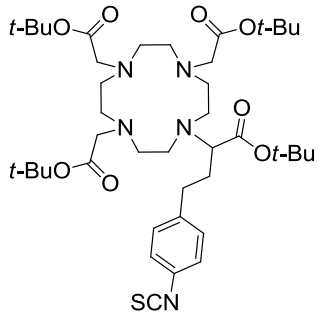

Thiophosgene (7.83 mmol, 0.40 mL) was added to the mixture of **15** (2.67 mmol, 2.00 g) and triethylamine (1 mL) in dichloromethane (20 mL). The reaction mixture was stired at room temperature for 24 h. The solvent was removed under reduced pressure and **16** was obtained by column chromatography as light brown solid (silica gel, 10% methanol/dihloromethane) (1.49 g, 71%).

^{1}H NMR (300 MHz, $CDCl_3$): δ 7.07 (s, 2H; Ar*H*), 3.51−1.56 (m, 27H; CH_2 ring, ArCH_2CH_2C*H*COO*t*Bu and CH_2COO*t*Bu), 1.55−1.28 (overlapping m, 36H; C(CH_3)$_3$).

^{13}C NMR (75 MHz, $CDCl_3$): δ 175.1, 172.8, 172.7 (*C*=O), 140.4, 137.8, 129.9, 129.3, 125.6 (Ar*C*), 82.3, 81.9, 81.7, 81.6 ((CH$_3$)$_3$*C*), 58.8 (*C*HCOO*t*Bu), 55.8, 55.5, 55.4, 52.5, 52.4, 51.9, 48.5, 48.2, 47.1, 44.6 (–*C*H$_2$–), 34.0 (Ar*C*H$_2$CH$_2$), 27.9, 27.8, 25.8.

FT-ICR/MS (m/z): $[M+H]^+$ calcd. for $C_{41}H_{68}N_5O_8S^+$, 790.47883; found 790.4777.

2,2',2''-(10-(1-carboxy-3-(4-nitrophenyl)propyl)-1,4,7,10-tetraazacyclododecane-1,4,7-triyl)triacetic acid (L-4)

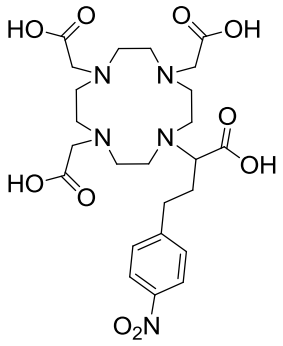

(0.13 mmol, 100 mg) was dissolved in formic acid and the mixture was stirred at 60 ^{o}C for 16 h. Formic acid was evaporated under reduced pressure. (67 mg, 94%).

^{1}H NMR (300 MHz, D_2O): δ 8.16 (d, *J*=8.4 Hz, 2H; Ar*H*), 7.48 (d, *J*=8.4 Hz, 2H; Ar*H*), 4.04−2.64 (br, 25H; CH_2 ring, ArCH_2CH$_2$C*H*COO*t*Bu and CH_2COO*t*Bu), 2.18-1.82 (br, 2H; ArCH$_2$CH_2CHCOO*t*Bu).

ESI-MS (m/z): $[M+H]^+$ calcd. for $C_{24}H_{36}N_5O_{10}^+$, 554.2; found 554.2.

Gd-DOTA complex CA-2

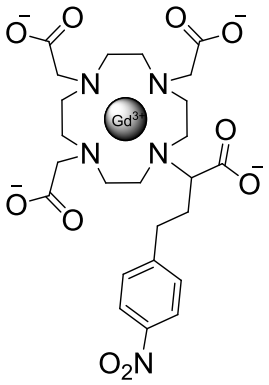

L-4 (40 mg, 0.072 mmol) was dissolved in water and pH was adjusted to 7.0 with aqueous sodium hydroxide (1 M). GdCl3·6H2O was added into the solution and pH was maintained to 7.0 with the sodium hydroxide solution. The mixture was stirred at room temperature for 24 h. Chelex was added into the reaction mixture to remove excess of Gd3+ ions. After filtration of chelex, water was removed under reduced pressure to get **CA-2** as brown solid (21 mg, 41%).

ESI-TOF/MS (m/z): $[M-H]^-$ calcd. for $C_{24}H_{31}GdN_5O_{10}^-$, 707.1317; found 707.1325.

tri-tert-butyl 2,2',2''-(10-(1-(tert-butoxy)-4-(4-(3-(6-((2-(3-(3',6'-dihydroxy-3-oxo-3H-spiro[isobenzofuran-1,9'-xanthen]-5-yl)thioureido)ethyl)amino)-6-oxo-5-(5-(2-oxohexahydro-1H-thieno[3,4-d]imidazol-4-yl)pentanamido)hexyl)thioureido)phenyl)-1-oxobutan-2-yl)-1,4,7,10-tetraazacyclododecane-1,4,7-triyl)triacetate (17)

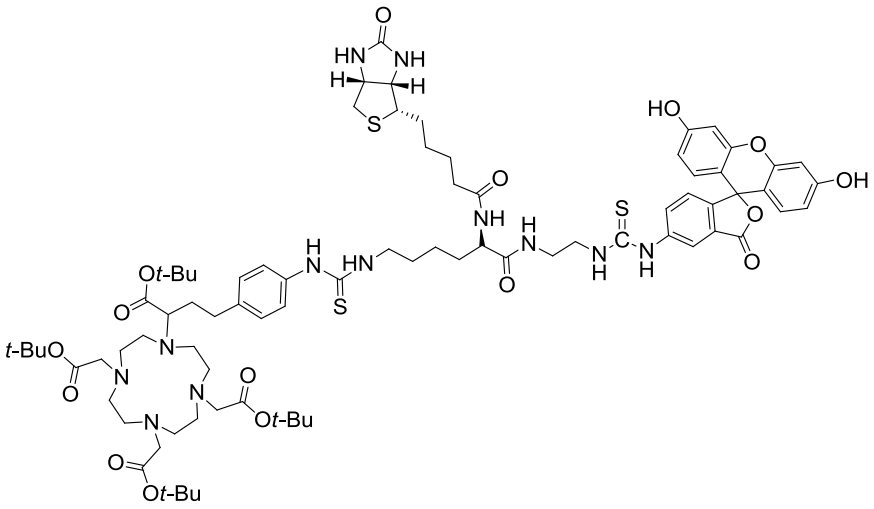

Compound **4** (0.12 mmol, 0.10 mg), compound **16** (0.19 mmol, 0.15 mg) and triethylamine (0.36 mmol, 0.05 mL) were dissolved in dimethylformamide (5 mL). The reaction mixture was stirred at 45^{o}C for 16 h with protection from direct light. The solvent was evaporated. The orange solid product was obtained by silica gel column chromotography (20% methanol/dichloromethane) to give protected monomeric chelator **17** as orange solid (0.20 g, 68%).

^{1}H NMR (300 MHz, CD_3OD): δ 8.27 (br, 1H; Ar*H*), 7.55–6.94 (br, 6H; Ar*H*), 6.92–6.38 (br, 6H; Ar*H*), 4.51–4.12 (br, 2H; SCH_2CHCH), 3.94-3.33 (br, 5H), 3.28-3.03 (br, 9H), 3.38–3.02 (br, 20H).

^{13}C NMR (75 MHz, CD_3OD): δ 183.0, 182.4 (*C*=S), 177.1, 176.4, 175.2, 174.6, 171.2, 166.1, 162.0 (*C*=O), 154.4, 142.3, 139.2, 138.7, 130.6, 129.5, 126.0, 125.7, 114.2, 111.8, 103.7 (Ar*C*), 82.3, 82.9, 82.8 ($C(CH_3)_3$), 63.3, 61.7, 59.5, 57.0, 56.9, 55.6, 55.5, 56.5, 55.2, 54.0, 53.9, 53.3, 45.4, 45.2, 41.2, 40.2, 40.1, 36.5, 32.7, 30.8, 29.8, 29.6, 29.4 (–*C*H– and –CH_2–), 28.6, 28.5, 28.4 ($C(CH_3)_3$), 26.9, 24.4, 24.1 (–CH_2–).

ESI-TOF/MS (m/z): $[M+H+Na]^{2+}$ calcd. for $C_{80}H_{113}N_{12}NaO_{16}S_3^{2+}$, 808.3723, found 808.3722.

2,2',2''-(10-(1-carboxy-3-(4-(3-(6-((2-(3-(3',6'-dihydroxy-3-oxo-3H-spiro[isobenzofuran-1,9'-xanthen]-5-yl)thioureido)ethyl)amino)-6-oxo-5-(5-(2-oxohexahydro-1H-thieno[3,4-d]imidazol-4-yl)pentanamido)hexyl)thioureido)phenyl)propyl)-1,4,7,10-tetraazacyclododecane-1,4,7-triyl)triacetic acid (L-5)

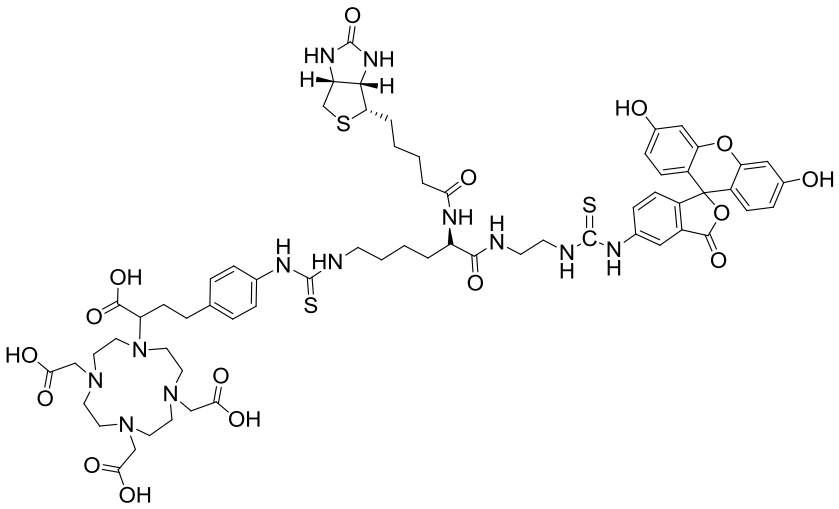

Protected monomeric chelator **17** (0.063 mmol, 100 mg) was dissolved in formic acid (4 mL). The reaction was stirred at 60 ˚C for 24 h. Formic acid was removed under reduced pressure. The residue was washed with diethylether at room tempearature to yield monomeric chelator **L-5** as orange solid (78 mg, 91%).

^{1}H NMR (300 MHz, D_2O): δ 7.58−6.86 (br, 9H; Ar*H*), 6.74 – 6.45 (br, 4H; Ar*H*), 4.64−4.05 (br, 2H; SCH_2CHCH), 3.82−0.70 (br, 51H;–CH_2– ring and –C*H*–).

ESI-TOF/MS (m/z): $[M+H]^+$ calcd. for $C_{64}H_{81}N_{12}O_{16}S_3^+$, 1369.5050, found 1369.5039; $[M+2H]^{2+}$ calcd. for $C_{64}H_{81}N_{12}O_{16}S_3^+$, 685,2562, found 685.2561.

Monomeric contrast agent MCA-2

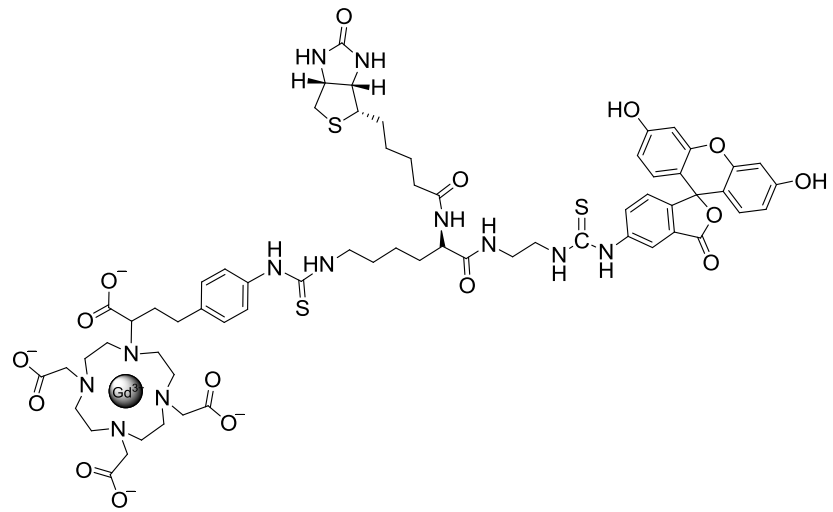

Monomeric chelator **L-5** (82 mg, 60 µmol) was dissolved in water and pH was adjusted to 7.0 with 0.1 M sodium hydroxide solution. $GdCl_3 \cdot 6H_2O$ (26 mg, 70 µmol) was added into the solution and pH was maintained to 7.0 with the sodium hydroxide solution. The mixture was stirred at room temperature for 24 h. Chelex®100 sodium form was added to the reaction mixture to remove excess of Gd^{3+} ions. After filtration of chelex, water was removed under reduced pressure to get **MCA-2** as orange solid (46 mg, 51%).

ESI-TOF/MS (m/z): $[M]^-$ calcd. for $C_{64}H_{76}GdN_{12}O_{16}S_3^-$,1522.3911; found 1522.3940.

Protected dendrimeric chealtor 18

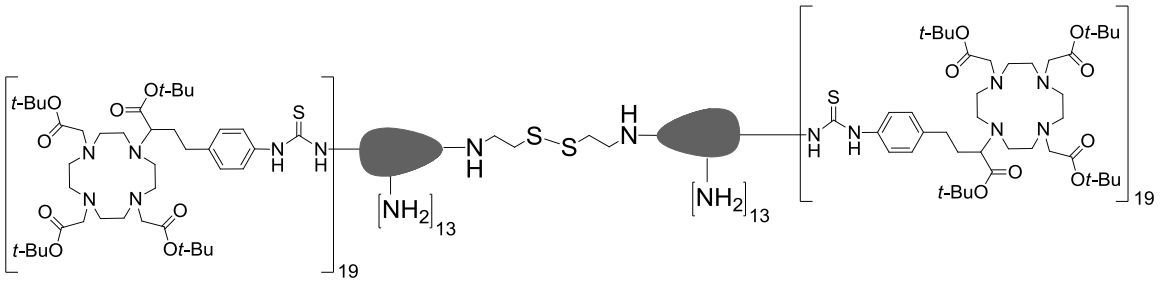

Cys-PAMAM-G4 (45.2 mg, 3.12 µmol) was dissolved in dimethylformamide. Compound **16** (240 mg, 0.30 mmol, 1.5 equiv. according to dendrimer surface groups) and triethylamine (56 µL, 0.40 mmol) was added. The reaction mixture was stirred at 45 °C for 48 h. The solvent was evaporated under reduced pressure and the residue was purified by lipophilic sephadex column using methanol as eluent. The dark brown dendrimer **18** was obtained (165 mg, 81%).

^{1}H NMR (300 MHz, $CDCl_3$): δ 7.49 (br, Ar*H*), 6.92 (br, Ar*H*), 4.38−1.56 (br), 1.56−1.21 (br, $C(CH_3)_3$).

MALDI-TOF/MS (m/z): $[M+45Na]^{2+}$ calcd. for $C_{2100}H_{3664}N_{430}Na_{45}O_{412}S_{39}$, 21876; found 21876.

Dendrimeric chelator 19

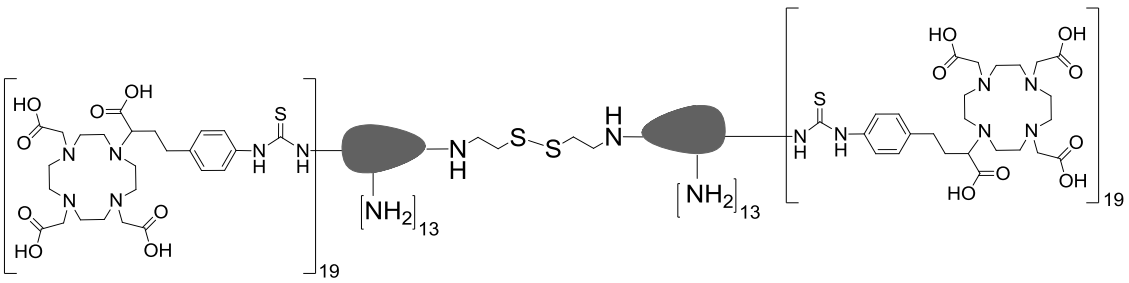

Protected dendrimeric chelator **18** (180 mg, 3.45 µmol) was dissolved in formic acid (5 mL) and the mixture was stirred at 60 ^{o}C for 16 h. Formic acid was evaporated under reduced pressure and the product was freeze-dried to give dendrimeric chelator **19** (120 mg, 84%).

^{1}H NMR (300 MHz, D_2O): δ 7.23 (br, Ar*H*). 4.45−0.40 (br).

MALDI-TOF/MS (m/z): $[M+21Na+17H_2O]^{2+}$ calcd. For $C_{1524}H_{2512}N_{430}Na_{21}O_{412}S_{38}(H_2O)_{17}$, 17717; found 17717.

Dendronic chelator 20

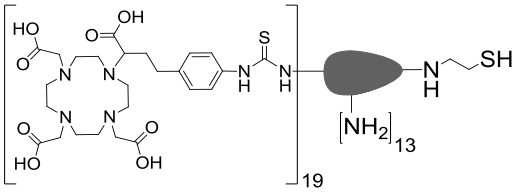

Dendrimeric chelator **19** (120 mg, 5.8µmol) was dissolved in water. TCEP (16.63 mg, 58 µmol) was added to cleave the sulfide bond. pH was adjusted to 7.0 with 0.1 M sodium hydroxide solution. The reaction mixture was stirred at room temperature for 1 hour. The reaction was monitored by TLC using Ellman's reagent. The appearance of a yellow spot confirmed the presence of thiol groups in the product. Dendronic chelator **20** was used without further purification in the next reaction.

Dendronic chelator L-6

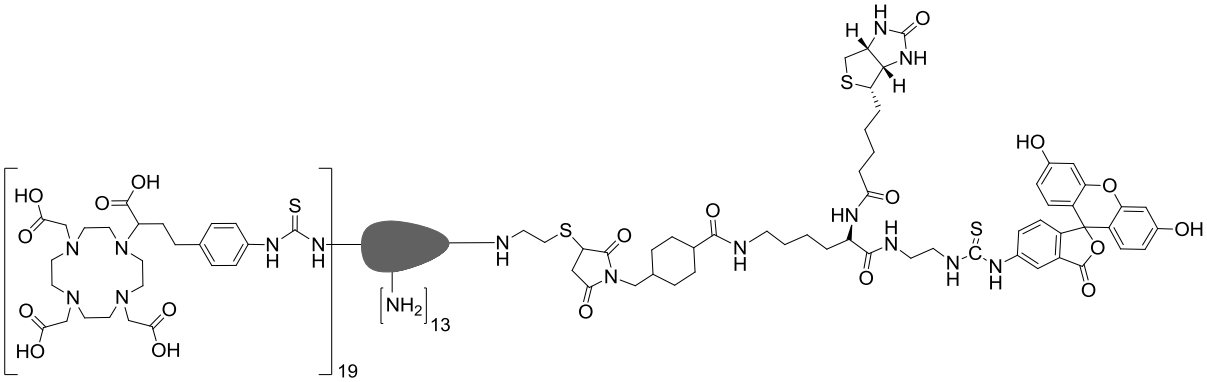

The pH was adjusted to 6.5−7.0 with hydrochloric acid. The solution of **10** was added to the reaction mixture and the pH was maintained to 6.5−7.0. The mixture was stirred at room temperature for 16 h. The unreacted dendronic chelator **20** was re-oxidized bubbling oxygen gas through to reaction mixture to get dendrimeric chelator **19**. Subsequently, the mixture was concentrated under reduced pressure and the excess amount of **10** and dendrimeric chelator **19**

were removed using G-15 sephadex column and water as eluent. Water was evaporated under reduced pressure and dendronic chelator **L-6** was lyophilized (110 mg, 87%).

^{1}H NMR (300 MHz, D_2O): δ 7.21 (br, Ar*H*), 4.09−0.51 (br).

MALDI-TOF/MS (m/z): $[M+16Na+8H_2O]^{2+}$ calcd. for $C_{838}H_{1350}N_{228}Na_{16}O_{225}S_{22}(H_2O)_8^{2+}$, 19347; found 19347.

Complex DCA-2

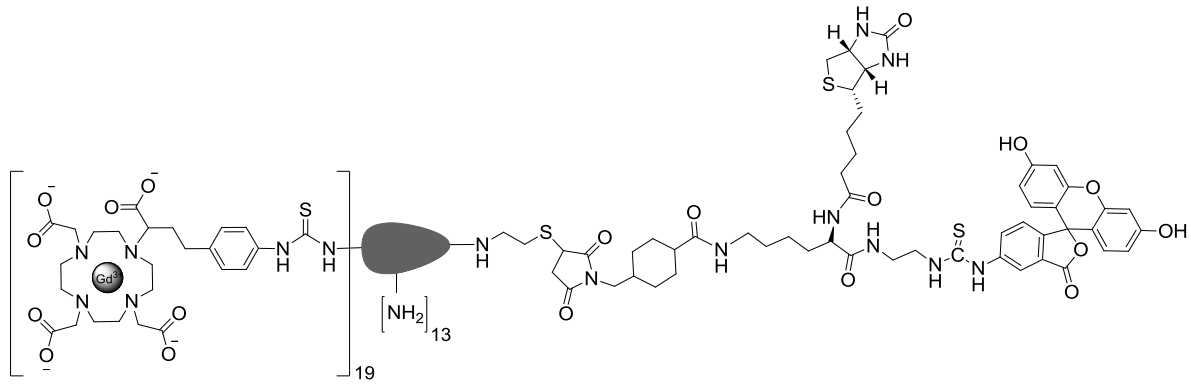

Dendronic chelator **L-6** (100 mg, 5.06 µmol) was dissolved in water and pH was adjusted to 7.0 with 0.1 M sodium hydroxide solution. $GdCl_3 \cdot 6H_2O$ (90 mg, 243 µmol) was added to the solution and pH was maintained to 7.0 with the sodium hydroxide solution. The mixture was stirred at room temperature for 24 h. EDTA (120 mg, 324 µmol) was added into the solution to remove excess Gd3+ while maintaining the pH at 7.0 with the aqueous sodium hydroxide solution. The mixture was stirred at room temperature for 24 h and the major part of GdEDTA and free EDTA was removed using water by G-15 sephadex column. The residues of GdEDTA and EDTA were removed by centrifugation using a centrifugal filter unit with 3 Kda molecular weight cut-off (102 mg, 79%).

MALDI-TOF/MS (m/z): $[M+37Na+37H_2O]^{2+}$ calcd. for $C_{838}H_{1274}Gd_{19}N_{228}Na_{37}O_{225}S_{22}(H_2O)_{37}^{2+}$, 11676; found 11676.

Benzyl (3-bromopropyl)carbamate (21)

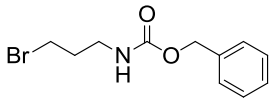

3-bromopropan-1-amine hydrobromide (20 g, 91 mmol) was dissolved in a mixture of water (50 mL) and dioxane (50 mL). Benzyl chloroformate (15.65 mL, 110 mmol) was added to solution dropwise and pH was maintained at 6.0-7.0 with 3.5 M potassium carbonate. The

mixture was kept at room temperature for 1 h. Excess CbZ was hydrolyzed with a solution of sodium hydroxide solution (2.0 M, 10 mL). The mixture was extracted with ether. The combined organic phase was washed with a solution of sodium hydroxide solution (1.0 M, 250 mL) once and with water twice (250 mL) and dried over sodium sulfate. The solvent was evaporated and the residue was purified by silica gel column chromotography (40% ethylacetate/hexane) to obtain bromide **21** as colourless oil (24g, %97).

^{1}H NMR (300 MHz, $CDCl_3$): δ 7.35 (s, 5H; Ar*H*), 5.10 (s, 2H; ArCH_2), 3.48−3.19 (m, 4H; BrCH_2CH_2CH_2NH), 2.06 (br, 2H; BrCH_2CH_2CH_2NH).

^{13}C NMR (75 MHz, $CDCl_3$): δ 156.4 (*C*=O), 136.3, 128.3, 127.9, 127.9 (ArC), 66.5 (Ar*C*H_2), 30.5, 32.3, 39.2 (Br*C*H_2*C*H_2*C*H_2NH).

ESI-MS (m/z): $[M+H]^+$ calcd. for $C_{11}H_{15}BrNO_2^+$, 272.0, found 272.0.

***tri-tert*-butyl 2,2',2''-(10-(3-aminopropyl)-1,4,7,10-tetraazacyclododecane-1,4,7-triyl)triacetate (22)**

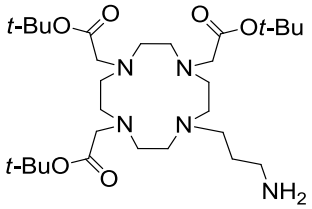

tri-tert-butyl 2,2',2''-(1,4,7,10-tetraazacyclododecane-1,4,7-triyl)triacetate (20 g, 38.9 mmol) and bromide **21** (13 g, 47.66 mmol) were dissolved in acetonitrile (200 mL). Potassium carbonate (10.74 g, 78 mmol) was added to the solution. The reaction mixture was kept at 70 °C overnight. Then potassium carbonate was removed by filtration. The solvent was evaporated under reduced pressure. The crude was dissolved in methanol (20 mL) and Pd/C catalyst (2.00 g) was added to the solution. The heterogeneous mixture was shaken for 16 h under a hydrogen atmosphere (30 psi) in a Parr hydrogenator apparatus. The catalyst was removed by filtration through the celite. The solvent was evaporated under reduced pressure. The residue was purified by silica gel column chromotography (10% methanol/dichloromethane) to give amine **22** as white solid (16.7 g, 75%).

^{1}H NMR (300 MHz, $CDCl_3$): δ 3.47−1.87 (br, 28H), 1.62 (br, 2H; NCH_2CH_2CH_2NH_2), 1.41 (s, 27H; C(CH_3)$_3$).

^{13}C NMR (75 MHz, $CDCl_3$): δ 172.4, 170.5 (*C*=O), 82.1, 81.8 (*C*$(CH_3)_3$), 57.6, 56.6, 50.6, 50.2, 49.8, 39.3(*C*H_2 ring), 27.9, 23.6 (C(*C*H_3)$_3$).

ESI-MS (m/z): $[M+H]^+$ calcd. for $C_{29}H_{58}N_5O_6^+$, 572.4, found 572.4.

***tri-tert*-butyl 2,2',2''-(10-(3-(2-bromoacetamido)propyl)-1,4,7,10-tetraazacyclododecane-1,4,7-triyl)triacetate (23)**

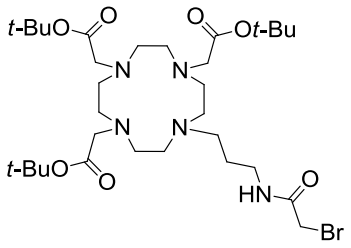

2-bromoacetic acid (2.36 g, 16.99 mmol) and N,N'-methanediylidenedicyclohexanamine (DCC) (3.5 g, 16.99 mmol) were dissolved in dichloromethane (40 mL). Amine **22** (8.83 g, 15.44 mmol) was dissolved in dichloromethane (20 mL) and added into the mixture. The resulting mixture was stirred at room temperature for 1 h. DCC was removed by filtration and the solvent was evaporated under reduced pressure. The residue was purified by silical gel column chromotography (10% methanol/dichloromethane) to obtain bromide **23** as off white solid (8.5, 79%).

^{1}H NMR (300 MHz, $CDCl_3$): δ 4.00 (d, *J*=6.1 Hz, 2H; CH_2Br), 3.66–1.60 (br, 28H), 1.49−1.32 (br, 27H; C(CH_3)$_3$).

^{13}C NMR (75 MHz, $CDCl_3$): δ 172.1, 170.2, 169.8, 167.4, 166.9 (*C*=O), 82.9, 82.5 (C(*C*H$_3$)$_3$), 56.7, 56.4, 55.7, 55.5, 53.4, 52.6, 51.6, 51.0, 50.2 (*C*H$_2$ ring), 47.8 (NHCH$_2$*C*H$_2$CH$_2$), 36.9 (NH*C*H$_2$CH$_2$CH$_2$), 29.4 (CH$_2$Br), 28.0, 27.9 (C(*C*H$_3$)$_3$), 27.7 (NHCH$_2$*C*H$_2$CH$_2$).

ESI-MS (m/z): $[M+H]^+$ calcd. for $C_{31}H_{59}BrN_5O_7^+$, 692.4, found 692.4.

2,2'-(ethane-1,2-diylbis(oxy))bis(N-benzylethanamine) (24)

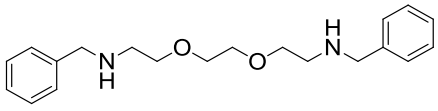

2,2'-(ethane-1,2-diylbis(oxy))diethanamine (20 g, 135 mmol) was added on moleculer sieves, then dichloromethane (200 mL) was added. Benzaldehyde (31.50 g, 297 mmol) was slowly added to the mixture. The reaction mixture was stirred at room temperature for 24h. Then sodium borohydride (10.21 g, 270 mmol) was suspended in ethanol (1.5 L) and added slowly into the mixture at 0 °C. The reaction mixture was stirred at 0 °C until the ice melted. Subsequently, it was stirred at room temperature for 48 h. The mixture was decanted to remove molecular sieves and the solvent was evaporated under reduced pressure. The crude

was dissolved in a mixture of dichloromethane and water. Then the mixture was filtered. Aqueous layer was acidified until pH 1 and extracted with dichloromethane to remove benzyl alcohol. Then pH was adjusted to 12 and extracted with dichloromethane to obtain compound **24** as colourless oil (38.7 g, 87%).

^{1}H NMR (300 MHz, $CDCl_3$): δ 7.38−7.18 (m, 10H), 3.67−3.54 (br, 8H; ArCH_2 and NHCH$_2$CH_2), 3.80 (s, 2H; OCH_2CH_2O), 2.87−2.74 (t, *J*=5.2 Hz, 4H; NHCH_2CH$_2$).
^{13}C NMR (75 MHz, $CDCl_3$): δ 140.0, 128.3, 128.1, 126.8 (Ar*C*), 70.4, 70.2 (*C*H$_2$O*C*H$_2$*C*H$_2$O*C*H$_2$), 53.7 (Ar*C*H$_2$), 48.5 (NH*C*H$_2$CH$_2$).
ESI-MS (m/z): $[M+H]^+$ calcd. for $C_{20}H_{29}N_2O_2^+$, 329.2, found 329.2.

***di-tert*-butyl 3,12-dibenzyl-6,9-dioxa-3,12-diazatetradecane-1,14-dioate (25)**

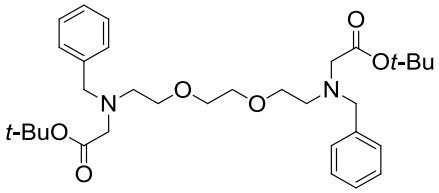

Compound **24** (10 g, 30.4 mmol) was dissolved in acetonitrile (100 mL) and potassium carbonate (10.52 g, 76 mmol) was added. Then tert-butyl 2-bromoacetate (9.4 mL, 64 mmol) was added dropwise to the mixture. The reaction mixture was stirred at 70 °C for 16 h. The solvent was evaporated under reduced pressure and the residue was purified by silica gel column chromotography (10% ethylacetate/dichloromethane) to obtain compound **25** as light yellow oil (12.74 g, 75 %).
^{1}H NMR (300 MHz, $CDCl_3$): δ 7.28−6.93 (br, 10H; Ar*H*), 3.67 (s, 4H; ArCH_2), 3.48−3.25 (br, 8H; CH_2OCH_2CH_2OCH_2), 3.12 (s, 4H; NCH_2CO), 2.72 (t, *J*=5.0 Hz, 4H; NCH_2CH$_2$), 1.28 (s, 18H; C(CH_3)$_3$).
^{13}C NMR (75 MHz, $CDCl_3$): δ 170.0 (*C*=O), 139.3, 129.7, 128.9, 128.2, 127.0 (Ar*C*), 80.7 (*C*(CH$_3$)$_3$, 70.3, 70.1 (OCH_2CH_2O), 58.6, 55.6, 53.0 N(CH_2)$_3$, 28.2 (C(*C*H$_3$)).
ESI-MS (m/z): $[M+H]^+$ calcd. for $C_{32}H_{49}N_2O_6^+$, 557.4, found 557.3.

***di-tert*-butyl 6,9-dioxa-3,12-diazatetradecane-1,14-dioate (26)**

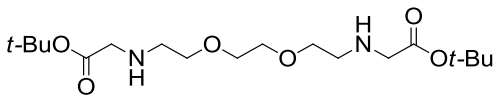

Compound **25** (21.0 g, 37.7 mmol) was dissolved in methanol (20 mL) and Pd(OH)$_2$/C catalyst (2.00 g) was added to this solution. The heterogeneous mixture was shaken for 16 h

under a hydrogen atmosphere (30 psi) in a Parr hydrogenator apparatus. The catalyst was removed by filtration through the celite. The solvent was evaporated under reduced pressure to obtain compound **26** as light yellow oil (13.8 g, 97%).

^{1}H NMR (300 MHz, $CDCl_3$): δ 3.64−3.51 (m, 8H; NHCH_2C(O) and CH_2OCH_2CH_2OCH_2), 3.28 (s, 4H; CH_2OCH_2CH_2OCH_2), 2.74 (t, *J*=5.5 Hz, 4H; NC$H_2$$CH_2$), 1.41 (s, 18H; C(C$H_3$)$_3$).

^{13}C NMR (75 MHz, $CDCl_3$): δ 171.3 (*C*=O), 80.9 (*C*$(CH_3)_3$), 70.5, 70.1 (*C*H_2O*C*H_2), 51.5, 48.6 (*C*H_2NH*C*H_2), 28.0 (C(*C*H_3)$_3$).

ESI-MS (m/z): $[M+H]^+$ calcd. for $C_{18}H_{37}N_2O_6^+$, 377.3, found 377.3.

***di-tert*-butyl 3-benzyl-6,9-dioxa-3,12-diazatetradecane-1,14-dioate (27)**

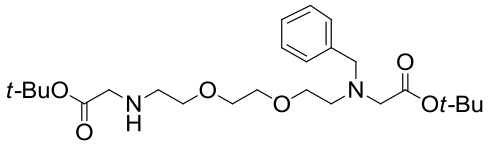

Compound **26** (26.6 mmol, 10 g) was dissolved in dimethylformamide (40 mL) and cesium carbonate (21.3 mmol, 6.95 g) was added. (chloromethyl)benzene (21.3 mmol, 2.70 g) was dissolved in dimethylformamide (20 mL) and added dropwise to the mixture. The resulting mixture was stirred at room temperature for 24 h. The solvent was removed under reduced pressure and dichloromethane (50 mL) was added to the residue. The insoluble salts were removed by filtration and the filtrate was concentrated under reduced pressure. The residue was dissolved in dichloromethane (200 mL) and extracted with water (2x200 mL). The combined organic layers were dried over sodium sulphate, filtered and concentrated under reduced pressure. Purification of the residue by silica gel column chromotography (3% methanol/dichloromethane) gave the mono benzyl amine derivative **27** as light yellow oil (5.21 g, 42%).

^{1}H NMR (300 MHz, $CDCl_3$): δ 7.44–7.10 (m, 5H, Ar*H*), 3.85 (s, 2H, NCH_2Ar), 3.59 (br, 8H CH_2OCH_2CH_2OCH_2), 3.39–3.21 (m, 4H, NCH_2COO*t*Bu), 3.01–2.68 (m, 5H, N*H*C$H_2$$CH_2$), 1.46 (s, 18H, C(C$H_3$)$_3$).

^{13}C NMR (75 MHz, $CDCl_3$): δ 171.1, 170.9 (*C*=O), 138.9, 128.8, 128.1, 126.9 (Ar*C*), 81.0, 80.6 (*C*$(CH_3)_3$), 70.2, 70.1, 70.0, 69.8, 58.5, 55.6, 52.9, 51.3, 48.5 (–*C*H_2–), 28.1, 27.9 (C(*C*H_3)$_3$).

ESI-TOF/MS (m/z): $[M+H]^+$ calcd. for $C_{25}H_{43}N_2O_6^+$, 467.3116, found 467.3119.

***di-tert*-butyl 3-benzyl-12-(2-oxo-2-((3-(4,7,10-tris(2-(tert-butoxy)-2-oxoethyl)-1,4,7,10-tetraazacyclododecan-1-yl)propyl)amino)ethyl)-6,9-dioxa-3,12-diazatetradecane-1,14-dioate (28)**

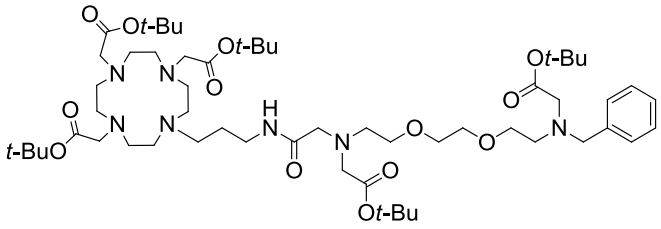

Compound **27** (5.79 mmol, 2.70 g) and **23** (6.94 mmol, 5.90 g) were dissolved in acetonitrile (50 mL) and potassium carbonate (17.37 mmol, 2.40 g) was added. The reaction mixture was stirred at 70 °C for 24 h. The insoluble materials were removed by filtration and the filtrate was concentrated under reduced pressure. The residue was dissolved in dichloromethane (200 mL) and extracted with water (2x200 mL). The combined organic layers were dried over sodium sulphate, filtered and concentrated under reduced pressure. The residue was purified by silica gel column chromotography (10% methanol/dichloromethane) to give compound **28** as light brown solid (4.4 g, 71%).

^{1}H NMR (300 MHz, $CDCl_3$): δ 8.31(br. s, 1H, N*H*), 7.27 (br., 5H, Ar*H*), 3.88−1.97 (m, 46H), 1.56–1.87 (m, 2H, $NCH_2CH_2CH_2$), 1.56−1.31 (m, 45H, $C(CH_3)_3$).

^{13}C NMR (75 MHz, $CDCl_3$): δ 172.4, 172.3, 172.2, 171.4, 170.2, 169.8, (*C*=O), 135.6, 129.7, 128.5, 127.7, (ArC), 82.5, 82.3, 81.5, 82.1, ($C(CH_3)_3$), 70.1, 69.2, 69.1, 67.1, 67.0, 59.6, 59.2, 58.8, 58.5, 56.7, 56.5, 55.5, 55.0, 54.2, 53.4, 52.9, 52.5, 51.8, 50.1, 37.4, 29.5, 28.0 (–CH_2–), 27.9, 27.7 ($C(CH_3)_3$).

ESI-TOF/MS (m/z): $[M+H]^+$ calcd. for $C_{56}H_{100}N_7O_{13}^+$, 1078.7374, found 1078.7360.

***di-tert*-butyl 3-(2-oxo-2-((3-(4,7,10-tris(2-(tert-butoxy)-2-oxoethyl)-1,4,7,10-tetraazacyclododecan-1-yl)propyl)amino)ethyl)-6,9-dioxa-3,12-diazatetradecane-1,14-dioate (29)**

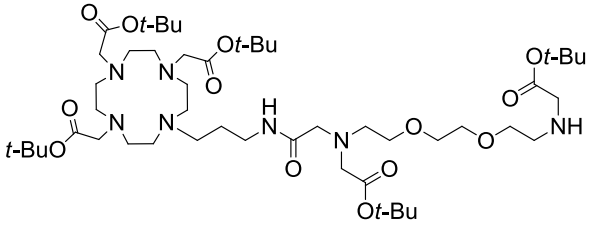

Benzyl amine **28** (3.9 g, 0.60 mmol) was dissolved in ethanol (15 mL) with 10% Pd-C (780 mg, 10% w/w) and shaken for 16 h in a Parr apparatus under H_2 (50 psi). The residue was obtained after reaction mixture was filtered and solvent was evaporated under reduced pressure. The residue was purified by silica gel column chromatography (10 % methanol/dichloromethane) to obtain the pure amine **29** as white fluffy powder (3.4 g, 95%).

^{1}H NMR (300 MHz, $CDCl_3$): δ 8.09 (br. s, 1H, N*H*), 3.84−1.94 (m, 44H), 1.87–1.59 (m, 2H, $NCH_2CH_2CH_2$), 1.55–1.25 (m, 45H, $C(CH_3)_3$).

ESI-TOF/MS(m/z): $[M+H]^+$ calcd. for $C_{49}H_{94}N_7O_{13}$, 988.6904, found 988.6895.

2-bromo-N-(4-nitrophenethyl)acetamide (30)

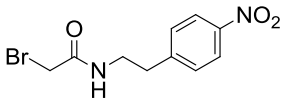

2-(4-nitrophenyl)ethanamine hydrochloride (5.0 g, 24.67 mmol) and and triethylamine (7.57 mL, 54.3 mmol) were dissolved in dichloromethane and cooled to 0 ^oC. A solution of bromoacetyl bromide (6.0 g, 29.7 mmol) in dichloromethane was added at the same temperature. After 20 minutes, the reaction completion was checked by TLC in 70% ethyl acetate/hexane. After completion of reaction, cold water (200 mL) was added to the reaction mixture and extracted with dihloromethane (2x200 mL). Organic phase was taken and the solvent was evaporated under reduced pressure. The crude was purified by silica gel column chromatography (70% ethylacteta/hexane; the polarity was increased by 10% ethyl acetate each time until 70%) to obtain bromide **30** as off white solid (3.8 g, 54%).

^{1}H NMR (300 MHz, $CDCl_3$): δ 8.16 (d, *J*=9.0 Hz, 2H; Ar*H*), 7.38 (d, *J*=9.0 Hz, 2H; Ar*H*), 3.85 (s, 2H; $BrCH_2$), 3.59 (q, *J*=7.0 Hz, 2H; $ArCH_2$), 2.97 (t, *J*=7.0 Hz, 2H; $NHCH_2CH_2$).

^{13}C NMR (75 MHz, $CDCl_3$): δ 165.6 (*C*=O), 146.8, 146.2, 129.6, 123.8 (Ar*C*), 40.7 $NHCH_2CH_2$, 35.3 ($ArCH_2$), 29.0 ($BrCH_2$).

ESI-TOF/MS (m/z): $[M+Na]^+$ calcd. for $C_{10}H_{11}BrN_2NaO_3^+$, 308.9918, found 308.9840.

***di-tert*-butyl 3-(2-((4-nitrophenethyl)amino)-2-oxoethyl)-12-(2-oxo-2-((3-(4,7,10-tris(2-(tert-butoxy)-2-oxoethyl)-1,4,7,10-tetraazacyclododecan-1-yl)propyl)amino)ethyl)-6,9-dioxa-3,12-diazatetradecane-1,14-dioate (31)**

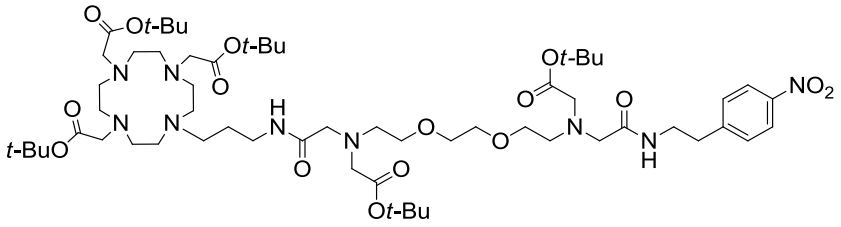

Compound **29** (2 g, 2.02 mmol) was dissolved in anhydrous acetonitrile (75 mL). Compound **30** (0.70 g, 2.44 mmol) and potassium carbonate (0.56g, 4.06 mmol) were added at room temrepature. The reaction mixture was stirred at 70 °C for 24 h. After cooling to room temperature, the insoluble materials were removed by filtration. The residue was dissolved into dichloromethane (200 mL) and extracted with water (2x200 mL). The organic layer was dried over sodium sulphate, filtered, and concentrated under reduced pressure. The solvent was removed under reduced pressure and the residue was purified by silica gel column chromotography (10% methanol/dichloromethane) to obtain protected monomeric chelator **31** as light brown solid (1.95 g, 81%).

^{1}H NMR (300 MHz, $CDCl_3$): δ 8.08 (br, 2H; Ar*H*), 7.39 (br, 2H; Ar*H*), 3.64−2.12 (m, 50H), 1.77–1.55 (br, 2H; $NHCH_2CH_2CH_2$), 1.40 (overlapping m, 45H; $C(CH_3)_3$).

^{13}C NMR (75 MHz, $CDCl_3$): δ 173.0, 172.0, 171.1, 171.0, 170.4, 169.9, 169.5 (*C*=O), 147.0, 146.1, 129.4, 123.1 (Ar*C*), 82.3, 82.0, 81.3, 80.9 ($C(CH_3)_3$), 69.7, 68.7, 58.6, 56.7, 56.3, 56.0, 55.2, 54.0, 52.7, 52.2, 51.4, 50.4, 49.7, 47.4, 39.2, 36.9, 35.1 (–CH_2–), 27.6, 27.3, 25.5 ($C(CH_3)_3$).

ESI-TOF/MS (m/z): $[M+H]^+$ calcd. for $C_{59}H_{104}N_9O_{16}^+$, 1194.7596, found 1194.7583.

***di-tert*-butyl 3-(2-((4-nitrophenethyl)amino)-2-oxoethyl)-12-(2-oxo-2-((3-(4,7,10-tris(2-(tert-butoxy)-2-oxoethyl)-1,4,7,10-tetraazacyclododecan-1-yl)propyl)amino)ethyl)-6,9-dioxa-3,12-diazatetradecane-1,14-dioate (L-7)**

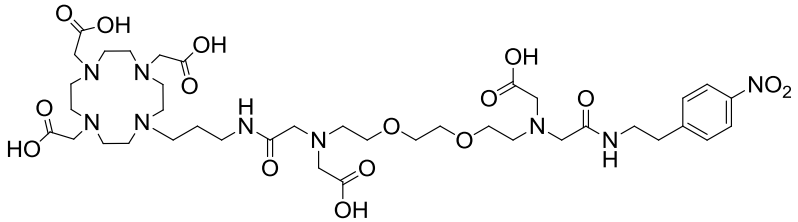

Protected monomeric chelator **31** (105 mg, 88 µmol) was dissolved in formic acid (5 mL) and the mixture was stirred at 60 ^{o}C for 16 h. Formic acid was evaporated under reduced pressure. The residue was dissolved in methanol (1 mL) and added slowly to diethyether (50 mL) under vigorous stirring. The solution was cooled to -20 °C for 16 h. The product was filtered and dried by lyophilizer to yield monomeric chelator **L-7** (65 mg, 81%).

^{1}H NMR (300 MHz, D_2O): δ 8.12 (d, *J*=8.3 Hz, 2H; Ar*H*), 7.45 (d, *J*=8.7 Hz, 2H; Ar*H*), 4.27−2.59 (m, 50H), 1.87 (br, 2H; $NHCH_2C\mathit{H}_2CH_2$).

^{13}C NMR (75 MHz, D_2O): δ 171.4, 169.7, 169.5, 165.4, 165.0 (*C*=O), 147.6, 146.3, 130.1, 123.7 (Ar*C*), 69.9, 69.8, 69.4, 64.5, 64.4, 60.8, 57.2, 57.0, 56.1, 55.8, 55.2, 54.9, 51.2, 50.3, 49.4, 49.3, 40.1, 37.0, 34.6, 32.9, 24.0 (–*C*H_2–).

ESI-TOF/MS(m/z):[M-H]$^-$ calcd. for $C_{39}H_{62}N_9O_{16}^-$, 912.4320, found 912.4317.

Monomeric smart contrast agent SCA-1

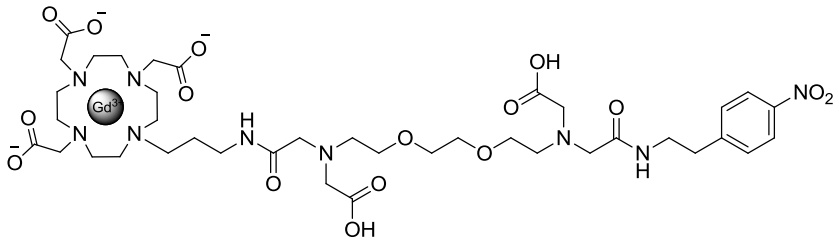

Monomeric chelator **L-7** (70 mg, 77 µmol) was dissolved in water and pH was adjusted to 7.0 with 0.1 M sodium hydroxide solution. $GdCl_3 \cdot 6H_2O$ (31.3 mg, 84 µmol) was added to the solution and pH was maintained to 7.0 with the sodium hydroxide solution. The mixture was stirred at room temperature for 24 h. Excess Gd^{3+} ions were removed by Chelex®100 sodium form and the solvent was evaporated under reduced pressure to obtain **SCA-1** as off-white solid (66 mg, 81%).

ESI-TOF/MS(m/z):[M-H]$^-$ calcd. for $[C_{39}H_{59}GdN_9O_{16}]^-$, 1067.3326, found 1067.3352.

***di-tert*-butyl 3-(2-((4-aminophenethyl)amino)-2-oxoethyl)-12-(2-oxo-2-((3-(4,7,10-tris(2-(tert-butoxy)-2-oxoethyl)-1,4,7,10-tetraazacyclododecan-1-yl)propyl)amino)ethyl)-6,9-dioxa-3,12-diazatetradecane-1,14-dioate (32)**

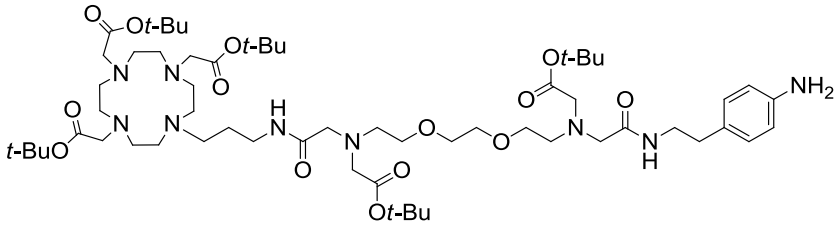

The mixture of compound **31** (1.85 g, 1.55 mmol) and Pd/C catalyst was shaken under a hydrogen atmosphere (3.0 bar) in a Parr hydrogenator. After completion of the hydogenation, the catalyst was removed by filtraion through celite column. The solvent was removed under reduced pressure to obtain **32** as light brown solid (1.75 g, 97%).

^{1}H NMR (300 MHz, $CDCl_3$): δ 6.79 (d, *J*=8.5 Hz, 2H; Ar*H*), 6.50 (d, *J*=8.3 Hz, 2H; Ar*H*), 3.46−1.93 (m, 50H), 1.59−1.45 (br, 2H; $NHCH_2C\mathit{H}_2CH_2$), 1.27 (overlapping m, 45H; $C(C\mathit{H}_3)_3$).

^{13}C NMR (75 MHz, $CDCl_3$): δ 173.0, 172.0, 170.9, 170.7, 170.5, 170.1, 169.8, 169.4 (*C*=O), 144.8, 128.9, 127.7, 114.7 (Ar*C*), 82.3, 81.9, 81.2, 80.9 ($\mathit{C}(CH_3)_3$), 69.7, 68.7, 58.7, 57.2, 56.7, 56.3, 56.0, 55.2, 53.9, 52.5, 52.1, 51.4, 50.4, 49.6, 48.5, 47.4, 40.1, 36.8, 34.4, 27.6 (–$\mathit{C}H_2$–), 27.5, 27.3, 25.5 ($C(\mathit{C}H_3)_3$).

ESI-TOF/MS(m/z): $[M+H]^+$calcd. for $C_{59}H_{106}N_9O_{14}^+$, 1164.75838, found 1164.78424.

***di-tert*-butyl 3-(2-((4-isothiocyanatophenethyl)amino)-2-oxoethyl)-12-(2-oxo-2-((3-(4,7,10-tris(2-(tert-butoxy)-2-oxoethyl)-1,4,7,10-tetraazacyclododecan-1-yl)propyl)amino)ethyl)-6,9-dioxa-3,12-diazatetradecane-1,14-dioate (33)**

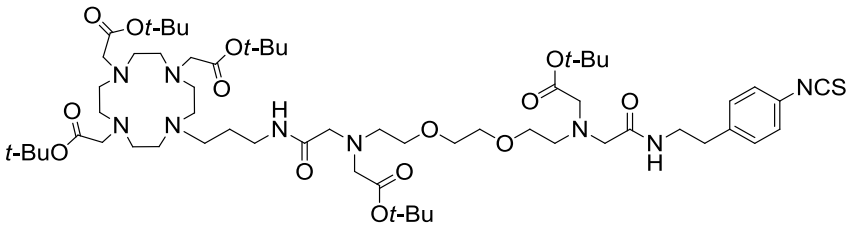

Compound **32** (1.5 g, 1.30 mmol) and triethylamine (0.54 mL, 3.86 mmol) were dissolved in dichloromethane (20 mL) and thiophosgene (0.2 mL, 2.61 mmol) was added. The reaction mixture was stirred at room temperature for 1 h. After completion of the reaction. The residue was dissolved into dichloromethane (200 mL) and extracted with water (2x200 mL) was added. The organic layer was dried over sodium sulphate, filtered, and concentrated under reduced pressure. The solvent was removed under reduced pressure. The residue was purified by silica gel column chromotography (10% methanol/dichloromethane) to obtain compound **33** as light brown solid. (0.9 g, 58%).

^{1}H NMR (300 MHz, $CDCl_3$): δ 7.09 (dd, *J*=22.8, 8.2 Hz, 4H; Ar*H*), 3.70−1.71 (br, 52H), 1.24 (br, 45H; $C(C\mathit{H}_3)_3$).

^{13}C NMR (75 MHz, $CDCl_3$): δ 172.3, 171.3, 170.7, 170.5, 170.4 (*C*=O), 138.6, 134.6, 129.8, 128.9, 125.5 (Ar*C*), 82.6, 82.3, 81.2, 81.1 ($\mathit{C}(CH_3)_3$), 70.0, 69.1, 69.0, 58.9, 56.8, 56.4, 55.5, 54.1, 53.3, 52.1, 51.7, 39.7, 37.1, 35.1, 27.9, 27.7, 27.6, 25.7 ($C(\mathit{C}H_3)_3$).

ESI-TOF/MS(m/z): $[M+H]^+$calcd. for $C_{60}H_{104}N_9O_{14}S$, 1206.74180, found 1206.74040.

Protected dendrimeric chelator 34

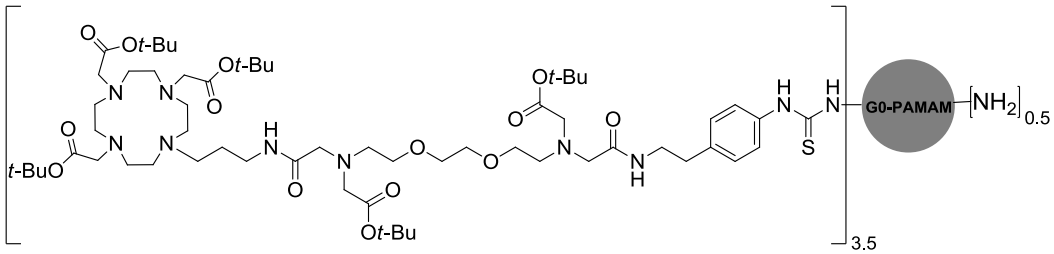

G0 PAMAM dendrimer (15 mg, 29 µmol) and compound **33** (210 mg, 174 µmol) were dissolved in dimethylformamide. Triethylamine (32.4 µL, 232 µmol) was added to the solution. The reaction mixture was stirred at 45 °C for 24 h. The solvent was evaporated and the unreacted ligand was removed using lipophilic sephadex column and methanol as eluent to obtain protected dendrimeric chelator **34** as brown solid (140 mg, 90%).

^{1}H NMR (300 MHz, $CDCl_3$):δ 7.50 (br, Ar*H*), 7.06 (br, Ar*H*), 3.83−1.55 (overlapping m), 1.41 (overlapping m, C(C*H*$_3$)$_3$).

^{13}C NMR (75 MHz, $CDCl_3$): δ 181.3 (*C*=S), 172.0, 171.2, 170.6, 170.4, 170.1, 169.7 (*C*=O), 138.0, 134.9, 128.5, 123.5 (Ar*C*), 81.7, 81.2 (*C*(CH$_3$)$_3$), 70.1, 69.9, 69.2, 68.9, 58.9, 56.6, 55.2, 54.1, 52.9, 52.4, 50.7, 49.9, 47.8, 40.1, 36.2, 35.0 (–*C*H$_2$–), 27.9, 23.3 (C(*C*H$_3$)$_3$).

MALDI-TOF/MS (m/z): $[M+6Na]^+$ calcd. for $C_{262}H_{460}N_{46}Na_6O_{60}S_4^+$ 5477, found 5475: $[M\cdot Na_2]^+$calcd. for $C_{202}H_{357}N_{37}O_{46}S_3$ 4179, found 4183.

Dendrimeric chelator L-8

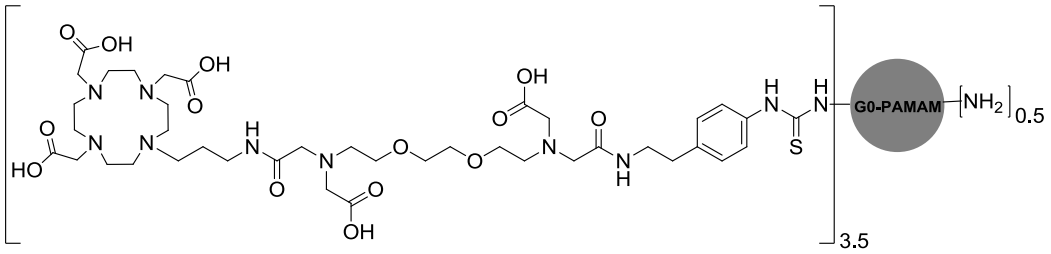

Protected dendrimeric chelator **34** (140 mg, 26 µmol) was dissolved in formic acid (5 mL) and the mixture was stirred at 60 ^{o}C for 16 h. Formic acid was removed under reduced pressure and the product was eluted from G-15 sephadex column using water to remove formic acid residual and dried by lyophilizer to obtain dendrimeric chelator **L-8** as brown solid (69 mg, 62%).

^{1}H NMR (300 MHz, D_2O): δ 7.21 (br, Ar*H*), 4.26−2.39 (overlapping m), 1.81 (br. s).

G0 dendrimeric smart contrast agent DSCA-1

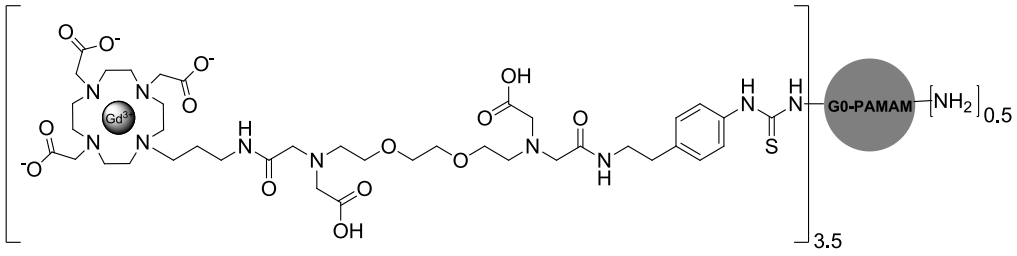

The dendrimeric chelator **L-8** (69 mg, 16 µmol) was dissolved in water and pH was adjusted to 7.0 with 0.1 M sodium hydroxide solution. $GdCl_3 \cdot 6H_2O$ (42.5 mg, 114 µmol) was added to the solution and pH was maintained to 7.0 with the sodium hydroxide solution. The mixture was stirred at room temperature for 24 h (34 mg, 43%). EDTA (120 mg, 324 µmol) was added to the solution to remove excess Gd^{3+} and pH was maintained to 7.0 with the sodium hydroxide solution again. The mixture was stirred at room temperature for 24 h. Excess EDTA was removed by centrifugation using centrifugal filter unit with 3 Kda molecular weight cut-off to obtain **DSCA-1** (102 mg, 79%).

MALDI-TOF/MS (m/z):$[M+4Na]^+$calcd. for $C_{182}H_{288}Gd_4N_{46}Na_4O_{60}S_4^+$, 4929, found 4930; $[M+3Na+3H_2O]^+$ calcd. for $C_{142}H_{228}Gd_3N_{37}Na_3O_{46}S_3(H_2O)_3^+$ 3880, found 3878.

Protected dendrimeric chelator 35

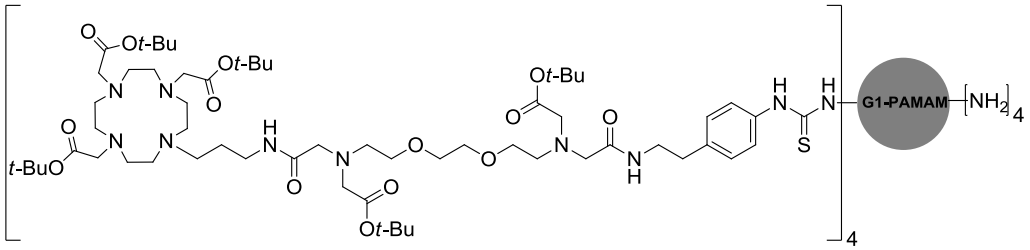

G1 PAMAM dendrimer (65 mg, 45 µmol) and compound **33** (650 mg, 539 µmol) were dissolved in dimethylformamide. Triethylamine (152 µL, 1.09 mmol) was added into the solution. The reaction mixture was stirred at 45 °C for 24 h. The solvent was evaporated and the unreacted ligand was removed by lipophilic sephadex column using methanol to obtain protected dendrimeric chelator **35** (388 mg, 77%).

^{1}H NMR (300 MHz, $CDCl_3$): δ 7.50 (br, Ar*H*), 7.06 (br, Ar*H*), 4.09–1.53 (overlapping m), 1.52–1.26 (overlapping m, C(CH_3)$_3$).

^{13}C NMR (75 MHz, $CDCl_3$): δ 181.4, 173.4, 173.0, 172.4, 172.0, 171.3, 171.3, 170.6, 170.5, 170.4, 170.2, 169.8 (*C*=O), 128.6, 123.6 (Ar*C*), 82.7, 82.3, 81.7, 81.3 (C(*C*H_3)$_3$), 70.2, 69.3,

69.0, 59.1, 56.9, 56.6, 56.3, 55.5, 55.3, 54.2, 52.9, 52.4, 51.8, 50.8, 50.3, 50.0, 47.9, 43.9, 40.3, 38.8, 37.2, 36.3, 35.2, 34.2 (–*C*H_2–), 28.0, 27.9, 27.7 (*C*(CH_3)$_3$).

Dendrimeric chelator L-9

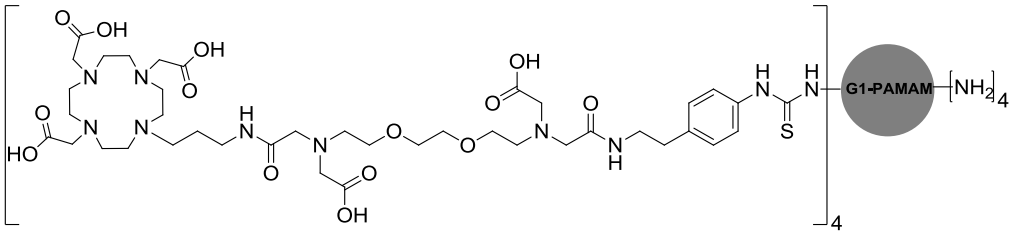

Protected dendrimeric chelator **35** (388 mg, 35 μmol) was dissolved in formic acid (5 mL) and the mixture was stirred at 60 ^oC for 48 h. Formic acid was removed under reduced pressure and the product was eluted through G-15 sephadex column to excess formic acid residual and dried by lyophilizer to obtain dendrimeric chelator **L-9** as light brown solid(300 mg, 97%).

^{1}H NMR (300 MHz, D_2O): δ 7.22 (br, Ar*H*), 4.25−2.50 (overlapping m), 1.83 (br. s).

G1 dendrimeric smart contrast agent DSCA-2

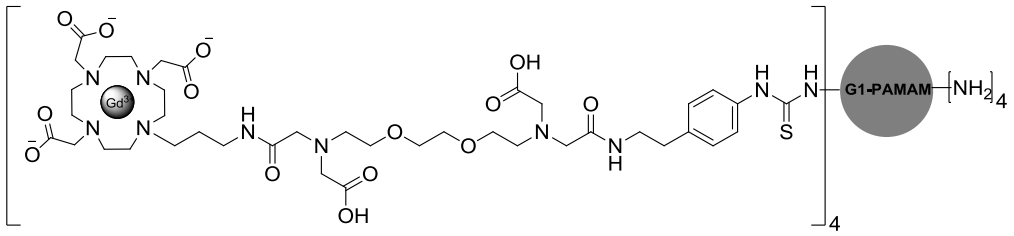

Dendrimeric chelator **L-9** (200 mg, 23 μmol) was dissolved in water and pH was adjusted to 7.0 with 0.1 M sodium hydroxide solution. $GdCl_3 \cdot 6H_2O$ (101 mg, 272 μmol) was added into the solution and pH was maintained to 7.0 with the sodium hydroxide solution. The mixture was stirred at room temperature for 24 h. EDTA (120 mg, 324 μmol) was added into the solution to remove excess Gd^{3+} and pH was maintained to 7.0 with the sodium hydroxide solution again. The mixture was stirred at room temperature for 24 h. Excess EDTA was removed by centrifugation using centrifugal filter unit with 3 Kda molecular weight cut-off to obtain **DSCA-2** as light brown solid (220 mg, 97%).

MALDI-TOF/MS (m/z): $[M+22Na+8H_2O]^+$ calcd. for $C_{222}H_{368}Gd_4N_{62}Na_{22}O_{68}S_4(H_2O)_8^+$, 6400, found 6402.

Protected dendrimeric chelator 36

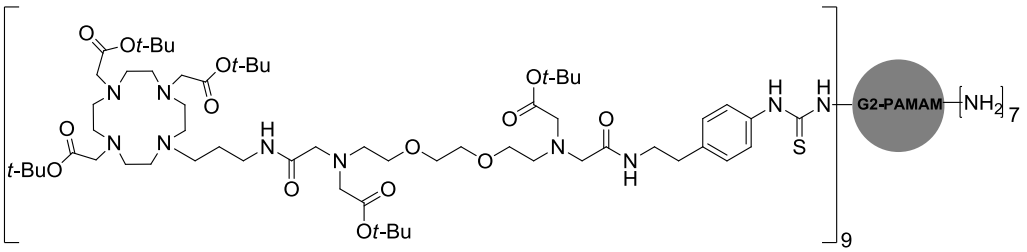

G2 PAMAM (60 mg, 18 µmol) and compound **33** (534 mg, 443 µmol) were dissolved in dimethylformamide. Triethylamine (93 µL, 664 µmol) was added into the solution. The reaction mixture was stirred at 45 °C for 24 h. The solvent was evaporated and the unreacted ligand was removed using lipophilic sephadex column and methanol as eluent to obtain protected dendrimeric chelator **36** as brown solid (260 mg, 63%).

^{1}H NMR (300 MHz, $CDCl_3$):δ 7.42 (br, Ar*H*), 7.02 (br, Ar*H*), 4.07−1.49 (br), 1.36 (br, C(CH_3)$_3$).

Dendrimeric chelator L-10

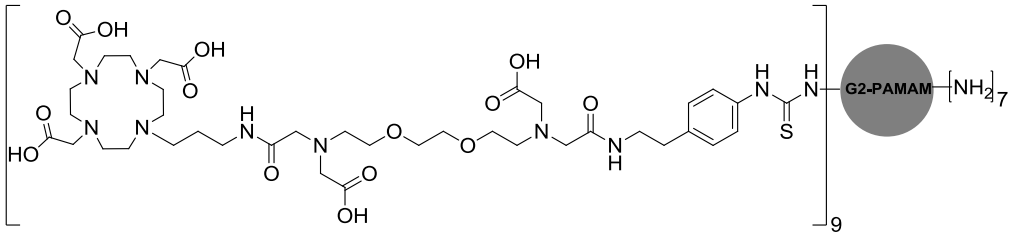

Protected dendrimeric chelator **36** (260 mg, 12 µmol) was dissolved in formic acid (5 mL) and the mixture was stirred at 60^{o}C for 48 h. Formic acid was removed under reduced pressure and the residue was eluted from G-15 sephadex column to remove formic acid residual and dried by lyophilizer to obtain dendrimeric chelator **L-10** as light brown solid (180 mg, 86%).

^{1}H NMR (300 MHz, D_2O): δ 7.22 (dd, ArH), 4.00−2.02 (overlapping m), 1.81 (br).

^{13}C NMR (75 MHz, D_2O): δ 181.2 (*C*=S), 173.2, 172.9, 172.2, 171.9, 171.1, 170.5, 170.4, 170.1, 169.7 (*C*=O), 137.6, 135.0, 128.5, 123.6 (Ar*C*), 82.6, 82.2, 81.5, 81.1 (*C*(CH_3)$_3$), 70.0, 69.9, 69.2, 68.9, 58.9, 56.7, 54.5, 55.2, 54.1, 52.8, 52.3, 50.6, 49.9, 47.7, 40.2, 38.7, 36.2, 35.1 (–*C*H_2–), 27.9, 27.7, 27.6, 23.3 (C(*C*H_3)$_3$).

G2 dendrimeric smart contrast agent DSCA-3

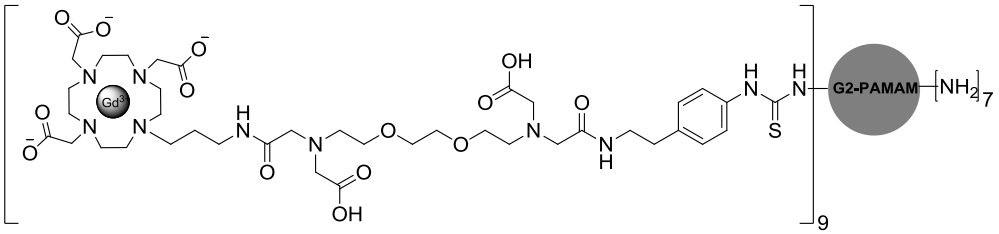

Dendrimeric chelator **L-10** (69 mg, 16 µmol) was dissolved in water and pH was adjusted to 7.0 with 0.1 M of sodium hydroxide. $GdCl_3 \cdot 6H_2O$ (42.5 mg, 114 µmol) was added into the solution and pH was maintained to 7.0 with the sodium hydroxide solution. The mixture was stirred at room temperature for 24 h. EDTA (120 mg, 324 µmol) was added into the solution to remove excess Gd^{3+} and pH was maintained to 7.0 with the sodium hydroxide solution again. The mixture was stirred at room temperature for 24 h. Excess EDTA was removed by centrifugation using centrifugal filter unit with 3 Kda molecular weight cut-off to obtain **DSCA-3** as light brown solid.

MALDI-TOF/MS (m/z): $[M+14Na+34H_2O]^+$ calcd. for $C_{502}H_{828}Gd_9N_{139}Na_{14}O_{154}S_9(H_2O)_{34}$ 13911, found 13911.

6. Appendix

Table 6-1. MRI signal intensity of contrast agent-treated Neutravidin™ agarose beads

	Raw T1-weighted Signal Intensity[a]				Normalized Signal Intensity (%)[b]		
Relaxation time (TR) (ms)	PBS	Dotarem	**MCA-2**	**DCA-2**	Dotarem	**MCA-2**	**DCA-2**
21	30205	31222	38155	163264	103.4	126.3	540.5
26	31995	33586	45928	213812	105.0	143.5	668.3
32	35320	37433	53900	273389	106.0	152.6	774.0
39	39842	42123	66493	345509	105.7	166.9	867.2
48	45392	49679	83102	428543	109.4	183.1	944.1
59	55074	59627	103428	526520	108.3	187.8	956.0
72	66754	73883	129923	635023	110.7	194.6	951.3
88	81962	90813	161655	759372	110.8	197.2	926.5
108	102114	112868	200831	890228	110.5	196.7	871.8
133	126681	141842	251670	1026923	112.0	198.7	810.6
163	154439	170959	305331	1150291	110.7	197.7	744.8
200	191450	211817	376278	1277859	110.6	196.5	667.5
246	235841	260353	457010	1391155	110.4	193.8	589.9
301	288802	321776	552587	1489933	111.4	191.3	515.9
370	353929	387588	662105	1570171	109.5	187.1	443.6
454	430660	470338	790276	1625685	109.2	183.5	377.5
557	518904	568493	929902	1662420	109.6	179.2	320.4
684	623150	679461	1087611	1684562	109.0	174.5	270.3
840	742443	810691	1261306	1694046	109.2	169.9	228.2
1031	879113	960147	1440590	1700071	109.2	163.9	193.4
1265	1023068	1106161	1605158	1693854	108.1	156.9	165.6
1553	1192878	1283991	1783411	1697225	107.6	149.5	142.3
1906	1374272	1470922	1947683	1696649	107.0	141.7	123.5
2340	1568880	1665124	2088443	1700061	106.1	133.1	108.4
2872	1754334	1858830	2200053	1695213	106.0	125.4	96.6
3525	1941373	2029596	2275666	1699271	104.5	117.2	87.5
4326	2100778	2184743	2329165	1699888	104.0	110.9	80.9
5310	2237934	2305895	2355081	1699088	103.0	105.2	75.9
6518	2343384	2396336	2367133	1706615	102.3	101.0	72.8
8000	2412255	2457246	2377609	1703788	101.9	98.6	70.6

a) Average pixel intensities from a region-of-interest encompassing each of the four CA-treated bead samples in T1-weighted images acquired at different relaxation times (TR). Values are averages from three CA-bead binding experiments.

b) Raw signal intensities were normalized and expressed as a percentage of the PBS control.

6.1 Relaxometric Ca^{2+} titrations

Relaxometric experiments were performed on a Bruker Avance III 300 MHz spectrometer, Germany. Upon addition of Ca^{2+}, the r_1 changes are shown below for each SCA.

Table 6-2. Ca^{2+} titration of **SCA-1**.

$[Ca^{2+}]$ (mM)	$[Gd^{3+}]$ (mM)	$[Ca^{2+}]/[Gd^{3+}]$	T_1 (ms)	r_1 (mM^{-1}/s^{-1})
0.00	3.00	0.0	100.39	3.20
0.30	2.97	0.1	91.12	3.58
0.59	2.94	0.2	82.56	4.00
0.87	2.91	0.3	75.13	4.45
1.15	2.88	0.4	69.07	4.90
1.43	2.86	0.5	63.91	5.35
1.70	2.83	0.6	59.35	5.83
1.96	2.80	0.7	55.41	6.31
2.22	2.78	0.8	51.96	6.80
2.48	2.75	0.9	49.68	7.19
2.73	2.73	1.0	48.76	7.39
2.97	2.70	1.1	48.84	7.45
3.21	2.68	1.2	49.30	7.44
3.45	2.65	1.3	49.61	7.46
3.68	2.63	1.4	49.95	7.48
3.91	2.61	1.5	50.33	7.48
4.91	2.59	2.0	50.68	7.49
6.15	2.56	2.5	51.34	7.46
7.37	2.54	3.0	51.91	7.44
8.57	2.52	3.5	52.51	7.41
9.75	2.50	4.0	52.96	7.41

r_1 relaxivity change of **SCA-1** was plotted versus equiv. Ca^{2+} per Gd^{3+} using the data in table 6-2 (Figure 6-1).

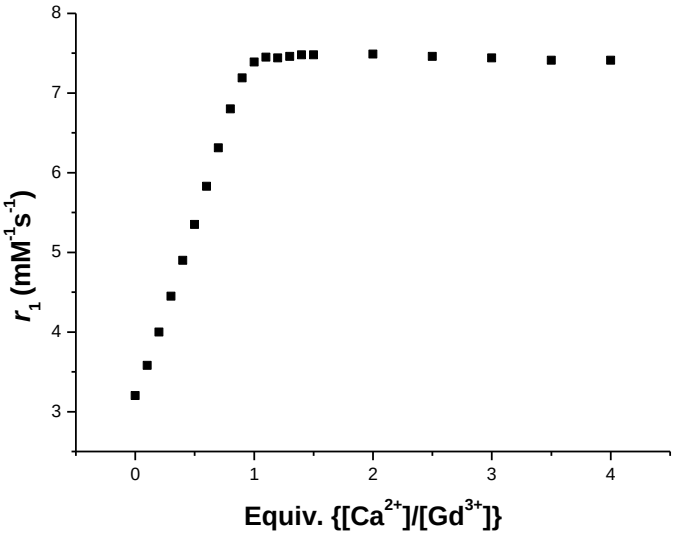

Figure 6-1. The Ca^{2+} dependent relaxivity response of **SCA-1**.

Table 6-3. Ca^{2+} titration of **DSCA-1**.

$[Ca^{2+}]$ (mM)	$[Gd^{3+}]$ (mM)	$[Ca^{2+}]/[Gd^{3+}]$	T_1 (ms)	r_1 (mM^{-1}/s^{-1})
0.00	3.00	0.0	96.74	3.33
0.30	2.97	0.1	92.24	3.53
0.59	2.94	0.2	87.62	3.76
0.87	2.91	0.3	82.79	4.03
1.15	2.88	0.4	78.35	4.30
1.43	2.86	0.5	73.63	4.63
1.70	2.83	0.6	69.29	4.98
1.96	2.80	0.7	65.28	5.34
2.22	2.78	0.8	61.50	5.73
2.48	2.75	0.9	58.26	6.11
2.73	2.73	1.0	56.96	6.31
2.97	2.70	1.1	57.12	6.35
3.21	2.68	1.2	57.45	6.37
3.45	2.65	1.3	57.74	6.39
3.68	2.63	1.4	58.06	6.41
3.91	2.61	1.5	58.38	6.43
4.91	2.59	2.0	58.89	6.43
6.15	2.56	2.5	59.40	6.43
7.37	2.54	3.0	59.63	6.46
8.57	2.52	3.5	60.48	6.42
9.75	2.50	4.0	61.05	6.41

r_1 relaxivity change of **DSCA-1** was plotted versus equiv. Ca^{2+} per Gd^{3+} using the data in Table 6-3 (Figure 6-2).

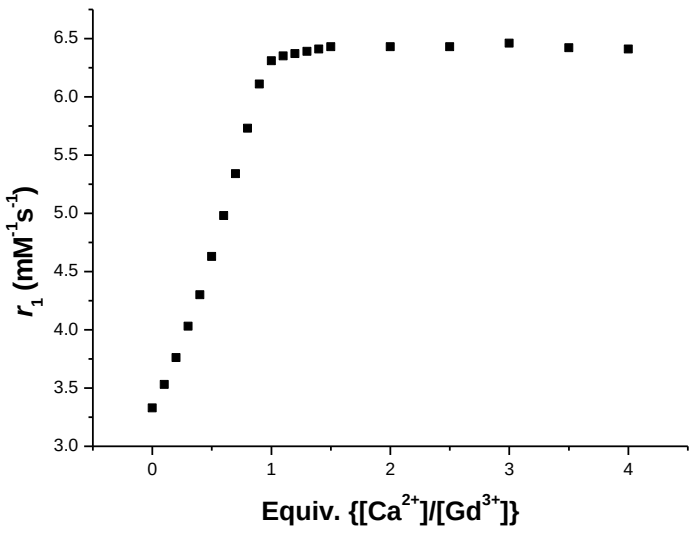

Figure 6-2. Ca^{2+} dependent relaxivity response of **DSCA-1**.

Table 6-4. Ca^{2+} titration of **DSCA-2**.

$[Ca^{2+}]$ (mM)	$[Gd^{3+}]$ (mM)	$[Ca^{2+}]/[Gd^{3+}]$	T_1 (ms)	r_1 (mM^{-1}/s^{-1})
0.00	3.00	0.0	95.90	3.36
0.30	2.97	0.1	94.58	3.44
0.59	2.94	0.2	92.38	3.56
0.87	2.91	0.3	90.27	3.68
1.15	2.88	0.4	87.74	3.83
1.43	2.86	0.5	85.12	3.99
1.70	2.83	0.6	82.70	4.15
1.96	2.80	0.7	79.91	4.34
2.22	2.78	0.8	77.10	4.54
2.48	2.75	0.9	74.32	4.76
2.73	2.73	1.0	71.78	4.98
2.97	2.70	1.1	69.05	5.23
3.21	2.68	1.2	67.12	5.43
3.45	2.65	1.3	65.48	5.62
3.68	2.63	1.4	64.08	5.80
3.91	2.61	1.5	63.20	5.93
4.91	2.59	2.0	62.14	6.09
6.15	2.56	2.5	62.16	6.14
7.37	2.54	3.0	62.45	6.16
8.57	2.52	3.5	62.76	6.18
9.75	2.50	4.0	63.12	6.20

r_1 relaxivity change of **DSCA-2** was plotted versus equiv. Ca^{2+} per Gd^{3+} using the data in Table 6-4 (Figure 6-3).

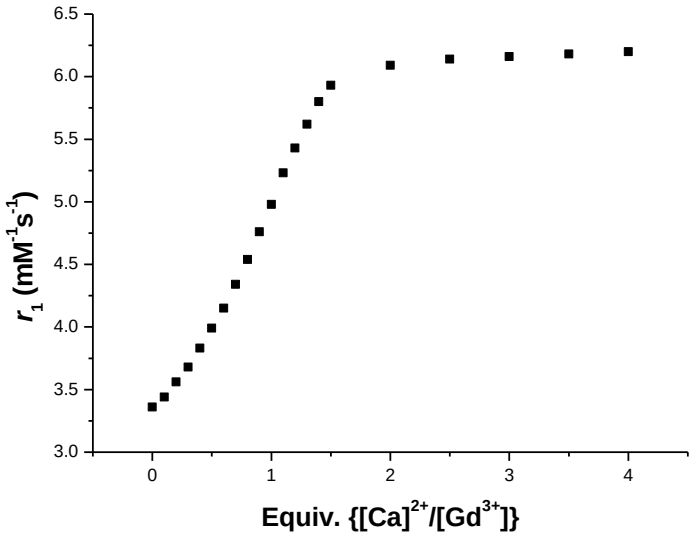

Figure 6-3. Ca^{2+} dependent relaxivity response of **DSCA-2**.

Table 6-5. Ca^{2+} titration of **DSCA-3**.

$[Ca^{2+}]$ (mM)	$[Gd^{3+}]$ (mM)	$[Ca^{2+}]/[Gd^{3+}]$	T_1 (ms)	r_1 (mM^{-1}/s^{-1})
0.00	3.00	0.0	95.27	3.38
0.30	2.97	0.1	93.12	3.50
0.59	2.94	0.2	90.53	3.64
0.87	2.91	0.3	87.38	3.81
1.15	2.88	0.4	84.09	4.00
1.43	2.86	0.5	80.62	4.22
1.70	2.83	0.6	77.04	4.46
1.96	2.80	0.7	73.45	4.73
2.22	2.78	0.8	69.99	5.02
2.48	2.75	0.9	66.59	5.33
2.73	2.73	1.0	63.21	5.67
2.97	2.70	1.1	60.23	6.01
3.21	2.68	1.2	57.81	6.33
3.45	2.65	1.3	57.34	6.44
3.68	2.63	1.4	57.62	6.46
3.91	2.61	1.5	57.98	6.48
4.91	2.59	2.0	58.27	6.50
6.15	2.56	2.5	58.67	6.51
7.37	2.54	3.0	59.13	6.51
8.57	2.52	3.5	59.58	6.52
9.75	2.50	4.0	60.06	6.52

r_1 relaxivity change of **DSCA-3** was plotted versus equiv. Ca^{2+} per Gd^{3+} using the data in Table 6-5 (Figure 6-4).

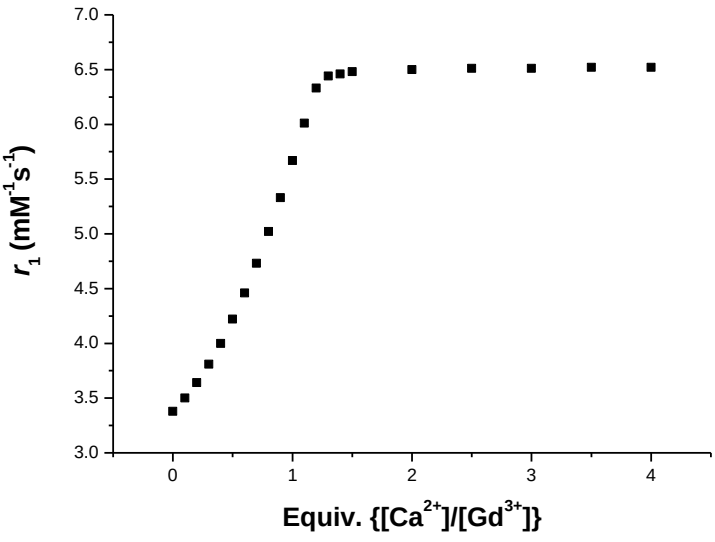

Figure 6-4. Ca^{2+} dependent relaxivity response of **DSCA-3**.

6.2 MALDI-TOF/MS and ^{1}H-NMR spectra of important compounds

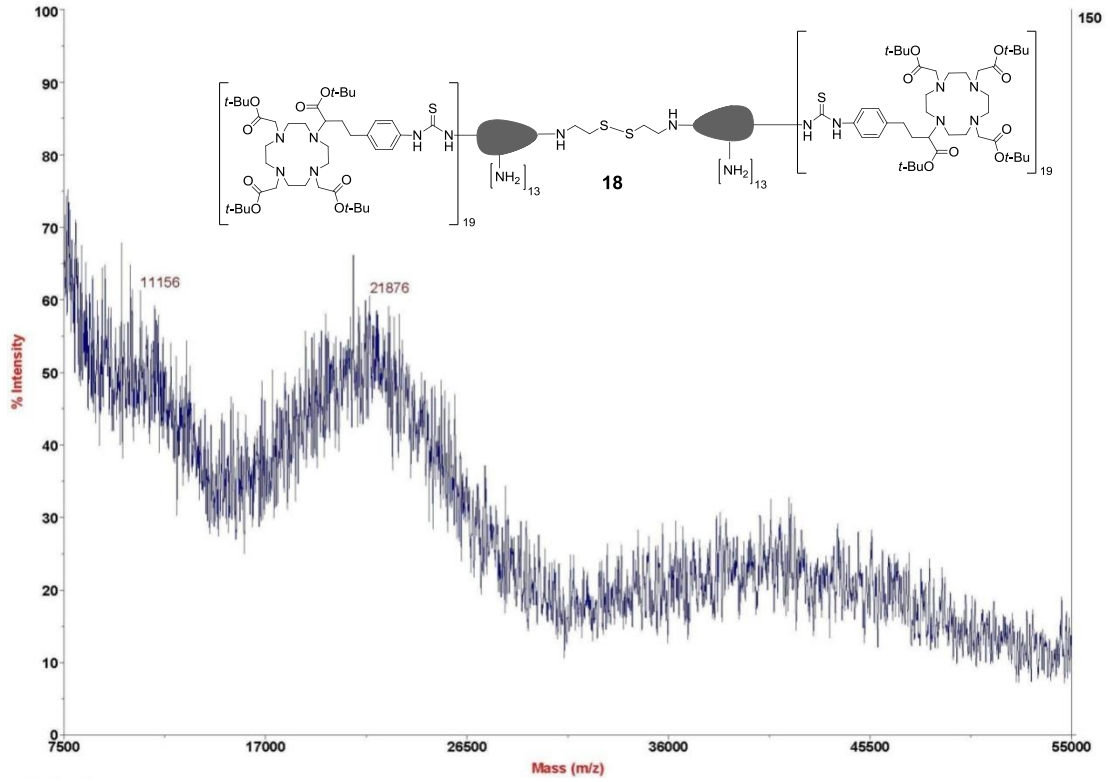

Figure 6-5. MALDI-TOF mass spectrum of **18**.

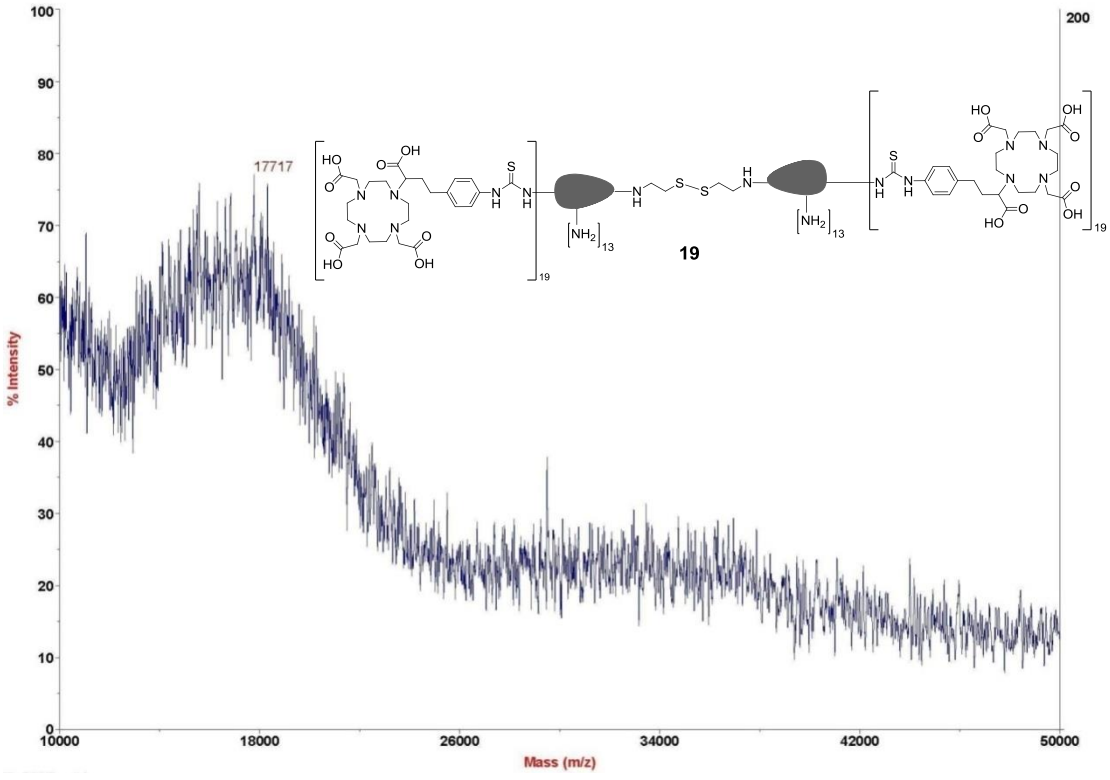

Figure 6-6. MALDI-TOF mass spectrum of **19**.

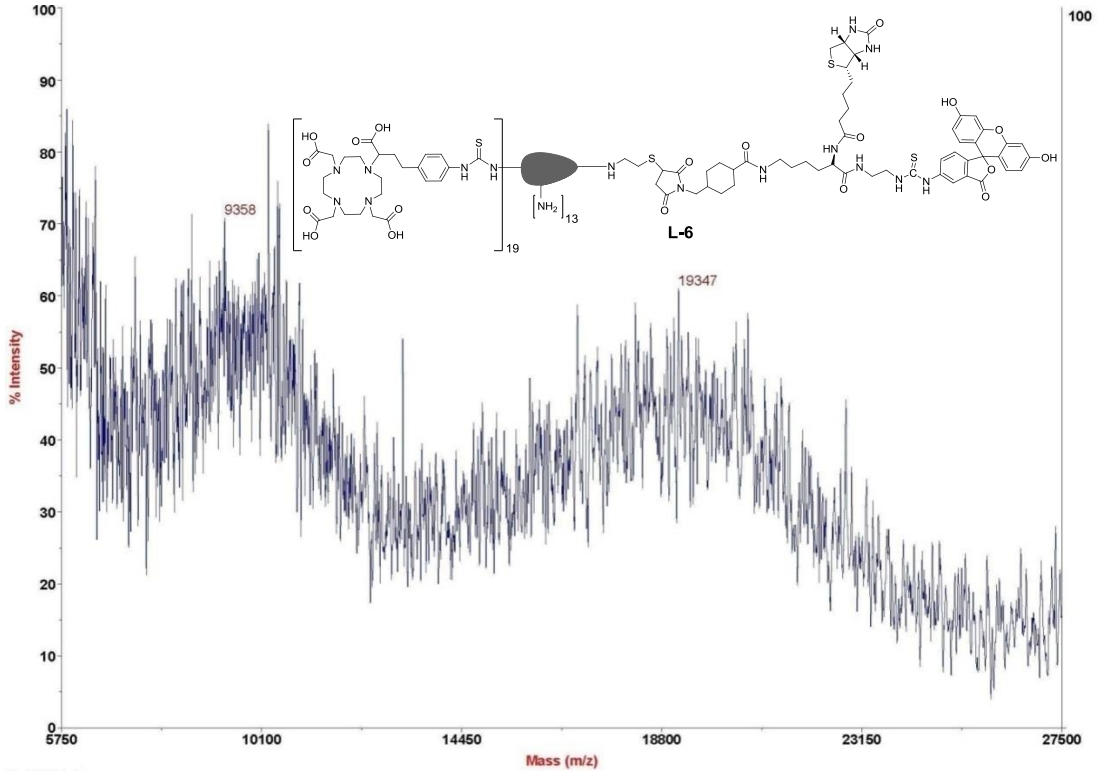

Figure 6-7. MALDI-TOF mass spectrum of **L-6**.

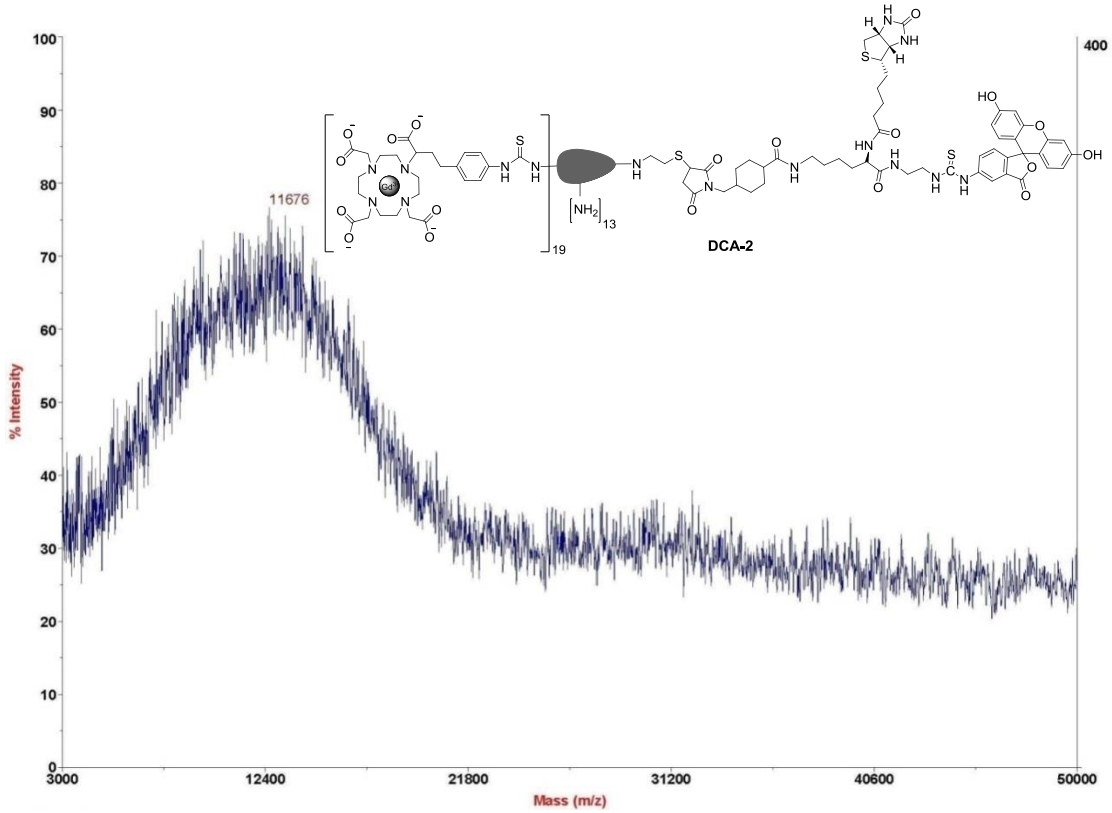

Figure 6-8. MALDI-TOF mass spectrum of **DCA-2**.

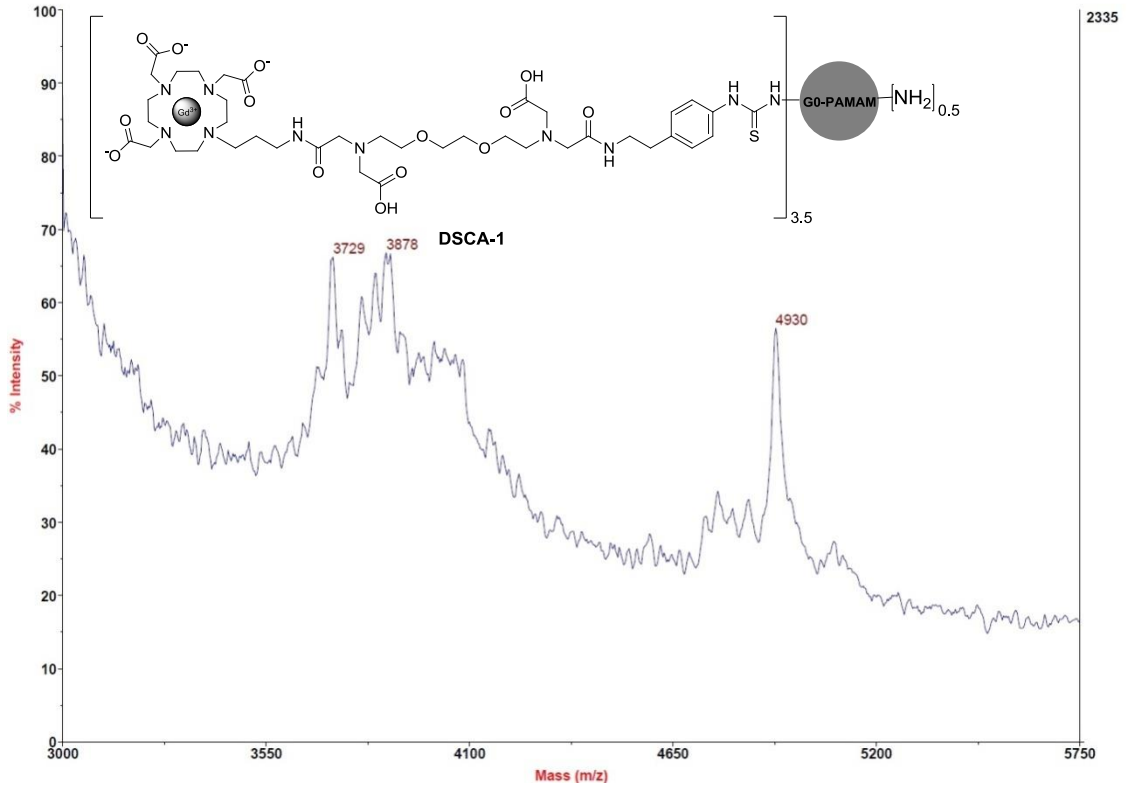

Figure 6-9. MALDI-TOF mass spectrum of **DSCA-1**.

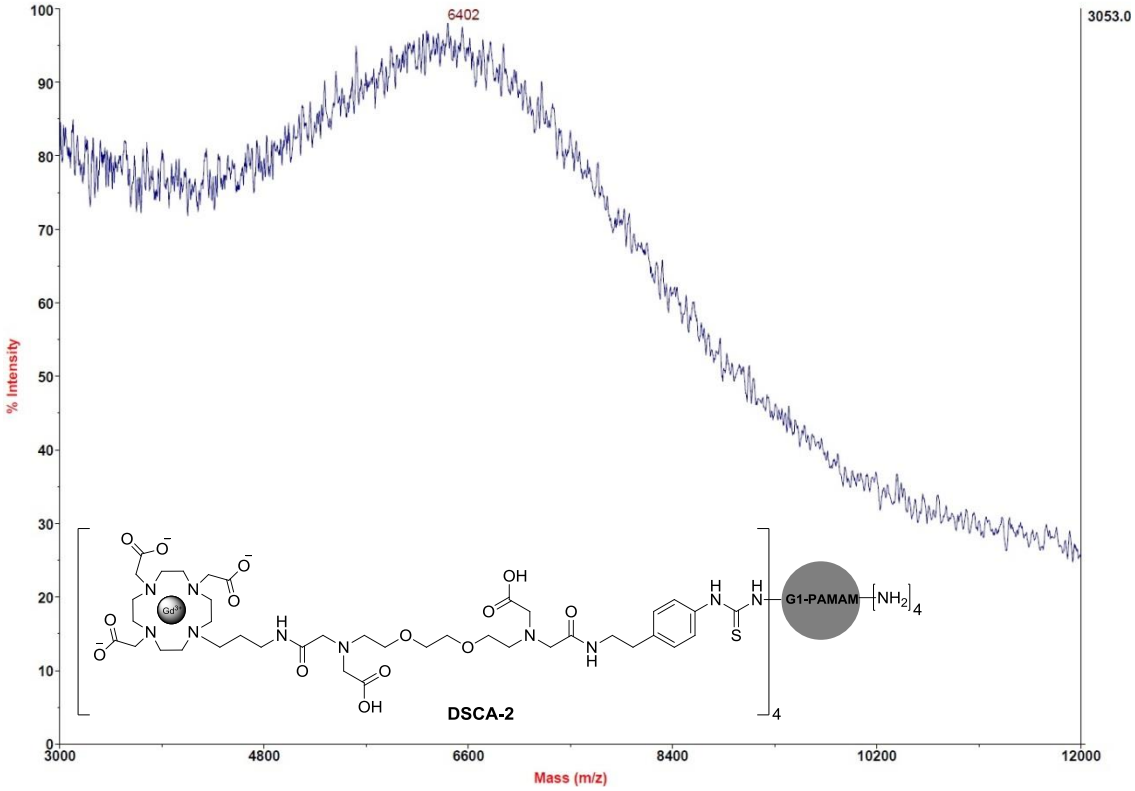

Figure 6-10. MALDI-TOF mass spectrum of **DSCA-2**.

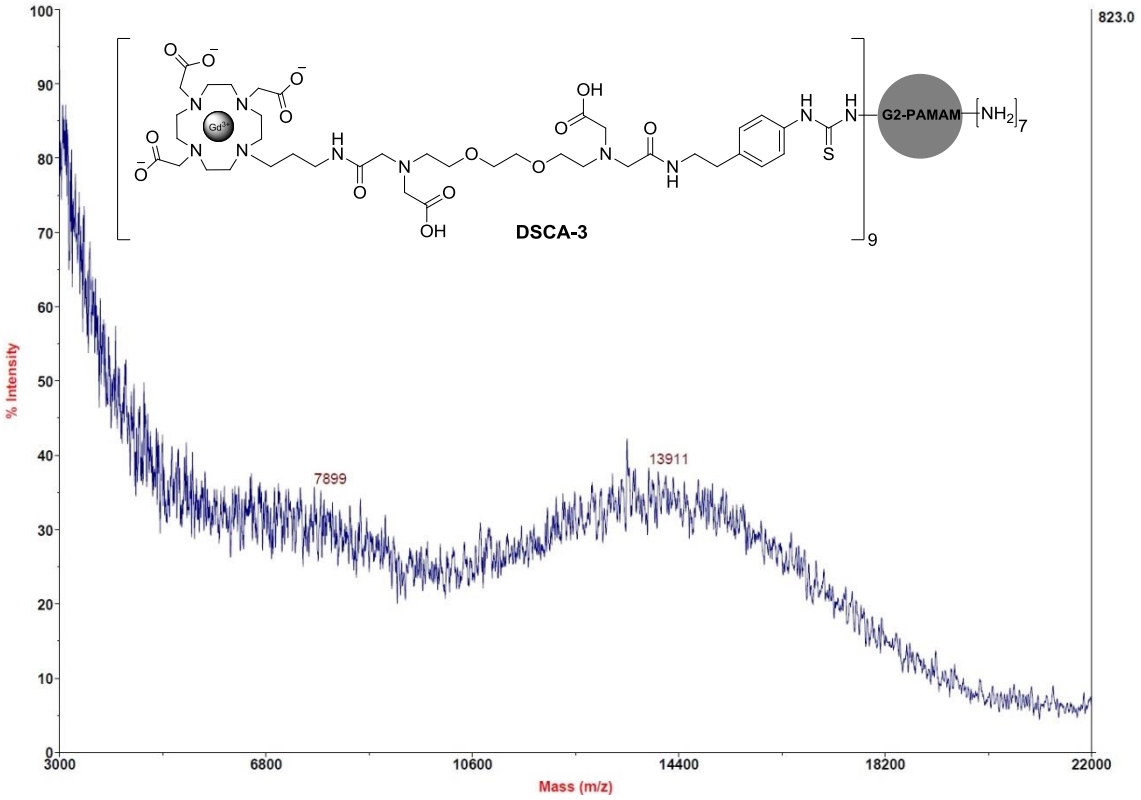

Figure 6-11. MALDI-TOF mass spectrum of **DSCA-3**.

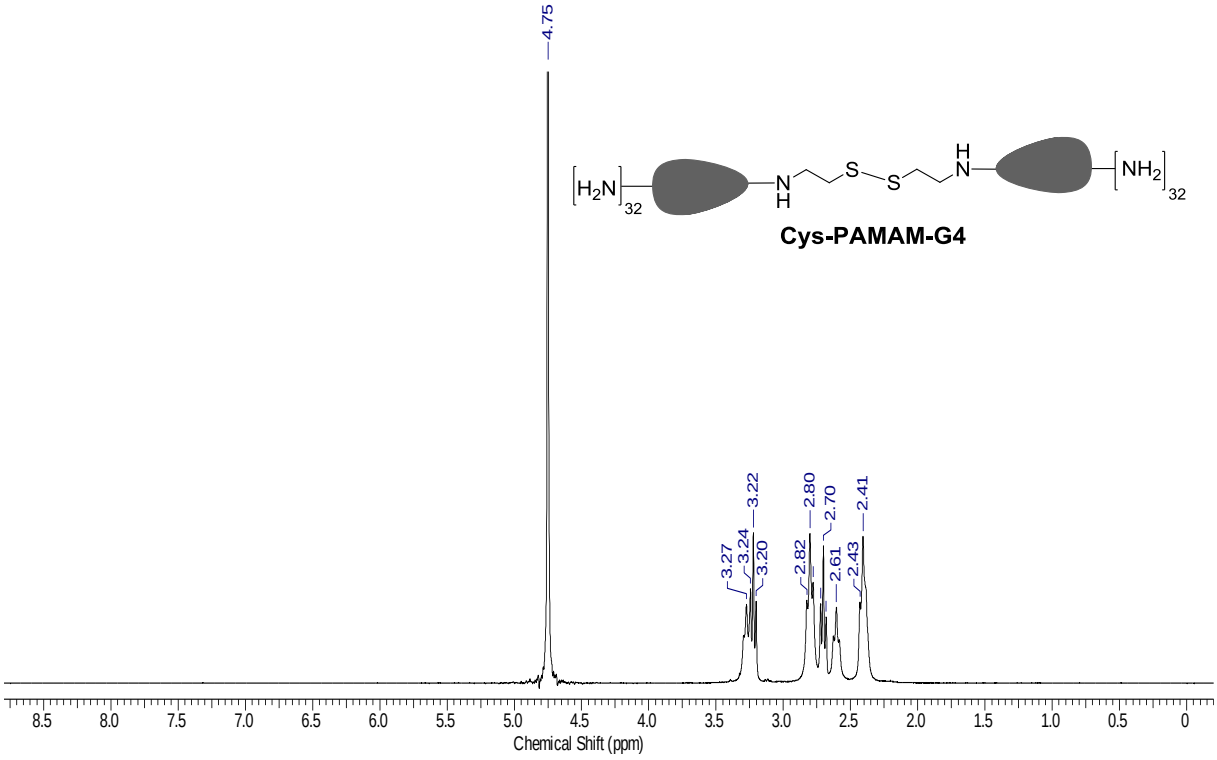

Figure 6-12. ^{1}H NMR spectrum of Cys-PAMAM-G4 (300 MHz, D_2O).

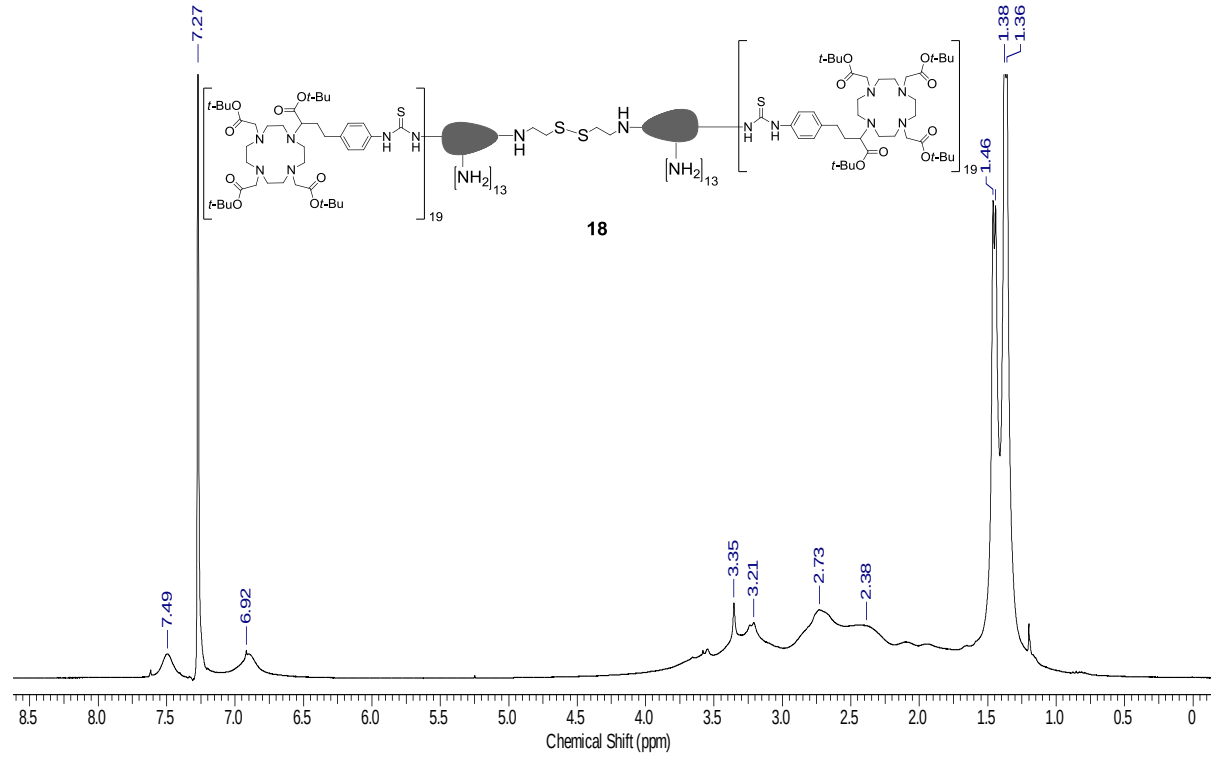

Figure 6-13. ^{1}H NMR spectrum of **18** (300 MHz, $CDCl_3$).

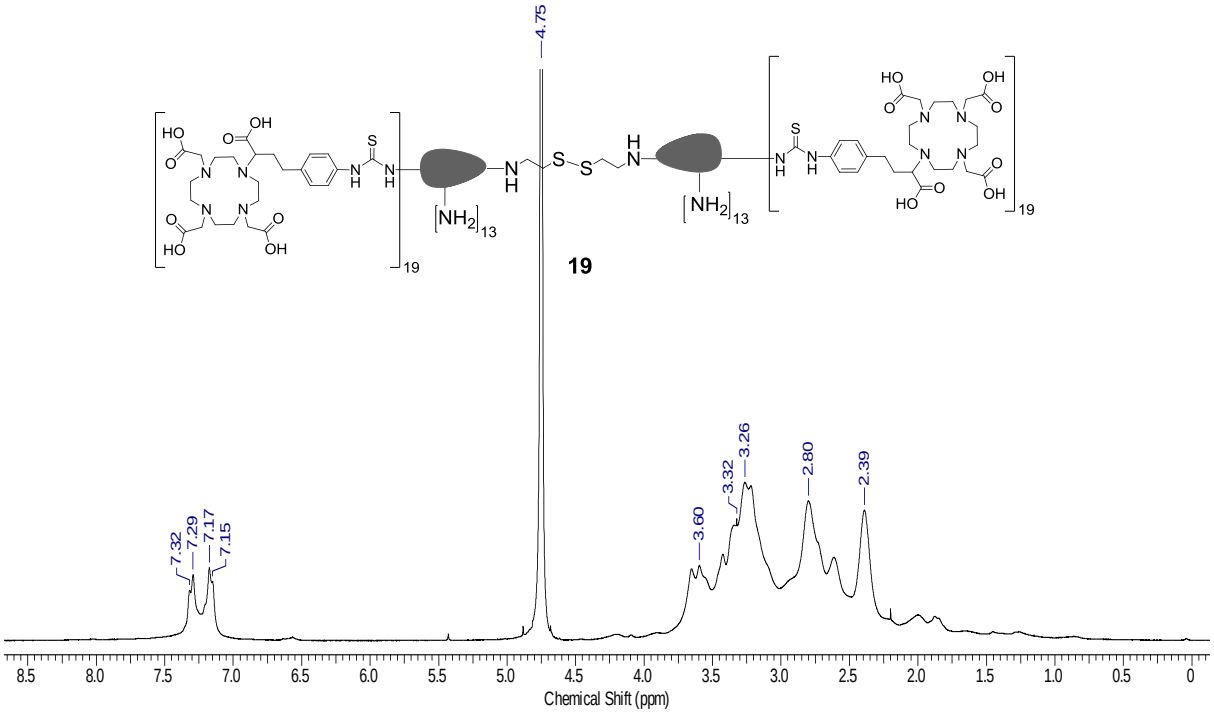

Figure 6-14. ^{1}H NMR spectrum of 1**9** (300 MHz, D_2O).

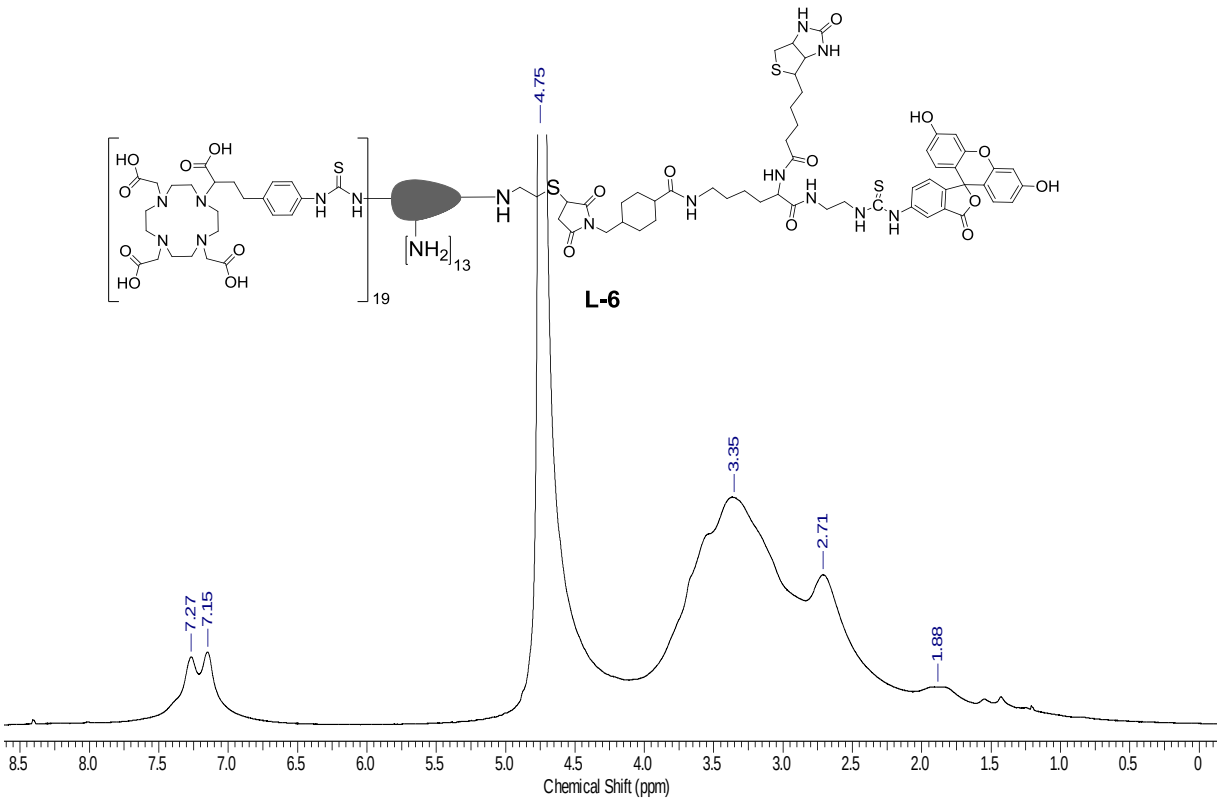

Figure 6-15. ^{1}H NMR spectrum of **L-6** (300 MHz, D_2O).

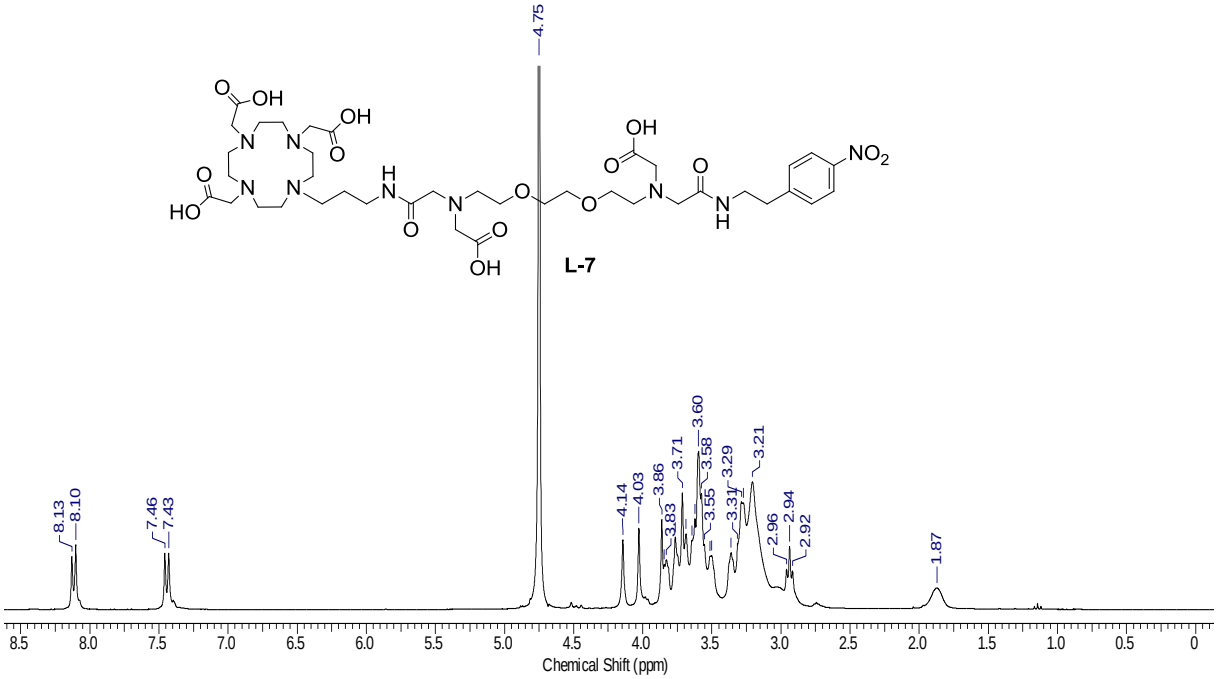

Figure 6-16. ^{1}H NMR spectrum of **L-7** (300 MHz, D_2O).

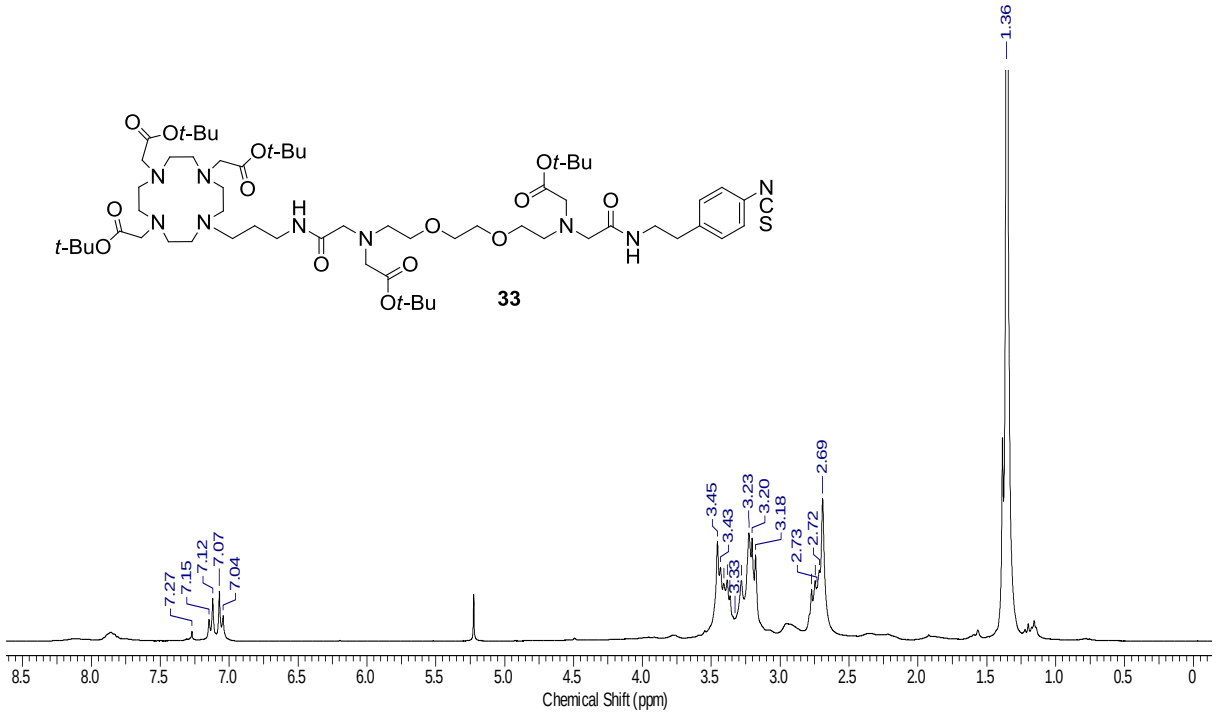

Figure 6-17. ^{1}H NMR spectrum of **33** (300 MHz, $CDCl_3$).

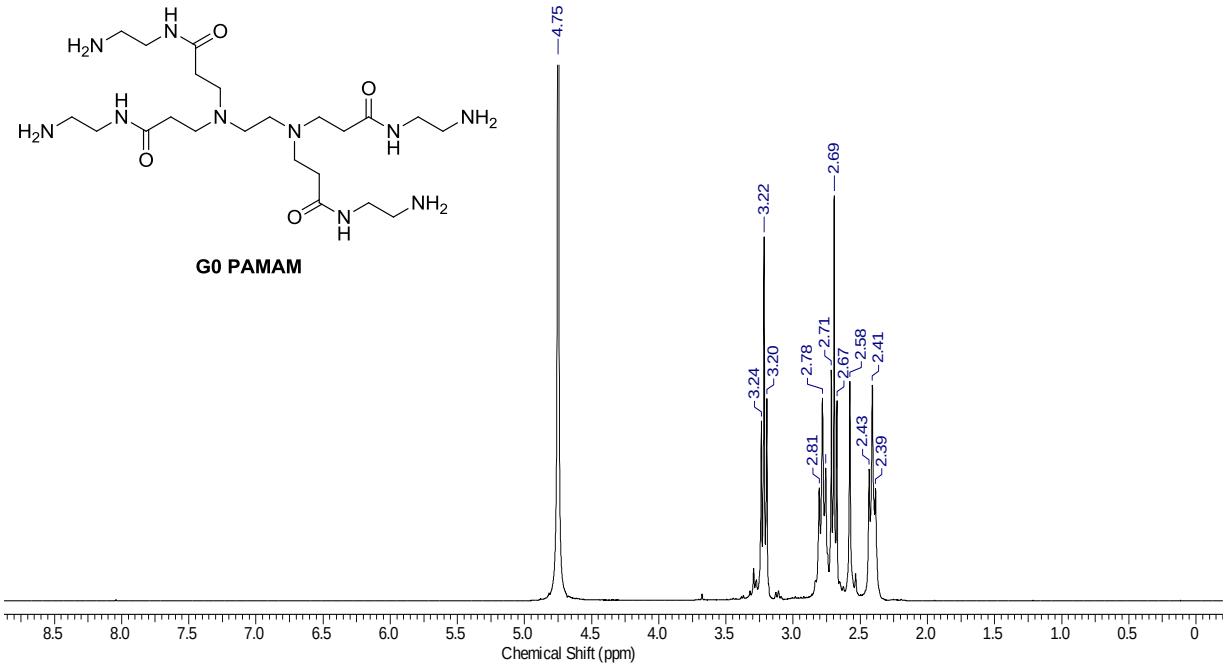

Figure 6-18. ^{1}H NMR spectrum of **G0 PAMAM** (300 MHz, D_2O).

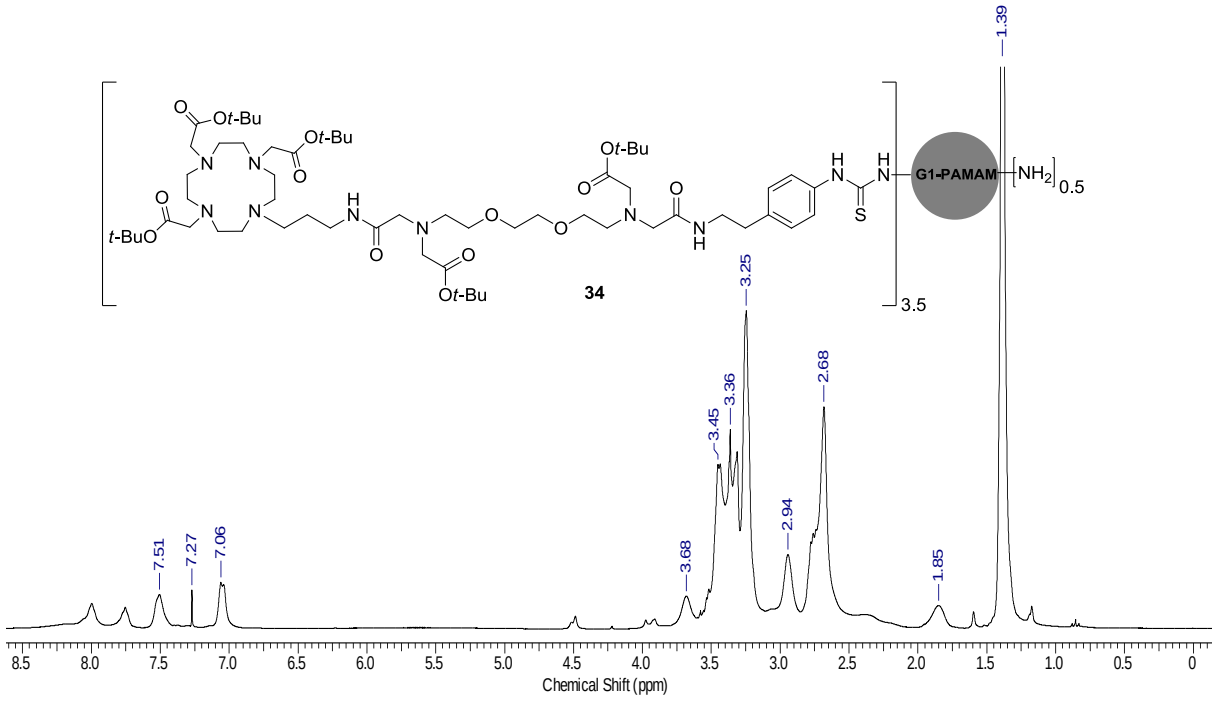

Figure 6-19. ^{1}H NMR spectrum of **34** (300 MHz, $CDCl_3$).

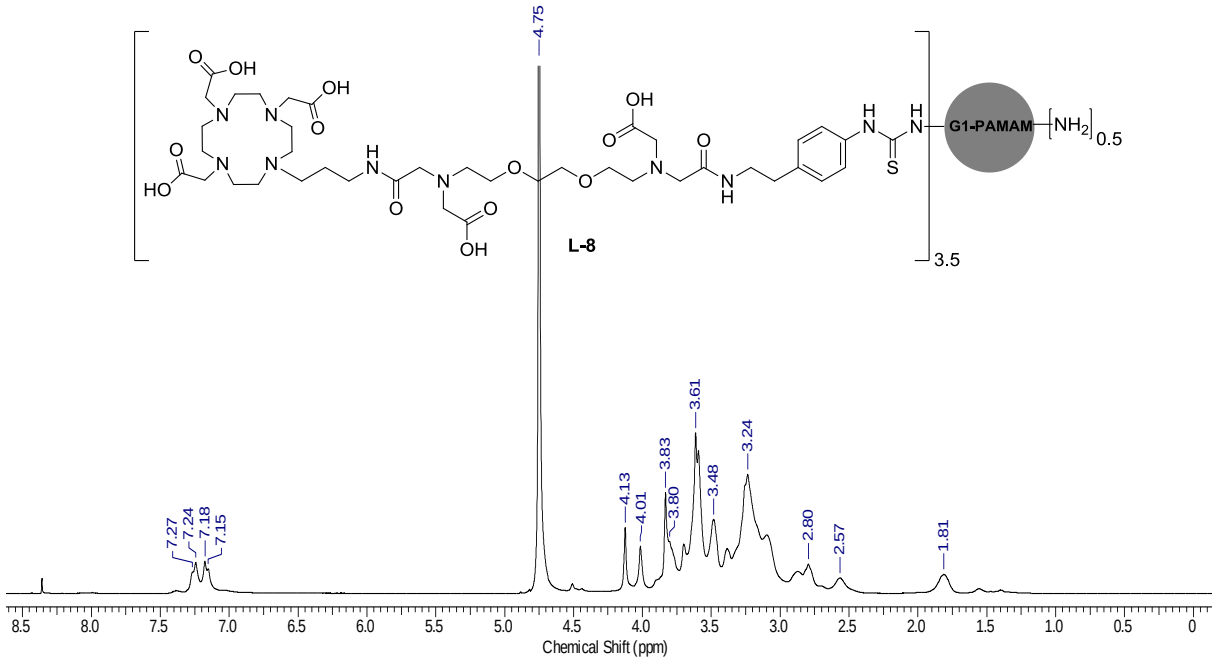

Figure 6-20. ^{1}H NMR spectrum of **L-8** (300 MHz, D_2O).

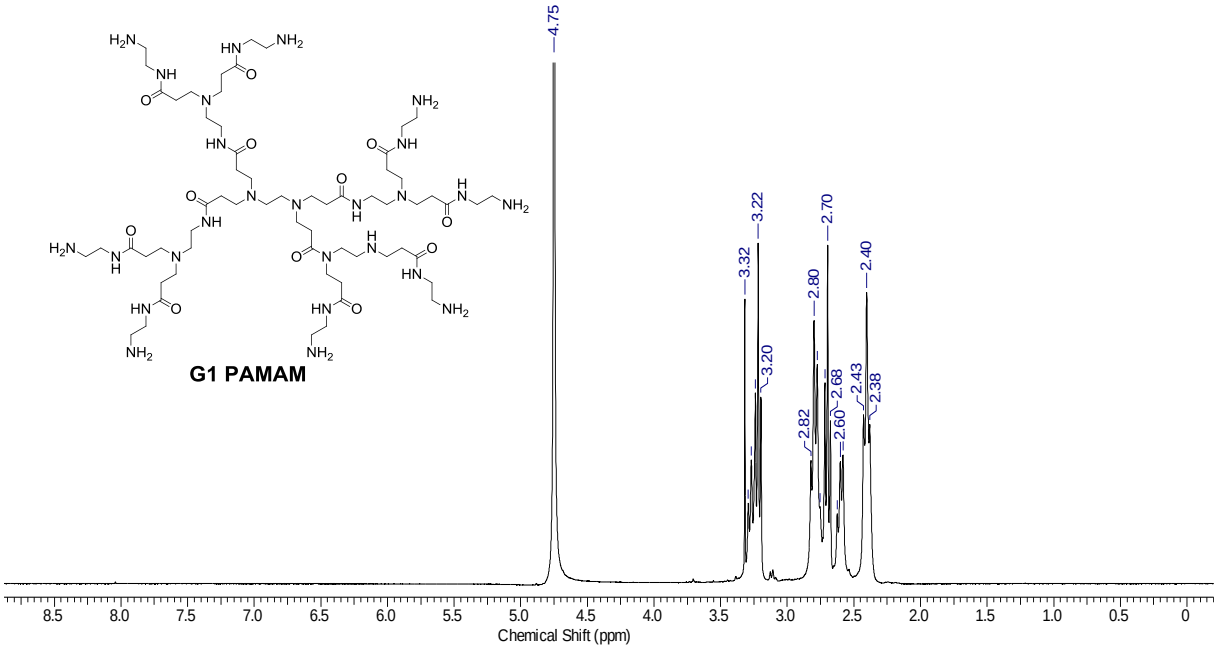

Figure 6-21. ^{1}H NMR spectrum of **G1 PAMAM** (300 MHz, D_2O).

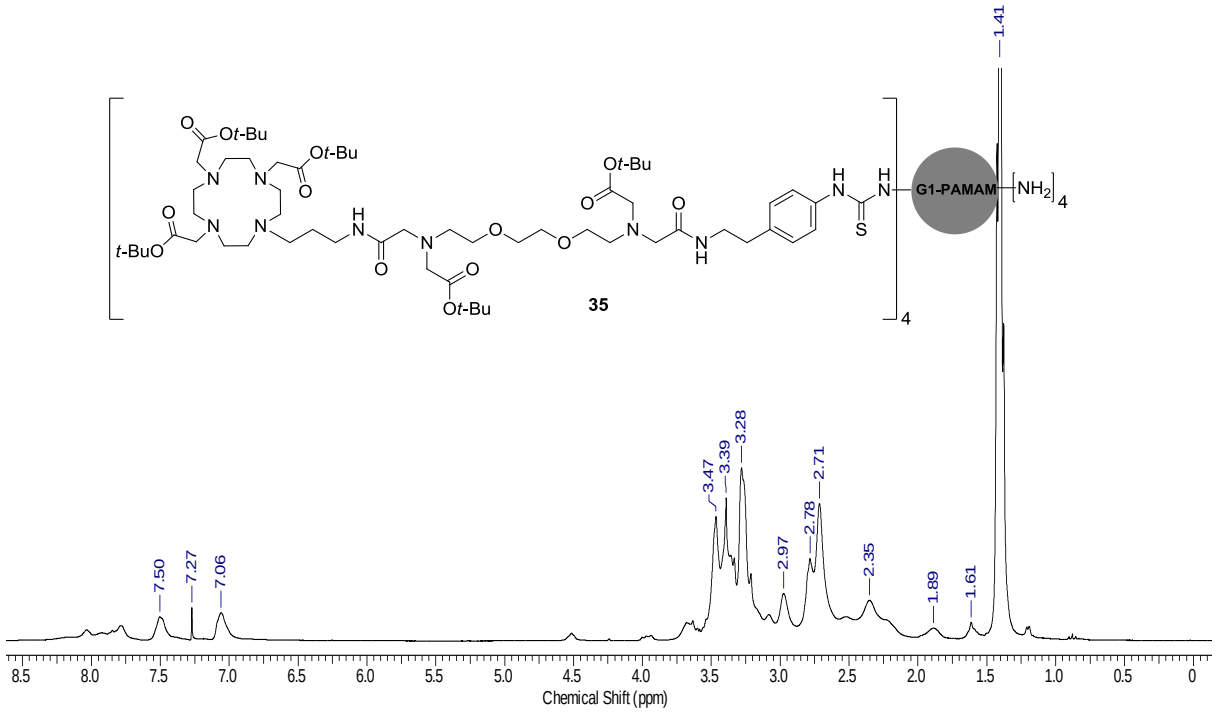

Figure 6-22. ^{1}H NMR spectrum of **35** (300 MHz, $CDCl_3$).

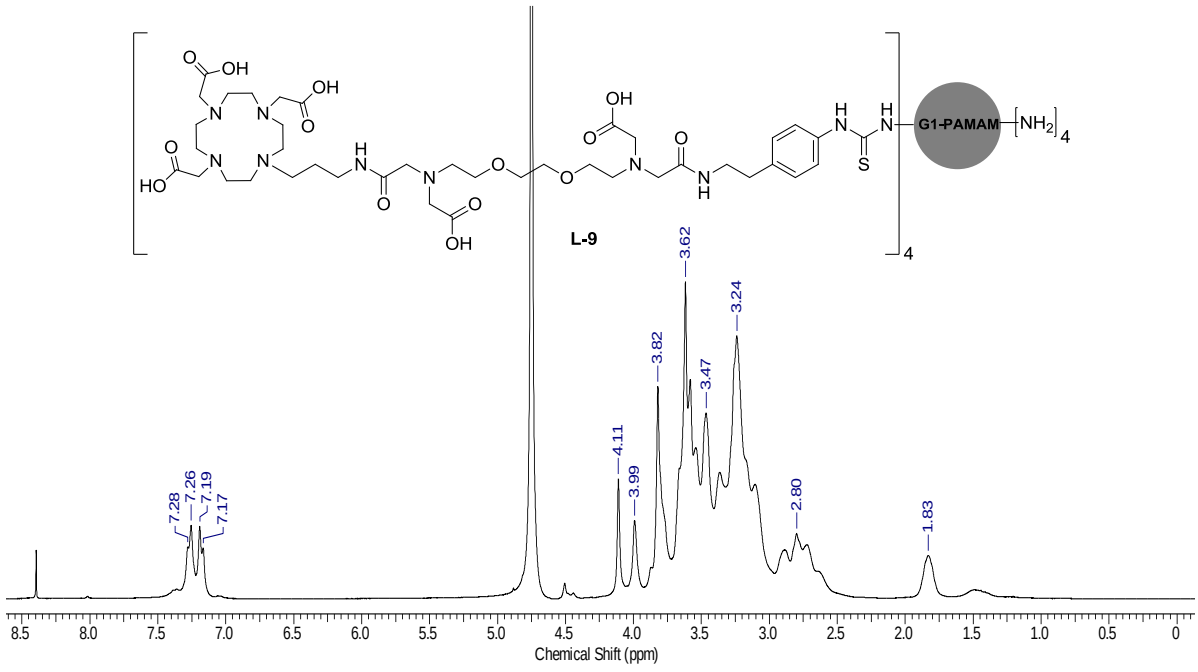

Figure 6-23. ^{1}H NMR spectrum of **L-9** (300 MHz, D_2O).

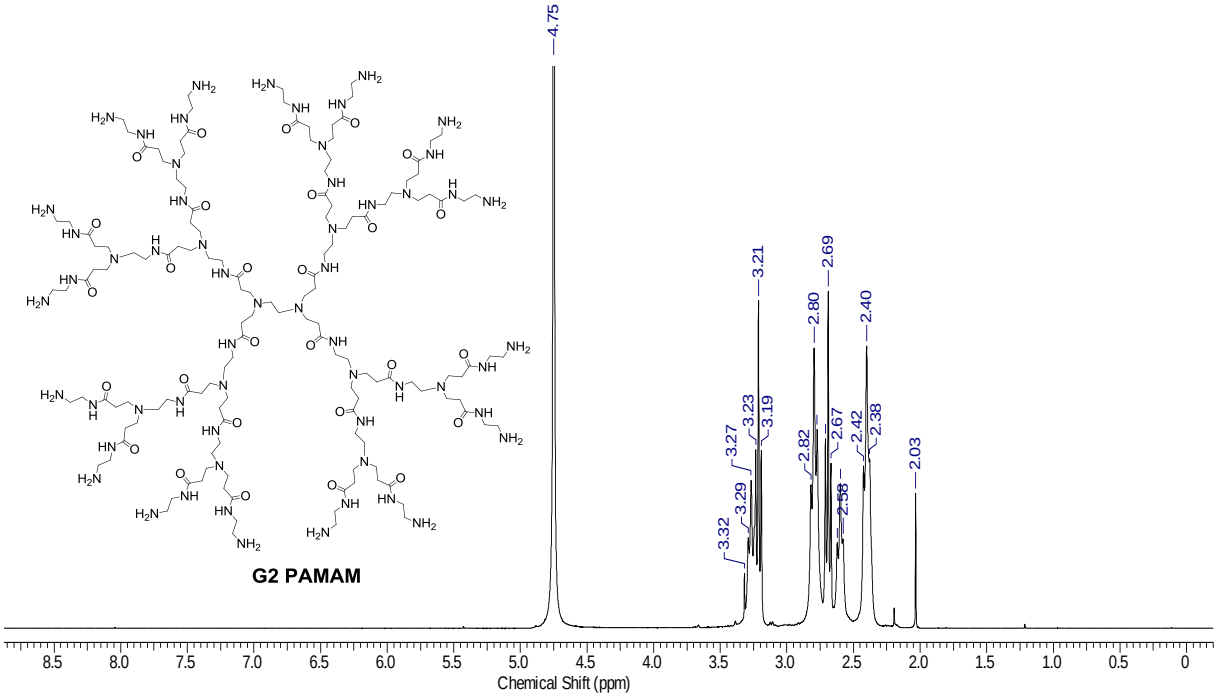

Figure 6-24. ^{1}H NMR spectrum of **G2 PAMAM** (300 MHz, D_2O).

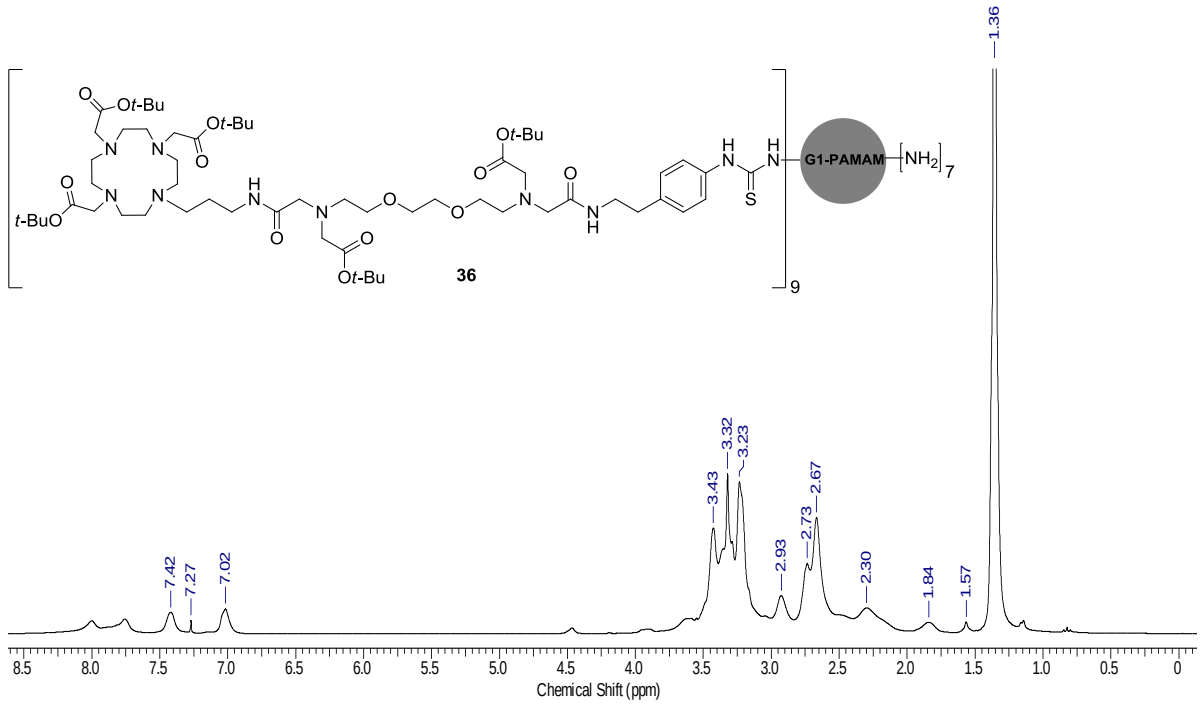

Figure 6-25. ^{1}H NMR spectrum of **36** (300 MHz, $CDCl_3$).

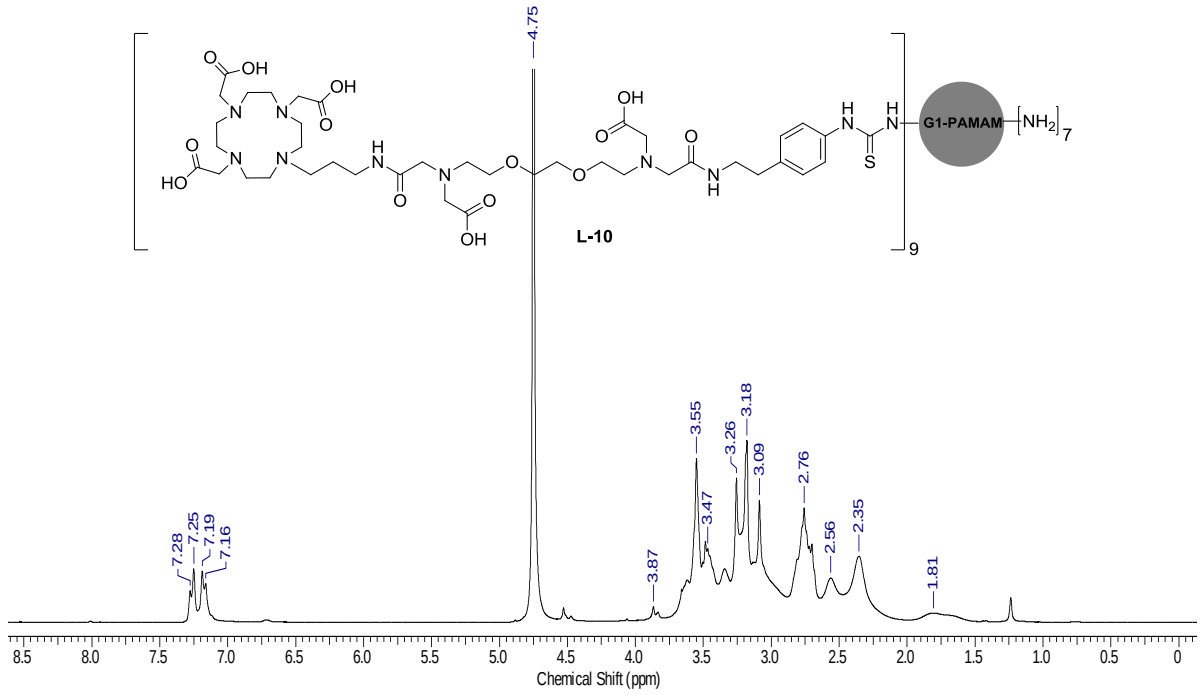

Figure 6-26. ^{1}H NMR spectrum of **L-10** (300 MHz, D_2O).

References

1. Modo, M.M.J.J. and J.W.M. Bulte, *Molecular and cellular MR imaging*. 2007, Boca Raton, Fla. London: CRC ;Taylor & Francis distributor. 421 p., 20 p. of plates.
2. Lauffer, R.E., *Paramagnetic Metal Complexes as Water Proton Relaxation Agents for NMR Imaging: Theory and Design.* Chemical Reviews, 1987. **87**(5): p. 901-927.
3. Krause, W., *Contrast agents I : magnetic resonance imaging*. Topics in current chemistry. 2002, Berlin ; London: Springer. viii, 249 p.
4. Caravan, P., et al., *Gadolinium(III) chelates as MRI contrast agents: Structure, dynamics, and applications.* Chemical Reviews, 1999. **99**(9): p. 2293-2352.
5. Merbach, A.E. and É. Tóth, *The chemistry of contrast agents in medical magnetic resonance imaging*. 2001, Chichester: Wiley. xii, 471 p.
6. Aime, S., et al., *Prototropic vs whole water exchange contributions to the solvent relaxation enhancement in the aqueous solution of a cationic Gd3+ macrocyclic complex.* Journal of the American Chemical Society, 1997. **119**(20): p. 4767-4768.
7. Aime, S., et al., *Prototropic and water-exchange processes in aqueous solutions of Gd(III) chelates.* Accounts of Chemical Research, 1999. **32**(11): p. 941-949.
8. Cotton, S., *Lanthanide and actinide chemistry*. Inorganic chemistry. 2006, Chichester: Wiley. xiv, 263 p.
9. Gries, H., *Extracellular MRI contrast agents based on gadolinium.* Contrast Agents I, 2002. **221**: p. 1-24.
10. Martell, A.E. and R.J. Motekaitis, *The determination and use of stability constants*. 1988, New York: VCH. x, 216 p.
11. Li, L., et al., *Superparamagnetic Iron Oxide Nanoparticles as MRI contrast agents for Non-invasive Stem Cell Labeling and Tracking.* Theranostics, 2013. **3**(8): p. 595-615.
12. Weissleder, R., et al., *Long-Circulating Iron-Oxides for Mr-Imaging.* Advanced Drug Delivery Reviews, 1995. **16**(2-3): p. 321-334.
13. Singh, N., et al., *Potential toxicity of superparamagnetic iron oxide nanoparticles (SPION).* Nano Rev, 2010. **1**.
14. Reimer, P. and B. Tombach, *Hepatic MRI with SPIO: detection and characterization of focal liver lesions.* European Radiology, 1998. **8**(7): p. 1198-1204.
15. Bulte, J.W.M. and D.L. Kraitchman, *Iron oxide MR contrast agents for molecular and cellular imaging.* Nmr in Biomedicine, 2004. **17**(7): p. 484-499.
16. Vögtle, F., G. Richardt, and N. Werner, *Dendrimer chemistry*. 2009, Weinheim: Wiley-VCH. xi, 342.
17. Vögtle, F. and V. Balzani, *Dendrimers*. Topics in current chemistry, 1970340-1022. 1998, Berlin ; London: Springer. 240p.
18. Egon BUHLEIER, W., Fritz VÖGTLE, *"Cascade"- and "Nonskid-Chain-like" Syntheses of Molecular Cavity Toplogies.* Communications, 1978. **2**: p. 155-158.
19. Hawker, C.J. and J.M.J. Frechet, *Preparation of Polymers with Controlled Molecular Architecture - a New Convergent Approach to Dendritic Macromolecules.* Journal of the American Chemical Society, 1990. **112**(21): p. 7638-7647.
20. Tomalia, D.A., J.B. Christensen, and U. Boas, *Dendrimers, dendrons, and dendritic polymers : discovery, applications, and the future*. 2012, Cambridge: Cambridge University Press. vii, 412 p.
21. Stiriba, S.E., H. Frey, and R. Haag, *Dendritic polymers in biomedical applications: From potential to clinical use in diagnostics and therapy.* Angewandte Chemie-International Edition, 2002. **41**(8): p. 1329-1334.

22. Roglin, L., E.H.M. Lempens, and E.W. Meijer, *A Synthetic "Tour de Force": Well-Defined Multivalent and Multimodal Dendritic Structures for Biomedical Applications.* Angewandte Chemie-International Edition, 2011. **50**(1): p. 102-112.
23. Majoros, I.J., et al., *PAMAM dendrimer-based multifunctional conjugate for cancer therapy: Synthesis, characterization, and functionality.* Biomacromolecules, 2006. **7**(2): p. 572-579.
24. Yellepeddi, V.K., A. Kumar, and S. Palakurthi, *Biotinylated Poly(amido)amine (PAMAM) Dendrimers as Carriers for Drug Delivery to Ovarian Cancer Cells In Vitro.* Anticancer Research, 2009. **29**(8): p. 2933-2943.
25. Kesharwani, P., K. Jain, and N.K. Jain, *Dendrimer as nanocarrier for drug delivery.* Progress in Polymer Science, 2014. **39**(2): p. 268-307.
26. Gillies, E.R. and J.M.J. Frechet, *Dendrimers and dendritic polymers in drug delivery.* Drug Discovery Today, 2005. **10**(1): p. 35-43.
27. Zhu, J.Y. and X.Y. Shi, *Dendrimer-based nanodevices for targeted drug delivery applications.* Journal of Materials Chemistry B, 2013. **1**(34): p. 4199-4211.
28. Ghobril, C., et al., *Dendrimers in nuclear medical imaging.* New Journal of Chemistry, 2012. **36**(2): p. 310-323.
29. Tomalia, D.A., L.A. Reyna, and S. Svenson, *Dendrimers as multi-purpose nanodevices for oncology drug delivery and diagnostic imaging.* Biochemical Society Transactions, 2007. **35**: p. 61-67.
30. Boas, U., J.B. Christensen, and P.M.H. Heegaard, *Dendrimers in medicine and biotechnology : new molecular tools*. 2006, Cambridge: RSC Publishing. ix, 179 p.
31. Roberts, J.C., M.K. Bhalgat, and R.T. Zera, *Preliminary biological evaluation of polyamidoamine (PAMAM) Starburst(TM) dendrimers.* Journal of Biomedical Materials Research, 1996. **30**(1): p. 53-65.
32. Rittner, K., et al., *New basic membrane-destabilizing peptides for plasmid-based gene delivery in vitro and in vivo.* Molecular Therapy, 2002. **5**(2): p. 104-114.
33. Vögtle, F. and D. Astruc, *Dendrimers II : architecture, nanostructure and supramolecular chemistry*. Topics in current chemistry, 2100340-1022. 2000, Berlin ; London: Springer. 311p.
34. Wiener, E.C., et al., *Dendrimer-based metal chelates: a new class of magnetic resonance imaging contrast agents.* Magn Reson Med, 1994. **31**(1): p. 1-8.
35. Polasek, M., et al., *PAMAM Dendrimers Conjugated with an Uncharged Gadolinium(III) Chelate with a Fast Water Exchange: The Influence of Chelate Charge on Rotational Dynamics.* Bioconjugate Chemistry, 2009. **20**(11): p. 2142-2153.
36. Langereis, S., et al., *Evaluation of Gd(III)DTPA-terminated poly(propylene imine) dendrimers as contrast agents for MR imaging.* Nmr in Biomedicine, 2006. **19**(1): p. 133-141.
37. Kaneshiro, T.L., et al., *Synthesis and Evaluation of Globular Gd-DOTA-Monoamide Conjugates with Precisely Controlled Nanosizes for Magnetic Resonance Angiography.* Biomacromolecules, 2008. **9**(10): p. 2742-2748.
38. Langereis, S., et al., *Dendrimers and magnetic resonance imaging.* New Journal of Chemistry, 2007. **31**(7): p. 1152-1160.
39. Nwe, K., L.H. Bryant, and M.W. Brechbiel, *Poly(amidoamine) Dendrimer Based MRI Contrast Agents Exhibiting Enhanced Relaxivities Derived via Metal Preligation Techniques.* Bioconjugate Chemistry, 2010. **21**(6): p. 1014-1017.
40. Misselwitz, B., et al., *Gadofluorine 8: initial experience with a new contrast medium for interstitial MR lymphography.* Magnetic Resonance Materials in Physics Biology and Medicine, 1999. **8**(3): p. 190-195.
41. Wisner, E.R., et al., *A modular lymphographic magnetic resonance imaging contrast agent: Contrast enhancement with DNA transfection potential.* Journal of Medicinal Chemistry, 1997. **40**(25): p. 3992-3996.
42. Mamedov, I., et al., *Dual-functional probes towards in vivo studies of brain connectivity and plasticity.* Chemical Communications, 2012. **48**(22): p. 2755-2757.

43. Konda, S.D., et al., *Specific targeting of folate-dendrimer MRI contrast agents to the high affinity fo late receptor expressed in ovarian tumor xenografts.* Magnetic Resonance Materials in Physics Biology and Medicine, 2001. **12**(2-3): p. 104-113.
44. Mamedov, G.A.a.I., *Cation-Responsive MRI Contrast Agents Based on Gadolinium(III).* Current Inorganic Chemistry, 2011. **1**(1): p. 76-90.
45. Sigel, A., et al., *Interrelations between essential metal ions and human diseases*. Metal Ions in Life Sciences,. 1 online resource (xxxvii, 573 pages).
46. Hanaoka, K., et al., *Selective sensing of zinc ions with a novel magnetic resonance imaging contrast agent.* Journal of the Chemical Society-Perkin Transactions 2, 2001(9): p. 1840-1843.
47. Aime, S., et al., *Paramagnetic Gd-Iii-Fe-Iii Heterobimetallic Complexes of Dtpa-Bis-Salicylamide.* Spectrochimica Acta Part a-Molecular and Biomolecular Spectroscopy, 1993. **49**(9): p. 1315-1322.
48. Matczak-Jon, E., et al., *Interactions of zinc(II), magnesium(II) and calcium(II) with iminodimethylenediphosphonic acids in aqueous solutions.* Journal of the Chemical Society-Dalton Transactions, 1999(20): p. 3627-3637.
49. McMahon, R.J., *Avidin–Biotin Interactions*. Methods in Molecular Biology, ed. J.M. Walker. 2008, UK: Humana Press.
50. Dirksen, A., et al., *A supramolecular approach to multivalent target-specific MRI contrast agents for angiogenesis.* Chemical Communications, 2005(22): p. 2811-2813.
51. Kobayashi, H., et al., *Avidin-dendrimer-(1B4M-Gd)(254): A tumor-targeting therapeutic agent for gadolinium neutron capture therapy of intraperitoneal disseminated tumor which can be monitored by MRI.* Bioconjugate Chemistry, 2001. **12**(4): p. 587-593.
52. Xu, H., et al., *Preparation and preliminary evaluation of a biotin-targeted, lectin-targeted dendrimer-based probe for dual-modality magnetic resonance and fluorescence Imaging.* Bioconjugate Chemistry, 2007. **18**(5): p. 1474-1482.
53. Boswell, C.A., et al., *Synthesis, characterization, and biological evaluation of integrin alphavbeta3-targeted PAMAM dendrimers.* Mol Pharm, 2008. **5**(4): p. 527-39.
54. Zhang, M.M., W.L. Zhu, and Y.X. Li, *Discovery of novel inhibitors of signal transducer and activator of transcription 3 (STAT3) signaling pathway by virtual screening.* European Journal of Medicinal Chemistry, 2013. **62**: p. 301-310.
55. Mattson, G., et al., *A Practical Approach to Cross-Linking.* Molecular Biology Reports, 1993. **17**(3): p. 167-183.
56. Tomalia, D.A., et al., *Structure control within poly(amidoamine) dendrimers: size, shape and regio-chemical mimicry of globular proteins.* Tetrahedron, 2003. **59**(22): p. 3799-3813.
57. Xu, R.Z., et al., *In vivo evaluation of a PAMAM-Cystamine-(Gd-DO3A) conjugate as a biodegradable macromolecular MRI contrast agent.* Experimental Biology and Medicine, 2007. **232**(8): p. 1081-1089.
58. Vögtle, F. and M. Ballauff, *Dendrimers III : design, dimension, function*. Topics in current chemistry, 2120340-1022. 2001, Berlin ; London: Springer. 198p.
59. Vibhute, S.M., et al., *Synthesis and characterization of pH-sensitive, biotinylated MRI contrast agents and their conjugates with avidin.* Organic & Biomolecular Chemistry, 2013. **11**(8): p. 1294-1305.
60. Xu, H., et al., *Toward improved syntheses of dendrimer-based magnetic resonance imaging contrast agents: New bifunctional diethylenetriaminepentaacetic acid ligands and nonaqueous conjugation chemistry.* Journal of Medicinal Chemistry, 2007. **50**(14): p. 3185-3193.
61. Corsi, D.M., et al., *Determination of paramagnetic lanthanide(III) concentrations from bulk magnetic susceptibility shifts in NMR spectra.* Magnetic Resonance in Chemistry, 2001. **39**(11): p. 723-726.
62. Squire, L.R. and M.J. Zigmond, *Fundamental neuroscience*. 2nd ed. 2003, San Diego, Calif. ; London: Academic. xix, 1426 p.

63. Chattopadhyay, N. and E.M. Brown, *Calcium-sensing receptor*. Endocrine updates. 2003, Boston ; London: Kluwer Academic. xvii, 286.
64. Logothetis, N.K. and B.A. Wandell, *Interpreting the BOLD signal.* Annual Review of Physiology, 2004. **66**: p. 735-769.
65. Logothetis, N.K., *What we can do and what we cannot do with fMRI.* Nature, 2008. **453**(7197): p. 869-878.
66. Bonnet, C.S. and E. Toth, *MRI probes for sensing biologically relevant metal ions.* Future Medicinal Chemistry, 2010. **2**(3): p. 367-384.
67. Atanasijevic, T., et al., *Calcium-sensitive MRI contrast agents based on superparamagnetic iron oxide nanoparticles and calmodulin.* Proceedings of the National Academy of Sciences of the United States of America, 2006. **103**(40): p. 14707-14712.
68. Li, W.H., S.E. Fraser, and T.J. Meade, *A calcium-sensitive magnetic resonance imaging contrast agent.* Journal of the American Chemical Society, 1999. **121**(6): p. 1413-1414.
69. Angelovski, G., et al., *Smart magnetic resonance imaging agents that sense extracellular calcium fluctuations.* Chembiochem, 2008. **9**(11): p. 1729-1734.
70. Angelovski, G., et al., *Investigation of a Calcium-Responsive Contrast Agent in Cellular Model Systems: Feasibility for Use as a Smart Molecular Probe in Functional MRI.* ACS Chem Neurosci, 2014.
71. Dhingra, K., et al., *Towards extracellular Ca2+ sensing by MRI: synthesis and calcium-dependent H-1 and O-17 relaxation studies of two novel bismacrocyclic Gd3+ complexes.* Journal of Biological Inorganic Chemistry, 2008. **13**(1): p. 35-46.
72. Hagberg, G.E., et al., *Diffusion properties of conventional and calcium-sensitive MRI contrast agents in the rat cerebral cortex.* Contrast Media & Molecular Imaging, 2014. **9**(1): p. 71-82.
73. Lehmann, S., et al., *Recording intracellular molecular events from the outside: glycosylphosphatidylinositol-anchored avidin as a reporter protein for in vivo imaging.* J Nucl Med, 2011. **52**(3): p. 445-52.
74. Lehtolainen, P., et al., *Targeting of biotinylated compounds to its target tissue using a low-density lipoprotein receptor-avidin fusion protein.* Gene Ther, 2003. **10**(25): p. 2090-7.
75. Mantyla, T., et al., *Targeted magnetic resonance imaging of Scavidin-receptor in human umbilical vein endothelial cells in vitro.* Magn Reson Med, 2006. **55**(4): p. 800-4.
76. Pinaud, F., et al., *Bioactivation and cell targeting of semiconductor CdSe/ZnS nanocrystals with phytochelatin-related peptides.* J Am Chem Soc, 2004. **126**(19): p. 6115-23.
77. Pinaud, F., et al., *Dynamic partitioning of a glycosyl-phosphatidylinositol-anchored protein in glycosphingolipid-rich microdomains imaged by single-quantum dot tracking.* Traffic, 2009. **10**(6): p. 691-712.